GeniSTELA - A Generalised Engineering Methodology for Thermal Analysis of Structural Members in Natural Fires

Hong Liang

BRE Centre for Fire Safety Engineering

University of Edinburgh

A thesis submitted for the degree of

Doctor of Philosophy

September 2008

I would like to dedicate this thesis to my loving family...

献给我亲爱的家人和朋友...

Declaration

The thesis writing and the research carried out has been completed solely by Hong Liang under the supervision of Dr. Stephen Welch, Professor Jose L. Torero and Professor Suresh Kumar. Where other sources are quoted, full references are given.

Hong Liang

September 2008

Abstract

The ability to predict the temperatures in protected steel structures is of vital importance for the progress of fire safety engineering. Existing methods are limited in several respects, typically being computationally restricted and limited to examination of the performance of specific components. This thesis investigates a generalised CFD-based methodology for thermal analysis of structural members in fire, developed to overcome these limitations.

A novel methodology has been developed, known as *GeniSTELA* (Generalised Solid ThErmal Analysis), which computes a "steel temperature field" parameter in each computational cell. The approach is based on a simplified 1D model for heat transfer, together with appropriate corrections for 2D and 3D effects, to provide a quasi-3D solution with a reasonable computational cost. It accommodates both uncertainties in the input parameters, such as member emissivities, and possible variants to the specification, e.g. member size and protection material properties, by means of many simultaneous thermal calculations. A framework for the inclusion of temperature/time-dependent thermal properties, including the effects of moisture and intumescence, has been established. Indicative values of intumescent material properties have been obtained by means of cone calorimeter testing. These are dependent on initial thickness and exposure heat flux. The corrections for 2D and 3D effects are based on simple physical considerations associated with different possible scenarios. Four cases where the precise nature of localised heating is important are treated in the quasi-3D model: junction effect, end effect, heat sink effect and axial temperature gradient. By predicting temperature of "virtual members" at every point in the computational domain a fundamental limitation of existing methods is bypassed, and by performing simultaneous calculations which span the range of cases of

possible interest, to provide a library of relevant solutions for any given fire scenario, the generality of the results is greatly increased.

GeniSTELA has been implemented as a submodel within the *SOFIE* RANS CFD code. The basic operation of the model has been verified and results compared to the empirical methods in EC3, indicating a satisfactory performance. The role of the surface temperature prediction has been examined and demonstrated to be important for certain cases, justifying its inclusion in the generalised method. The models for 3D corrections have been verified and their significance assessed. The computational requirements are addressed considering a number of aspects such as the number of simultaneous parametric cases, the required frequency of *GeniSTELA* steel temperature field computation and, hence, the overall balance between fluid and solid-phase analysis. These confirm the practical utility of the tool in simultaneously running a large number of parametric variants.

Validation of the model is undertaken with respect to standard testing in fire resistance furnaces, examining the fire ratings of different practical protection systems, and the BRE large compartment fire tests, which looked at protected steel indicatives in full-scale post-flashover fires; in both cases, a satisfactory agreement is achieved. Model sensitivities are reported which reveal the expected strong dependencies on certain properties of thermal protection materials.

The intended operation of the generalised model is demonstrated in application to test scenarios, such as the hypothetical benckmark test scenario, with simultaneous computation of 72 parametric variants. The methodology is confirmed as a comprehensive, but practical, tool for structural fire design, providing far more flexibility in assessing the thermal response of steel structures to fire than has been available hitherto, with potential to improve the efficiency and safety of the relevant constructions. Suggestions are made for the further developments required to consider generalised structural response.

Publications

The following papers have been produced as a result of this research:

Journal papers

Liang, H. and Welch, S. and Torero, J. L.(2008). Development of an engineering methodology for thermal analysis of protected structural members in fire. Invited submission to *International Journal on Advanced Steel Construction*.

Conference papers

Liang, H. and Welch, S.(2006). A novel engineering tool for thermal analysis of structural members in natural fires. In *Proc. of 4th Int. Workshop on Structures in fire*, Aveiro, Portugal.

Liang, H. and Welch, S. and Stratford, T. and Kinsella, E.V.(2007). Development and validation of a generalised engineering methodology for thermal analysis of structural members in fire. In *Proc. of 5th Int. Seminar Fire and Explosion Hazards*, Edinburgh, UK.

Liang, H. and Welch, S.(2007). Development of an engineering methodology for thermal analysis of protected structural members in fire. In *Proc. of 3rd Int. Conf. on Steel and Composite Structures*, Manchester, UK.

Liang, H. and Welch, S.(2007). Application of a generalised engineering methodology for thermal analysis of structural members in fire. In *Proc. of Advance Research Workshop on Fire Computer Modelling*, San-

tander, Spain.

Liang, H. and Welch, S.(2007). *GeniSTELA* - A generalised engineering methodology for thermal analysis of protected steel work. In *Proc. of Steel in Fire Forum Workshop*, Swinden Technology Centre Moorgate, Rotherham, UK.

Liang, H. and Welch, S.(2008). *GeniSTELA* - A generalised engineering methodology for thermal analysis of structural members in natural fires. *9th International IAFSS Symposium*, Karlsruhe, Germany.

User guide

Liang, H.(2007). *GeniSTELA* Manual (Generalised Solid Thermal Analysis) v1.0.. (To be published)

Acknowledgements

Grateful acknowledgement is to my supervisor Dr. Stephen Welch for his guidance and encouragement during my research as well as his kindness and patience.

Acknowledgements are also to Professor Dougal Drysdale, Professor Jose Torero, Professor Suresh Kumar, Dr. Asif Usmani, Dr. Guillermo Rein, Dr. Tim Stratford and Dr. Rochan Upadhyay for their supports and valuable suggestions.

Thanks to BEng student Emmett Kinsella for providing the intumescent test data. Useful comments on intumescent properties were also received from Yong Wang and Matthias Barthol-mai, and Daniel Joyeux and Mario Fontana via *IAFSS* email list.

Further thanks to all the members of the BRE Centre for Fire Safety Engineering at the University of Edinburgh and the staff at BRE Garston, near London.

Special thanks to my family and my friends, especially Dr. Imjai, for their encouragements and supports.

I would also like to thank BRE Trust for the financial support during my research. Besides, the work has formed part of *FireGrid*. This project was/is co-funded by the Technology Strategy Board's Collaborative Research and Development programme, following an open competition. All supports are appreciated.

Table of Contents

List of Figures

List of Tables

Notation

Alphabetic symbols

A	is the cross section area, $[m^2]$
A_m	is the surface area of the member per unit length, $[m^2/m]$
A_m/V	is the section factor for unprotected steel members, $[1/m]$
A_p	is the appropriate area of fire protection material per unit length of the member, $[m^2/m]$
A_p/V	is the section factor for steel members insulated by fire protection material, $[1/m]$
A_s	is the surface area of the member per unit length, $[m^2/m]$
b_{flange}	is the flange width, $[m]$
c_a	is the specific heat of steel, $[J/(kg \cdot K)]$
c_p	is the specific heat, $[J/(kg \cdot K)]$
$c_{p,eff}$	is the effective specific heat with the change of temperature and effect of intumescence, $[J/(kg \cdot K)]$
c_{p,H_2O}	is the specific heat capacity of water, $c_{p,H_2O} = 10^3$ $[J/(kg \cdot K)]$
d_p	is the thickness of the fire protection material, $[m]$
d_{web}	is the web depth, $[m]$
E	is the energy term, $[J]$
E	is the young's modulus (modulus of elasticity), $[N/mm^2]$
E	is the emission of a surface at anytime, $[W/m^2]$
E_b	is the emission of the black body surface at anytime, $[W/m^2]$
E_{system}	is the total energy in the system, $[J]$
Gr	is the Grashof number, $[-]$
h	is the opening height, $[m]$
h, h_c	is the convective heat transfer coefficient, $[W/(m^2 \cdot K)]$
$\dot{h}_{net}$	is the design value of the net heat flux per unit area, $[W/m^2]$
K	is the stiffness, $[N/m]$
k	is the thermal conductivity, $[W/(m \cdot K)]$
$KTFactor$	is the temperature effect factor, by default, $3e^{-6}$ $[-]$
k_s	is the thermal conductivity, $[W/(m \cdot K)]$
k_{sh}	is the correction factor for the shadow effect, $[-]$
k_0	is the dry thermal conductivity, $[W/(m \cdot K)]$

L	is the length of structural component, $[m]$
L	is the latent heat capacity of water, $L = 2.176 \times 10^6$ $[J/kg]$
l	is the characteristic length scale dimension of the surface, $[m]$
m	is the material mass change rate due to intumescence, $[kg/kg]$
mu	is the value of viscosity $[m^2/s]$
n	is the shape factor power for intumescent model, $[-]$
Nu	is the dimensionless Nusselt number, $[-]$
P	is the perimeter of the member per unit length, $[m/m]$
Pr	is the dimensionless Prandtl number, $[-]$
$\dot{Q}$	is the fire growth rate, $[kW/s]$
$\mathrm{Q}\,\vert_A$	is the net rate of heat flow out of the control surface, by conduction, convection and radiation or combined modes, $[J/s]$
q	is the heat flux $[W/m^2]$
$q_{b,emitted}$	is the heat flux emitted from a black body, $[W]$
q_c	is the convective heat flux per unit area, $[W/m^2]$
q_{cond}	is the conduction heat flux vector, $[W/m^2]$
q_{conv}	is the convection heat flux vector, $[W/m^2]$
q_r	is the radiative heat flux per unit area, $[W/m^2]$
q_{rad}	is the radiation heat flux vector, $[W/m^2]$
q''	is the convection heat flux, $[W/m^2]$
q''_x	is the heat flux in x direction, $[W/m^2]$
R	is the time-dependent expansion factor for intumescent materials, $[-]$
R_f	is the final expansion factor, $[-]$
Re	is the dimensionless Reynolds number, $[-]$
$\dot{S}_e\,\vert_{\mathrm{V}}$	is the rate of other work done (or conversion of energy) on the control volume, $[J/s]$
T	is the relevant temperature, $[K]$
$T_{ambient}$	is the ambient temperature, $[K]$
T_{lower},T_{mid}	
T_{upper}	is the critical temperatures where scaling factor changes, $[K]$
T_g	is the gas temperature, $[^\circ C]$
T_H	is the local gas temperature, $[K]$
T_{ilower}, T_{imid}	
T_{iupper}	is the critical temperatures where scaling factor changes due to energy effect, $[K]$
$T_{rad,inv}$	is the inverted radiative temperature, $[K]$
T_s	is the steel temperature, $[K]$
T_{s1}, T_{s2}	is the two surface temperatures respectively, $[K]$
t	is the specific time of interest, $[s]$
t_{web}	is the web thickness, $[m]$
t_0	is the length of the incubation period, $[s]$
ΔT	is the temperature change, $[K]$
Δt	is the time interval, $[seconds]$

u	is the x-component of velocity, $[m/s]$
V	is the volume of the member per unit length, $[m^3/m]$
V_s	is the volume of the member per unit length, $[m^3/m]$
v	is the y-component of velocity, $[m/s]$
$\dot{\mathrm{W}}_{\mathrm{p}}\,\vert_{\mathrm{A}}$	is the rate of pressure work done on the control surface, $[J/s]$
$\dot{\mathrm{W}}_{g,e}\,\vert_{\mathrm{V}}$	is the rate of gravitational and electromagnetic work done on the control volume, $[J/s]$
$\dot{\mathrm{W}}_{\mu}\,\vert_{\mathrm{A}}$	is the rate of viscous work done on the control surface, $[J/s]$
w	is the z-component of velocity. $[m/s]$
w_p	is the weight factor for protection layers, $[-]$
x	is the x-coordinate direction, $[m]$
x^*	is the spatial variable, $[-]$
δx	is the material layers thickness $[m]$
y	is the y-coordinate direction, $[m]$
z	is the z-coordinate direction, $[m]$

Greek letters

α	is the absorptivity, [−]
α_f	is the fire-growth coefficient, $[kW/s^2]$
χ	is an appropriate length scale, [−]
Δ	difference or change [−]
δ	thermal penetration depth $[m]$
κ	is the gas absorption coefficient or called extinction coefficient, [−]
λ_p	is the thermal conductivity of the fire protection system, $[W/(m \cdot K)]$
μ	is the viscosity, $[kg/(m \cdot s)]$
∇	is the divergence vector, $[1/m]$
ω_m	is the initial moisture content of the material, $[kg/kg]$
π	pi constant, 3.141592654 [−]
ρ	is the density of the control system, $[kg/m^3]$
ρ_a	is the unit mass of steel, $[kg/m^3]$
ρ_p	is the unit mass of the fire protection material, $[kg/m^3]$
ρ_s	is the unit mass of steel, $[kg/m^3]$
ρ_{eff}	is the effective density with the change of temperature and effect of intumescence, $[kg/m^3]$
σ	is the Stefan-Boltzmann constant, $\sigma = 5.669 \times 10^{-8}$ $[W/(m^2 \cdot K^4)]$
$\theta_{a,t}$	is the steel temperature at time t, $[°C]$
$\theta_{g,t}$	is the ambient gas temperature at time t, $[°C]$
ε	is the emissivity coefficient, [−]
ε_f	is the emissivity of the fire, [−]
ε_g	is total gas emissivity, [−]
ε_m	is the structural member emissivity, [−]
ε_{res}	is the resultant emissivity, [−]
ε_s	is the emissivity of the steel member, [−]
ε_t	is the total strain including mechanical strain and thermal strain, [−]

Subscripts

a	Ambient
a	Steel
avg	Average
b	Black body
c	Convective
$cond$	Conduction
$conv$	Convective
eff	Effective value
env	Environmental, i.e. effective conditions seen from point of interest
f	Fire
g	Gas
H	Hot cell
$lower$	Lower moisture plateau temperature
m	Members
mid	Middle moisture plateau temperature
net	Net heat flux
p	Protection material
$poly0$	Polynomial curve parameter for power of zero
$poly1$	Polynomial curve parameter for power of one
$poly2$	Polynomial curve parameter for power of two
r	Radiative
rad	Radiation
s	Steel
$system$	Structure system
$upper$	Upper moisture plateau temperature
web	Steel beam web
1	Protection layer side 1
2	Protection layer side 2
$1,0$	Surface temperature at gas-solid interface on sides 2
$2,0$	Surface temperature at gas-solid interface on sides 2

Superscripts

$\cdot$	Signifies rate of change as in $\dot{q}$
$'$	Single prime (signifies 'per unit width')
$''$	Double prime (signifies 'per unit area')
n	n^{th} time step

Abbreviations

ABAQUS	FEM package
ANSYS	FEM program
CFD	Computational Fluid Dynamics
DIANA	FEM program
DTRM	Discrete Transfer Radiation Model
DTF	Discrete Transfer Radiation Model
EBU	Eddy BreakUp combustion model
EC	Structural Eurocode
FDS	CFD PROGRAM (Fire Dynamics Simulator)
GeniSTELA	Solid-phase field thermal model (Generalised Solid ThErmaL Analysis)
GeniSTRUC	Solid-phase field mechanical model (Generalised STRUCtural analysis)
JOSEFINE	Graphical User Interface (JASMINE or SOFIE Fire Interface)
RANS	Reynolds Averaged Navier-Stokes
SOFIE	Fire field model solver (Simulation Of Fires In Enclosures)
STELA	Embedded mesh solid-phase solver (Solid ThErmaL Analysis)
VESTA	CFD Program (Vuur En STroming Analysator)

Chapter 1

Introduction

1.1 Background to the Project

Over the last two decades, attempts to consider more realistically the effects of fire on structures have intensified. This increasing interest in assessing the performance of structures in fire is driving the development of an array of modelling methodologies to be used in fire safety engineering design. Traditionally, most code-based design has been based on simple calculations, referencing measured fire performance in standard tests. These sorts of codes make some provision for design analysis of steel-framed buildings on the basis of the predicted response of structures to "natural" fire exposures. However, in the context of "whole-frame" mechanical analysis, the member temperatures are normally still prescribed very crudely and conservatively, often taking a single worst case temperature value for an entire enclosure. The progressive shift towards performance-based design has opened the door to use of advanced methods based on numerical models. These approaches will not replace standard testing, but they can already be used in a complementary fashion, to extend the application of test data and to better account for localised heating effects for natural fires.

Some simplified modelling methods have also been established, such as the protected member equation in Eurocode 3 (EC3) (BSI, 2005a), but as with all semi-empirical methods the results will tend to be conservative and there are of necessity a number of simplifying assumptions. Computational fluid dynamics (CFD)-based methodologies can in principle provide a much more detailed description of the thermal environment and the effects of localised heating, which

could be used in conjunction with thermal analysis models to examine structural performance. In previous work (Kumar *et al.*, 2005), a dedicated fine-mesh thermal modelling tool, known as *STELA* (Solid ThErmaL Analysis), has been implemented with the RANS CFD code *SOFIE* (Lewis *et al.*, 1997). However, this research suggests that detailed thermal analysis of structural members in the context of simulations of full-scale building fires remains problematic. This is partly due to the difference of scale between the mesh which can be afforded for the fire and that required for the thermal analysis of the structure, a particular problem with structured meshes, and also the generally high computational demands for coupled analysis. Moreover, existing approaches are limited to a specific structural arrangement of interest since it is necessary to define all model parameters in advance. Simulations including the CFD simulation must be repeated if details such as the structural geometry or the thermal properties are changed, a very inefficient procedure. In the consequence, there is a clear need for much more general and flexible procedures to assess the performance of structures in fire.

A novel methodology for generalised thermal analysis of structural members in fire, but still within the context of a CFD fire simulation, has been developed under the BRE Trust funded project. The methodology is known as *GeniSTELA* (Generalised Solid ThErmaL Analysis). This is based on computation of a set of "steel temperature field" parameters within the whole of the CFD calculation domain, accommodating, by means of simultaneous calculations, both uncertainties in the input parameters and possible variants to the specification. Hence the need for repeat simulations is bypassed. Furthermore, by predicting the "virtual member" temperatures at each point in space the limitations of existing methods with regards to the position of the structural component are overcome. Considering the potentially great computational costs associated with the large numbers of thermal analysis calculations required (equal to the number of gas-phase cells times the number of variants studied in the simultaneous calculations), approximate methods are employed to reduce the full 3D thermal response problem down to treatments which are essentially 1D but which include appropriate representations of the heat transfer processes in the other dimensions to reconstruct a quasi-3D solution. The further development, in particular, the modelling representations for the effects of moisture and intumescent performance in fire has also been addressed. *GeniSTELA* has been implemented as a submodel within the

SOFIE RANS CFD code.

Two full-scale tests simulation examples are provided to validate the method. The first is a standard fire resistance test apparatus, based on the Warrington $9m^3$ wall furnace, and the second is the post-flashover BRE large compartment fire test. A furnace test is chosen in order to decouple uncertainties in temperature prediction from the thermal response problem whilst at the same time assessing the latter in the context of results available from testing. The results of the furnace simulation are used to verify the model for thermal response of protected components, referencing expected performance based on fire resistance ratings. The compartment fire test also permits assessment of the predictive captivities for the steel temperature field, but for the more general case of natural fire exposures. However, it is a challenge to first reproduce the measured thermal fields, though in this case the heat release rates can be determined at least approximately by reference to crib mass loss data (Lennon & Moore, 2003; Schleich *et al.*, 2003; Welch *et al.*, 2007). Another significant uncertainty in natural fire derives from the lack of information on the optical properties of the combustion gases which were not measured, but sensitivities can be considered based on some assumed values (Welch *et al.*, 2007).

The computational requirements are assessed considering a number of aspects such as the number of simultaneous parametric cases, the required frequency of the *GeniSTELA* steel temperature field computation and, hence, the overall balance between fluid and solid-phase analysis. These confirm the practical utility of the tool in simultaneously running a large number of parametric variants, of the order 100 parallel cases. The model is applied to a hypothetical benchmark test scenario (Kumar *et al.*, 2006), demonstrating its practical use.

Overall, *GeniSTELA* is a comprehensive, but practical, tool for structural fire design, providing far more flexibility in assessing the thermal response of steel structures to fire than has been available hitherto, with potential to improve the efficiency and safety of the relevant constructions. It has also been exploited as an example of integrated models for fire and structural response under the *FireGrid* project, which is aimed to establish a cross-disciplinary collaborative community to pursue fundamental research for developing real time emergency

response systems, using the Grid technique, beginning with fire emergencies (UoE, 2007).

1.2 Aims and Objectives

The ultimate aim of the project is to develop a novel simulation methodology, which is based on computational fluid dynamics (CFD), for generalised thermal analysis of structural members in natural fires. The research intends to analyse the overall thermal performances of structural members by a combination of analytical formulation and numerical modelling, in a generalised fashion in consideration of a broad range of possible component geometries and specifications, as well as the likely variations in other essential parameters such as emissivity. To achieve this aim, the specific objectives are as presented as follows:

- To fully understand the relevant mechanisms of fire modelling
- To develop a verified CFD-based engineering methodology for simulating the structural members by including computation of a general "steel temperature field" parameter within the whole of the calculation domain
- To investigate the sensitivities of the methodology to intrinsic uncertainties in the input parameters such as configuration factors, member emissivity and fire emissivity, as well as the possible variants to the specification such as member section size, protection thickness etc., and finally identify the key controlling parameters
- To verify and validate the methodology with regards to experimental tests
- To optimize the code by the means of simultaneous calculation of multiple cases under the same fire environment
- To examine the practical use of the methodology, relating to the accuracy and efficiency
- To prepare recommendations on implementation and use of such a methodology, as appropriate, to encourage take-up by practitioners

1.3 Layout of the Thesis

Chapter 2: Literature Review

This chapter reviews the fundamental theories and state-of-art researches relating to thermal analysis of structures in fire. It starts from the fire behaviours to the fundamentals of CFD as well as heat transfer to structural members, reviewing the theoretic background knowledge for later conceptual model development. Besides, certain material thermal properties that might have a strong effect on the thermal response predictability have been examined. This chapter concludes with a comparative study of existing research methodologies and expresses the necessity for further research in thermal analysis of structures in fire.

Chapter 3: Methodology

A generalised modelling methodology is developed and described here both as a conceptual and numerical model. It has been developed on the base of the energy balance and heat transfer theory as described in the previous chapter. The representation of heat transfer processes in the other dimensions when they become significant have been included. Temperature and time- dependent thermal properties for protection materials are considered, encompassing moisture and intumescent effects. Assumptions along with the methodology development are also described.

Chapter 4: Implementation, Verification and Validation

A brief description of the methodology implementation is given here, based on spreadsheet and Fortran CFD code. It also shows how the parameters are prepared within *GeniSTELA*. The simulation of a single protected universal beam subjected to a localised fire test has been described for initial model verification. Following that, verification of certain details of the model, such as the 3D effects and surface temperature calculation procedure using Newton-Raphson iterations has been presented. Two full-scale experimental tests are introduced, Warrington fire resistance furnace test and the BRE Cardington large compartment fire test, representing two different fire situations. They are simulated using *GeniSTELA* and studied together with many other parameters. The results are stated and analysed in this chapter. They are used for *GeniSTELA* further verification and are compared with the measured results for model validation.

Chapter 5: Application and Exploitation

In order to investigate the practical use of *GeniSTELA*, the computational requirements have been assessed in this chapter and optimized by adjusting the *GeniSTELA* calling frequency in comparison with the fluid field simulation. This procedure has been found to be efficient and not detrimental to the final results. The simultaneous calculations of multiple cases with varying parameters or specifications within afforded CPU cost have been conducted within *GeniSTELA*. The application of *GeniSTELA* to a hypothetical benchmark test scenario is demonstrated with 72 simultaneous cases, illustrating the generality and feasibility of *GeniSTELA*. At the end of the chapter, literature review and discussion of the existing structural response analysis methodologies are presented. A proposal of a simplified structural analysis model within *GeniSTELA* is suggested as a possible follow-up project.

Chapter 6: Conclusions

A summary of the work undertaken and outcomes of the study is presented. It concludes that *GeniSTELA* has been confirmed as a practical and generalised thermal analysis methodology in terms of several aspects, covering the steel temperature field prediction accuracy, material properties submodels, reliability and computational efficiency. Ideas for future research needs and focus are given in terms of increasing the generality of *GeniSTELA*, widening its application as well as complementary research in the structural fire safety field.

Appendices

More details for certain aspects are provided in the appendices. **Appendix A** describes the calculation of the weight factor which is a factor to consider the transient heating of the protected material. **Appendix B** describes the representative term for junction effect correction and its derivations, including the length scale variable and the net heat flux difference caused by the junction effect. **Appendix C** describes the derivation of temperature dependent and moisture inclusive thermal properties, covering specific heat and thermal conductivity. **Appendix D** is the list of 72 parametrical variables adopted in the benchmark test scenario demonstration.

Chapter 2

Literature Review

2.1 Introduction

This chapter presents relevant literature available on the thermal analysis of structures in fire. It outlines some of the fundamental aspects in the fire safety engineering, heat transfer and thermal analysis of structures in fire. Heat transfer fundamentals including conjugate heat transfer as well as material thermal properties are investigated. Focused on the thermal analysis aspect, an overview of some commonly used or representative analysis methodologies available so far is given. Modelling methodologies are also reviewed and discussed as a complement to the empirical or analytical methodologies.

2.2 Fire behaviour

Significant impacts of fires on structures have been long observed, especially fires in enclosures such as the multi-story buildings, schools, hospitals and the underground parking lots (Ghojel, 1998). Attempts have arisen to consider more realistically the effects of fire on structures. The effective prediction of the effects becomes significantly important, involving the understanding of the nature of fire, the interaction between fire and structural members and the prediction methodologies.

A good understanding of the fundamentals of fires in UK from an engineering standpoint could be attributed to Drysdale (Drysdale, 1999), who outlines in detail the development of fire as it goes through a series of processes from its inception, through spread and growth to its fully developed stage. The development of a fire is therefore divided into three distinct phases. The first phase is called ignition and initial development of fire, or namely, pre-flashover. The second phase is fully developed fire phase, or post-flashover and the third phase is the decay of fire. A typical fire growth curve is as illustrated in Figure 2.1 below:

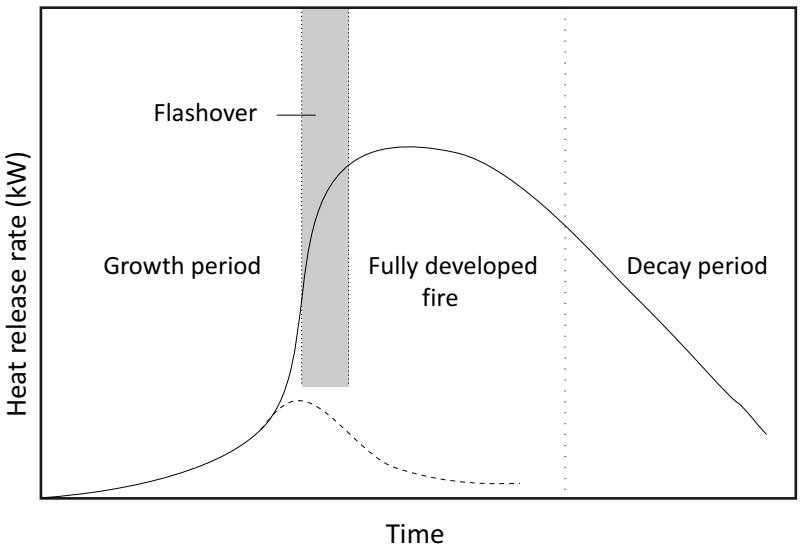

Figure 2.1: Development of a well-ventilated compartment fire (Drysdale, 1999) (The broken line represents either depletion of fuel prior to flashover or an extinguished fire)

Many other researchers have also tried to determine the fire growth rate. For instance, a parabolic growth rate for the pre-flashover fire, commonly referred to as a t-squared fire, is given by Alpert as specified in the *SFPE* handbook (Alpert, 2002):

$$\dot{Q} = \alpha_f (t - t_0)^2 \tag{2.1}$$

where

$\dot{Q}$ is the fire growth rate, $[kW/s]$
α_f is the fire-growth coefficient, $[kW/s^2]$
t_0 is the length of the incubation period, $[s]$
t is the specific time of interest, $[s]$

Typical values for α_f obtained by Thomas and Bullen (Thomas & Bullen, 1979) are presented in Table 2.1:

Table 2.1: Parameters used for t-squared fires

Description	Typical Scenario	α_f $[kW/s^2]$
Slow	Densely packed paper products	0.00293
Medium	Mattress/Armchair	0.01172
Fast	Pallets stacked 1m high	0.04690
Ultrafast	High rack storage	0.18760

Following flashover, most exposed surfaces of combustible items are assumed to be burning and the rate of heat release develops to a maximum, at the same time, high temperature will develop and be sustained until the fuel has largely been consumed. The rate of burning is expressed as the rate of mass loss. Two regimes of burning, "ventilation controlled" and "fuel controlled", are considered as explained by Thomas et al (Thomas *et al.*, 1967). The "ventilation controlled" regime, is the regime when the rate of burning is found to be independent of the amount of fuel, but increased with the size of the ventilation opening, as also studied by Kawagoe (Kawagoe, 1958) in early Japanese work on the burning of wood cribs in enclosures. In contrast with the "ventilation controlled" regime, when a ventilation opening is enlarged, the rate of burning becomes independent of the size of the opening and is determined instead by the surface area and burning characteristics of fuel, such is so-called "fuel controlled" regime.

Fire curves, expressed as the temperature-time relationships, are commonly used to represent the fire behaviour in design. Three levels of typical and widely used curves are the nominal fire curves, the parametric fire curves as given in Eurocode 1 (EC1) (BSI, 2002a) and the natural fire curves, the latter implying the real fire behaviour. EC1 (BSI, 2002a) specifies three nominal fire curves, which are the standard fire curve, normally known as ISO 834 standard fire curve, the external fire curve as well as the hydrocarbon fire curve. They are the simplest way to represent the behaviour of a fire, but do not represent real fire scenarios since the

cooling stage of the fire is not considered, and do not take into account ventilation, fuel load, compartment size or thermal characteristics of the compartment boundary. They are typically used in the performance-based structural fire engineering design as endorsed by the design codes (Bailey, 2006a). Parametric fire curves given in EC1 Annex A (BSI, 2002a) allow the time-temperature relationship to be estimated over the duration of the anticipated fire. Ventilation, fuel load, compartment size and boundary characteristics are considered. They are also easy to use and with the aid of spreadsheets, fire predictions can be easily derived. However, they are only valid for a maximum fire compartment floor area of $500m^2$ without openings in the roof and maximum compartment height of $4m$. They are also limited to fire compartments with mainly cellulosic-type fire loads and compartments with linings that have a value of thermal inertia between 100 and 2200 $J/(m^2 s^{1/2} K)$.

Natural fire curves are needed sometimes when the accuracy of the fire prediction becomes important and the scenarios are outside the prediction scope of EC1 (BSI, 2002a). Those curves generally could be obtained from either experimental test data or from computational modelling. Zone models are simple computer models that divide the considered fire compartment into separate zones, usually a hot and a cold layer, where the condition in each zone is assumed to be uniform. For each zone, the temperature is calculated with the consideration of the resolution of mass conservation and energy conservation equations, the exchange of mass between the internal gas, the external gas and the fire, and the exchange of energy between the fire, internal gas, walls and openings, as one-zone or two-zone models explained in EC1 Annex D (BSI, 2002a). One of the representative models is *MRFC* (Multi Room Fire Code), which is a zone model to calculate the physical data during a fire such as the temperature distribution in gases and structures and smoke transport inside a complex building and between the building and outside (Kumar *et al.*, 2002). Many others are available such as *CFAST*, *ASET*. Zone models are easy to use, fast to run, mostly only take several seconds to compute and relatively more practical. Because of their simplicity, zone models can achieve first order approximations to real fire behaviour. But in terms of complex fire situations, the accuracy of the predicted results may suffer.

A more sophisticated modelling technique is the use of computational fluid dynamics (CFD) to predict fire growth and obtain compartment temperatures. CFD

fire models, also known as field models, solve the fundamental equations describing the fluid flow and heat transfer phenomena associated with fire. They are therefore able to predict the fire in any arbitrary complexity, associating with offering the advantage of the accuracy and the detail of the results. Normally, CFD models are characteristically defined by the way in which turbulence is modelled. Thus, CFD codes can simplistically be divided into three groups, with models based on Reynolds-Averaged Navier-Stokes (RANS), Large Eddy Simulation (LES) and Direct Numerical Simulation (DNS). A detailed model comparison has been studied by Jowsey (Jowsey, 2006). Currently available CFD models, which are either fire dedicated programs or general purpose software which has been applied in fire modelling, include *FDS, JASMINE, SOFIE, MEFE, SPLASH, UNDSAFE, STAR-CD, FLUENT, CFX* (Fernandez-Pello & Rein, 2004) and *FLACS* (Gexcon, 2008). *FLACS* is a an advanced tool for the modelling of ventilation, gas dispersion, vapour cloud explosions and blast in complex process areas. It is mainly used for explosion. Except *FLACS*, all other codes are incompressible codes, giving solution of the incompressible Reynolds-Averaged Navier-Stokes (RANS) equation. With the advent of performance-based codes, the CFD based models are increasingly being used as general tools for fire safety engineering due to several advantages. On the other hand, the models require a great deal of experience in the use and place a high demand on computing resources and time. Attention is paid for choosing efficient and economic methodologies in practice. Figure 2.2 below shows a representative example of the different fire curves as aforementioned, annotated together with the key characteristics as well as the controlling factors during the fire development.

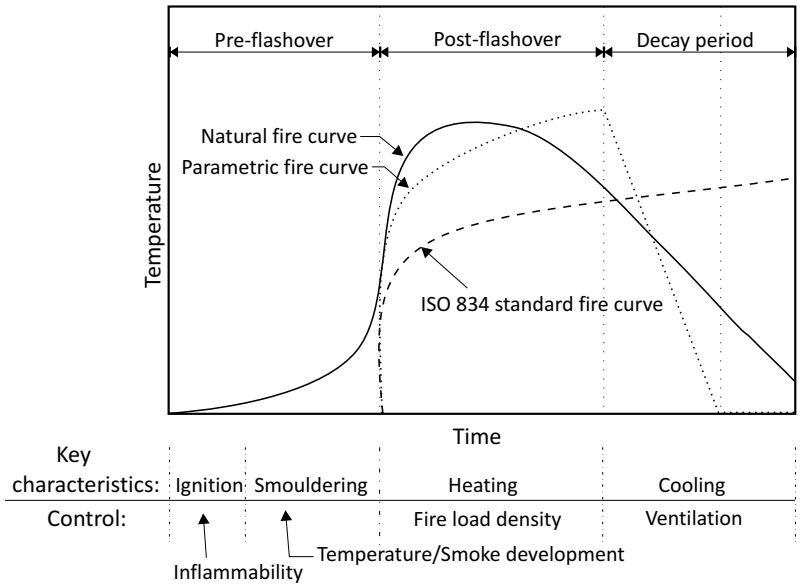

Figure 2.2: Temperature profile of natural fire curve, ISO 834 standard fire curve and parametric fire curve

2.3 Heat transfer

2.3.1 Heat transfer mechanisms

The heat produced by a fire flows between regions that are not in thermal equilibrium; more precisely speaking, it flows from areas of high temperature to areas of low temperature. Heat transfer therefore arose as a science which seeks to predict the energy transfer that may take place between material bodies as a result of the temperature difference. There are three heat transfer modes: conduction, convection and radiation, as described extensively in literature (Drysdale, 1999; Holman, 1988; Incropera & Dewitt, 1996). As referred in Figure 2.3 below, conduction is identified as the mode in which the heat passes through the substance of the body itself, while, in convection, heat is transferred by relative motion of portions of the heated body, and in radiation, heat is transferred direct between distant portions of the body by electromagnetic radiation (Carslaw & Jaeger, 1959; Christopher, 1999; Özisik, 1985).

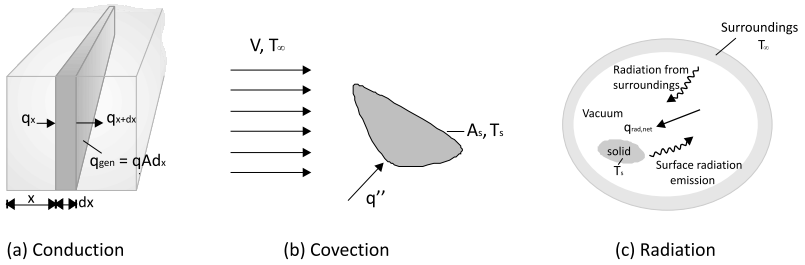

Figure 2.3: Conduction, convection, and radiation heat transfer modes

The heat transfer rate, termed as "heat flux" (Incropera & Dewitt, 1996), is used to quantify the heat transfer process. It is defined as the amount of heat per unit time per unit cross-sectional area (Drysdale, 1999). For one-dimensional heat transfer by conduction, the rate of heat transfer per unit area is proportional to the normal temperature gradient. French mathematical physicist Joseph Fourier applies the following expression 2.2 for calculating the conduction heat flux, called Fourier's law:

$$q_x^{''} = -k \cdot \frac{dT}{dx} \tag{2.2}$$

where
k is the thermal conductivity, $[W/(m \cdot K)]$
$q_x^{''}$ is the heat flux in x direction, $[W/m^2]$

The quantity k varies with different materials and their temperatures. For example, it could be as small as $0.026W/(m \cdot K)$ for air and as big as $387W/(m \cdot K)$ for copper at specific temperature (Pitts & Sissom, 1977). More detailed literature is reviewed and described in the next section together with other material thermal properties.

Convection heat transfer is the heat transfer between a solid surface and the surrounding fluid. The transfer process occurs close to the surface within a region known as the boundary layer. It is normally classified as either forced convection or free (or natural) convection according to the nature of the flow. As it stands, forced convection is the convection caused by external means, such as a fan or a pump. Free (or natural) convection, the flow is caused via expansion and buoyancy forces, which arise from density differences caused by temperature variations in the fluid. Regardless of the particular nature of the convection heat

transfer process, the appropriate heat transfer rate equation is of the form expressed in Equation 2.3, which describes the convection heat flux transfers from the fluid to the surface. This expression is also known as Newton's law of cooling.

$$q'' = h \cdot (T_\infty - T_s) \tag{2.3}$$

where

h is the convective heat transfer coefficient, $[W/(m^2 \cdot K)]$
q'' is the convection heat flux, $[W/m^2]$

In general, the convective heat transfer coefficient depends on the characteristics of the system, the geometry of the solid and the properties of the fluid including the flow parameters, and is also a function of temperature change. The evaluation of convective heat transfer coefficient for different situations has been one of the major problems in heat transfer and fluid dynamics. Typical values lie in the range $5 \sim 25 W/(m^2 \cdot K)$ for free convection and $10 \sim 500 W/(m^2 \cdot K)$ for forced convection in air (Drysdale, 1999). The detailed literature review for convective heat transfer coefficient could be found in the next section.

Unlike the mechanisms of conduction and convection, radiation heat transfer does not require the presence of a material medium. The energy of the radiation field is transported by electromagnetic waves. Thermodynamic considerations (Christopher, 1999; Drysdale, 1999; Holman, 1988) show that an ideal thermal radiator, or blackbody, will emit energy at a rate proportional to the fourth power of the absolute temperature of the body and directly proportional to its surface area. Stefan-Boltzmann law of thermal radiation applies:

$$q_{b,emitted} = \sigma \cdot A \cdot T^4 \tag{2.4}$$

where

σ is the Stefan-Boltzmann constant, $\sigma = 5.669 \times 10^{-8}$ $[W/(m^2 \cdot K^4)]$
$q_{b,emitted}$ is the heat flux emitted from a blackbody, $[W]$

However, generally a real surface will not radiate as much energy as the blackbody, but still follows the fourth power of the temperature proportionality. Emissivity,

a term to describe the radiative property of the surface, is a measure of the efficiency of a surface in emitting energy relative to a blackbody. As a consequence, the heat flux emitted by a real surface is given by:

$$q_{emitted} = \varepsilon \cdot \sigma \cdot A \cdot T^4 \tag{2.5}$$

where

ε is the emissivity coefficient, [–]

Actually, the radiation heat transfer phenomena could be far more complex than stated above. In reality, not only one surface is involved in the heat emission. For the radiation heat transfer case where two faces involved, the radiation heat flux exchanges between two surfaces could be described as:

$$q''_{rad} = \varepsilon \cdot \sigma \cdot (T_{s1}^4 - T_{s2}^4) \tag{2.6}$$

where

T_{s1}, T_{s2} are the two surface temperatures respectively, $[K]$

Moreover, not all the radiation leaving one surface will reach the other surface due to the heat loss to the surroundings. Several researchers have tried to consider those effects, such as Holman (Holman, 1988), who introduced F_G, a geometric "view factor" function to denote the fraction of energy leaving from one surface and arriving at the other. He also introduced F_ε, an emissivity function. Hamilton and Morgan (Hamilton & Morgan, 1952) have presented generalised relations for parallel and perpendicular rectangles in terms of "shape factors". Siegel and Howell (Siegel & Howell, 1980) et al. have extended the "configuration factor", namely "view factor" or "shape factor" to more complex geometries and provided a very complete catalog of analytical relations and graphs. Some others have studied the emissivity value ε and they found that the emissivities of various substances vary widely with wavelength, temperature, and surface condition.

In general, a real fire would involve one or all of the above three basic mechanisms of heat transfer. However, Carslaw and Jaeger (Carslaw & Jaeger, 1959) claim that in liquids and gases convection and radiation are of paramount importance,

but in solids convection is altogether absent and radiation usually negligible. Drysdale (Drysdale, 1999) also claims that "it is often found that one predominates at a given stage, or in a given location". This is evidenced by the fact that when a body is heated and its temperature rises, it will lose heat partly by convection and partly by radiation, depending on the emissivity and the value of convective heat transfer coefficient. Convection dominates at low temperature ($T < 150 \sim 200°C$) while radiation becomes increasingly dominant above $400°C$. These facts imply that simplified methods for heat transfer prediction could be adopted and may provide an appropriate basis for heat transfer analysis in the solid phase.

2.3.2 Heat transfer analysis

The analysis of heat transfer is based on the principle of energy conservation, because the variation in temperature during the heat transfer process is governed by the same principle. The principle of energy conservation states that the total energy of all the participants in any process must remain unchanged throughout the process. More specifically speaking, when applied to a control volume or a control mass, the sum of the flow of energy and the heat across the system, the work done on the system, and the energy stored and converted within the system, is zero, as also expressed in Equation 2.7 (Kaviang, 2002) below:

$$\mathrm{Q}\,|_A = -\frac{\partial E}{\partial t}\,|_\mathrm{V} - \dot{\mathrm{E}}_\mathrm{u}\,|_\mathrm{A} + \dot{\mathrm{W}}_\mathrm{p}\,|_\mathrm{A} + \dot{\mathrm{W}}_\mu\,|_\mathrm{A} + \dot{\mathrm{W}}_{g,e}\,|_\mathrm{V} + \dot{S}_e\,|_\mathrm{V} \tag{2.7}$$

where

$\mathrm{Q}\,\vert_A$	is the net rate of heat flow out of the control surface, by conduction, convection and radiation or combined modes,$[J/s]$
$-\frac{\partial E}{\partial t}\,\vert_\mathrm{V}$	is negative of rate of energy storage in the control volume, $[J/s]$
$-\mathrm{E_u}\,\vert_\mathrm{A}$	is negative of net rate of kinetic energy flow out of the control surface, $[J/s]$
$\dot{\mathrm{W}}_\mathrm{p}\,\vert_\mathrm{A}$	is the rate of pressure work done on the control surface, $[J/s]$
$\dot{\mathrm{W}}_\mu\,\vert_\mathrm{A}$	is the rate of viscous work done on the control surface, $[J/s]$
$\dot{\mathrm{W}}_{g,e}\,\vert_\mathrm{V}$	is the rate of gravitational and electromagnetic work done on the control volume,$[J/s]$
$\dot{S}_e\,\vert_\mathrm{V}$	is the rate of other work done (or conversion of energy) on the control volume, $[J/s]$

For heat transfer analysis of structures in a real fire, a control volume with constant pressure is normally assumed. The energy conservation equation (Equation 2.7) is therefore reduced as Equation 2.8, providing no additional work done on this control volume.

$$\nabla \cdot (q_{cond} + q_{conv} + q_{rad}) = -\frac{\partial}{\partial t}\rho c_p T \tag{2.8}$$

where

∇	is the divergence vector, $[1/m]$
q_{cond}	is the conduction heat flux vector, $[W/m^2]$
q_{conv}	is the convection heat flux vector, $[W/m^2]$
q_{rad}	is the radiation heat flux vector, $[W/m^2]$
ρ	is the density of the control system, $[kg/m^3]$
c_p	is the specific heat of the control system, $[J/(kg \cdot^\circ C)]$
T	is the temperature of the control system at time t, $[^\circ C]$
$-\frac{\partial}{\partial t}\rho c_p T$	is the time rate of sensible heat storage or release, $[W/m^3]$

The above equation is also called differential-volume energy equation, and is widely used as the governing equation for heat transfer analysis of structures in fire.

2.3.3 Conjugate heat transfer

Attention is to be paid to the *coupled* effects of conduction and free or natural convection and radiation, which is also called conjugate heat transfer, since it appears frequently in practice. Theoretically speaking, the term "conjugate heat transfer" (Yapici & Basturk, 2004) is used to describe the processes that involve

variations of temperature within solids and fluids, due to thermal interaction between the solids and fluids. In another words, the conjugate heat transfer is the coupling of the three modes of heat transfer: convection and radiation heat transfer in the fluid and the conduction heat transfer inside the adjacent solid surfaces (Papanicolaou *et al.*, 2001; Patankar, 1978).

Accurate solution of a conjugate heat transfer problem demands simultaneous solution of Navier-Stokes equations in the solid and in the fluid part of the computational domain, which might cause the difficulty. Patankar (Patankar, 1978) used a harmonic-mean procedure to solve the conjugate heat transfer problem. In this procedure, the problem is solved by using a calculation domain that includes both the fluid and solid regions, with the outer surface of the wall coinciding with the boundary of the domain. Thus, the boundary conditions for both the velocity and temperature fields can easily be supplied at the outer surface of the wall. Developed methods based on Finite Difference Methods (FDM), Finite Volume Methods (FVM) or Finite Element Methods (FEM) arise and could deal very successfully with the problem of interest. However, they all include some artificial assumptions, including assignment of large values for the fluid viscosity in the solid regions and the use of harmonic mean of physical properties at the solid-fluid interface. The final results are determined in an iterative way. The Boundary Element Method (BEM) could reduce the unknowns and simplify the preparation of computational models since only the boundary mesh is involved in solving the conjugate heat transfer problem. Nevertheless, this type of method could not tackle complex flow situations. Work on coupling of two individual methods for conjugate heat transfer has been carried out by some researchers, such as the coupling of FDM and BEM by He, Kassab et al. (He *et al.*, 1995), but an additional iteration procedure is required by this methodology. In practice, an appropriate method is chosen for particular case of interest.

2.4 Material thermal properties

Due to the heat transfer, the properties or behaviours of structural members vary with the internal energy change, and the structural elements behave quite differently under the fire exposure according to their material properties. The key dominating material thermal properties for a building structure analysis subjected

to fire are the specific heat (c), thermal conductivity (k), the convection coefficient (h), the emissivity (ε) as well as the absorptivity (α). The moisture effect and intumescent effect are considered especially for the first two material thermal properties because the effect is normally significant. Appropriate determination of all these properties is therefore required. Experimental measurements may be made to determine these properties of different materials or directly provided by the manufacturer. However, it is often the case that they are not directly available and approximations are required in this case.

There are many literature reports of these properties for building elements. For instance, Harmarthy (Harmarthy, 1995) reviews information on the properties of building materials, including concrete and brick, with particular reference to high temperature (fire exposure) conditions. The International Energy Agency has collated information on material properties (Kumaran, 1996). Guidelines are also available for certain properties.

2.4.1 Specific heat

Specific heat, c, is defined as the quantity of heat that is required to increase the temperature of unit mass by 1 K (Kumaran, 1996). It has the unit of $J/(kg \cdot K)$.

In general, gas phase specific heat is a function of temperature and species concentrations and can vary by about 20% for a typical enclosure fire. Normally, a constant within $1000 \sim 1200 J/(kg \cdot K)$ is adopted or if possible, it is expressed as a function of gas temperature and species concentrations, like in *JASMINE* (BRE, 2003; Miles & Kumar, 2003) and *SOFIE* (Rubini, 1997).

For the widely used building material, steel, Eurocode3 (EC3) (BSI, 2005a) determines the specific heat as follows:

Table 2.2: Specific heat of steel c_a $[J/(kg \cdot K)]$ in EC3 (BSI, 2005a)

$c_a = 425 + 7.73 \times 10^{-1}\theta_a - 1.69 \times 10^{-3}\theta_a^2 + 2.22 \times 10^{-6}\theta_a^3$	$(20°C \leq \theta_a < 600°C)$
$c_a = 666 + 13002 \div (738 - \theta_a)$	$(600°C \leq \theta_a < 735°C)$
$c_a = 545 + 17820 \div (\theta_a - 731)$	$(735°C \leq \theta_a < 900°C)$
$c_a = 650$	$(900°C \leq \theta_a < 1200°C)$

The variation is also illustrated as in the following figure.

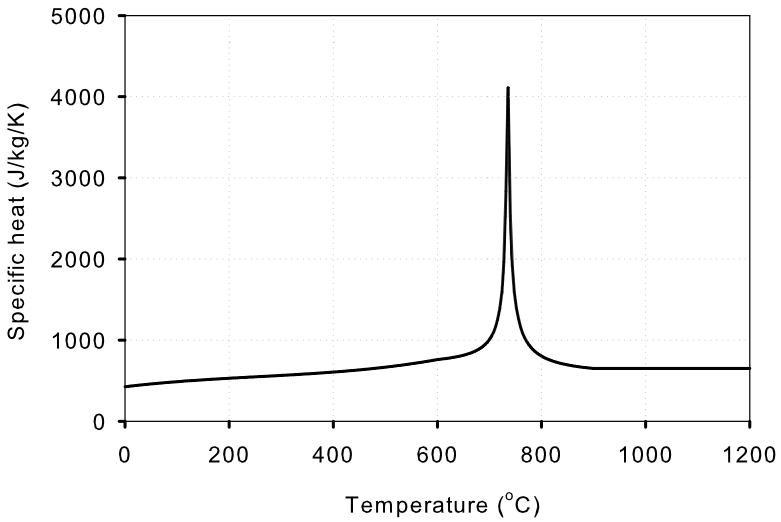

Figure 2.4: Specific heat of carbon steel as a function of the temperature

The above equation is valid for carbon steel; for stainless steel, the thermal properties could be obtained from EC3 Annex C (BSI, 2005a).

The performances of fire protection materials are far more complex than steel. Their thermal properties can be assessed using the test procedures followed by design codes ENV 13381-1 (BSI, 2005b), ENV 13381-2 (BSI, 2002c) for protective member or ENV 13381-4 (BSI, 2002b) for applied protection to steel members as appropriate.

2.4.2 Thermal conductivity

Thermal conductivity, k, is the rate at which heat is conducted across unit cross-sectional area when there is unit temperature gradient perpendicular to this area. It has the unit of $W/(m \cdot K)$ (Goldsmid, 1965). In the early stage, constant values are adopted for materials at specific temperatures. As aforementioned, Pitts and Sissom (Pitts & Sissom, 1977) and others provide a table of typical values for thermal conductivity of some common materials at 0 or 20 $°C$. Those values indicate the relative orders of magnitude to be expected in practice. Nevertheless,

the thermal conductivity is often strongly temperature dependent. Not until the 1980's, data on thermal conductivity as a function of temperature are available for many pure materials (e.g. (Kaye & Laby, 1986)), but such information for combustible solids and building materials remains fragmentary (Abrams, 1979; Harmarthy, 1995). The thermal conductivity change of some typical gases, liquids and solids including insulting materials are available in certain text books, such as the one by Holman (Holman, 1997).

EC3 (BSI, 2005a) gives the thermal conductivity of carbon steel as a function of the temperature. Table 2.3 below shows the function and the variation of the thermal conductivity with temperature is also illustrated graphically in Figure 2.5.

Table 2.3: Thermal conductivity of steel $\lambda_\alpha[W/(m \cdot K)]$ in EC3 (BSI, 2005a)

$\lambda_\alpha = 54 - 3.33 \times 10^{-2}\theta_a$	$(20°C \leq \theta_a < 800°C)$
$c_a = 27.3$	$(800°C \leq \theta_a < 1200°C)$

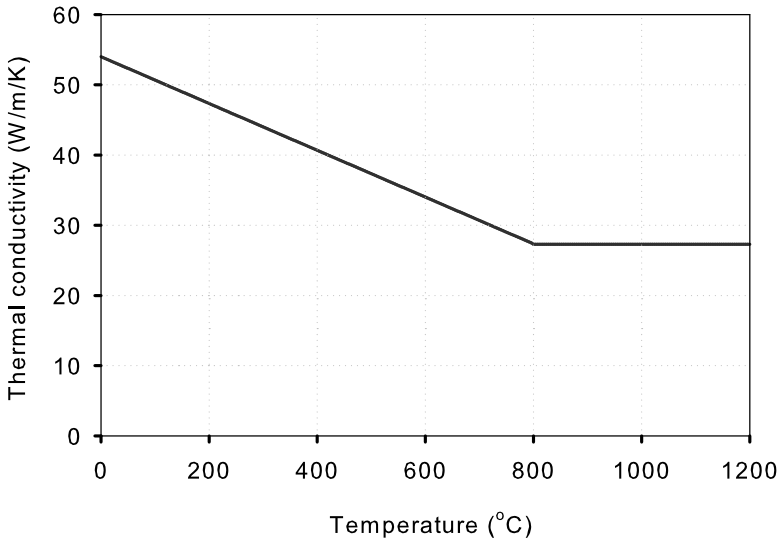

Figure 2.5: Thermal conductivity of carbon steel as a function of the temperature

Similarly, the thermal conductivity for stainless steel is available in EC3 Annex C (BSI, 2005a) and that for protection materials is assessed using the test pro-

cedures followed by the aforementioned design codes as appropriate.

2.4.3 Moisture effect

As is well known, water will evaporate if provided with sufficient heat. This process will lead to an increase in the pore pressures. Together with the gradients in temperature and mass concentration, water vapour will be forced to move through the material, hence affecting the heat transfer process. Research has found that the presence of small amounts of water can have a profound effect on the effective specific heat capacities of different materials and hence on the overall heat transfer. Similarly, thermal conductivities are also affected by moisture, with the value for moisture containing specimens being much greater than that of the dry material, even at quite low water concentrations. It is therefore essential to account for specific heat and thermal conductivity dependencies on moisture concentration, particularly in simple lumped parameter models which neglect moisture migration itself. (Welch, 2000)

Even though the specific heat and thermal conductivity properties have already been well presented as a function of temperature, most early methods made no explicit reference to moisture effects such as the method used in finite element model *FIRES-T* (Bizri *et al.*, 1974). Although the predicted temperature gradients did show a good agreement with experiment, in certain circumstances, the effect of moisture is not negligible. Other models such as that by Harada and Terai (Harada & Terai, 1988) have been proposed with the intention of explicitly accounting for moisture effects but not the mass transfer of the moisture within the material. Later on in the 1960's, a method was derived by Harmarthy (Harmarthy, 1965) for determining the fire endurance at some given moisture content. Similar methods are also available from other researchers. One of the important model is that proposed by Wickström (Wickström, 1979), known as *TASEF*, which has found fairly extensive application in prediction of the thermal response of steel and composite structures to fire. *TASEF* uses temperature-dependent conductivity and specific heat values and employs a modified enthalpy to account for the effect of moisture subjected to evaporation in concrete. Good agreement in terms of temperature has also been found by Anderberg and Forsén

(Anderberg & Haksever, 1982). Though lots of advanced models have been developed to address the moisture effect, it is rather complex, and thus, well validated empirical equations or simpler models are suggested under certain circumstances.

2.4.4 Intumescent effect

Intumescent materials are an increasingly popular form of fire protection, due to a number of advantages arising from the fact that they can be applied as thin, aesthetically pleasing, coatings either before or after construction (Bailey, 2006a; Goode, 2004; Jimenez *et al.*, 2006). Besides, intumescent coatings are with high durability, and they do not readily flake off when stuck. They are relatively quick to apply and easy to maintain. They are therefore increasingly used in particular for complex structures where normal protection materials could not be applied easily.

Intumescent coatings, when in contact with high temperatures, will swell and form a layer of carbonaceous char which has much greater thickness than the initial state. The char subsequently acts as a thermal barrier to effectively protect the substrate against increase in temperature. During the process of intumescence, the material properties are severely changed along with mass transport and endo- and exothermic reactions. These properties include thermal conductivity, specific heat, density and thickness of the intumescent layer. The effective values of those thermal properties related to the thickness change are hereafter used to describe the intumescent effects.

Typically, the standard testing of intumescent coatings is done by full-scale test, with associated extensive efforts and costs. A simpler and affordable procedure, based on calibrated models, is thus under investigation. Several research studies have been carried out to determine the effective intumescent thermal properties by differently scaled experimental tests, in conjunction with some form of numerical analysis. These include bench-scale cone calorimeter tests and small-scale furnace tests on coated plates (Bartholmai & Schartel, 2007; Bartholmai *et al.*, 2003), and furnace tests on cellular beams (Bailey, 2006b). Bartholmai and Schriever conducted studies on typical water-based and solvent-containing intumescent systems (Bartholmai *et al.*, 2003) and later on a high-performance

material, i.e., epoxy resin containing boric acid and phosphate-based flame retardant (Bartholmai & Schartel, 2007). The results from the former showed a significant slow down of temperature increase between 200 $\sim$ 300 $^{\circ}C$ due to intumescence, i.e. the formation of an insulating char and other co-acting energy absorbing processes; temperature influences during the latter tests also resolved a damping effect at 150 $^{\circ}C$ due to the endothermic reaction of boric acid, which also releases water that could take a noticeable amount of heat away from the material. The thermal properties were characterized as a single parameter called effective thermal conductivity, λ/d, which incorporates all the intumescent induced influences. In this expression, λ is the temperature-dependent thermal conductivity and d is the time-dependent intumescent thickness. The effective thermal conductivity is affected by fundamental changes in the material as it intumesces. It is found from the results that larger initial coating thickness provides lower effective thermal conductivity and vice versa. Other literature is also available to specify the expansion ratios, for example, Desanghere and Joyeux (Desanghere & Joyeux, 2005) report that an expansion ratio equals to 10 could be assumed in general, while Goode (Goode, 2004) suggests 15 $\sim$ 30. Hence, the final intumescent thickness is determined by multiplying the initial intumescent thickness with the expansion ratio for that particular intumescent material. Tests by Swedish company FSD (Fire Safety Design AB) have also determined a table of effective thermal conductivity for intumescent materials (FSD, 2002). The values are calculated as the average constant value of thermal conductivity in the range of 400 $\sim$ 800 $^{\circ}C$ corresponding to each specimen. More accurate steel temperature prediction could be obtained when the temperature has increased above 400 $^{\circ}C$. It is therefore more efficient and reliable for design purposes, where critical values are required. However, the predicted temperature is found to be underestimated at the earlier stage of heating since a constant conductivity value is adopted (FSD, 2002). A more generalised method is required for taking account of the intumescent effects on thermal properties.

2.4.5 Convection heat transfer coefficient

From the Newton's law of cooling, Equation 2.3, convective heat transfer coefficient, h, could be defined as the proportionality coefficient between the heat flux and the thermodynamic driving force for the flow of heat, i.e., the temperature

difference. It is often known to be a function of the fluid properties (thermal conductivity, density and viscosity), the flow parameters (velocity and nature of the flow) and the geometry of the surface (dimensions and angle to the flow) (Drysdale, 1999). It therefore depends strongly on conditions in the boundary layer, which are influenced by surface geometry, nature of the fluid motion and a range of fluid thermodynamic and transport properties. Due to the complexity of convection heat transfer mechanism, the related coefficient remains the largest uncertainty in calculating convective heat fluxes to structural elements. A wide range of research has been done in the literature and is presently underway. Drysdale states that typical values for convection heat transfer coefficient lie in the range $5 \sim 25\ W/(m^2 \cdot K)$ for free convection and $10 \sim 500\ W/(m^2 \cdot K)$ for forced convection in air (Drysdale, 1999). In design practice, EC1 (BSI, 2002a) adopts the values summarized in Table 2.4 below:

Table 2.4: Convection parameters

Exposure condition	Heat transfer coefficient $[W/(m^2 \cdot K)]$
Standard temperature-time curve	25
External fire curve	25
Hydrocarbon curve	50
Natural fire models - simplified fire models	35
Natural fire models - advanced fire models	35
None (unexposed face)	4

By convention, the convection heat transfer coefficient is expressed in a dimensionless form as:

$$h = \frac{Nu \cdot k}{l} = \frac{\mu \cdot c_p \cdot Nu}{d \cdot Pr} \tag{2.9}$$

where

h is the convection heat transfer coefficient, $[W/(m^2 \cdot K)]$
l is the characteristic dimension of the surface, $[m]$
k is the thermal conductivity of the fluid, $[W/(m^2 \cdot K)]$
Nu is the dimensionless Nusselt number, $[-]$
Pr is the dimensionless Prandtl number, $[-]$
c_p is the thermal capacity of air, $[J/(kg \cdot K)]$
μ is the viscosity, $[kg/(m \cdot s)]$

In literature, a value of 0.72 is suggested for Prandtl number, Pr (Jones & Whitelaw, 1982) and the viscosity μ can be evaluated from an empirical correlation using Sutherland's Law (Anderson, 1997).

The above equation could calculate either a local or average convection heat transfer coefficient when, consistently, a local or average Nusselt number is used. Thus, the determination of this coefficient purely converts as the determination of the dimensionless Nusselt number, Nu.

Literature (Holman, 1997) found that for a given geometry, the local Nusselt number Nu could be expressed as a function of spatial variable, local Reynolds number and Prandtl number:

$$Nu = f(x^*, Re, Pr) \tag{2.10}$$

where
x^* is the spatial variable, [–]
Re is the dimensionless Reynolds number, [–]

The average heat transfer coefficient is obtained by integrating over the surface of the body and is therefore independent of the spatial variable x^*. As a consequence, the average Nusselt number $\bar{N}u$ is a function of Reynolds number and Prandtl number only:

$$\bar{N}u = \frac{\bar{h} \cdot l}{k} = f(Re, Pr) \tag{2.11}$$

Many different forms of the exact expressions are discovered in the literature such as that by Rohsenow and Choi (Rohsenow & Choi, 1961), Kanury (Kanury, 1975) and Williams (Williams, 1982). They recommended a list of convective heat transfer correlations in terms of the nature of the flow and configuration of the surfaces, encompassing both forced and free convection. The table of lists is also available in the text book by Drysdale (Drysdale, 1999). Powell (Powell, 2004) summarized the Nusselt number expressions in an even more general fashion. He divided the expressions into a hierarchy as shown in Figure 2.6. Hence, three levels of decisions must be made to find the appropriate expression for Nusselt

number calculation.

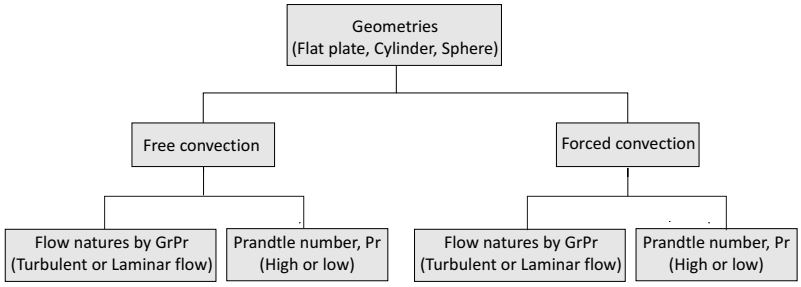

Figure 2.6: Hierarchy for choosing appropriate Nusselt number expressions

2.4.6 Emissivity

Emissivity, ε, is known as the ratio of radiation emitted by a surface to that of a black body at the same temperature. Thus, it is obvious that the emissivity for an ideal emitter (black body) ε_b equals to 1. In general term, the emissivity has spectral dependence denoted by ε_λ, where $\varepsilon_\lambda = \frac{E_\lambda}{E_{b,\lambda}}$, E_λ is the spectral emission while $E_{b,\lambda}$ is the spectral, hemispherical blackbody emissive power, given by the Planck law (Christopher, 1999; Kaviang, 2002). However, while considering only the total emissivity, which represents an average over all possible directions and wavelengths, the definition of emissivity may be expressed formally as:

$$\varepsilon = \frac{E}{E_b} \tag{2.12}$$

where
ε is the emissivity of a surface at anytime, $[-]$
E is the emission of a surface at anytime, $[W/m^2]$
E_b is the emission of the black body surface at anytime, $[W/m^2]$

Comprehensive total emissivity charts were first developed by Hottel (Hottel & Sarofim, 1967) and a comprehensive set of tables of emissivity was also produced by Touloukian and Dewitt (Touloukian & Dewitt, 1972), while modern formulations have been summarized for the emissivities, especially those of gases (Edwards & Menard, 1964; Edwards & Balakrishnan, 1972, 1973). Total emissivity charts for water vapour and carbon dioxide allow the determination based

on knowledge of partial pressure and temperature of each gas and the associated path length. Correction factors for the emissivities are provided (Smith *et al.*, 1982) for the effect of the band overlap of water vapour and carbon dioxide (Jowsey, 2006). It is important to note that emissivity ε depends on surface finish and temperate. For metals, it increases with an increase in the temperature while for non-metals, it generally decreases with temperature. Most tables available give values of emissivity for various standard surface conditions and temperature. Positively, in most engineering problems, where radiation interchange occurs between surfaces at comparable absolute temperatures, it is usually adequate to assume that the emissivity is independent of temperature and therefore wavelength. However, notable exceptions occur when thermal radiation from the sun, or from high-temperature sources such as gas flames, to surfaces at or around room temperature are considered (Drysdale, 1999).

For most structural fire problems, the emissivity properties of the combustion products and the structure are of paramount importance. Therefore, the literature of interest here is that related to the relevant fire or gas emissivity and structural member emissivity. Strictly speaking, the emissivity of fire ε_f is different from that of gas ε_g. The former considers all fire involved participating media, generally including gas and soot, while the latter specifies gaseous components only. They are equal only in idealized circumstances. However, for simplicity, mostly they are assumed to be the same in the design codes. The Society of Fire Protection Engineers (SFPE) Handbook Chapter 1 $\sim$ 4 (SFPE, 2002) and the Australian Fire Engineering Guidelines (AFEG) (ABCB, 2001) calculate the emissivity ε_g of a smoke layer based on the theory of radiation through a participating medium using:

$$\varepsilon_g = 1 - e^{-\kappa L} \tag{2.13}$$

where

κ is the gas absorption coefficient or called extinction coefficient, [–]

L is the radiation path length, which is related to the volume of smoke layer and thus in turn, to the size of the compartment, [m]

ε_g is total gas emissivity, [–]

Within the above equation, Equation 2.13, the gas absorption coefficient κ value is recommended as 0.8 by the Australian Fire Engineering Guidelines (AFEG)

(ABCB, 2001). However, it usually varies strongly with wavelength, and substantially with temperature and pressure for a real gas (Siegel & Howell, 1992). Its value would even depend on the concentrations of individual gas components for a mixture of gas. Therefore, assuming a constant value for κ is too simplistic, rendering an unrealistic evaluation for the gas properties. In most fires in structures, the pressure in the compartment can be assumed to be at 1 atm and an average wavelength at a temperature can be calculated for certain gas species. Thus, the value of the absorption coefficient κ, and hence ε_g, can be related to temperature alone for a fixed size of compartment (Wong, 2005).

In addition, the above general form could be part of the fundamentals in radiation heat transfer, however, for fire resistance design purposes, normally ε_g is treated as a constant, cf. *SFPE* (SFPE, 2002). For steel temperature prediction, an assumption is mostly made that the fire and the steel member are treated as two parallel planes in a nonradiating medium (Wong, 2005). A resultant emissivity ε_{res} therefore results, which remains constant throughout the thermal response period, and is given in Equation 2.14 below, the same as that in EC3 (BSI, 2005a):

$$\varepsilon_{res} = \frac{1}{(1/\varepsilon_f) + (1/\varepsilon_s) - 1} \approx \varepsilon_s \cdot \varepsilon_f \tag{2.14}$$

where
ε_{res} is the resultant emissivity, [–]
ε_f is the emissivity of the fire, [–]
ε_s is the emissivity of the steel member, [–]

The choice for the values of ε_f and ε_s has been under investigation by researchers for some time but no consensus has been reached. For instance, EC1 (BSI, 2002a) suggests that the emissivity of the fire is taken in general as $\varepsilon_f = 1$, and $\varepsilon_s = 0.8$ unless given in the material related fire design Parts of EC2 (BSI, 2003a) for concrete structures to EC6 (BSI, 2003b) for masonry structures, and EC9 (BSI, 2003c) for aluminium structures, giving $\varepsilon_{res} = 0.8$. In EC3 Part 1-2 Fire Design (BSI, 2005a), the emissivity related to the steel surface is specified to be 0.7 for carbon steel and equal to 0.4 for stainless steel, accordingly giving $\varepsilon_{res} = 0.7$ and $\varepsilon_{res} = 0.4$. Whereas the UK National Application Document preceding EC3 recommends $\varepsilon_f = 0.8$ and $\varepsilon_s = 0.8$, giving $\varepsilon_{res} = 0.64$ (in the full EN version of EC3, a value of 0.7 for ε_{res} is to be used.) SBI (SBI, 1976) recommends that $\varepsilon_f = 0.85$ and $\varepsilon_s = 0.8$ for most fire situations, giving $\varepsilon_{res} = 0.7$ for a steel column

fully engulfed in fire. Besides, $\varepsilon_f = 1$ is used as an conservative and appropriate assumption (Hostikka, 2003), though Hostikka has also tried to estimate the lower limit of ε_f by a computational model calculation. The set of ε_f and ε_s has sometimes been treated as adjustment factors to match experimental results rather than reflecting the true thermal properties related to the fire tests. A single values of ε_{res} surely would not fit all experimental results, also confirmed by Smith and Stirland (Smith & Stirlad, 1983). Mooney (Mooney, 1992) has also pointed out that ε_{res} is temperature-dependent and Ghojel (Ghojel, 1998) concurred. Data for ε_g can also be found from Edwards and Matavosian (Edwards & Matavosian, 1984). Recently, simple analytical expressions for the gas absorptivity and emissivity have been developed using a regression technique for design of structures in fire by Wong and Ghojel (Wong *et al.*, 1998). They found an approximate equation for ε_g under 1 atm pressure to be:

$$\varepsilon_g = 0.458 - 1.29 \times 10^{-4} T_g \tag{2.15}$$

where

T_g is the gas temperature, $[^\circ C]$

The above value developed is based on an average radiation path length $L = 3.6m$, but in reality it varies with the size of the compartment. As a consequence, a correct radiation path length L is required in practice, for a better approximation.

2.4.7 Absorptivity and reflectivity

Absorptivity, α, is often defined as the ratio of impinging radiation flux or so-called irradiation absorbed by a surface to the impinging radiation flux (Kaviang, 2002).

When radiant energy strikes a material surface, part of the radiation is reflected, part is absorbed and part is transmitted, as shown in Figure 2.7 below:

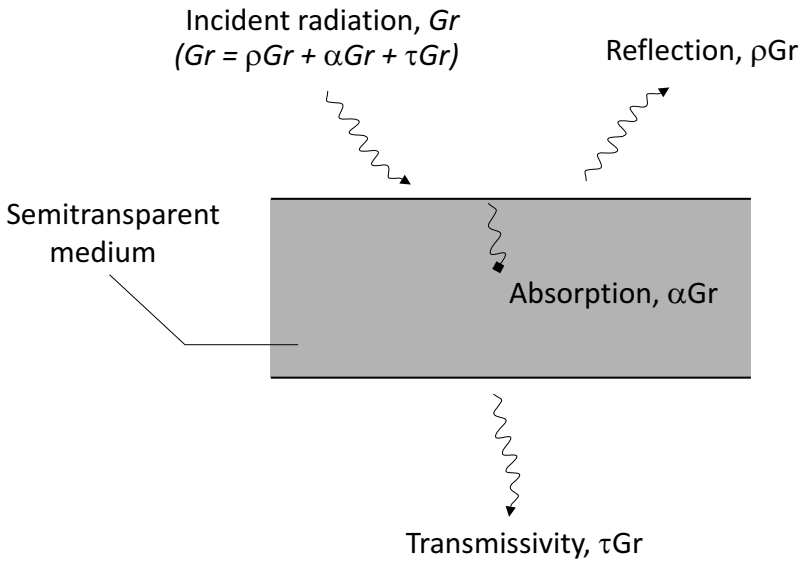

Figure 2.7: Absorption, reflection and transmission processes associated with a semitransparent medium

The fraction reflected is defined as the reflectivity ρ, the fraction absorbed as the absorptivity α and the fraction transmitted as transmissivity τ. These fractions therefore have the relation as in Equation 2.16:

$$\rho + \alpha + \tau = 1 \tag{2.16}$$

Most gases transmit thermal radiation while reflect and absorb very little. Therefore, they normally have a high value of transmissivity τ and low value of reflectivity ρ and absorptivity α. On the contrary, most solid bodies do not appreciably transmit thermal radiation, so that for many applied problems the transmissivity τ may be taken as zero. Then:

$$\rho + \alpha = 1 \tag{2.17}$$

Nevertheless, consider the case of a number of small bodies in a large enclosure, in a thermal steady state and in thermal equilibrium with each other and the enclosure. This is the case which is not unrepresentative of conditions existing in many scenarios with structures in fire compartments. Even though gases in general have a low value of absorptivity α, for this case, Kirchoff's law of radiation

applies.

$$\alpha = \varepsilon \tag{2.18}$$

Since the bodies are small, they have negligible effect on the radiative properties of the enclosure. The enclosure therefore acts as a black body, absorbing all incident radiation and emitting radiation diffusely. The incident radiation is taken as equal to the emitted radiation. (Christopher, 1999)

2.5 Thermal Analysis of structures in fire

"By definition 'Thermal Analysis' (TA) is the term applied to a group of methods and techniques in which a physical property of a substance is measured as a function of temperature, while the substance is subjected to a controlled temperature programme - Warne, S. St. J.". (Warne, 1991)

The use of thermal analysis techniques has increased rapidly in the past ten years and their field of application is widening continuously. The scope of the literature study here is limited to the thermal analysis of structures in fire. In general, the thermal analysis of heat transfer to structural members can be divided into two parts:

- The transfer of heat by convection and radiation across the boundary from a fire to a member
- The transfer of heat by conduction within a member

This analysis could be extremely complex, especially for materials that retain moisture and have a low thermal conductivity (Bailey, 2006a).

2.5.1 Thermal analysis methodologies state-of-art

Generally speaking, there are two main methods, experimental investigation and theoretical calculation (Patankar, 1978), which exist to represent the fire effects on

structures. Although the experimental investigation involving full-scale scenarios would give quite reliable information, it is more expensive and often impossible, particularly in the case of large-scale scenarios. The theoretical calculation, on the other hand, would have the advantages of low cost, high speed, ability to simulate realistic and ideal conditions, easy modification and repetition.

Within the theoretical prediction, the simplest method of defining the temperature profile through the cross-section is to use test data presented in tables or charts, which are published in codes or design guides. Malhotra (Malhotra, 1982) developed a series of graphs for estimating the steel temperature of members exposed to the standard fire exposure, based on the lumped heat capacity. This method is limited to the standard fire exposure and considers a limited knowledge of the fire protection material. Jeanes (Jeanes, 1984) created a series of temperature-time graphs of protected steel beams. Lie (Lie, 1972) presents graphical representations of the exact solutions to the governing differential equations for the temperature of protected steel members exposed to the standard fire. Similar to method of Jeanes, this method applies to American W-shape sections. It is assumed that heat transfer is one-dimensional through the insulation layer and that there is a uniform temperature throughout the steel cross-section. Although useful in some cases, the test data are generally based on standard fire conditions (BSI, 1999, 2001).

Other methods then appear with the capability to deal with the case when structures under a design fire which incorporates different growth, maximum temperature and decay characteristics with respect to the standard fire temperature-time curve. They are often based on the energy balance of the structural element exposed to convective and radiative heat fluxes from the fire.

An empirical calculation method to estimate the temperature response of unprotected and protected steel is presented in EC3 (BSI, 2005a). The method is based on a lumped mass model, in which it is assumed that the temperature is uniform within the cross-section.

For *unprotected* steelwork, the increase of temperature $\Delta\theta_{a,t}$ of the steel member during a time interval Δt is determined from (BSI, 2005a):

$$\Delta\theta_{a,t} = k_{sh}\frac{A_m/V}{c_a\rho_a}\dot{h}_{net}\Delta t \tag{2.19}$$

where

k_{sh}	is correction factor for the shadow effect, $[-]$
A_m/V	is the section factor for unprotected steel members, $[1/m]$
A_m	is the surface area of the member per unit length, $[m^2/m]$
V	is the volume of the member per unit length, $[m^3/m]$
c_a	is the specific heat of steel, $[J/(kg \cdot K)]$
$\dot{h}_{net}$	is the design value of the net heat flux per unit area, $[W/m^2]$
Δt	is the time interval, $[seconds]$
ρ_a	is the unit mass of steel, $[kg/m^3]$

For the *protected* steelwork, the increase of temperature $\Delta\theta_{a,t}$ of the steel member during a time interval Δt is determined from (BSI, 2005a):

$$\Delta\theta_{a,t} = \frac{\lambda_p A_p/V}{d_p c_a \rho_a}\frac{(\theta_{g,t}-\theta_{a,t})}{(1+\phi/3)}\Delta t - (e^{\phi/10}-1)\cdot\Delta\theta_{g,t} \tag{2.20}$$

with:

$$\phi = \frac{c_p\rho_p}{c_a\rho_a}d_p A_p/V$$

where

A_p/V is the section factor for steel members insulated by fire protection material, $[1/m]$
A_p is the appropriate area of fire protection material per unit length of the member, $[m^2/m]$
V is the volume of the member per unit length, $[m^3/m]$
P is the perimeter of the member per unit length, $[m/m]$
c_a is the temperature dependant specific heat of steel, $[J/(kg \cdot K)]$
c_p is the temperature dependant specific heat of the fire protection material, $[J/(kg \cdot K)]$
d_p is the thickness of the fire protection material, $[m]$
Δt is the time interval, $[seconds]$
$\theta_{a,t}$ is the steel temperature at time t, $[°C]$
$\theta_{g,t}$ is the ambient gas temperature at time t, $[°C]$
$\Delta\theta_{g,t}$ is the increase of the ambient gas temperature during the time interval Δt, $[K]$
λ_p is the thermal conductivity of the fire protection system, $[W/(m \cdot K)]$
ρ_a is the unit mass of steel, $[kg/m^3]$
ρ_p is the unit mass of the fire protection material, $[kg/m^3]$

As with all empirical equations, the above calculation method requires only simple hand calculations and consequently has great flexibility and simple implementation. Nevertheless, it should be applied to situations that are similar to the tests used to derive the equation, and can not be used for intumescent coatings. A sensitivity study carried out by Wong and Ghojel (Wong & Ghojel, 2003) also indicates that the method has limited use for insulation with relatively high density and high conductivity, though debates are ongoing.

A Eurocode-based extended model has been proposed but with better defined parameters (Ghojel, 1998; Wong & Ghojel, 2005). This heat transfer model for structural steel is based on temperature-dependent gas properties evaluated using the method given by Edwards and Matavosian (Edwards & Matavosian, 1984). It is determined from the following energy balance equation:

$$q_r + q_c = \frac{c_s V_s \rho_s}{A_s}\frac{dT}{dt} = \frac{c_s \rho_s}{(P/A_s)}\frac{dT}{dt} \tag{2.21}$$

with:

$$q_r = \varepsilon_g \cdot \sigma \cdot T_g^4 - \alpha_g \cdot \sigma \cdot T_s^4$$

$$q_c = h_c(T_g - T_s)$$

where

- q_r is the radiative heat flux per unit area, $[W/m^2]$
- q_c is the convective heat flux per unit area, $[W/m^2]$
- c_s is the specific heat of steel and is assumed to be vary with steel temperature as $c_s = 3.8 \times 10^{-7} T_s^2 - 2 \times 10^{-4} T_s + 0.472$, $[J/(kg \cdot K)]$
- V_s is the volume of the member per unit length, $[m^3/m]$
- ρ_s is the unit mass of steel, $[kg/m^3]$
- A_s is the surface area of the member per unit length, $[m^2/m]$
- h_c is the convective heat transfer coefficient, $[W/(m^2 \cdot K)]$
- ε_g is the total gas emissivity at temperature T_g over the mean beam length of the enclosure, $[-]$, and the mean beam length is the characteristic dimension of the thickness of the gas-layer transmitting energy and is taken equal to $L_c = 3.6V_g/A_s$
- α_g is the total gas absorptivity for radiation from a black surface at temperature T_s absorbed over the mean beam length by a gas at temperature T_g, $[-]$
- σ is the Stefan-Boltzmann constant, $\sigma = 5.67 \times 10^{-8}$, $[W/(m^2 \cdot K^4)]$

Note that within the above model, the convective heat transfer coefficient is assumed to change linearly from zero at the start of combustion to a maximum value when the temperature of the gases and the steel element become equal, and remain constant afterwards, as expressed below:

$$\begin{cases} h_c = \frac{50}{t_{g=s}} \cdot t \quad [W/(m^2 \cdot K)], & t \leq t_{g=s} \\ h_c = 10 \quad [W/(m^2 \cdot K)], & t > t_{g=s} \end{cases} \tag{2.22}$$

This model can be used for all types of fires in enclosures with known temperature-time histories and good results are yielded compared to the example tests. Another advantage is that this is a simple model but accounts for real gas behaviour and does not require long computational times. However, it is only valid on the basis of several assumptions, for instance, the temperature variations are confined to a thin boundary layer close to the enclosure inner wall, and uniform steel temperature is assumed throughout the cross-section. More assumptions are described in the paper produced by Ghojel (Ghojel, 1998). These assumptions limit

the application of this modelling methodology.

Based on the same differential equations for heat transfer by Wickström (Wickström, 1985) as that of the Eurocode design method for unprotected steelwork, Melinek and Thomas (Melinek & Thomas, 1987) demonstrate an alternative exact solution using Laplace Transformation. This empirical method could give better estimations, especially for insulation with high density and high conductivity, but it is quite complex to evaluate the parameters related to the thermal resistance of the insulation.

Due to the limitations of the empirical methodologies, and the non-linear transient nature of the unsteady heat transfer problem in the real world, advanced performance based methodologies are required for heat transfer analysis, when parametric curves, zone models or CFD models are used (Bailey, 2006a). Those advanced methodologies are either based on Finite Difference Methods (FDM), Finite Volume Methods (FVM) or Finite Element Methods (FEM) as mentioned in the conjugate heat transfer analysis methodology section. Although FDM and FEM can be applied in 1, 2 or 3 dimensions and, within the limitations of the input parameters, provide a completely general solution to the transient heat conduction problem (Harmarthy, 1993), a number of sensitivity checks need to be made for each calculation in order to determine that the solution is sufficiently independent of numerical parameters (e.g. grid resolution and length of the numerical time step) (Welch, 2004). In addition, the major uncertainties in the use of these methods relate to the description of surface heat transfer, such as the convective heat transfer coefficient and the surface emissivities, and to the temperature dependent material properties, particularly when moisture is present or intumescent protection material is used, which are often approximately represented, typically leading to conservative predictions. For a more accurate or detailed prediction, full 3D analysis, with more exact representations of material properties, is normally required, however, it would be more computationally demanding in terms of setup and run-time. In addition, difficulties arise to transfer data from fire model to thermal model in a seamless and efficient manner. Moreover, in many cases, the essential part of the heat transfer is essentially 1D in nature, and there may be no need for full 3D analysis. Rubini (Rubini, 1996) mentioned that the FVM may be considered as a hybrid, lying between classical FDM and FEM. From a finite difference perspective, FVM may be considered as

an integral technique applied to the conservative forms of the governing partial equations. From a finite element perspective, FVM may be considered as a special case of the method of weighted residuals, in which the weighting function is chosen to be unity over a control volume and zero everywhere else. The FVM offers a number of attractions in comparison to both the FDM and FEM. As a consequence of the integration over a volume, the method guarantees that the basic quantities of mass, momentum and energy will remain conserved in the discrete algebraic representation of the equations. Secondly the integral approach provides a more intuitive association between the physical processes occurring across the bounding surfaces of a volume and the governing partial differential equations (Rubini, 1996). Therefore, the research of interest here is the FVM.

With the development of both fire behaviour prediction methods and heat transfer analysis methods, the research on the interface between the two has been paid more attention, since there are great potential to improve the flexibility, generalization and computational demands of the structure performance prediction methodologies in fire, with the effective link between the two. The traditional simplified methodologies are uncoupled, obtaining the structure temperature results directly from input fire conditions at each time step, such as EC3. Normally, a simple assumption of the thermal boundary conditions is made, such as structural surface temperature is equivalent to the gas temperature or a constant value is assumed for the convective heat transfer coefficient. The prediction is quite general and conservative as explained previously for EC3 methodology. Commercial programs are also available using the uncoupled method, including *VULCAN* (widely used in Buro Happold and University of Sheffield) or *ABAQUS* (used in Arup). Although they could provide general structure-fire modelling, they are quite complex to use in terms of fire application and expensive. Other uncoupled methodologies use either submodel techniques (e.g. *SOFIE* conjugate thermal model used in BRE or *ANSYS* used in Buro Happold) or embedded grid approach (e.g. *STELA* model used in BRE). The former uses the thermal analysis model as a submodel for the fire model, which requires the numerical grid for the structural component to be consistent with the fire grid, resulting in great computational demands for detailed structural analysis. The latter allows the independent mesh between the structure grid and the fire grid. This is quite useful when complex structure is considered; high resolution grid could be generated without increasing the fire grid numbers. However, the so-called small cell

problem would be associated with this methodology. Near the embedded boundary, the grid cells may be orders of magnitude smaller than regular Cartesian grid cells in the gas phase. Since standard explicit finite volume methods take the time step to be proportional to the size of a grid cell, this would typically require small time steps near an embedded boundary. Nowadays, research to develop a numerical method that overcomes the time step restriction, while seeking an appropriate justification near the solid-fluid interface as well as in the whole domain is widely spread, using coupling techniques. Several approaches have been proposed either commercially or academically. Those approaches could be categorized as two main strategies: one-way coupling and two-way coupling. In the one-way coupling, the fire development is calculated entirely independent of the thermal response, based on pre-defined boundary conditions, using CFD methodology. From the fire model, certain time and space varying information, such as gas temperature, convective flow characteristics and radiation heat flux are then transferred to the thermal response model. Interpolation of these data between the different temporal and spatial scales used by the models is required. Thereafter, the thermal response model, using either CFD or FEM, calculates the temperature distribution in the structural elements on the basis of the interpolated output of the fire development model. Because the thermal response of the structure is not directly represented in the fire simulation, the structural components may optionally be completely omitted from the fire model, thus providing great flexibility (Welch *et al.*, 2008). Currently, the following codes are implemented and explored as one-way coupling within the *FIRESTRUC* project (Welch *et al.*, 2008): *JASMINE-SAFIR*, *SOFIE-SAFIR*, *VESTA-SAFIR*, *FDS-ANSYS* and *JASMINE-STELAb*. In Arup, *FDS* is normally used as the fire prediction model and thermal model, while FEM *ABAQUS* is used for structural fire modelling. Recently, a fire post-processing model is developed to generalize the heat fluxes imposed on all surfaces by a fire and thus properly characterize the thermal boundary conditions. In this modelling methodology, the heat fluxes are defined at all points on the structure by considering full spatial and temporal distribution. It has been implemented into *FDS* and *ABAQUS* codes (Jowsey, 2006). Also at NIST, a Fire Structure Interface (FSI) methodology has been developed to calculated the coupled heat transfer problem. It makes use of a mixture of analytical and computational techniques to cope with the widely disparity of length and time scales that control the physical processes simulated in FDS and whatever structural analysis code is chosen for use (Baum, 2005). In the

two-way coupling, the surface temperature of the structure is calculated taking the in-depth heat penetration into account, using one or more thermal response models, and transferred back to the fire development model. *VESTA-DIANA* and *JASMINE-STELA* are examples of the two-way coupling. This method needs to be considered only when there is a more significant interaction of fire and structure, or when more accurate analysis is required and greater computational costs can be sustained. Mostly, one-way coupling would be sufficient (Welch *et al.*, 2008).

Based upon the pros and cons of fire prediction models mentioned before in the section on fire behaviour, the current and future mainstream for the fire prediction is likely to be methodologies based on CFD modelling. Hence, for the thermal analysis, it would also rely on theoretical calculation by using computational numerical modelling methodologies, especially CFD models.

In this work, the *SOFIE* (Simulation of Fires in Enclosures) CFD code has been exploited. The reasons to explore *SOFIE* CFD code is firstly, it is a RANS code which is computationally more reasonable than DNS or LES code. DNS code requires grid resolution to be as fine as the Kolmogorov microscale, and it is impossible for current computing resources to solve such detailed fire flows at any practical scale (Jowsey, 2006). LES codes always require 3D, and must have a time-step short enough to capture most of the important turbulent motion. It is therefore computationally more expensive than RANS code. Another reason is that it is possible to select the time steps for performing the radiation calculation, an advantage compared with other code such as *FDS*, providing more flexibility.

The background of *SOFIE* is that it is an advanced CFD code written at Cranfield University (Rubini, 1997), used for simulation of the overall fire and structure behaviour, including prediction of the heating regime and the thermal response of the steel (Welch & Ptchelintsev, 1997). It employs a finite volume pressure correction procedure to solve the governing density weighted Navier-Stokes equations (Abbott & Basco, 1989) in a general curvilinear coordinate system. The standard $k-\varepsilon$ turbulence model is employed with buoyancy modifications. Combustion is accounted for by assuming that the rate of heat release is limited by turbulent mixing of the fuel and oxidant, as modelled by an eddy breakup combustion model, or using flamelet models. The enthalpy source term includes the

net energy absorbed or emitted by radiation and the rate of heat release determined by the combustion model. (Welch & Rubini, 1997)

Two representative heat transfer models within the *SOFIE* CFD code, i.e. the default *SOFIE* conjugate thermal model and the embedded mesh *STELA* model, have been studied with regards to the BRI beam test (Kumar *et al.*, 2005) to examine the thermal response.

1) SOFIE conjugate thermal model
This is a 3D thermal model using conjugate heat transfer at solid-fluid interface, based on a structured grid which must be consistent with CFD grid, that is to say, the same numerical grid is required in the solid as that in the gas phase.

2) STELA 3D model
STELA model is a 3D finite-volume model, integrated into the *SOFIE* (and *JASMINE*) CFD code, for calculating the thermal response of structural elements to fire gases. The code was developed by BRE/FRS for predicting the thermal response of structural elements (i.e., beams or columns) when exposed to fire conditions in an attempt to overcome some of the grid resolution problems of the conventional model. The solver is integrated into the FRS CFD codes to provide a means for running a simultaneous simulation of the gas and solid phase behaviour under fire conditions. The main application envisaged is for protected and composite members, where the thermal behaviour is hard to predict using simpler models. The temperature development of such components in fire conditions is highly sensitive to the non-linear thermal properties of the constituent materials. In particular, the effects of moisture and intumescence are often very significant and these are accommodated in the model. (BRE, 2003)

STELA model is similar to the *SOFIE* conjugate thermal model; the difference is the *STELA* model uses an independent high resolution grid in component, which could allow finer grid for structural elements. However, the accuracy is still limited by the resolution of the boundary, i.e. the size of the interface cells in the plane of the solid surface.

In this simulation case, there are 2 cells across the flange width and each cell size is $3mm$ when the *SOFIE* conjugate thermal model is used; while in the *STELA*

model, there are around 6 cells across the flange width and $1mm$ per cell. The cell numbers used in the *STELA* model are three times more than *SOFIE* conjugate thermal model in each direction. Overall, as a 3D calculation code, *STELA* would need $3 \times 3 \times 3 = 27$ times more cells than other model.

Figure 2.8 below compares steel temperature against location for the BRI beam test and the two computer modelling prediction results.

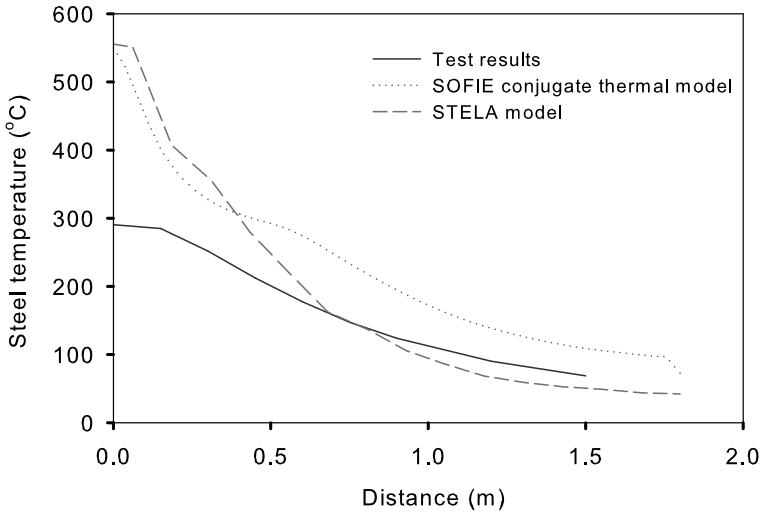

Figure 2.8: BRI beam test results comparison with different methods at 600s

By analysis of the results, it can be seen that the results from the numerical analysis are qualitatively consistent with the experimental results, which demonstrates the potential of CFD method for the thermal behaviour simulation of structures in natural fires. However, the numerical models are not perfect, and it can be seen that an error arises towards the middle of the beam. The prediction results are higher than the experimental results, which might be partly due to the over-prediction of gas-phase temperatures and partly due to the neglect of the axial conduction. Besides, to resolve solid phase heat transfer, if it is solved by means of the conjugate heat transfer treatment, such as the *SOFIE* conjugate thermal model, sufficiently small cells are needed. As a result, there are inevitably severe limitations due to restrictions on cell size when a structured grid is used. Though in the *STELA* 3D model, small cells are provided, they are still limited by the CFD cell size at the interface. The fine grid into the solid may result in great

computational demands in terms of time and memory and may often be impractical for real projects, especially for large-scale equipment. Moreover, in each simulation, both models give only one result, as fixed set of parameters such as the member position and geometry as well as the protection material properties.

2.5.2 Necessity for further research

On the base of the literature survey, it is found that the existing methodologies in general have the following limitations irrespective of the accuracy of prediction.

- Limited to one specific component of interest
- Computationally demanding with problems of resolving component in gas phase and fine grid size needed in solid phase

Therefore, development of a novel but practical methodology that would bypass the limitations of existing methodologies and provide possible advantages in terms of generalisation of the results is highly desirable.

Chapter 3

Methodology

3.1 Introduction

When protected steelwork is exposed to fire, heat is transferred to the structure through a layer of insulation. The transient heating response of the member can in principle be described using conventional methods based on numerical heat transfer. However, full 3D analysis impose great computational demands, due to the large numbers of cells required in order to adequately resolve the steep thermal gradients during the initial heating. Even if the computational resource is available, in simple deterministic models there is no direct mechanism to accommodate uncertainties in the thermal properties and member specification. To overcome these problems, with an appropriate balance between accuracy and tractability, a novel quasi-3D analysis methodology has been developed, known as *GeniSTELA* (Generalised Solid ThErmaL Analysis). This is achieved by constructing a generalised 1D model and further considering the 2D or 3D effects within the heat transfer processes by appropriate approximations and corrections. The computations are performed in each gas-phase CFD cell in the computational domain. The heat transfer within the structure and CFD calculation are solved separately and then coupled together by exchanging data, such as temperatures and velocities at their mutual boundaries at the end of the time step. In this novel methodology, the CFD results are provided from *SOFIE* CFD code and then supplied as boundary conditions for quasi-3D heat transfer calculation. The CFD results could also be provided from other CFD codes, such as *FDS, CFX, JASMINE*, but *SOFIE* is used here due to its flexibility for radiation calculation. For generalisation and accuracy, heat transfer submodels are also implemented

within *GeniSTELA* to treat the important factors which might have great impact on the transient thermal response, such as the convection coefficient and material thermal properties. The details of the model development are described in this chapter.

3.2 Generalised 1D model

3.2.1 1D model governing equations

The generalised 1D model is constructed through analysing the heat transfer to and within an element in an idealised protected steel member assumed to be exposed to heat on two faces, as shown in Figure 3.1 below:

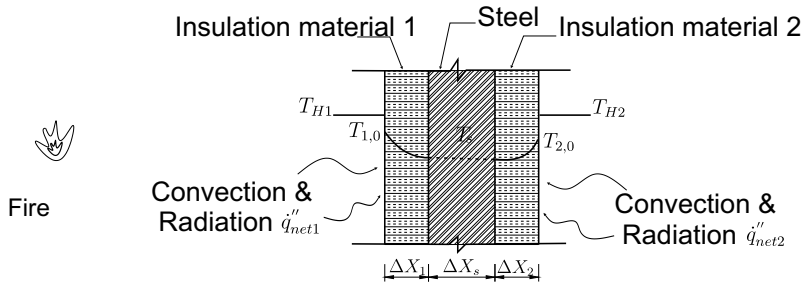

Figure 3.1: Schematic of heat transfer to protected steel member

This element is supposed to be representative of a slice of a protected steel structure, e.g. a finite section of a flange or a web; two faces are used to allow for situations where the exposure conditions on each side might vary, encompassing also the case of hollow sections with very different exposures on the inside of the structure, though in that case the insulation thickness on the inside is reduced to zero. This element is applicable for most steel sections widely used in the building industry, with specified boundary conditions. Table 3.1 below lists a few steel sections and specifies boundary conditions for each of them.

Table 3.1: General steel sections

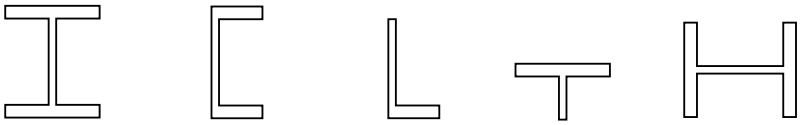

This is the same as the representative element, with no modifications of the boundary conditions.

Heating comes from only the external surface of the element, adiabatic condition is assumed for the inner surface, and the modified boundary conditions are: $T_{H2} = 0$, $T_{2,0} = 0$ and $\Delta x_2 = 0$.

The generalised 1D model provides a modelling framework which exploits a simple thermal penetration model for the protection coupled to an essentially lumped parameter representation of the steel heating. The governing equations for this model are derived by considering the net energy balance together with surface heat transfer boundary conditions (Carslaw & Jaeger, 1959), as given below:

Energy balance equation:

$$\frac{\partial E_{system}}{\partial t} = \dot{q}''_{net} \tag{3.1}$$

i.e. $\rho_s \cdot c_s \cdot \frac{\partial T_s}{\partial t} \cdot \Delta x_s + w_{p1} \cdot \rho_1 \cdot c_{p1} \cdot \frac{\partial T_1}{\partial t} \cdot \Delta x_1 + w_{p2} \cdot \rho_2 \cdot c_{p2} \cdot \frac{\partial T_2}{\partial t} \cdot \Delta x_2 =$
$h_{c1} \cdot (T_{H1} - T_{1,0}) + \dot{q}''_{r1} - \varepsilon_{m1} \cdot \sigma \cdot T_{1,0}^4 + h_{c2} \cdot (T_{H2} - T_{2,0}) + \dot{q}''_{r2} - \varepsilon_{m2} \cdot \sigma \cdot T_{2,0}^4$

The terms shown in the expanded equation here represent, respectively, the transient heating of the steel and protection layer on each side, and the convection, radiation and re-radiation for each surface of the protected member. A semi-empirical treatment is adopted for transient heating, allowing for spatially- and temporally-varying temperature gradients within the solid. The boundary conditions are supplied from the heat transfer solution for the surfaces, using the

following equations:

$$\dot{q}''_{net1} = \frac{k_1}{w_{p1} \cdot \Delta x_1} \cdot (T_{1,0} - T_s) \tag{3.2}$$

i.e. $$h_{c1} \cdot (T_{H1} - T_{1,0}) + \dot{q}''_{r1} - \varepsilon_{m1} \cdot \sigma \cdot T^4_{1,0} = \frac{k_1}{w_{p1} \cdot \Delta x_1} \cdot (T_{1,0} - T_s)$$

$$\dot{q}''_{net2} = \frac{k_2}{w_{p2} \cdot \Delta x_2} \cdot (T_{2,0} - T_s) \tag{3.3}$$

i.e. $$h_{c2} \cdot (T_{H2} - T_{2,0}) + \dot{q}''_{r2} - \varepsilon_{m2} \cdot \sigma \cdot T^4_{2,0} = \frac{k_2}{w_{p2} \cdot \Delta x_2} \cdot (T_{2,0} - T_s)$$

For the purpose of accounting for the transient energy storage in the protection layer, the influence of the change of steel temperature on the protection layer temperatures is included only indirectly, referencing the rate of change on the previous time step.

Moreover, the thermal properties of protection materials are critical to the transient response, and hence have been treated in a generalised and reliable fashion within *GeniSTELA*. The framework for incorporating temperature/time-dependent characteristics, including moisture and intumescence effects are described later on in the material properties section.

3.2.2 Variables

Weight factors

Within the above governing equations, the weight factors, w_{p1},w_{p2}, are defined in terms of the thermal penetration depth of the protection, given in the form of Equation 3.4, detailed derivation is presented in **Appendix A**:

$$w_{p1} = \min\{\frac{\delta_1}{\Delta x_{p1}}, 1\}, w_{p2} = \min\{\frac{\delta_2}{\Delta x_{p2}}, 1\} \tag{3.4}$$

with:

$$\delta_1 = 2 \cdot \left(\frac{k_1 \cdot t}{c_{p1} \cdot \rho_1}\right)^{1/2}, \delta_2 = 2 \cdot \left(\frac{k_2 \cdot t}{c_{p2} \cdot \rho_2}\right)^{1/2}$$

where

w_{p1}, w_{p2}	are the weight factors for protection on each side, respectively, [–]
δ_1, δ_2	are the thermal penetration depth for protection on each side, respectively, $[m]$

Convection coefficient

The convective heat transfer coefficients, h_{c1}, h_{c2}, are treated generally as a function of Nusselt number, Nu, with consideration of a series of influencing factors such as convection types, component geometries, and velocity sizes. Though it is known from literature that for materials with low density and high thermal resistance, i.e. low thermal conductivity, the accuracy in evaluating the values of the heat transfer coefficient has little effect on the final steel temperature prediction (Wong & Ghojel, 2003), in general, the convective heat transfer calculated by CFD is highly sensitive to the numerical methods and turbulence models employed in CFD (Zhai & Chen, 2004), in particular in the low temperature regime. Therefore, it is crucial to adopt a general form for the convective heat transfer coefficient rather than an approximate empirical fit, i.e. a constant value.

Since *GeniSTELA* is not explicitly modelling the flow over the member, the convective heat transfer coefficient is estimated from correlations in the literature for Nusselt number, giving an average value of $h = k \cdot \frac{Nu}{L}$, where, L is the characteristic length-scale; k can be obtained from the Prandtl number, i.e. $= mu \cdot \frac{c_p}{k}$; thus,$h = mu \cdot c_p \cdot \frac{Nu}{(L \cdot Pr)}$ Within this formula, value of viscosity mu is obtained from an empirical correlation according to the Sutherland's law which makes it a function of temperature (Anderson, 1997). The determination of the Nusselt number Nu is rather complex. Study of a wide range of literature has been carried out during the research and a list of Nusselt number Nu expressions has been compiled according to the following classification procedures, as also demonstrated previously in Figure 2.6:

- Identify the mechanism that drives the flow, where three possibilities are considered, i.e. forced convection, natural convection and mixed convection
- Inspect the surface geometry, in which the most commonly used geometries are flat plate, cylinder and sphere, others also include tube bank, annulus, duct, hexagon etc.

- If the flow driving force has been identified as natural convection, the surface's orientation with respect to gravity is specified as horizontal, vertical or inclined
- If the flow driving force has been identified as forced convection, the flow direction is specified as parallel to axis, normal to axis or oblique to axis

The above classification procedure not only determines the approach for the Nusselt number Nu calculation, but also affects the characteristic length L that is used for convective coefficient calculation. For example, for a cylinder oriented normal to a flow that is driven by forced convection, the characteristic length L equals the length of that cylinder, while for a horizontal cylinder driven by natural convection, characteristic length L equals half of the cylinder perimeter, i.e. $L = \pi \cdot D/2$.

For simplicity but also covering frequent and practical usage, *GeniSTELA* has finalised and implemented a Nusselt number Nu for flat plate calculations as provided in Table 3.2 below. The selection of either vertical or horizontal direction is decided in the code at present. 'SensVari.txt' file would be another option for future improvement.

Table 3.2: Calculations for Nusselt number, Nu of flat plate in *GeniSTELA*

free convection	Vertical	$Nu = 0.638 \cdot Gr^{0.25} \cdot Pr^{0.5} \cdot (0.861 + Pr)^{0.25}$	(a)
	Horizontal	$Nu = (\frac{0.825+0.387 \cdot Ra^{(1/6)}}{(1+(0.492/Pr)^{(9/16)})^{(4/9)}})^{2.0}$	(b)
forced convection	Laminar	$Nu = 0.664 \cdot Re^{0.5} \cdot Pr^{(1/3)}$	(c)
	Turbulent	$Nu = 0.228 \cdot Re^{0.731} \cdot Pr^{(1/3)}$	(d)

3.3 Quasi-3D model

In the context of *GeniSTELA*, use of a fundamentally 1D treatment is essential, considering the costs of doing a full 3D analysis in every computational cell and including a sufficient number of parametric variations. However, adoption of a simple 1D model for thermal analysis could clearly lead to some modelling inaccuracies. These could in principle be in either direction, resulting in either conservative (over-design) or non-conservative (unsafe) results. The former aspect is not a major concern since the method is in any case far more flexible than

other simple models, and by using generalised treatments conservatism is already greatly reduced. The latter aspect is a more obvious problem, and in order to overcome it, methods for treating important 2D and 3D effects are needed. A number of corrections factors have been implemented in the model, encompassing the phenomena indicated in Figure 3.2(b). Specific corrections are made for the "junction effect", "end effect", "heat sink effect" and "axial temperature gradient effect", for which the precise nature of localised heating is important. The significance of these corrections can also be found by comparison with the simulation results from other models, e.g. those of *STELA*, cf. Figure 3.2(a).

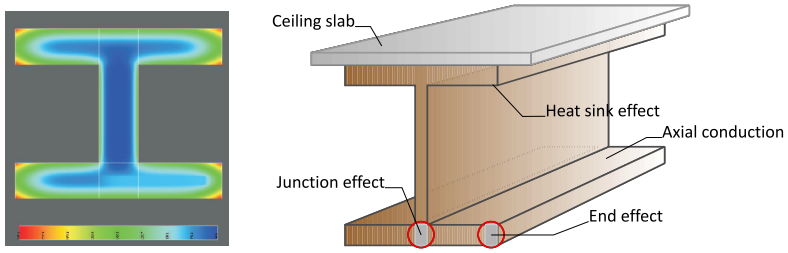

(a) Temperature profile from STELA (b) 3D corrections

Figure 3.2: Cross-section of the beam with locations of possible correction effects

3.3.1 Junction effects

This correction accounts for the effects of the connection between two different parts of a member under differential heating, e.g. when the main exposure is from below a flange or directly onto the web. In the case where the dominant heating comes from below a flange, for cells in the region of the junction between flange and web, a possible heat sink effect to the cooler structure above the junction needs to be considered. This caters both for the case where the web is cooler, due to having no direct exposure to the dominant radiative heating, and thus some heat would possibly be lost into the web by conduction, and the case where the upper flange of the member is attached to a ceiling slab remaining cool. The effect in depressing the flange temperature can be accommodated in the quasi-3D conceptual model by including an additional term, on the right-hand side of the 1D model governing equation, Equation 3.1. This additional term is expressed as Equation 3.5 and it equals the net heat flux/energy by junction effect $\dot{q}_{rad,junct}$.

$$- k_s \cdot \left(\frac{T_s - T_{web}}{\chi} \right) \tag{3.5}$$

where

T_{web} is the independently evaluated web temperature, equals the steel temperature without junction effect, $[K]$

T_s is the steel temperature considering junction effects, $[K]$

k_s is the thermal conductivity, $[W/(m \cdot K)]$

χ is an appropriate length scale which is a function of the section geometry (section breadth and depth, and flange and web thicknesses), as expressed as $\chi = 4wf/(2fd + wb)$. Here, f is the flange thickness, $w = t_{web}$ is the web thickness, $d = d_{web}$ is the web depth, $b = b_{flange}$ is the flange width. The detailed derivation of the term is described within **Appendix B**.

Therefore, the steel temperature difference between the one with and without the junction effect correction is $\Delta T_{s,junct} = T_s - T_{web} = -\frac{\dot{q}_{rad,junct} \cdot \chi}{k_s}$. In order to reduce the additional computational cost caused by solving the modified governing equation, the junction effect for steel temperature is treated simply by adding the difference $\Delta T_{s,junct}$ term on the basis of the uncorrected steel temperature $T_{s,avg}$, as expressed below:

$$T_{s,junct} = T_{s,avg} + \Delta T_{s,junct} = T_{s,avg} - \frac{\dot{q}_{rad,junct} \cdot \chi}{k_s} \tag{3.6}$$

In this expression, $\dot{q}_{rad,junct}$ is the net heat flux caused by the junction effect. It is established as follows and the detailed derivation procedure is described together with the aforementioned length scale in **Appendix B**:

$$\dot{q}_{rad,junct} = \left(\frac{k_s \cdot t_{web}}{b_{flange} \cdot d_{web}}\right) \cdot (T_s - T_{ambient}) \cdot \left(1 - \frac{h_c \cdot d_{web}}{k_s}\right) + \frac{t_{web}}{b_{flange}} \cdot \varepsilon_m \cdot \sigma \cdot (T_{ambient}^4 - T_s^4) \tag{3.7}$$

where

k_s is the thermal conductivity, $[W/(m \cdot K)]$

t_{web} is the web thickness, $[m]$

d_{web} is the web depth, $[m]$

b_{flange} is the flange width, $[m]$

T_s is the steel temperature considering junction effects, $[K]$

$T_{ambient}$ is the ambient temperature, $[K]$

When the dominant heating comes directly onto the web, a reverse of the above analysis can be conducted to determine the heat sink into an unexposed flange. It should be noted that in both cases, the effect of the redistribution of heat by conduction serves only to reduce the predicted peak member temperatures, meaning that the initial uncorrected 1D model predictions are expected to be on the conservative side.

3.3.2 End effects

Along the length of the flange, the steel temperature changes, especially for the cells in the two ends of the flange, which might be a worst case position for temperature by virtue of the fact that they are exposed to heat arriving from two different directions, i.e. their heated surface is larger. The heating might be expected to be relatively uniform when convection is dominant and a simple correction referencing the true flange surface area can be used. A more complex case results when the radiative heat flux dominates; if the radiation arrives mainly from below, then the end cell behaves no differently from any other flange cell, or may even be cooler due to the extra surface area for heat loss; if the radiation arrives only from the side, then conductive loss to the unexposed material elsewhere in the flange means that the end cell temperature will be depressed, and probably lower than a typical web cell temperature in the same member. At intermediate conditions, the temperature in the end cell, T_s^+, is perturbed and needs carefully consideration; a possible approximate treatment is given below:

$$T_s^+ = T_{s,avg} + \frac{\Delta T_s}{2} \tag{3.8}$$

Where, $T_{s,avg}$ is the average steel temperature along the flange length, which is equal to the middle point temperature, obtained from the original solution for governing equation, Equation 3.1, or as per solution Equation (c) in Table 3.4 in the next section where detailed solutions are explained. And ΔT_s is the temperature difference between the flange end-point and the mid-point, by considering the effects of radiation from the side: $\Delta T_s = \frac{b \cdot \dot{q}_{rad,side}}{k}$, where b is flange width. In theory, this correction is sufficient for the end effect correction. However, it is found to be rather difficult to determine $\dot{q}_{rad,side}$ since the heat flux intensity,

$\dot{q}_{rad}$ could not be simply adopted to represent $\dot{q}_{rad,side}$. It is actually the net heat flux considering both heat flux intensity and re-radiation. The determination of re-radiation would couple back to the unknown end cell temperature T_s^+, resulting in difficulty in solving the problem.

Another more realistic scaled correction regards to the local cell correction is proposed and finally adopted into *GeniSTELA*. To start with, a unidirectional heat flux problem is considered, as seen in Figure 3.3 below, which could be categorized as 1D heat transfer problem. The local steel temperature correction is the same as that in 1D model, $\Delta T_{s1} = \Delta T_s = \frac{(K_1+K_2)}{2}$, whose derivation procedure is explained in detail in the solution section.

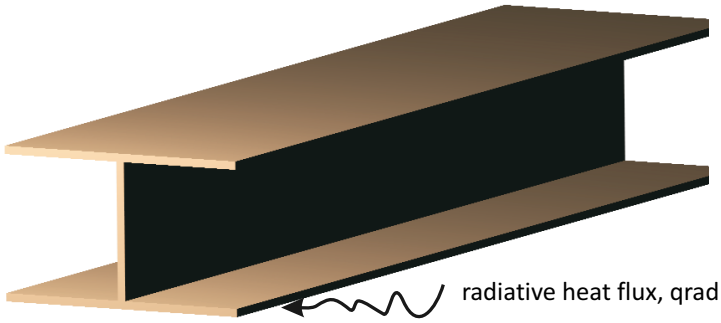

Figure 3.3: Structural element embedded in an environment with unidirectional heat flux

For the case where there is only lateral heat flux, Figure 3.4, the energy spreads over the flange thickness, but heats through the flange breadth.

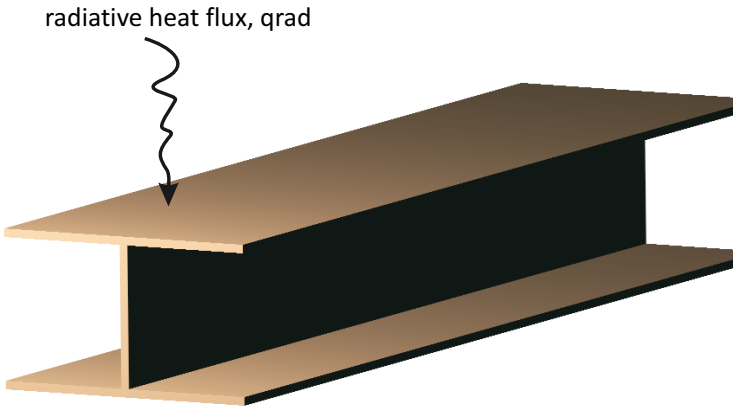

Figure 3.4: Structural element embedded in an environment with lateral heat flux only

Compared with the unidirectional heat flux case in Figure 3.3, it heats through the overall flange breadth b instead of heating through the thickness. If a slice of unit length material is selected, Figure 3.3 could be expressed as $\frac{\dot{q}_{rad}\cdot(b\cdot 1)}{b} = \dot{q}_{rad}$ while Figure 3.4 as $\frac{\dot{q}_{rad}\cdot(t\cdot 1)}{b} = \dot{q}_{rad}\cdot(\frac{t}{b})$. Considering the steel temperature change is driven by the heat flux energy, the steel temperature correction for case in Figure 3.4 could be scaled as $\Delta T_{s2} = \Delta T_s \cdot (\frac{t}{b}) = \frac{(K_1+K_2)}{2} \cdot (\frac{t}{b})$. For a more complex but common case with uniform environment and lateral heat flux occurring at the same time, a combination of the above two cases is considered, as shown in Figure 3.5

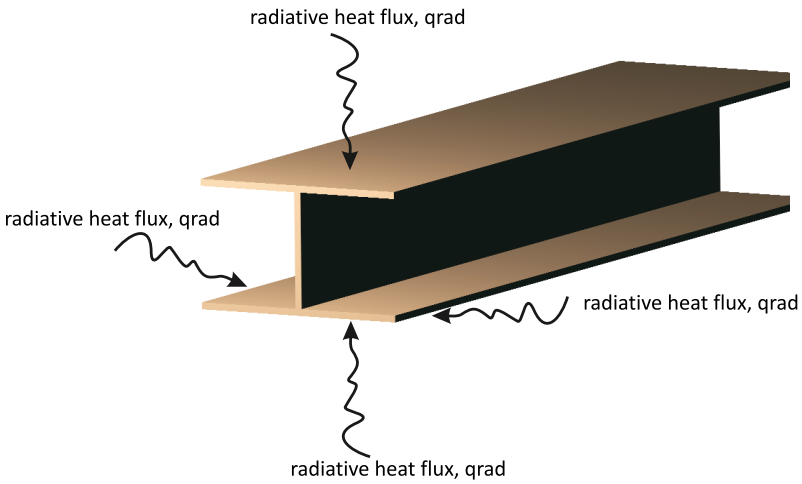

Figure 3.5: Structural element embedded in a uniform heat flux environment

For a single side, the overall steel temperature change is expressed as $\Delta T_{s3} = \Delta T_{s1} + \Delta T_{s2} = \Delta T_s + \Delta T_s \cdot (\frac{t}{b}) = \Delta T_s \cdot (1 + \frac{t}{b})$. Thus, the side effect correction equals $\Delta T_{s\_1side} = \Delta T_{s3} - \Delta T_{s1} = \Delta T_s \cdot (\frac{t}{b})$ for a single side case, and $T_{s\_side} = \Delta T_s \cdot (\frac{2t}{b})$ for two sides. As a general tool, an extra correction is considered for one sided heat flux, such as the case where the beam reaches an adiabatic boundary, as shown in Figure 3.6.

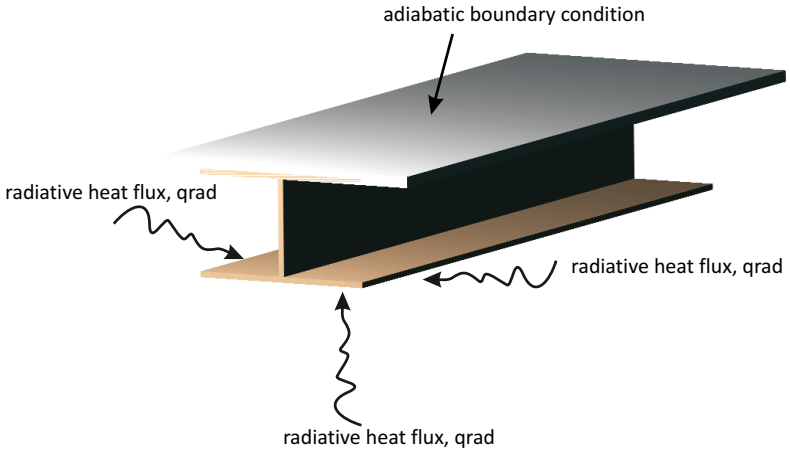

Figure 3.6: Structural element attached to an adiabatic boundary condition

The steel temperature correction equals $\Delta T_{s\_uniflux} = \frac{1}{2} \cdot \Delta T_{s\_1side} = \Delta T_s \cdot (\frac{t}{2b})$.

Compared with the general case (Figure 3.5), the correction term in this case is four times smaller, which could be negligible. In summary, the end effect correction for both sides flux is $\Delta T_{s,end} = \Delta T_s \cdot (\frac{2t}{b}) = \frac{(K_1+K_2)}{2} \cdot (\frac{2t}{b})$ and hence has been adopted in *GeniSTELA*.

3.3.3 Heat sink effects

This case considers the thermal effects when a structural member is in contact with a ceiling slab. Here, the upper flange in the model is assumed to be cooler than the rest of the member, and can be ignored. For the lower flange, heat sink effects may lead to an overly-conservative solution and a correction might be justified. The solution, together with the correction for this case, is similar to that for junction effects described above.

3.3.4 Axial temperature gradients

When the structure passes from a cold layer into a hot layer, i.e. a column or even in very deep section beams, the temperature may change greatly with height. The former situation could introduce significant modelling errors but the latter is normally likely to be less significant in terms of peak temperatures and thus is neglected here. It is however important to note that any resulting modelling errors will be on the conservative side. This can be explained by the fact that the temperatures of cells in the hot layer are reduced by axial conduction to the cooler structure below, whilst the temperatures of the cooler cells are increased - but still remain *below* those of the structure where it is exposed to the highest temperatures. The governing equation for analysis of a single cell at an intermediate height in a column running through a thermally stratified layer is:

$$h_{c1} \cdot (T_{H1} - T_{1,0}) + \dot{q}''_{r1} - \varepsilon_{m1} \cdot \sigma \cdot T_{1,0}^4 + h_{c2} \cdot (T_{H2} - T_{2,0}) + \dot{q}''_{r2} - \varepsilon_{m2} \cdot \sigma \cdot T_{2,0}^4 + \frac{k_s}{\delta_{x,upper}} \cdot (T_{s,upper} - T_s) - \frac{k_s}{\delta_{x,lower}} \cdot (T_s - T_{s,lower}) = 0 \tag{3.9}$$

Compared to the 1D model governing equations, two additional correction terms

$\frac{k_s}{\delta_{x,upper}} \cdot (T_{s,upper} - T_s)$ and $\frac{k_s}{\delta_{x,lower}} \cdot (T_s - T_{s,lower})$ appear, due to the heat conduction effects, where *upper* is a characteristic hot layer temperature and *lower* signifies conditions in a cold(er) layer. The significance of the correction terms depends on the location of the element in question with respect to the bounding temperatures. The model loops over the full height of the compartment, tracking the peak incident heat flux gradient locations, which includes both radiative and convective heat flux from the surroundings and is the temperature driver in the solid phase. Hence the two additional axial gradient correction terms are applied to the steel temperature when the column is positioned at that specific location. Here, in order to avoid the additional computational expense of performing the necessary calculations, no further attempt is made to take into account more detailed steel temperature profiles over the height of the column. Instead, based on the fact that the steel temperature change with time is proportional to the inverted radiation, i.e., the local radiative temperature, the model obtains the above two correction terms as per the following descriptions.

For the lower temperature cell that cools down the present cell temperature, the correction equals $\frac{k_s}{\delta_{x,lower}} \cdot (T_s - T_{s,lower})$.

In the short term, the steel temperature has not yet risen to the local radiative temperature, so the net heat flux that drives the steel temperature change would be as given in Equation 3.10.

$$h_c \cdot (T_H - T_{ambient}) + \varepsilon_m \cdot \sigma \cdot T_{rad,inv}^4 - \varepsilon_m \cdot \sigma \cdot T_{ambient}^4 \tag{3.10}$$

where

h_c	is the convective heat transfer coefficient, $[W/(m^2 \cdot K)]$
ε_m	is the steel member emissivity, $[-]$
σ	is the Stefan-Boltzmann constant, $\sigma = 5.669 \cdot 10^{-8}$ $[W/(m^2 \cdot K^4)]$
T_H	is the local gas temperature, $[K]$
$T_{ambient}$	is the ambient temperature, $T_{ambient} = 298.15[K]$
$T_{rad,inv}$	is the inverted radiative temperature, $[K]$

Since the steel temperature change with time is proportional to the net heat flux, that is to say, $\frac{dT_s}{dt} \propto [h_c \cdot (T_H - T_{ambient}) + \varepsilon_m \cdot \sigma \cdot T_{rad,inv}^4 - \varepsilon_m \cdot \sigma \cdot T_{ambient}^4]$, the relation between the lower cell and present cell temperature change could be expressed as in Equation 3.11 below:

$$\Delta T_{s,lower} = \Delta T_s \cdot [\frac{h_{c,lower} \cdot (T_{H,lower} - T_{ambient}) + \varepsilon_{m,lower} \cdot \sigma \cdot T^4_{rad,inv,lower} - \varepsilon_m \cdot \sigma \cdot T^4_{ambient}}{h_c \cdot (T_H - T_{ambient}) + \varepsilon_m \cdot \sigma \cdot T^4_{rad,inv} - \varepsilon_m \cdot \sigma \cdot T^4_{ambient}}] \tag{3.11}$$

with:

$$\Delta T_{s,lower} = T_{s,lower} - T_{ambient}$$

$$\Delta T_s = T_s - T_{ambient}$$

In the longer term, the steel temperature eventually reaches the local radiative temperature at the same cell location, and the following relation is obtained:

$$T_{s,lower} = T_s \cdot [\frac{T_{rad,inv,lower}}{T_{rad,inv}}] \tag{3.12}$$

Substituting Equation 3.11 or 3.12 into the main correction term regarding either short or long term corrections gives Equation 3.13 for short term lower temperature cell axial correction and Equation 3.14 for longer term correction:

$$\frac{k_s}{\delta_{x,lower}} \cdot (T_s - T_{s,lower}) = \frac{k_s}{\delta_{x,lower}} \cdot (T_s - T_{s,ambient}) \cdot \{1 - [\frac{h_{c,lower} \cdot (T_{H,lower} - T_{ambient}) + \varepsilon_{m,lower} \cdot \sigma \cdot T^4_{rad,inv,lower} - \varepsilon_m \cdot \sigma \cdot T^4_{ambient}}{h_c \cdot (T_H - T_{ambient}) + \varepsilon_m \cdot \sigma \cdot T^4_{rad,inv} - \varepsilon_m \cdot \sigma \cdot T^4_{ambient}}]\} \tag{3.13}$$

$$\frac{k_s}{\delta_{x,lower}} \cdot (T_s - T_{s,lower}) = \frac{k_s}{\delta_{x,lower}} \cdot (T_s - T_{s,ambient}) \cdot \{1 - [\frac{T_{rad,inv,lower}}{T_{rad,inv}}]\} \tag{3.14}$$

Following the same steps, the axial correction for upper temperature cell is:

$$\frac{k_s}{\delta_{x,upper}} \cdot (T_{s,upper} - T_s) = \frac{k_s}{\delta_{x,upper}} \cdot (T_s - T_{s,ambient}) \cdot \{ [\frac{h_{c,upper} \cdot (T_{H,upper} - T_{ambient}) + \varepsilon_{m,upper} \cdot \sigma \cdot T^4_{rad,inv,upper} - \varepsilon_m \cdot \sigma \cdot T^4_{ambient}}{h_c \cdot (T_H - T_{ambient}) + \varepsilon_m \cdot \sigma \cdot T^4_{rad,inv} - \varepsilon_m \cdot \sigma \cdot T^4_{ambient}}] - 1\} \tag{3.15}$$

$$\frac{k_s}{\delta_{x,upper}} \cdot (T_{s,upper} - T_s) = \frac{k_s}{\delta_{x,upper}} \cdot (T_s - T_{s,ambient}) \cdot \{ [\frac{T_{rad,inv,upper}}{T_{rad,inv}}] - 1\} \tag{3.16}$$

It is determined that either axial correction should be considered or not, or either short term or long term corrections should be applied, depending on the ratio of the steel temperature increment and the temperature increment caused by inverted radiation. As a consequence, an additional variable χ_axial is introduced, and denoted as $\chi\_axial = \frac{\Delta T_s}{(T_{rad,inv} - T_{ambient})}$ for the case when $T_{rad,inv}$ is greater than $T_{ambient}$, while $\chi\_axial = 0$ when $T_{rad,inv}$ equals to $T_{ambient}$. The axial correction is applied when χ_{axial} is greater than zero. Besides, when it reaches a certain degree, by default 50%, significant increase of the steel temperature has been observed, leading to a reasonable assumption of the long term correction, and afterwards, the long term correction is assumed to apply to all the following time steps.

Strictly speaking, the above axial correction is based on a non-time-varying boundary condition hypothesis. It is a simplified assumption for a constant fire environment, but not applicable for arbitrary variation of the thermal boundary condition, such as the scenario where the local radiative temperature might rise suddenly or fall immediately. Since the long term driver for the steel temperature increase is more of a concern, for the case where the local radiative temperature rises suddenly, a hypothesis of eventually reaching thermal equilibrium is made and long term axial correction applies. For the case where the local radiative temperature falls immediately, such as the cooling stage, the axial correction would only reduce the steel temperature, leading to a conservative result. The "worst" case would therefore be considered as the normal 1D case without axial correction.

In addition, it is important to note that these effects are only critical where they

negatively impact the performance of the member, i.e. increase the solid temperatures, and in the majority of cases the opposite is true, i.e. the default procedure is a good representation of the "worst" case. Thus, while it is vital to show that these possible corrections have been appropriately considered, their effect on the final results is expected to be fairly limited and should be applied only when critical.

3.4 Brief Summary

In summary, the governing equations for the quasi-3D model can be summed up as in Table 3.3 below:

Table 3.3: Summary of the governing equations for quasi-3D model

Simple 1D model: $\rho_s \cdot c_s \cdot \frac{\partial T_s}{\partial t} \cdot \Delta x_s + w_{p1} \cdot \rho_1 \cdot c_{p1} \cdot \frac{\partial T_1}{\partial t} \cdot \Delta x_1 + w_{p2} \cdot \rho_2 \cdot c_{p2} \cdot \frac{\partial T_2}{\partial t} \cdot \Delta x_2$ $= h_{c1} \cdot (T_{H1} - T_{1,0}) + \dot{q}''_{r1} - \varepsilon_{m1} \cdot \sigma \cdot T^4_{1,0}$ $+ h_{c2} \cdot (T_{H2} - T_{2,0}) + \dot{q}''_{r2} - \varepsilon_{m2} \cdot \sigma \cdot T^4_{2,0}$	(a)
1D model with axial gradient corrections: $\rho_s \cdot c_s \cdot \frac{\partial T_s}{\partial t} \cdot \Delta x_s + w_{p1} \cdot \rho_1 \cdot c_{p1} \cdot \frac{\partial T_1}{\partial t} \cdot \Delta x_1 + w_{p2} \cdot \rho_2 \cdot c_{p2} \cdot \frac{\partial T_2}{\partial t} \cdot \Delta x_2$ $= h_{c1} \cdot (T_{H1} - T_{1,0}) + \dot{q}''_{r1} - \varepsilon_{m1} \cdot \sigma \cdot T^4_{1,0} + h_{c2} \cdot (T_{H2} - T_{2,0})$ $+ \dot{q}''_{r2}$ - $\varepsilon_{m2} \cdot \sigma \cdot T^4_{2,0} + \frac{k_s}{\delta_{x,upper}} \cdot (T_{s,upper} - T_s)$ - $\frac{k_s}{\delta_{x,lower}} \cdot (T_s - T_{s,lower})$	(b)
Junction effect or heat sink effect corrections : $\Delta T_{s,junct} = -\frac{\dot{q}_{rad,junct} \cdot \chi}{k_s}$	(c)
End effect corrections: $\Delta T_{s,end} = \Delta T_s \cdot \frac{2t}{b} = \frac{(K_1+K_2)}{2} \cdot \frac{2t}{b}$,	(d)

As a one-way coupling methodology, which passes information from CFD calculation to the thermal analysis, the above quasi-3D model passes the following information from CFD calculation. Those include grid number information nx, ny, nz, time step $delta_t$, radiative heat flux q_{r1}, q_{r2}, local gas temperature T_{H2}, T_{H2} and velocity variables u, v, w, which are used for convective heat transfer coefficient calculation.

To reduce the great computational demands caused by repeated calculation of the above governing equations, and to calculate the thermal responses of the material in a generalised fashion by inclusion of all the above effects, the quasi-3D model

is proposed as a single solution to Equations (a) and (b) in Table 3.3 where axial gradient effects cannot be ignored, together with two additional difference terms $\Delta T_{s,junct} = -\frac{\dot{q}_{rad,junct} \cdot \chi}{k_s}$ and $\Delta T_{s,end} = \Delta T_s \cdot \frac{2t}{b}$ specifying the junction effect or heat sink effect and the end effect respectively.

For simplicity, *GeniSTELA* model ignored the shadow effect even though it would be possible to treat shadow effects in the more general sense, i.e. with information on directional radiation effects, to compute the flux to each part of the member. Nevertheless, this would result in additional great computational cost and the complexity of generalizing member orientation in the model.

3.5 Numerical Solutions

As is well-known in numerical heat transfer, the above situation in the governing equation (Equations (a) and (b) in Table 3.3) represents a strongly coupled problem, with the net heat fluxes at the gas-solid interface very much dependent on the surface temperature, but both also related to the transient thermal response of the structure itself. Numerical instabilities might become evident if inadequate solution procedures are used; these are overcome with a specific modelling strategy here. This solution procedure is based upon using the heat transfer equation boundary conditions, Equations 3.2 and 3.3, and iterating by the Newton-Raphson method to update the surface temperature, and thereafter, with the updated surface temperature as a boundary condition, solving the overall energy balance equation (Equations (a) and (b) Table 3.3) by the Runge-Kutta method to obtain the steel temperature. During the analysis, while using the Newton-Raphson procedures to obtain the values of the surface temperatures, the convergence is checked by examining the absolute errors $|T_{1,0}(i) - T_{1,0}(i-1)|$ and $|T_{2,0}(i) - T_{2,0}(i-1)|$ within each time step, where n represents the time step and i represents the iteration number. By default (in the spreadsheet implementation), five iterations are carried out and reasonably good convergence typically results; in the CFD implementation, iterations are performed until a sufficient degree of convergence is achieved (e.g. 0.1% temperature error). The Runge-Kutta integration is used to accommodate rapid rates of change of gas temperature, to which thermal exposures are related in a strongly non-linear fashion via the radiation terms, and to provide an implicit element to the solution, since the

evolving steel temperature is coupled back on itself via its influence on surface temperature. For simplicity, the equations for a 2^{nd}-order Runge-Kutta (or Euler-Cauchy) procedure are provided, which also act as a sufficient solution procedure. The steel temperature at n^{th} time step is obtained:

Simple 1D model:

$$T_s^{(n)} = T_s^{(n-1)} + \frac{1}{2}(K_1^{(n)} + K_2^{(n)}) \tag{3.17}$$

1D model with axial gradient corrections:

$$T_{s\_axial}^{(n)} = T_{s\_axial}^{(n-1)} + \frac{1}{2}(K_{1\_axial}^{(n)} + K_{2\_axial}^{(n)}) \tag{3.18}$$

where:

$$K_1^{(n)} = \Delta t \cdot f(T_s^{(n)}, t^{(n)}) = \Delta t \cdot f(\bar{T}_{1,0}^{(n)}(i_{converged}), \bar{T}_{2,0}^{(n)}(i_{converged}))$$

$$K_2^{(n)} = \Delta t \cdot f(T_s^{(n)} + K_1^{(n)}, t^{(n)}) = \Delta t \cdot f(T_{1,0}^{(n)}(j_{converged}), T_{2,0}^{(n)}(j_{converged}))$$

while,

$$f(\bar{T}_{1,0}^{(n)}(i), \bar{T}_{2,0}^{(n)}(i)) = \left\{ \begin{array}{l} h_{c1} \cdot (T_{H1}^{(n)} - \bar{T}_{1,0}^{(n)}(i)) \\ +\dot{q}''_{r1} - \varepsilon_{m1} \cdot \sigma \cdot \bar{T}_{1,0}^{(n)}(i)^4 \\ +h_{c2} \cdot (T_{H2}^{(n)} - \bar{T}_{2,0}^{(n)}(i)) \\ +\dot{q}''_{r2} - \varepsilon_{m2} \cdot \sigma \cdot \bar{T}_{2,0}^{(n)}(i)^4 \\ -\frac{(\bar{T}_{1,0}^{(n)}(i) - \bar{T}_{1,0}^{(n-1)}(i))}{\Delta t} \cdot \Delta x_1 \cdot w_{p1} \cdot \rho_1 \cdot c_{p1} \\ -\frac{(\bar{T}_{2,0}^{(n)}(i) - \bar{T}_{2,0}^{(n-1)}(i))}{\Delta t} \cdot \Delta x_2 \cdot w_{p2} \cdot \rho_2 \cdot c_{p2} \end{array} \right\} \cdot \frac{1}{\Delta x_s \cdot \rho_s \cdot c_s}$$

$$f(T_{1,0}^{(n)}(j), T_{2,0}^{(n)}(j)) = \left\{ \begin{array}{l} h_{c1} \cdot (T_{H1}^{(n)} - T_{1,0}^{(n)}(j)) \\ +\dot{q}''_{r1} - \varepsilon_{m1} \cdot \sigma \cdot T_{1,0}^{(n)}(j)^4 \\ +h_{c2} \cdot (T_{H2}^{(n)} - T_{2,0}^{(n)}(j)) \\ +\dot{q}''_{r2} - \varepsilon_{m2} \cdot \sigma \cdot T_{2,0}^{(n)}(j)^4 \\ -\frac{(T_{1,0}^{(n)}(j) - T_{1,0}^{(n-1)}(j))}{\Delta t} \cdot \Delta x_1 \cdot w_{p1} \cdot \rho_1 \cdot c_{p1} \\ -\frac{(T_{2,0}^{(n)}(j) - T_{2,0}^{(n-1)}(j))}{\Delta t} \cdot \Delta x_2 \cdot w_{p2} \cdot \rho_2 \cdot c_{p2} \end{array} \right\} \cdot \frac{1}{\Delta x_s \cdot \rho_s \cdot c_s}$$

And with axial gradient correction,

$$K_{1\_axial}^{(n)} = \Delta t \cdot f_{axial}(T_{s\_axial}^{(n)}, t^{(n)}) = \Delta t \cdot f_{axial}(\bar{T}_{1,0}^{(n)}(i_{converged}), \bar{T}_{2,0}^{(n)}(i_{converged}))$$

$$K_{2\_axial}^{(n)} = \Delta t \cdot f_{axial}(T_{s\_axial}^{(n)} + K_{1\_axial}^{(n)}, t^{(n)}) = \Delta t \cdot f_{axial}(T_{1,0}^{(n)}(j_{converged}), T_{2,0}^{(n)}(j_{converged}))$$

while,

$$f_{axial}(\bar{T}_{1,0}^{(n)}(i), \bar{T}_{2,0}^{(n)}(i)) = \left\{ \begin{array}{l} h_{c1} \cdot (T_{H1}^{(n)} - \bar{T}_{1,0}^{(n)}(i)) \\ +\dot{q}''_{r1} - \varepsilon_{m1} \cdot \sigma \cdot \bar{T}_{1,0}^{(n)}(i)^4 \\ +h_{c2} \cdot (T_{H2}^{(n)} - \bar{T}_{2,0}^{(n)}(i)) \\ +\dot{q}''_{r2} - \varepsilon_{m2} \cdot \sigma \cdot \bar{T}_{2,0}^{(n)}(i)^4 \\ -\frac{(\bar{T}_{1,0}^{(n)}(i) - \bar{T}_{1,0}^{(n-1)}(i))}{\Delta t} \cdot \Delta x_1 \cdot w_{p1} \cdot \rho_1 \cdot c_{p1} \\ -\frac{(\bar{T}_{2,0}^{(n)}(i) - \bar{T}_{2,0}^{(n-1)}(i))}{\Delta t} \cdot \Delta x_2 \cdot w_{p2} \cdot \rho_2 \cdot c_{p2} \\ +\frac{k_s}{\delta_{x,upper}} \cdot (\bar{T}_{s,uppper}^{(n)} - \bar{T}_s^{(n)}) \\ -\frac{k_s}{\delta_{x,lower}} \cdot (\bar{T}_s^{(n)} - \bar{T}_{s,lower}^{(n)}) \end{array} \right\} \cdot \frac{1}{\Delta x_s \cdot \rho_s \cdot c_s}$$

$$f_{axial}(T_{1,0}^{(n)}(j), T_{2,0}^{(n)}(j)) = \left\{ \begin{array}{l} h_{c1} \cdot (T_{H1}^{(n)} - T_{1,0}^{(n)}(j)) \\ +\dot{q}''_{r1} - \varepsilon_{m1} \cdot \sigma \cdot T_{1,0}^{(n)}(j)^4 \\ +h_{c2} \cdot (T_{H2}^{(n)} - T_{2,0}^{(n)}(j)) \\ +\dot{q}''_{r2} - \varepsilon_{m2} \cdot \sigma \cdot T_{2,0}^{(n)}(j)^4 \\ -\frac{(T_{1,0}^{(n)}(j) - T_{1,0}^{(n-1)}(j))}{\Delta t} \cdot \Delta x_1 \cdot w_{p1} \cdot \rho_1 \cdot c_{p1} \\ -\frac{(T_{2,0}^{(n)}(j) - T_{2,0}^{(n-1)}(j))}{\Delta t} \cdot \Delta x_2 \cdot w_{p2} \cdot \rho_2 \cdot c_{p2} \\ +\frac{k_s}{\delta_{x,upper}} \cdot (T_{s,upper}^{(n)} - T_s^{(n)}) \\ -\frac{k_s}{\delta_{x,lower}} \cdot (T_s^{(n)} - \bar{T}_{s,lower}^{(n)}) \end{array} \right\} \cdot \frac{1}{\Delta x_s \cdot \rho_s \cdot c_s}$$

Within these equations, the initial and intermediate surface temperatures, $T_{1,0}^{(n)}$ & $T_{2,0}^{(n)}$ and $\bar{T}_{1,0}^{(n)}$ & $\bar{T}_{2,0}^{(n)}$, respectively, are obtained through application of the Newton-Raphson procedure to solve Equation 3.2 and 3.3, in conjunction with the initial steel temperature, in the first case, and the estimated steel temperature between two time steps, $T_s^{(n)} = T_s^{(n-1)} + K_1^{(n-1)}$, in the second case.

Repeating the above procedure, the final thermal responses including the insulation temperature which is adopted as the effective insulation temperature, surface temperature, and the steel temperature from quasi-3D model at n^{th} time step can

be obtained as given below:

Table 3.4: Thermal responses obtained from quasi-3D model

Surface temperature	$T_{1,0}^{(n)}(i_{converged}), T_{2,0}^{(n)}(i_{converged})$	(a)
Insulation temperature	$T_{eff,insulation}^{(n)} = \frac{T_{1,0}^{(n)}(i_{converged})+T_{2,0}^{(n)}(i_{converged})}{2} \cdot w_p$ where: $T_1^{(n)}(i_{converged}) = \frac{T_{1,0}^{(n)}(i_{converged})+T_s^{(n)}}{2}$ $T_2^{(n)}(i_{converged}) = \frac{T_{2,0}^{(n)}(i_{converged})+T_s^{(n)}}{2}$	(b)
Steel temperature	For the case without axial gradient correction: $T_{s\_final}^{(n)} = T_{s\_1D}^{(n)} + \Delta T_{s,junct} + \Delta T_{s,end}$ $= T_{s\_1D}^{(n)} - \frac{\dot{q}_{rad,junct} \cdot \chi}{k_s} + (\frac{K_1^{(n)}+K_2^{(n)}}{2})(\frac{2t}{b})$	(c)
	Or with axial gradient correction: $T_{s\_final}^{(n)} = T_{s\_axial}^{(n)} + \Delta T_{s,junct} + \Delta T_{s,end}$ $= T_{s\_axial}^{(n)} - \frac{\dot{q}_{rad,junct} \cdot \chi}{k_s} + (\frac{K_1^{(n)}+K_2^{(n)}}{2})(\frac{2t}{b})$	(d)

3.6 Material properties

The aforementioned model might be considered as a reasonable representation of the *fundamental* aspects of the heat transfer phenomena. However, in practice several factors are found to have a great impact on the transient response, in particular the thermal properties of the protection materials, which affect the surface temperature and thus the steel temperature. It is known that these properties are often strongly temperature/time-dependent and the use of constant values may result in significant errors in some cases. The methodology developed here aims at generalising the thermal analysis to accommodate all important phenomena. Conventional approaches to treatment of moisture effects have been implemented, referencing modified specific heats and thermal conductivities (Liang & Welch, 2006). The effects of intumescence, which is clearly of great practical relevance to the case of protected structures, are also extended. In order to do so, geometrical and density variations have been explicitly treated.

3.6.1 Moisture effects

The temperature-dependent characteristics and moisture effects are incorporated in certain parameters for generalisation of the methodology. These are treated by varying the relevant thermal properties of the material, in particular, the specific heat and thermal conductivity, by means of an additional temperature-dependent source term in the energy equation representing latent heat effects. The effective specific heat comprises the dry specific heat and one additional part considering the temperature dependent properties and moisture effects, denoted as $c_p^{'}$ in Figure 3.7. A similar principle applies to the effective thermal conductivity derivation as to the effective specific heat. As shown in Figure 3.8 below, the thermal conductivity is defined as increasing linearly to a peak value k_{peak} at the temperature of T_0, which equals $(k_0+\alpha\cdot\Delta T)\cdot(\omega_m \cdot KFactor^{KPower}+1)^{(1/KPower)}$, and then decreasing linearly to the dry material thermal conductivity, of a value of $(k_0 + \alpha \cdot \Delta T)$. Here α, also known as $KTfactor$, is a linear rate of change with temperature; ΔT is the temperature change relative to the zero Celsius temperature degree condition, $\Delta T = T - T_z$; $KFactor$ is the empirical moisture enhancement factor and $KPower$ is the empirical moisture enhancement power. By comparison with some model fits to fire resistance test data (Welch, 2000), values of the series of factors $KTFactor$, $KFactor$, and $KPower$ are typically adopted as 3E-06, 10 and 4, respectively. For other frequently used protection materials, such as the sprayed fibre type or board type, the moisture correction to the thermal conductivity is neglected, since this would only be appropriate for enhancing thermal conductivity when moisture can move from exposed to unexposed surfaces. In those cases, a unity value is adopted for both $KFactor$ and $KPower$, and $KTFactor$ varies with different materials. When the moisture effect needs to be considered for thermal conductivity and specific heat corrections, to match with reality, the moisture content itself is considered to be varying with temperature and time and it is simply considered as a linear change with each of these parameters. It is assumed that the moisture content is precisely equal to the initial value at temperature below the boiling range, dropping to zero as the temperature rises through this range, and remaining at zero thereafter. The final expressions for the effective values are demonstrated in Table 3.5 and Table 3.6. The detailed derivations of the additional temperature and moisture-dependent source terms for both thermal property parameters are available in **Appendix C**.

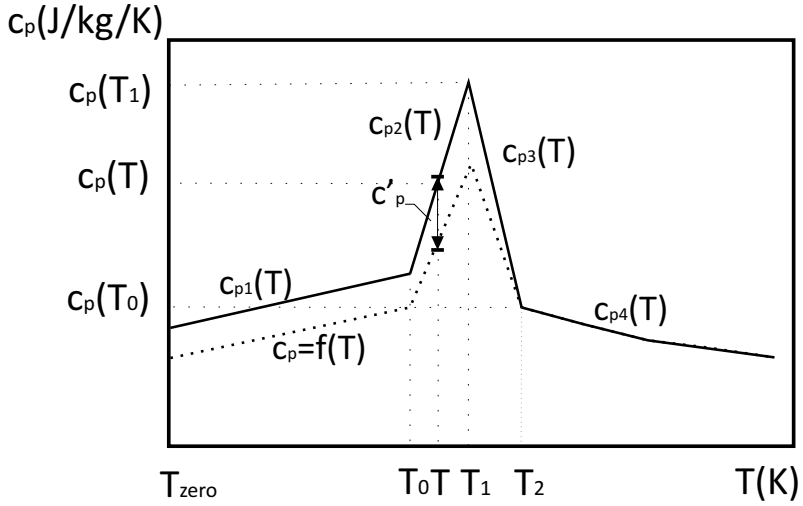

Figure 3.7: Specific heat vs. temperature

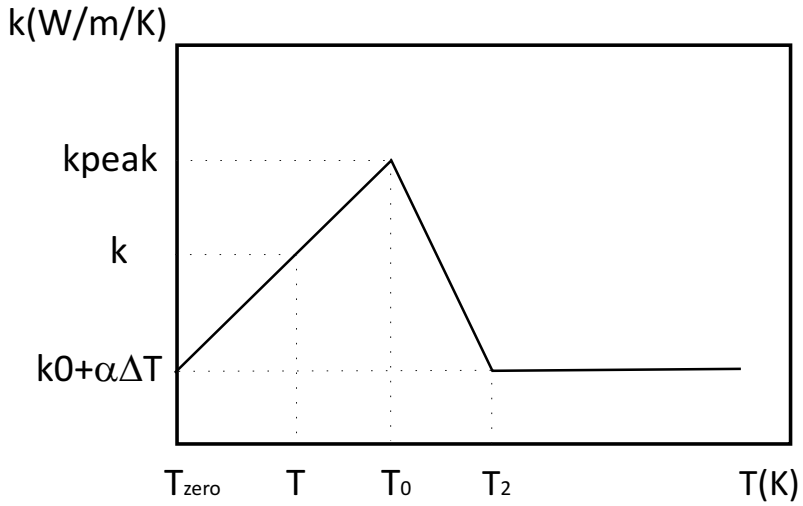

Figure 3.8: Thermal conductivity vs. temperature

Table 3.5: Effective specific heat, c_p

$c_p = c_{p1}(T) = f(T) + c_{p,H_2O} \cdot \omega_m$	$(T_z \leq T < T_0)$
$c_p = c_{p2}(T) = f(T) + c'_{p2}(T)$ $= f(T) + \omega_m \cdot [\frac{4L}{(T_2-T_0)} \cdot (\frac{T-T_0}{T_2-T_0}) + c_{p,H_2O} \cdot (\frac{T_2-T}{T_2-T_0})]$	$(T_0 \leq T < T_1)$
$c_p = c_{p3}(T) = f(T) + c'_{p3}(T)$ $= f(T) + \omega_m \cdot [\frac{4L}{(T_2-T_0)} \cdot (\frac{T_2-T}{T_2-T_0}) + c_{p,H_2O} \cdot (\frac{T_2-T}{T_2-T_0})]$	$(T_1 \leq T < T_2)$
$c_p = c_{p4}(T) = f(T)$	$(T \geq T_2)$

Table 3.6: Effective thermal conductivity, k

$k = (\frac{T-T_z}{T_0-T_z}) \cdot [k_{peak} - (k_0 + \alpha \cdot \Delta T)] + (k_0 + \alpha \cdot \Delta T)$	$(T_z \leq T < T_0)$
$k = (\frac{T_2-T}{T_2-T_0}) \cdot [k_{peak} - (k_0 + \alpha \cdot \Delta T)] + (k_0 + \alpha \cdot \Delta T)$	$(T_0 \leq T < T_2)$
$k = (k_0 + \alpha \cdot \Delta T)$	$(T \geq T_2)$

Where

c_p	is the dry material specific heat or initial specific heat, which is a function of temperature and it is normally obtained through the tests data, $[J/(kg \cdot K)]$
L	is the latent heat capacity of water, $L = 2.176 \cdot 10^6$ $[J/kg]$
T	is the relevant temperature, $[K]$
ΔT	is the temperature change, $[K]$
ω_m	is the initial moisture content of the material, $[kg/kg]$
c_{p,H_2O}	is the specific heat capacity of water, $c_{p,H_2O} = 10^3$ $[J/(kg \cdot K)]$
k_0	is the base value of the thermal conductivity at zero Celsius degree temperature, $[W/(m \cdot K)]$

3.6.2 Intumescent effects

Intumescent coatings offer a passive protection against heat and flame spread. They increase their thickness under the influence of heat, and thus build up a multicellular structure of low thermal conductivity that provides an efficient heat barrier. At the same time, an endothermic chemical reactions take some heat away from the protected material (Bartholmai *et al.*, 2003). They therefore are found to represent an increasingly common method of providing fire protection to the structural steel, that is used more and more in modern architectural designs, whilst at the same time maintaining aesthetic appearance. Accompanying the chemical and physical changes in the intumescent materials under heating, the thermal properties of those materials will change significantly. Based on literature survey, considering the effects of geometrical expansion, a simple conceptual model would suggest that thermal equivalence to a finite thickness problem can be achieved by simply scaling the thermal conductivity by the layer thickness, $d(d = 1m)$, giving an effective thermal conductivity, k/d. Density is scaled in the same way, and specific heat by the inverse of d, but these two parameters always appear as factors of each other, so these scalings vanish in the term $\rho \cdot c_p$.

The description of the temperature-dependent intumescent thickness, d, can be determined from an expression for the expansion ratio. The initial submodel for

the intumescent property calculation postulates that the expansion ratio R would fit the general form:

Table 3.7: Calculation of expansion ratio, R

$R = 1$	$T < T_{lower}$	(a)
$R = 1 + \frac{1}{2}(R_f - 1)(\frac{T - T_{lower}}{T_{mid} - T_{lower}})^n$	$T_{lower} \leq T < T_{mid}$	(b)
$R = R_f - \frac{1}{2}(R_f - 1)(\frac{T_{upper} - T}{T_{upper} - T_{mid}})^n$	$T_{mid} \leq T < T_{upper}$	(c)
$R = R_f$	$T \geq T_{upper}$	(d)

where

R	is the time-dependent expansion factor, [–]
R_f	is the final expansion factor, [–]
n	is the shape factor power, [–]
T	is the current averaged intumescent temperature, [K]
$T_{lower}, T_{upper}, T_{mid}$	are critical temperatures where scaling factor changes, [K]

Here, besides the relevant temperature limits, the critical controlling parameters are the shape factor n and the overall expansion ratio R_f. An approximate calibration has been initially performed by comparison with test data, including the results of Bartholmai (Bartholmai *et al.*, 2003) giving a value of $n = 2$. Taking an approximate temperature range from the DTG results of the latter study, and assuming $R_f = 10R$, gives the following curve:

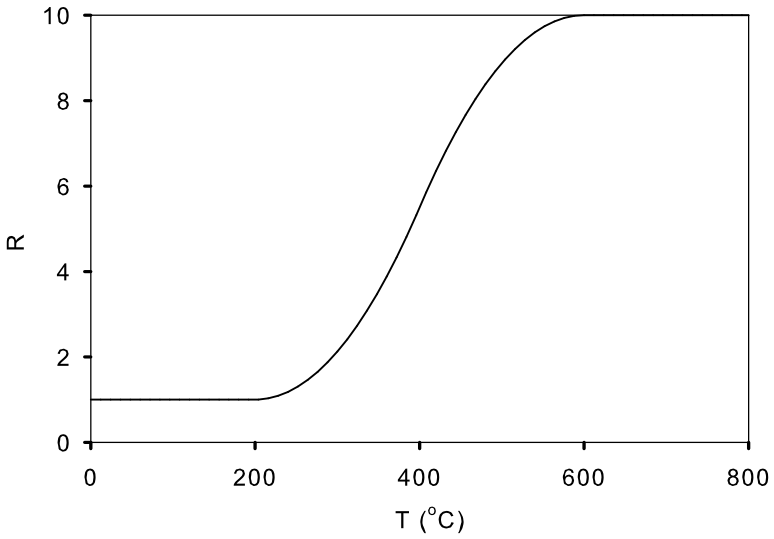

Figure 3.9: Scaling factor R change with temperature

In fact, a variety of overall 1D expansion ratios have also been reported in the literature as in the previous chapter.

The key parameter for the thermal model is the conductivity, or its scaled value, i.e. k/d . The conductivity itself is affected by fundamental changes in the material as it intumesces (Bartholmai & Schartel, 2007; Bartholmai *et al.*, 2003; Tan *et al.*, 2004). Unfortunately, the effect is non-linear and very dependent on initial thickness, and most pronounced at the smaller thicknesses typical of real applications; hence, there would appear to be no substitute for its direct experimental determination. The various literature results would suggest an initial increase followed by a fall during intumescence and finally a sharp rise during material degradation. The initial model adopts fitted values derived from the results of Bartholmai (Bartholmai & Schartel, 2007), as shown in Figure 3.10 below.

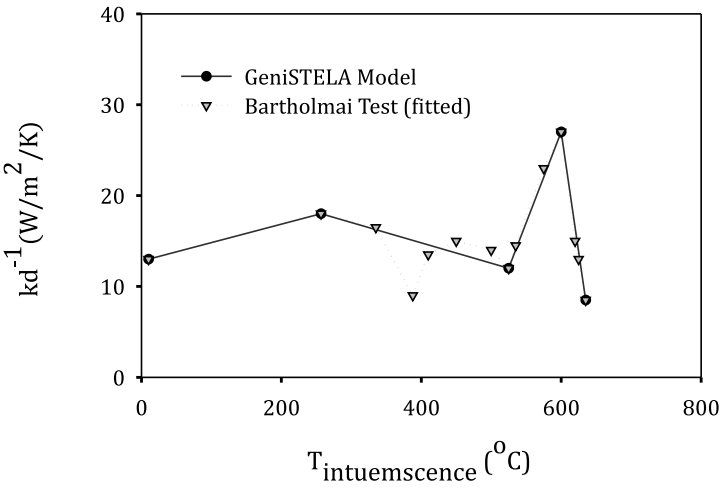

Figure 3.10: Comparison of thermal conductivity between generalised model and Bartholmai test (Bartholmai & Schartel, 2007)

In comparison with the initial model, the final model adopts fitted values derived from the results of cone calorimeter tests, which have been carried out at the University of Edinburgh as part of an undergraduate thesis project (Kinsella, 2007).

3.6.2.1 Cone calorimeter tests

Cone calorimeter testing was carried out according to ISO-5660 (BSI, 1993) in order to investigate derivation of the temperature/time-dependent thermal properties of intumescent materials. A single intumescent paint was examined (a white thin-film water-borne coating, Steelguard FM585, supplied by Ameron coatings). It was applied to an Aluminium block, of area $100 \times 100mm$ by $15mm$ depth and thermocouples were physically attached (not welded) to the back of the block and at the interface between the block and the intumescent. 12 samples with three intumescent thicknesses ($1mm$, $2mm$, $5mm$), together with an uncoated control specimen, were tested at four irradiance levels (30, 60, 75, 90 kW/m^2). Their intumescent expansion ratio was approximated by measuring peak char thickness after the test and their effective thermal conductivity deduced from calibration of a one-dimensional thermal model implemented in a spreadsheet. For this, the conduction heat transfer through the intumescent layer is simply equated to the sensible enthalpy increment of the substrate block, minus a heat

loss term; the latter was scaled from the value deduced for the final conditions of the test (when thermal equilibrium is assumed to apply so that it can be equated to the net heat flux from the cone), weighted by the normalized ratio of the temperature difference between the rear of the block and the ambient conditions. A summary of the results is provided in Table 3.8 and a photograph example of post-test condition of the expanded intumescent material is shown in Figure 3.11:

Table 3.8: Summary of intumescent tests parameters

Test No.	Heat flux $[kW/m^2]$	Approx.initial thickness $[mm]$	Approx.final thickness $[mm]$	Expansion ratio $[-]$	Nominal k/d $[W/m^2/K]$
1	30	1	27	27	30
2	30	2	22	11	23
3	30	5	47	3.4	18
4	60	1	24	24	28
5	60	2	38	19	20
6	60	5	60	10	12
7	75	1	28	28	25
8	75	2	46	23	15
9	75	5	66	13	10
10	90	1	45	45	20
11	90	2	66	33	12
12	90	5	79	16	9

Figure 3.11: Photograph illustrating final condition of intumescent in test 5

The final measured thicknesses in Table 3.8 show that the overall expansion ratio is not very strongly related to the initial intumescent layer thickness, suggesting that it is mainly the surface material intumescing to create a thermal barrier. Nevertheless, Figures 3.12 ∼ 3.14 show that the block temperatures plateaued at lower levels with higher initial thicknesses (shown by the locations of the right-hand ends of the curves), consistent with the fact that greater amounts of intumescent do provide a better insulation effect. The effective (normalized) thermal conductivities are rather variable (and some data points are missing in the lower temperature range for the $60kW/m^2$ plot), but there is a clear trend to lower values at greater thicknesses, consistent with the provision of extra insulation. However, this effect is exposure dependent and Figure 3.15 shows a better intumescent performance, i.e. reduced normalized conductivity, at higher fluxes (Test 12). This must be partly due to the relatively greater expansion thicknesses at high fluxes, hence larger normalizing parameter d, but other effects may also be relevant. Finally, it should be noted that the intumescent thicknesses used here are greater than typical design specifications for the product tested, due to practical considerations (though c. $1mm$ is required for some larger members) but this testing was not intended to be a material performance assessment. However, results of this type could in principle be used to provide guidance on representing intumescent thermal properties for use in *GeniSTELA* for any other products.

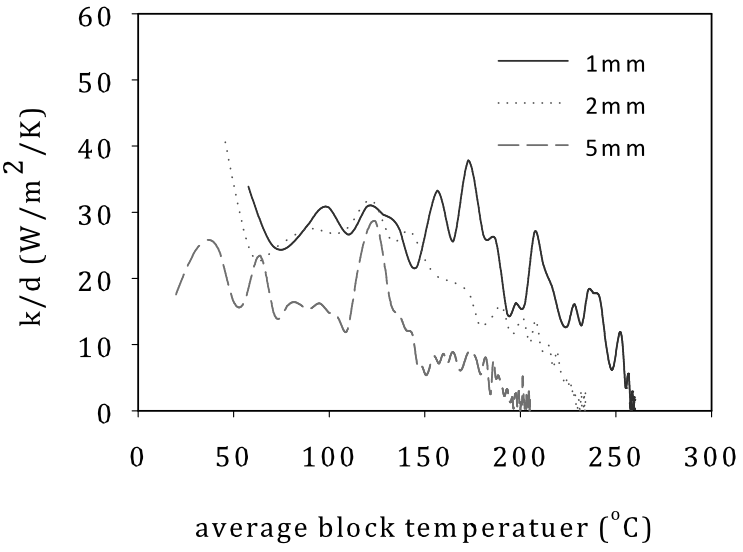

Figure 3.12: Effective thermal conductivity at $30kW/m^2$

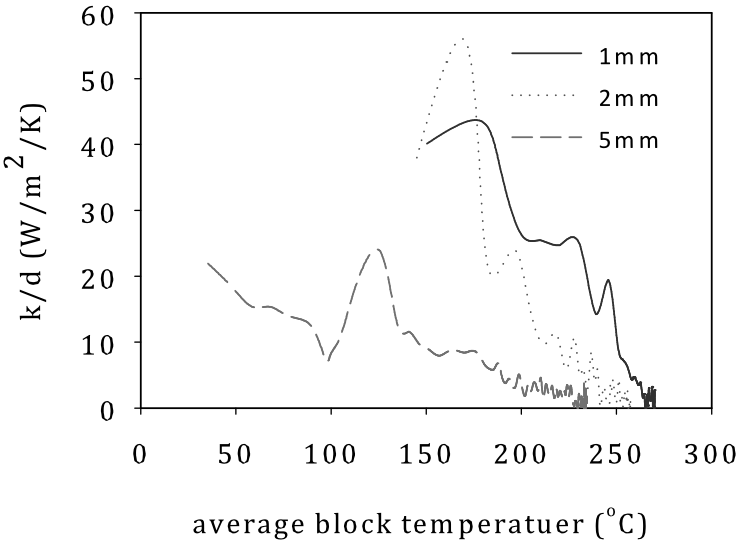

Figure 3.13: Effective thermal conductivity at $60kW/m^2$

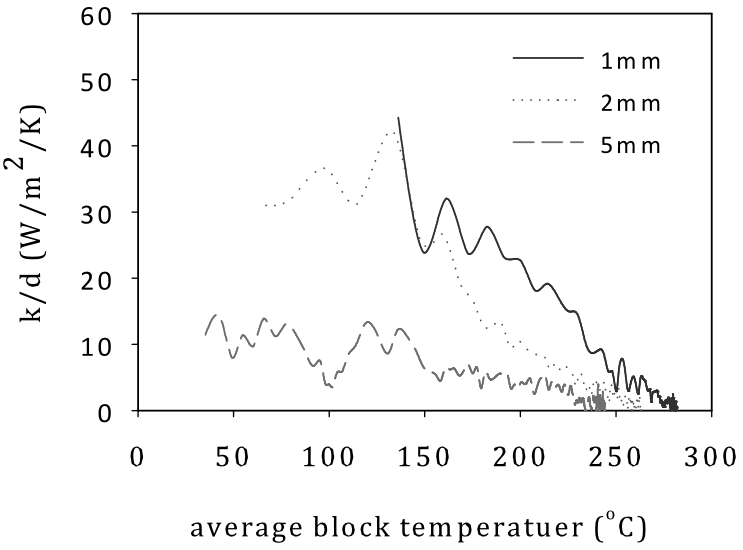

Figure 3.14: Effective thermal conductivity at $90kW/m^2$

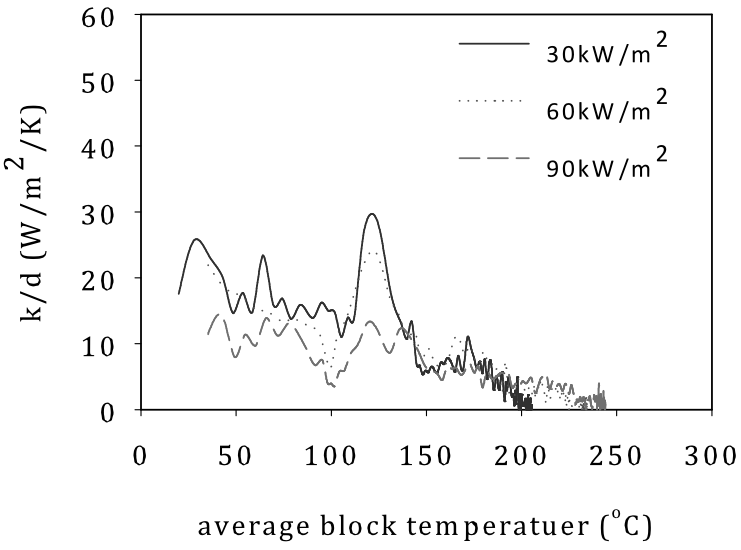

Figure 3.15: Effective thermal conductivity for intumescent with $5mm$ thickness

3.6.2.2 Intumescent submodel summary

Based on the initial model, referencing the literature and comparing with the cone tests, *GeniSTELA* adopts an intumescent material property submodel in a more generalised fashion, with the capability to calculate the temperature-dependent and intumescent affected effective density, specific heat and thermal conductivity. These dependencies are summarized as follows. Note that where notations have been defined previously, they are not repeated here.

a. Effective density:

$$\rho_{eff} = \rho \cdot m \tag{3.19}$$

where

ρ is the material density at initial dry condition, $[kg/m^3]$

ρ_{eff} is the effective density with the change of temperature and effect of intumescence,$[kg/m^3]$

m is the material mass change rate due to intumescence, $[kg/kg]$

With the process of intumescence, intumescent materials will lose mass. The material mass change rate m here is used to consider the temperature geometry effect and is derived as demonstrated in Table 3.9.

Table 3.9: Calculation of mass change rate, m

$m = 1$	$T < T_{lower}$	(a)
$m = 1 - \frac{1}{2}(1 - \frac{1}{R_f})(\frac{T - T_{lower}}{T_{mid} - T_{lower}})^n$	$T_{lower} \leq T < T_{mid}$	(b)
$m = \frac{1}{R_f} + \frac{1}{2}(1 - \frac{1}{R_f})(\frac{T_{upper} - T}{T_{upper} - T_{mid}})^n$	$T_{mid} \leq T < T_{upper}$	(c)
$m = \frac{1}{R_f}$	$T \geq T_{upper}$	(d)

b. Effective specific heat:

Intumescent materials not only affect the material geometry during the intumescence process, but also take away the material heat energy. The intumescent material submodel embedded within *GeniSTELA* thereafter takes both effects into account. The determination of effective specific heat is summarized in Table 3.10.

Table 3.10: Calculation of effective specific heat, $c_{p,eff}$

$c_{p,eff} = c_p \cdot R$	$T < T_{lower}$	(a)
$c_{p,eff} = c_p \cdot R + \frac{1}{(T_{ilower}+T_{imid})/2} \cdot [\frac{T}{(T_{ilower}+T_{imid})/2} - \frac{1}{2}] \cdot E$	$T_{lower} \leq T < T_{mid}$	(b)
$c_{p,eff} = c_p \cdot R - \frac{1}{(T_{ilower}+T_{imid})/2} \cdot [\frac{T}{(T_{ilower}+T_{imid})/2} - \frac{5}{2}] \cdot E$	$T_{mid} \leq T < T_{upper}$	(c)
$c_{p,eff} = c_p \cdot R_f$	$T \geq T_{upper}$	(d)

where

c_p is the material specific heat at initial dry condition, $[J/(kg \cdot K)]$

$c_{p,eff}$ is the effective specific heat with the change of temperature and effect of intumescence, $[J/(kg \cdot K)]$

R is the time-dependent expansion factor, defined as in Table 3.7 before, $[-]$

E is the energy term, a value of $2e^6$ is adopted in this model, $[J]$

$T_{ilower}, T_{iupper}, T_{imid}$ are critical temperatures where scaling factor changes due to energy effect, $[K]$

c. Effective thermal conductivity:

Similarly as for the other two effective thermal property calculations, the effective thermal conductivity due to intumescence has been scaled. It equals the initial thermal conductivity divided by expansion ratio factor R. A different point is that temperature dependent properties are considered in the first place; while for specific heat and density, constants are used as the initial value. This is due to the fact that the thermal conductivity plays a significant role in intumescence. The effective thermal conductivity is finally expressed as:

$$k_{p,eff} = k_p \cdot R \tag{3.20}$$

with:

$$k_p = f(k_0, T) \tag{3.21}$$

Consistent with the temperature dependent function for thermal conductivity in *JOSEFINE* (BRE, 2003), *GeniSTELA* used the following equations to represent

a general temperature-varying thermal conductivity:

$$k_p = (k_0 + KTFactor \cdot T) \cdot (k_{poly2} \cdot T^2 + k_{poly1} \cdot T + k_{poly0}) \tag{3.22}$$

where

k_0	is the dry thermal conductivity, $[W/(m \cdot K)]$
$KTFactor$	is a temperature effect factor, $3e^{-6}$ $[-]$
$k_{poly0}, k_{poly1}, k_{poly2}$	are variables used to fit with the experiment, $[-]$

3.7 Assumptions

Due to the complexity of fire flow and structural responses within the compartment, it is rather difficult to predict accurately the performance. As a consequence, some approximate assumptions with no significant penalty for the overall performance prediction are made to ease the difficulty of solving the problem, summarized as follows.

- *GeniSTELA* is considered as a field model giving field thermal response predictions.
- It couples CFD calculation with simple heat transfer within the structural components. In the model, the simple structural components are omitted from the CFD model, on the assumption that their interference with the flowfield is minor, which is normally true for most natural fire phenomena. This assumption greatly improves the computational efficiency of *GeniSTELA*, since the CFD program need only be run once, allowing simultaneous calculations with varying structure related parameters as well.
- For the 1D numerical model construction, several assumptions are made, as per below:
  - From the energy aspect, as also seen in the energy balance equation (Equation 3.1), the transient state assumption is made for both steel and protection layers, which could give a more accurate solution.
  - From the temperature distribution aspect, as seen in the two boundary condition equations (Equations 3.2 and 3.3), quasi-steady state approximations are used. Here, the introduction of a weight factor

covers the transient heating effect, thus thus the method is referred to as "quasi-steady state" rather than "steady state". Besides, ρ_s, c_{ps} are much greater than ρ_1, c_{p1} and ρ_2, c_{p2}, the transient effect on the steel temperature can be well expressed in the main governing equation (Equation 3.1). Though the fully transient state can also be solved for boundary conditions, it is obviously much more complicated and the difference on the boundary condition is tiny using either fully transient state or quasi-steady state.

- For the boundary condition, a method similar to the Neumann time-varying boundary condition is adopted, in which the heat flux due to radiation and convection at the fire interface is specified. The temperature of the insulation layer at the fire interface is determined as a surface temperature which considers the heat loss through radiation and convection from the fire gas to the insulation surface. The heat loss is negligible for most of the insulation materials, such as intumescent paint, gypsum plaster, ceramic blanket, etc., with high thermal resistance, where thermal energy can be effectively "blocked" by insulation and accumulated at the fire interface, rendering a negligible temperature difference compared to the fire gas. However, it could cause significant errors for protection materials with a relatively low thermal resistance, such as concrete, as also investigated by Wong and Ghojel (Wong & Ghojel, 2003). Consequently, as a general engineering tool, *GeniSTELA* considers the heat loss through surface radiation and convection from the fire gases to the insulation surface.

- For the 2D/3D effects corrections, the following assumptions are also made.
  - The junction effect correction only considers the heat conduction within the member. This assumption is made by the reason that the whole system is heat balanced, as confirmed in 1D model. No heat is self-generated within the component, but only flows from one place to another.
  - For the end effect correction, it is assumed that the radiation heat fluxes from different directions are equal at the edge of the component. Thus, the overall energy from radiation equals that of a single direction radiation heat flux multiplying with main direction numbers according to different cases. Though the radiation in fact arrives over

the surface of a sphere from all directions, it is quite complex and taking this detail into account would be greatly demanding computationally as it would involve passing directional informational. Strictly, application of both uni- and bi-directional radiative fluxes should be accommodated in the model analysis, with the most conservative result assumed (in order to avoid running parallel calculations for all possible component orientations). However, though there is provision of the code for differentiating for two heating faces, it is considered that the simplified treatment in *GeniSTELA*, i.e. assumed uniform radiative fields, could provide sufficiently accurate results for the final thermal response prediction. Therefore, the results presented in the thesis are obtained from *GeniSTELA* by considering only the case where heat comes equally from both sides of the protected structural element. As mentioned before, this is due to the simple fact that in order to do anything more elaborate, i.e. to take directional effects into account, requires more information. Specifically, it would be possible to look at the effects of assuming different orientations of beam and column (most simplistically, in orthogonal directions, i.e. four orientation cases - these could be further parameters in the 'SensVari.txt' parameters file) but this could only be linked for heat flux boundary conditions at the cost of a much more detailed computation of the face fluxes, i.e. using the directional radiance values. Since it would not have been practically possible to do the later, a simple solution would be to look at the two extremes of uniform heating (same incident flux on each face) and purely unidirectional heating, where an equivalent total power is specified for the incident radiation. Hence, this part of study has now been extended to consider the case where the heat flux comes from one direction, i.e. if there are important directional effects.

It should be noted that it is only possible to establish a true equivalence in the boundary conditions in terms of radiation, since the convective flux is confounded by the thermal response of the member. This is most easily achieved by simply setting the convective heat transfer coefficient to zero, a scenario which corresponds to the remote heating scenario, i.e. where the heat source(s) are distant from the member.

A comparison of the increment of steel temperature with time between unidirectional heat flux and uniform (i.e. bidirectional) heat flux definitions is made for two different cases. In the first, the radiative heat flux used is equivalent to $1000°C$ radiative temperature on each side. For unidirectional heating, this corresponds to $1220°C$ on the exposed side (and ambient on the unexposed side); these values are high but are intended to represents a realistic upper limit for large fire scenarios. A second case, with a much more moderate $500°C$ equivalent temperature driver, is also studied to investigate the generality of the result. The steel temperature rise for both cases is shown below in Figures 3.16 and 3.17.

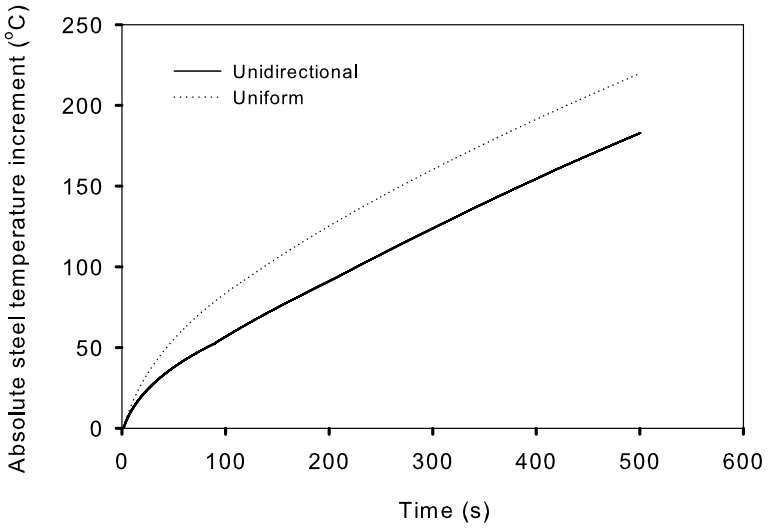

Figure 3.16: The absolute steel temperature increment between unidirectional and uniform heat flux for $1000°C$ equivalent heat flux on both sides

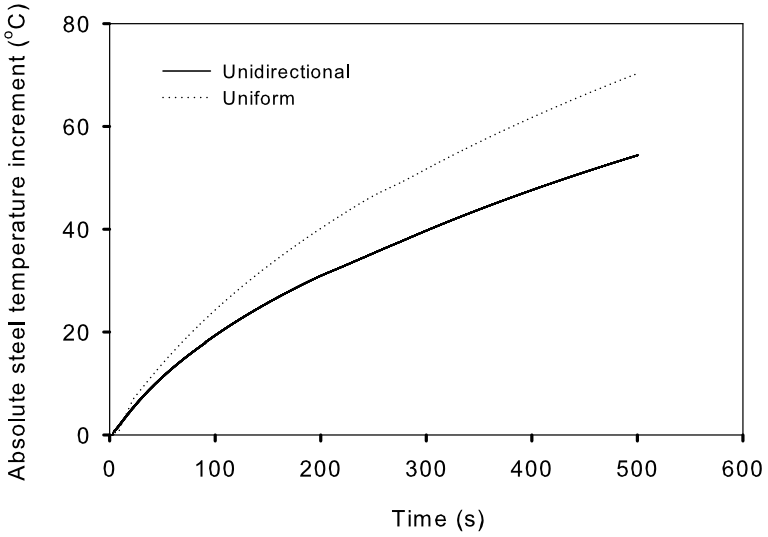

Figure 3.17: The absolute steel temperature increment between unidirectional and uniform heat flux for $500°C$ equivalent heat flux on both sides

It is found that with unidirectional heating, the steel temperature rise is slower than uniform heating. The difference is increasing while the overall heat energy is increasing. The ratio of the two prediction results both lie around 0.8, as seen in Figure 3.18 below, i.e., the difference is about 20%. However, in reality, this is a rather artificial scenario and pure remote radiative heating is unlikely since some degree of convective heating would normally exist (though it could be negligible when the steel temperature is very high, where convection is relatively small with regards to the radiation). For most cases, the above result provides an indication of the upper limit for the difference, that is to say, it would not be greater than 20%, though more cases would need to be examined to investigate the generality of this conclusion. However, it is encouraging that the differences are relatively low; moreover, the uniform heating predicts more conservative steel temperature results. This confirms that it may not always be necessary to specifically consider the effect on differential thermal exposures and large errors are not anticipated for practical scenarios. However, where there is confidence that localized fires will be present, it may be worth providing an explicit treatment of one side heating in order to generate more

accurate steel temperature predictions.

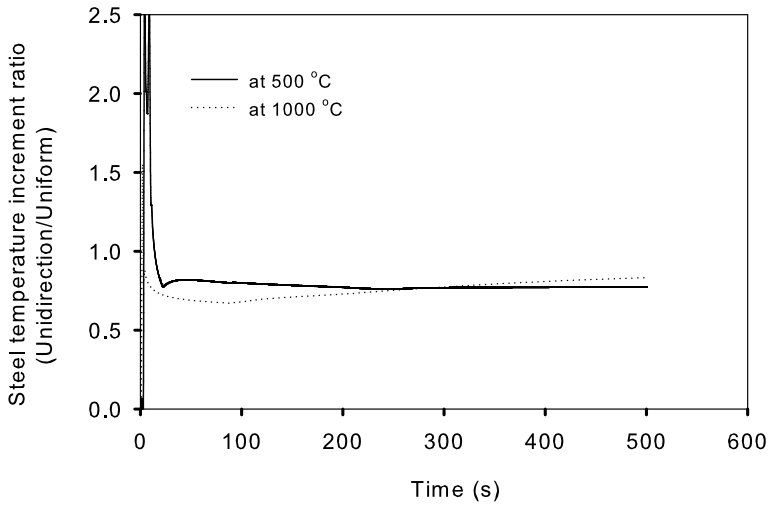

Figure 3.18: Steel temperature increment ratio between unidirectional heating and uniform heating

The effect of these assumptions is further discussed in the later chapters.

Chapter 4

Implementation, Verification and Validation

4.1 Introduction

For the practical application of the methodology, the above conceptual model has been implemented firstly as spreadsheet-based localised model and then as CFD linked model called *GeniSTELA* within the *SOFIE* RANS CFD code (Rubini, 1997). Thereafter, it has been examined with a single universal beam insulated over the entire profile and subjected to a localised fire for initial verification of the model. The influences of input parameters are studied by exercising the model with different sets of input parameter values. The performance of the model was assessed by performing sensitivity studies, looking at the effects of a range of numerical and physical parameters. Comparisons were also made with the results from the EC3 protected member equation (BSI, 2005a). Altogether, three main aspects have been examined to verify *GeniSTELA* - the model predictions, the significance of 3D effects corrections, and the significance of the Newton-Raphson procedure for updating the protection surface temperature, respectively.

Two cases are used for further verification and validation of the model: standard tests in fire resistance furnaces and the post-flashover BRE large compartment fire test. Comparison with the test results permits model validation whilst model capabilities are demonstrated by considering a range of parameters of interest, including member size and protection material properties. The results enable

identification of the critical parameters which affect the thermal performance.

4.2 Model Implementation

The spreadsheet-based model implementation is the development stage of the method. It was used for the purpose of sensitivity studies and to test the modelling method. The CFD linked model implementation serves the purpose to link the quasi-3D thermal analysis model to CFD, exploiting the calculated radiation fields and local gas temperatures. For both implementations, a relatively simple treatment has been adopted, with a lumped parameter model being used for the steel and the coupled thermal response of the protection layer modelled with an analytical treatment for transient heating, allowing for spatially and temporally varying temperature gradients within the solid. Representative values are used for some parameters such as the initial conditions, the dry thermal properties, etc. and exact values are used for several possible factors that might affect the transient response, such as the temperature-dependent thermal properties In the CFD implementation, the main input parameters are provided externally in a data file, called 'SensVari.txt'. The decision as to whether *GeniSTELA* should carry out the simulation on the basis of the simple 1D conceptual model alone, or exploiting the corrected quasi-3D conceptual model, is made at run time. To define this, the implementation allows the logical correction flag to be modified through the input data file. *GeniSTELA* is therefore a coupled CFD-thermal analysis methodology.

4.3 Initial Verification

A case of a universal beam insulated over the entire profile has been studied by modelling with *GeniSTELA*. The prediction have been verified by comparison with simplified thermal calculations, including the (empirical) Eurocode specified methodology (EC3) (BSI, 2005a) for protected steelwork and by conducting a sensitivity study. Two types of models, i.e. the basic 1D conceptual model and the full quasi-3D model, have been studied, in order to verify the significance of the correction terms. A modified model based on *GeniSTELA* has been studied to

verify the significance of the interactions with the protection surface temperature between the solid and the gas phase. The modified model replaces the existing Newton-Raphson procedure to update the protection surface temperature with a value equal to the local gas temperature, approximating to an adiabatic case (assuming convection is dominant). This part of the study has also been compared with the literature, especially the studies carried out by Wong and Ghojel (Wong & Ghojel, 2003) and Wickström (Wickström, 1985, 2007).

4.3.1 Problem definition

The case studied for initial verification is a universal beam insulated over the entire profile subjected to a localised fire. The element used was an I-section steel beam of overall dimensions $3.6m \times 0.254m \times 0.254m$; the thickness of the web was $8.6mm$ and the flange $14.2mm$. The beam was insulated with Fendolite MII sprayed fibre fire protection material of thickness $12.5mm$. It was positioned below a ceiling slab consisting of Perlite (mineral fibre) board of dimensions $3.6m \times 1.83m \times 0.024m$ and at a height of $1m$ above the upper surface of the burner. A propane burner of $0.3m$ diameter was located below the center of the ceiling assembly, providing a $100kW$, $10min$ steady fire. Figure 4.1 below illustrates the model setup for this specified problem.

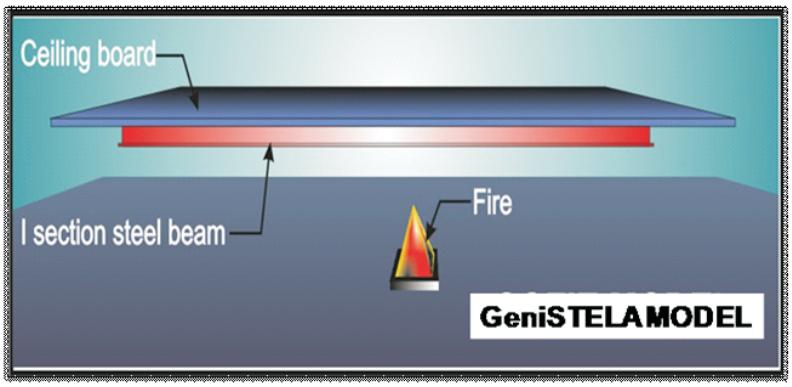

Figure 4.1: Profile insulated steel beam subjects to a localised fire

The steel material properties used in the model were based on the Eurocode (EC3) and the protection material properties were the same as that supplied

from the manufacturer. A 1% moisture content was assumed together with a surface emissivity equal 1.0. All of the parameters are input into the 'SensVari.txt' file. Besides, due to symmetry, one quarter of the element is modelled to reduce the computational effort.

4.3.2 Model prediction

The model based on the EC3 (BSI, 2005a) methodology together with the *GeniSTELA* model have been used to simulate the aforementioned case. The relevant gas temperature and inverted radiation temperature from CFD calculation are shown in Figure 4.2. The comparison results in terms of the steel temperature prediction between empirical methods EC3 (BSI, 2005a) and *GeniSTELA* are presented in Figure 4.3. The results are obtained from a location 1.075m above the fire source, 2.05m away from the center of the beam in the axial direction and 0.406m away from the central line of the beam web.

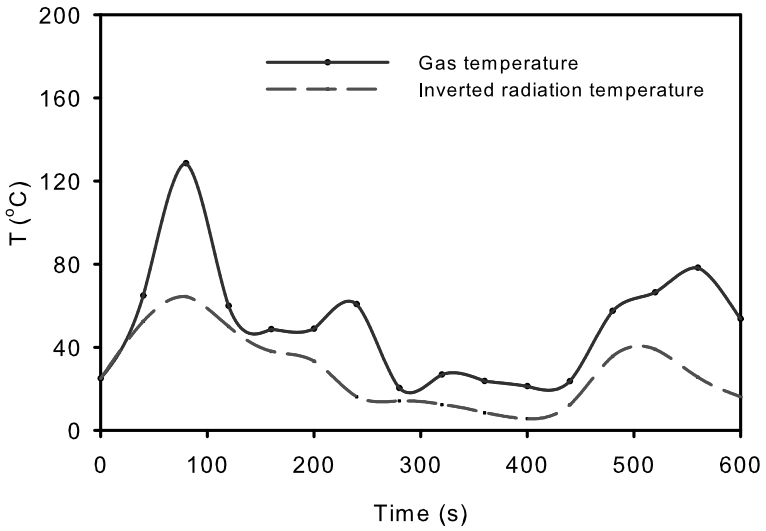

Figure 4.2: Gas temperature and inverted radiation temperature obtained from CFD calculation

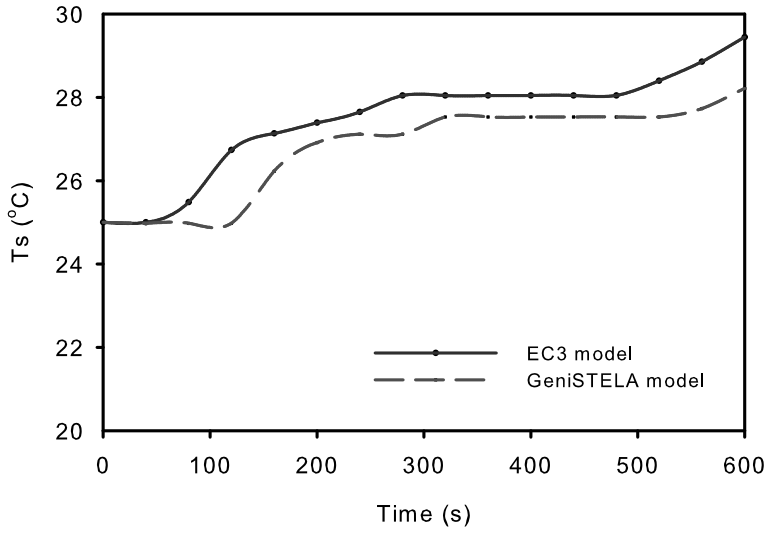

Figure 4.3: Comparison of steel temperature prediction using *GeniSTELA* and EC3 methodology (BSI, 2005a)

In general, the results are consistent with each other in terms of the prediction trend. There are discrepancies in a few aspects, but these may be resulted from the more advanced treatment provided by the *GeniSTELA* methodology over EC3 (BSI, 2005a) empirical methodology. Firstly, it is seen that in the first 100 seconds, a flat plateau is observed from the *GeniSTELA* prediction, which is an evidence of the transient heating in the protection. From literature review, the transient heating is found to be important during the heat transfer process, but this has been oversimplified in the EC3 (BSI, 2005a) method. Prediction from EC3 (BSI, 2005a) method is higher than the *GeniSTELA*, which might due to the over conservative drawback of the empirical method itself, since the temperature rise in EC3 (BSI, 2005a) is driven by the local gas temperature, where the inverted radiation temperature is not taken into account. This might cause serious errors, especially when the structure is in the cold layer where convection dominates, the EC3 (BSI, 2005a) prediction would be undermined due to the low local gas temperature.

In addition, unlike other models which could only provide one simulation result for one specific case with a fixed set of parameters, *GeniSTELA* provides field simulation results within one simulation. Figures 4.4 and 4.5 present an example

of field results at the end of 600s, which are the illustrations of gas temperature field and steel temperature field prediction, respectively. The beam inside each of the graph is a "virtual" beam, which could be anywhere within the compartment. There are several fluctuations in the steel temperature field prediction result, which is caused by the radiation ray effect in the CFD calculation. This could be solved by increasing the ray numbers. However, with the increasing of the ray numbers, the computational cost would also be increased. The present ray numbers are enough to demonstrate the field result prediction here.

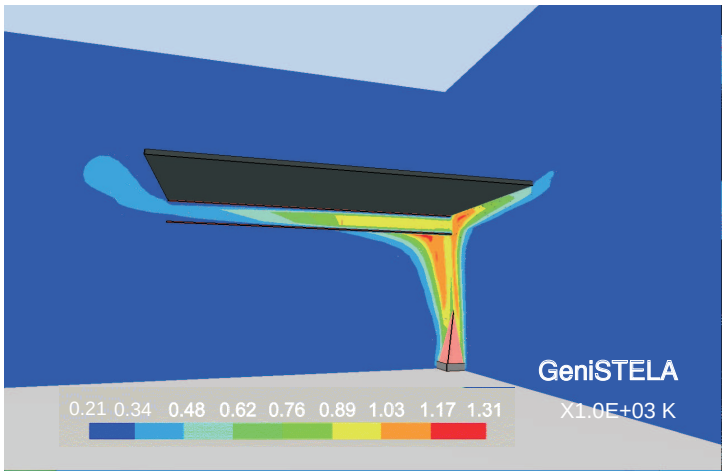

Figure 4.4: Gas temperature field prediction

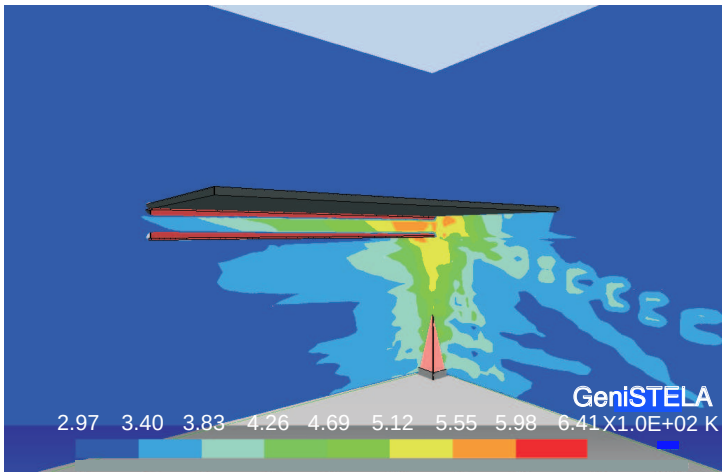

Figure 4.5: "Virtual" steel temperature field prediction

GeniSTELA is further studied with varying parameters, such as the member size and member thermal properties, for instance, emissivity. Figures 4.6 and 4.7 below demonstrate examples of changing the steel member thickness and protection material parameters in terms of the material types and protection thickness. The results are obtained from a location $0.899m$ above the fire source, $1m$ away from the center of the beam in the axial direction and $0.15m$ away from the center line of the beam web. A similar study has been done previously with the empirically-based EC3 method (BSI, 2005a), and the sensitivity study results have been compared. The results prove that the model is highly sensitive to the change of some of these parameters, and the change in *GeniSTELA* is found to be compatible with that from EC3 methodology. That is to say, with bigger flange thickness and/or with thicker protection layers, the lower steel temperature that will be predicted, thus enabling the initial verification of *GeniSTELA*.

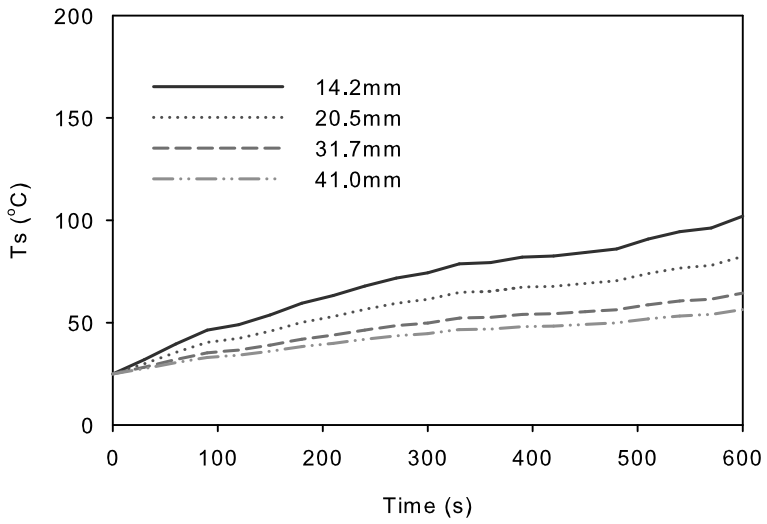

Figure 4.6: Steel flange thickness effect

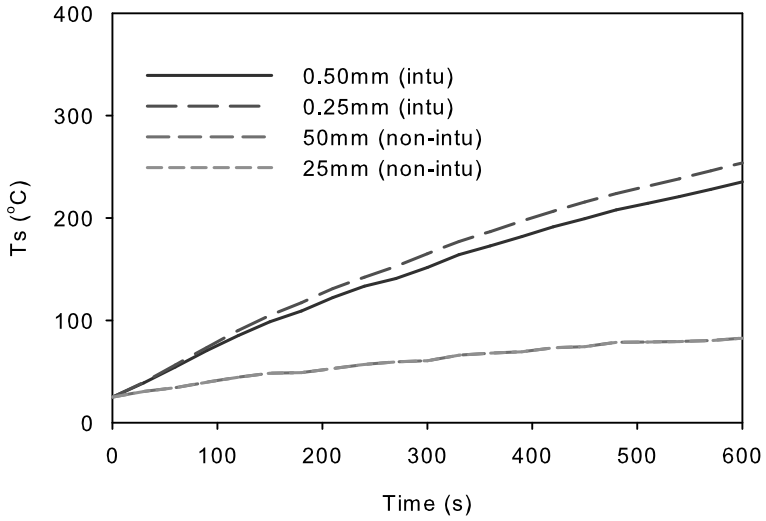

Figure 4.7: Protection thickness effect

4.3.3 3D effects corrections significance

Based on the above case study, *GeniSTELA* model has been examined and verified in more detail. Firstly, the 3D correction effects have been investigated. Two types of models based on *GeniSTELA* have been applied to this case, one of which uses quasi-3D model with consideration of 3D correction effects, while the other does not include those corrections, using the basic 1D model. The comparison results from the two types of models are presented as follows, which based on three possible "worst case" cell locations, denoted as cell 1, 2 and 3 in the representative Figure 4.8 below:

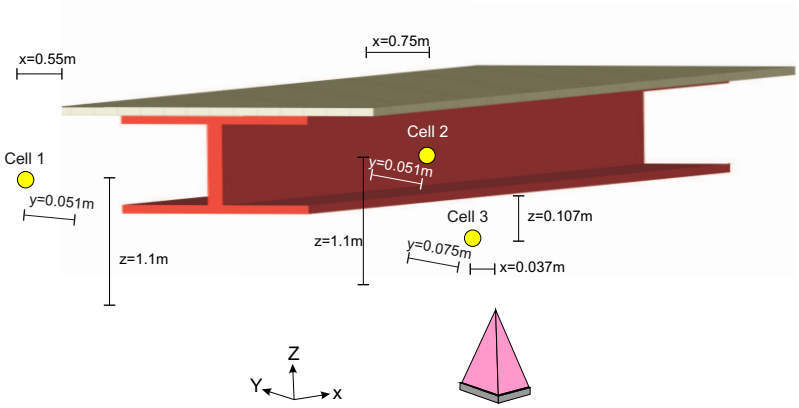

Figure 4.8: Cell locations for 3D effects correction

The related grid numbers in the modelling mesh for each cell of interest are as follows:

- Cell 1: $x = 9$, $y = 21$, $z = 28$
- Cell 2: $x = 35$, $y = 21$, $z = 28$
- Cell 3: $x = 56$, $y = 36$, $z = 20$

Figure 4.9 shows the steel temperature prediction against time while Figure 4.10 shows that along the axial distance for all three locations. Half of the axial distance is plotted, and the scale ranges from the end cell of the beam to the middle cell along the beam in the axial direction.

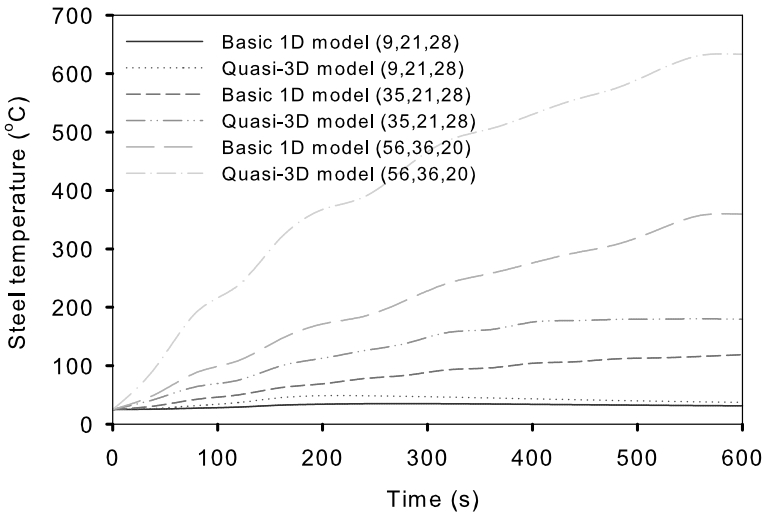

Figure 4.9: Steel temperature prediction against time using models with and without 3D corrections

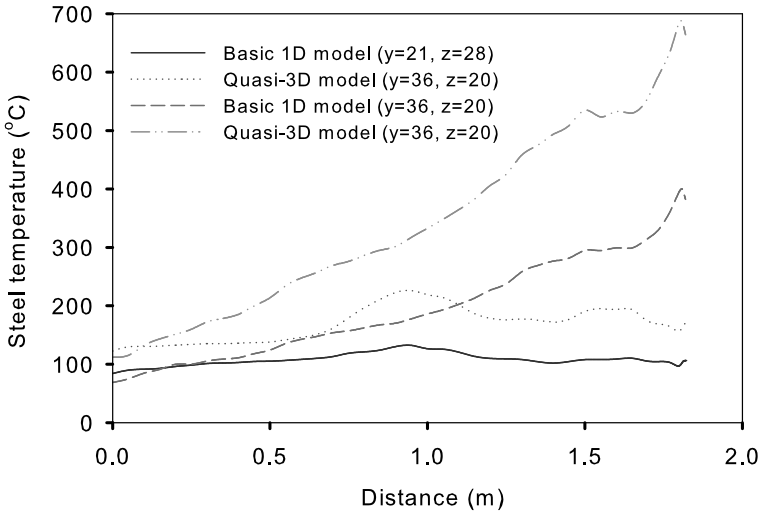

Figure 4.10: Steel temperature prediction along the axial distance using models with and without 3D corrections

The percentage differences using the two types of models have also been plotted as in Figures 4.11 and 4.12.

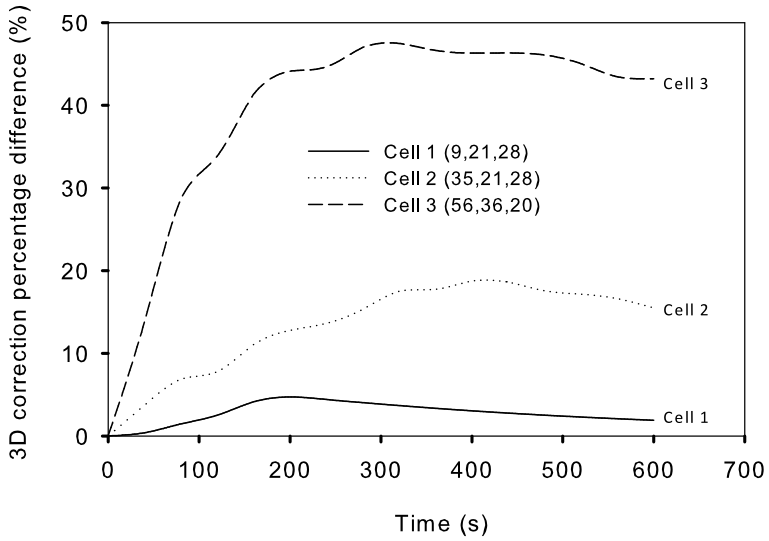

Figure 4.11: Percentage difference in steel temperature prediction against time using models with and without 3D corrections

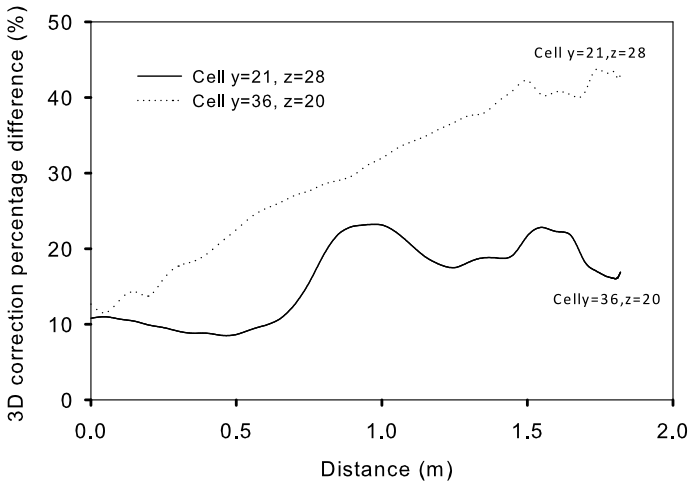

Figure 4.12: Percentage difference in steel temperature prediction along the axial distance using models with and without 3D corrections

The above 3D corrections are done for column or beam in a vertical direction. It is found from the figures that generally, when adopting the 3D corrections, the prediction results are higher than the one without 3D corrections. Nevertheless, those 3D effect corrections are found to be as small as within 5% when it located far away from the steel beam (Cell 1 in Figure 4.11), but the temperature prediction is highly affected when the cell is underneath or very close to the beam,

as that of Cell 3. This is true since when the fire source, where the main radiation comes from, is set right below the beam, the heat flux travels less distance than to other locations, thus less heat loss. More energy will reach the beam, strongly affecting the steel temperatures in the particular cells close to the beam and vice versa. More significant 3D effects have been observed in Cell 2, since even though it is located in the same horizontal level, it is closer to the fire source. Taking the cell away from the beam into consideration, i.e, Cell 1, the percentage difference of the cell temperature prediction is within 5%, and even for Cell 2 within 20%, which means the 3D effect could be ignored in those locations. In practice, the 3D effect corrections are test scenario dependent, and they should be used when necessary. For example, the end effect correction is important for a localized fire case, the junction effect correction for elements having no direct exposure to the dominant radiative heating, and the axial correction for the case when a big temperature gradient is subjected. The results here confirm that the 3D effect corrections could be often be ignored, as already implemented in the *GeniSTELA* where those effects are only turned on when they make results worse.

4.3.4 Newton-Raphson procedure significance

In the *GeniSTELA* model, a Newton-Raphson (NR) procedure is used to update the protection surface temperature which is then used for the steel temperature calculation in the same time step. Some literature states that the protection surface temperature might not significantly affect the final steel temperature prediction (BSI, 2005a; Wong & Ghojel, 2003). Therefore, a simple assumption is suggested, such as that in EC3 (BSI, 2005a), in which the protection surface temperature is simply considered hot, i.e., the same as the effective local gas temperature. That is to say, the radiation heat flux loss is zero when it travels through the gas phase to the solid surface. The significance has been studied here by a comparison of two types of models, one of which uses Newton-Raphson (NR) procedure to update the protection surface temperature, as that in the *GeniSTELA* model, while the other adopts the simple assumption. The comparison results of the final steel temperature against time and that along the axial distance have been reported and demonstrated as in Figures 4.13 and 4.14. Within those figures, the legend "NR model" represents the model that adopts

the Newton-Raphson procedure to update the surface temperature and "Simplified model" represents the model using the aforementioned simple assumption where surface temperature is assumed the same as the local gas temperature.

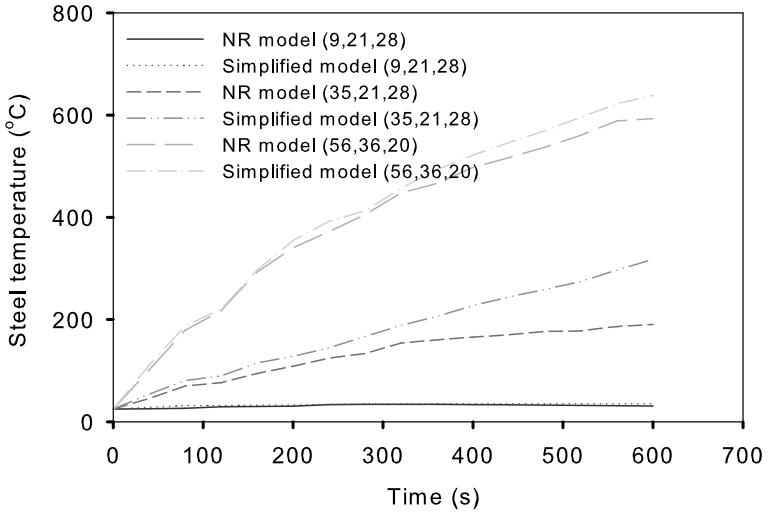

Figure 4.13: Steel temperature prediction against time using two different types of models for surface temperature calculation

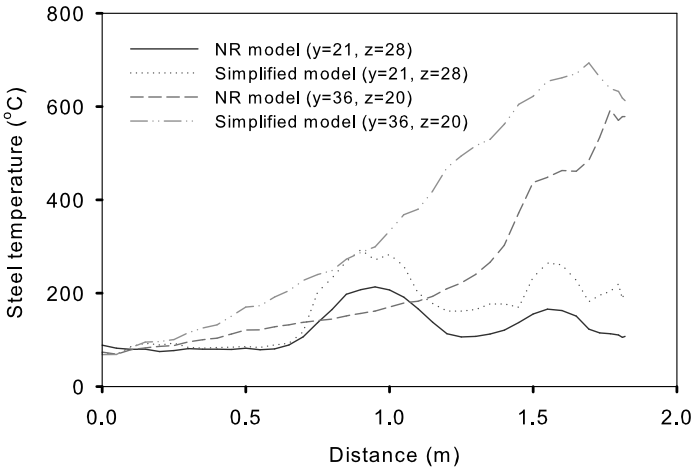

Figure 4.14: Steel temperature prediction along the axial distance using two different types of models for surface temperature calculation

Similarly, the percentage differences of those two types of models have been anal-

ysed and shown in Figures 4.15 and 4.16 as below:

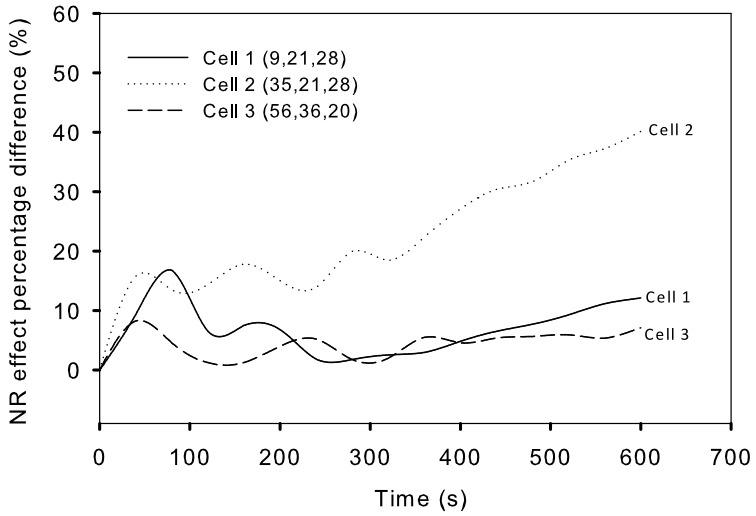

Figure 4.15: Percentage difference in steel temperature against time using two different types of models for surface temperature calculation

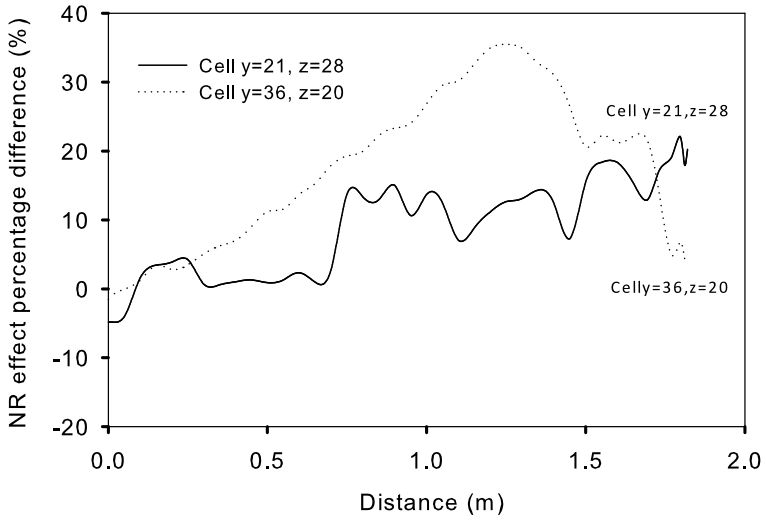

Figure 4.16: Percentage difference in steel temperature prediction along the axial distance using two different types of models for surface temperature calculation

The above results show that, when the cell of interest is considered as the cell far away from the fire source or from the structural member, the effect of either

using Newton-Raphson procedure or simplified assumption to predict the surface temperature is relatively small, within 20%. However, the effect becomes significant when the cells are located close to the fire source. This is because at those locations near the fire source, the local gas temperature is higher, and the simple assumption leads to a high surface temperature, with knock-on effect on the steel temperature. This could result in a big error since the heat energy driving steel temperature rise is not only related to the absolute surface temperature, but also to the temperature difference between the local gas temperature and the surface temperature. Therefore, at the locations where there is big difference between local gas temperature and the element surface temperature, possible significant effects of reasonably predicting the final steel temperature might occur. This confirms the necessity of using Newton-Raphson procedure within *GeniSTELA*.

A sensitivity study with varying protection material properties has been carried out. Results below are based on two types of protection materials: high density concrete and Fendolite MII, which are the representatives of the following two types of insulations respectively: insulations with high density and conductivity and insulations with low density and conductivity. It should be noted that high density concrete is not a typical protection material in practice, and it is only used for test purpose here. The thermal properties of concrete used are: $\rho_p = 2600kg/m^3$, $c_p = 677J/kg/K$, $k_0 = 1.0W/m/K$ and that of Fendolite MII used are: $\rho_p = 680kg/m^3$, $c_p = 970J/kg/K$, $k_0 = 0.19W/m/K$. A thickness of $0.0125m$ has been applied for both types of protection. An example of the results for cell locations 2 are shown in Figure 4.17 here.

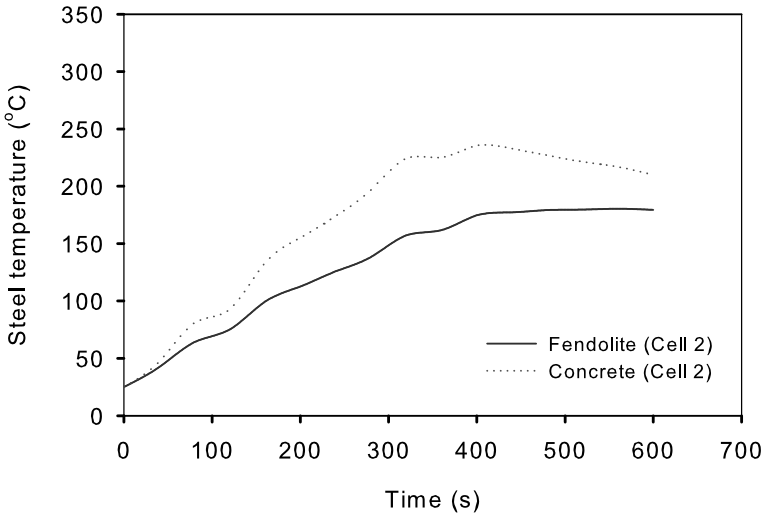

Figure 4.17: Steel temperature prediction for two types of protection materials at Cell 2

The percentage differences in terms of steel temperature prediction for the two types of protection materials, when using either NR model or Simplified model models for surface temperature, are also displayed as in Figure 4.18.

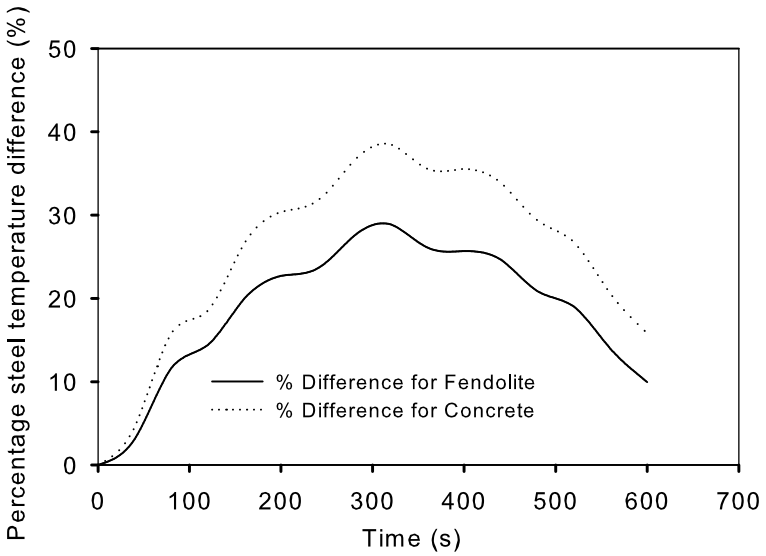

Figure 4.18: Percentage steel temperature difference using models with and without NR procedure for two types of protection materials

From the results, it is clearly seen that the difference between using two types of model for surface temperature is greater when the member is protected with high density and conductivity protection materials, to a maximum extent of 15% greater than that for low density and conductivity material. A similar study has been carried out by Wong and Ghojel (Wong & Ghojel, 2003), using two types of protection material: concrete and fibre board protection. By comparison, the above results confirmed that the difference would be significant when the insulation has high density and conductivity, in which case, the accuracy of protection surface temperature prediction is of paramount importance and the exact solution using Newton-Raphson procedure for surface temperature prediction is required.

The CPU time for the two types of models has also been checked. It is found that, for each time step, the absolute difference is within $0.3s$ and percentage difference is within 20%. For the overall CPU time spent during the simulation, the difference is tiny, less than 1% for $600s$ simulation. The results show that the additional CPU caused by the Newton-Raphson iteration procedure is negligible. The implementation of this procedure into *GeniSTELA* will not do any harm regarding the computational cost, but would help with the solution accuracy, especially for the case when the protection surface temperature has great impact on the final steel temperature prediction.

4.3.5 Brief summary

In summary, the above studies are conducted in terms of the prediction capabilities, the 3D effects corrections significance as well as the Newton-Raphson procedure significance within *GeniSTELA*. The results show sufficient evidence that *GeniSTELA* could give sufficiently accurate field results with reasonable computational costs. The correction terms and Newton-Raphson procedure adopted within *GeniSTELA* are necessary as part of a general thermal analysis methodology. The results indicate that *GeniSTELA* could be a potentially applicable generalised methodology and therefore, necessitates further investigations of *GeniSTELA*.

4.4 Verification and Validation

According to *AIAA* (American Institute of Aeronautics and Astronautics) (AIAA, 2005), the verification is like to solve the equation right while validation is to solve the right equation. The verification is a low level activity which is the process of determining that a model implementation accurately represents the developer's conceptual description of the model and the solution to the model, while the validation is a high level activity, which is the process of determining the degree to which a model is an accurate representation of the real world from the perspective of the intended uses of the model. Briefly speaking, verification is to test the correctness of the solution to the modelling while validation is to test the efficiency of the model to the real physical phenomenon. Similar definitions are also available by Roache (Roache, 1998).

The study described in the last section provides the initial verification of *GeniSTELA* based on a simple protected beam problem. To ensure its general application, verification and validation processes regarding practical test cases are demanded. In this work, two full-scale application examples are provided to further verify and validate the method. The first case is a standard fire resistance test apparatus, based on the Warrington $9m^3$ wall furnace, and the second is the post-flashover BRE large compartment fire test. A furnace test is chosen in order to decouple uncertainties in temperature prediction from the thermal response problem whilst at the same time assessing the latter in the context of results available from testing. For this to work, it is clearly essential that the basic CFD model must reproduce the standard temperature-time curve, as a minimum, and to achieve this could be quite challenging, not least because no detailed information is normally available on the gas flow rates in furnace testing. Nevertheless, it is possible to achieve a match at least at the level of the overall furnace temperatures by iteratively adjusting the gas flow rates, as has been reported previously (Welch & Rubini, 1997). The results of the furnace simulation are used to verify the model for thermal response of protected components, referencing expected performance based on fire resistance ratings. The compartment fire test also permits assessment of the predictive captivities for the steel temperature field, but for the more general case of natural fire exposures. Again, it is a challenge to first reproduce the measured thermal fields, though in this case the fuel supply rates can be determined at least approximately by reference to crib mass loss data (Lennon & Moore, 2003; Schleich *et al.*, 2003; Welch *et al.*, 2007). Another

significant uncertainty in natural fire derives from the lack of information on the optical properties of the combustion gases which these were not measured, but sensitivities can be considered based on some assumed values (Welch *et al.*, 2007).

4.4.1 Test scenarios

Two cases, the Warrington full-size fire resistance furnace test and the BRE large compartment fire test, are studied. Their experimental details are described below.

4.4.1.1 Warrington fire resistance test furnace

a. Experimental arrangement

Figure 4.19 shows a view of the fire resistance test furnace with the front specimen removed. The internal dimensions of specimen and exhaust walls are $3.08m$ high by $3.06m$ wide; the width of the furnace, i.e. distance between the specimen wall and the exhaust wall shown at the rear, is $0.93m$. There are a total of fourteen burners arranged opposite each other in two sets of seven. Here, the test specimen is taken to be a steel sheet of thickness $50mm$; all the other walls are lined with a ceramic material, approximately $150mm$ in thickness. The default material properties, for ambient conditions, are listed in Table 4.1 below. Note that even though the test specimen is large compared with the furnace enclosure, *GeniSTELA* is still applicable since the structural element would not influence the air flow within the enclosure, unless heating would come from different directions, which is not the case in this test. Therefore, the results from the one-way coupling *GeniSTELA* methodology is still reliable.

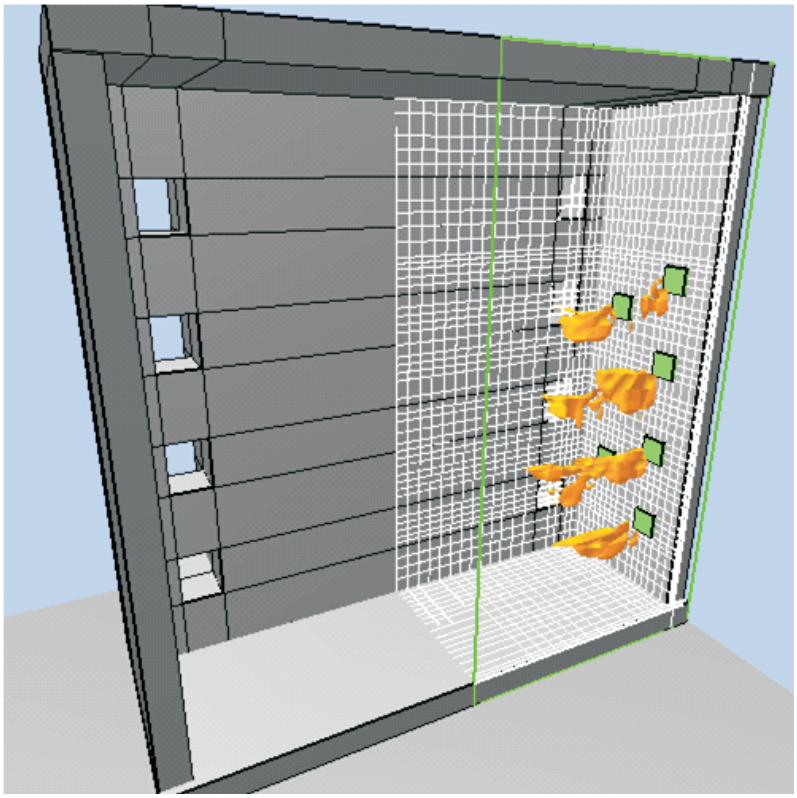

Figure 4.19: Illustration of the Warrington wall furnace geometry

Table 4.1: Physical parameter values of steel and ceramic at ambient temperature (Welch & Rubini, 1997)

	Steel	Ceramic
Thermal conductivity $[W/m/K]$	42.0	0.34
Specific heat capacity $[J/kg/K]$	530	1000
Density $[kg/m^3]$	7850	880
Surface emissivity $[-]$	0.80	0.90

This is a gas-fired furnace with natural gas supplied to the center slot of the burner quarls and sufficient air for a stoichiometric balance via a surrounding duct. In the test, a total of 18 $1.5mm$ thermocouples were used to monitor the gas-phase temperatures. Nine were located $100mm$ from the specimen surface, three positioned on the furnace center line, and three offset $0.7m$ towards the burners on each side. The vertical positions were $0.52m$, $1.43m$ and $2.34m$ from the floor. The other nine thermocouples are located near the exposed specimen surface at equivalent locations (Welch & Rubini, 1997). The positions of the

thermocouples are shown in Figure 4.20.

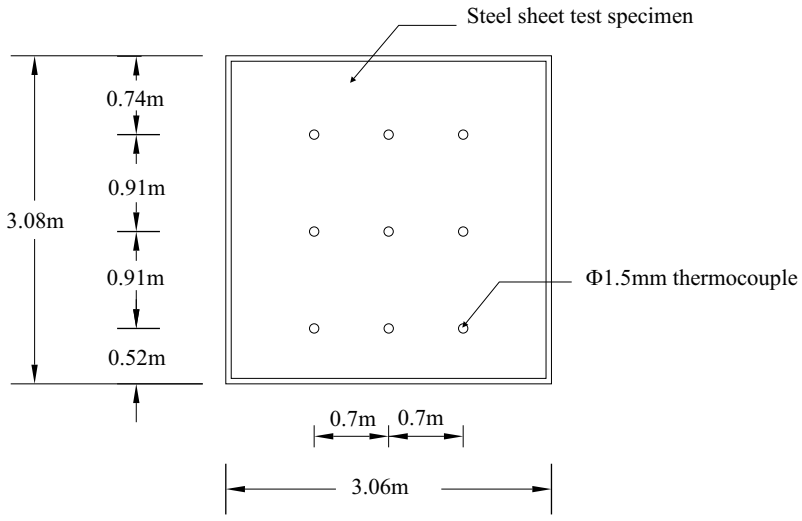

Figure 4.20: Position of the thermocouples in $X - Z$ plane

b. Experimental data

Unfortunately, detailed measurements of gas flow rates are not typically recorded in standard fire tests; however, a nominal value of $2160cu - ft(gas)/hr$ was available for this furnace providing an initial guideline. In simulations with a steel specimen it was found necessary to boost this by a factor of up to three in order to achieve a match with the standard heating curve, i.e. based on the predicted thermocouple temperatures. Figure 4.21 shows the adopted time variation of the overall gas and air flows together with the heat release rate for a single burner.

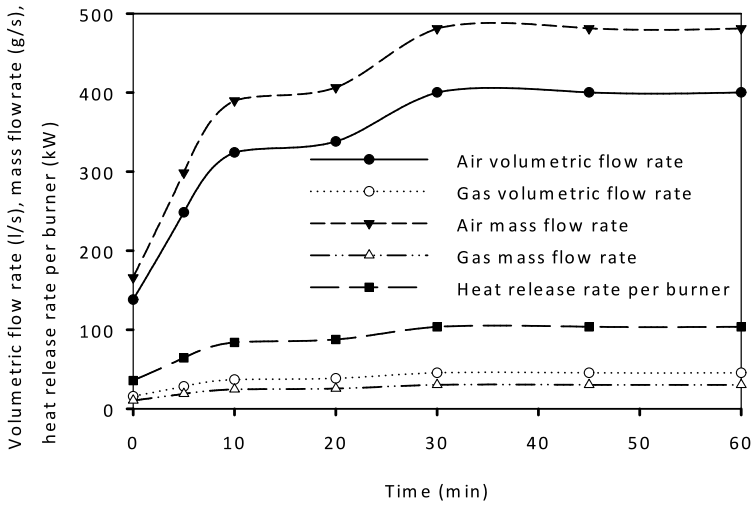

Figure 4.21: Time variation of air and gas flow rates, and burner heat release rate

4.4.1.2 BRE large compartment

a. *Experimental details*

A series of eight full-scale fire tests were undertaken at BRE as part of the European Coal and Steel Community (ECSC) research project, for validation of the Natural Fire Safety Concept (NFSC2). These tests were carried out in a large compartment, nominally $12m \times 12m$ in plan, with a ventilation factor of approximately $0.09m^{1/2}$ and fire loading of $40kg/m^2$ wood or equivalent wood and plastic fuel (Lennon & Moore, 2003; Schleich *et al.*, 2003; Welch *et al.*, 2007). The test variants looked at the effects of ventilation conditions (by varying opening position and geometry), fire load composition (using different fuels, but maintaining the same calorific value) and thermal insulation of the compartment boundaries (by changing the wall lining materials). The detailed analysis of the experimental measurements has been reported for test 8, and the same test is studied here for *GeniSTELA* application. The test details from *in situ* measurements at the time of the test are summarised in Table 4.2 below (Lennon & Moore, 2003; Welch *et al.*, 2007).

Table 4.2: Summary of BRE large compartment test 8

Parameters	**Descriptions**
Fire load type	Cellulosic and plastic – 80% wood and 20% plastic
Geometry	Internal room geometry 12 m x 12 m plan by 2.95 m high
Ventilation conditions	Opening at the front only: full-height doorway centered on each symmetric half of the compartment Geometry: 3.60m wide x 2.95m high with opening factor $0.084\text{m}^{1/2}$
Materials	Light-weight concrete blocks (masonry walls) Precast concrete (ceiling slabs) Steel - 254x254UC73 section (main beams and columns) Sprayed fibre fire protection material (Fendolite MII) applied over underside of ceiling slabs and on beams and columns
Measured parameters	1. Fuel mass loss rate (8 cribs) 2. Gas temperatures 3. Heat fluxes (steel billets measurement devices) 4. Wall temperatures 5. Gas velocities The detailed measurement locations are accessible [6].

The basic nominal/ambient material properties are listed in Table 4.3 below:

Table 4.3: Material properties for BRE large compartment fire test

Material	Thickness $[m]$	Conductivity $[W/m/K]$	Density $[kg/m^3]$	Specific heat capacity $[J/kg/K]$
Light-weight concrete	0.19	0.42	1375	753
Precast concrete	0.15	1.5	2400	1500
Fendolite MII	0.025	0.19	680	970

Figure 4.22 show the pre-test conditions and fire development for tests 1 and 8 (test 1 used no plastic in the fuel load, but was otherwise the same as test 8).

(a) Right hand opening in BRE large compartment prior to test 8

(b) Right hand opening showing early fire development in test 8

(c) Front opening showing later fire development in test 8

Figure 4.22: Pre-test conditions and fire development for tests 1 and 8

a. *Experimental data*

A variety of thermal parameters were measured in the test, encompassing temperatures, velocities and heat fluxes in the gas phase, as well as steel temperatures in protected beams, columns and indicatives, with and without protection, in the solid phase (Lennon & Moore, 2003; Schleich *et al.*, 2003; Welch *et al.*, 2007).

4.4.2 Results and analysis

4.4.2.1 Warrington fire resistance test furnace

The standard heating curve was approximated by running simulations based on the gas/air inflow specifications given in Figure 4.21, cf. (Welch & Rubini, 1997). 30576 cells were used for a symmetric half geometry, using one second time steps, eddy breakup combustion, convected scalar soot (1.2% in inflows) and *DTRM* radiation (2×4 rays). The characteristic furnace temperature was obtained from the weighted average of the predicted thermocouple temperatures at the nine

measurement locations used in the test (see Figure 4.20). Thermocouple temperature predictions were obtained from the in-built thermocouple simulation model (Kumar *et al.*, 2005; Welch & Ptchelintsev, 1997), based on a specification of cylindrical 1.5mm diameter wires. The predicted values varied quite markedly around the furnace, cf. Figure 4.23, as noted previously (Welch & Ptchelintsev, 1997),and there is a knock-on effect on the steel temperature predictions, which peak in the region of the burners, cf. Figure 4.24.

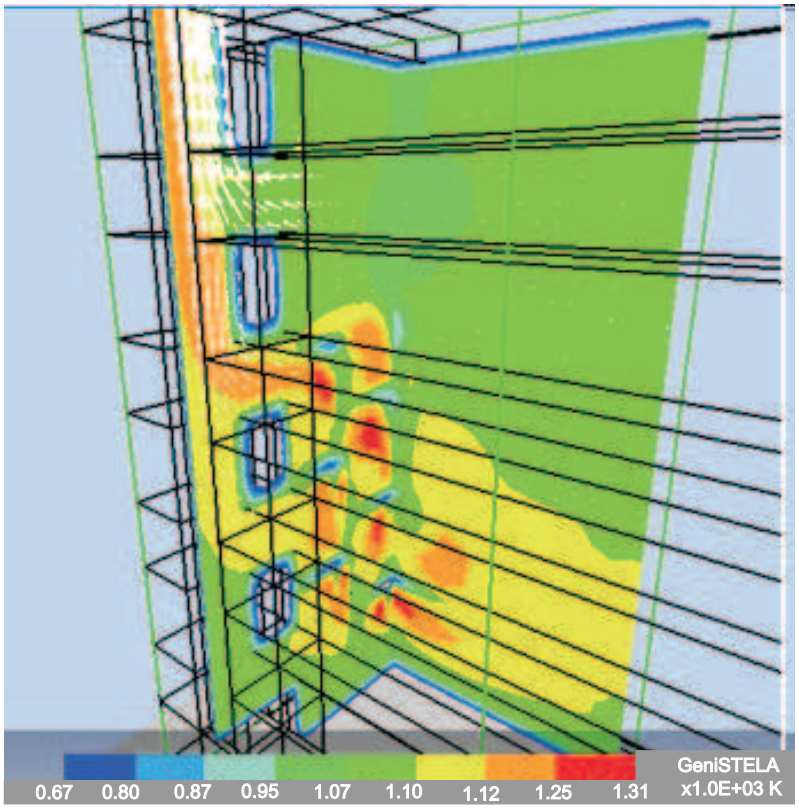

Figure 4.23: Predicted gas temperature field at 1 hour

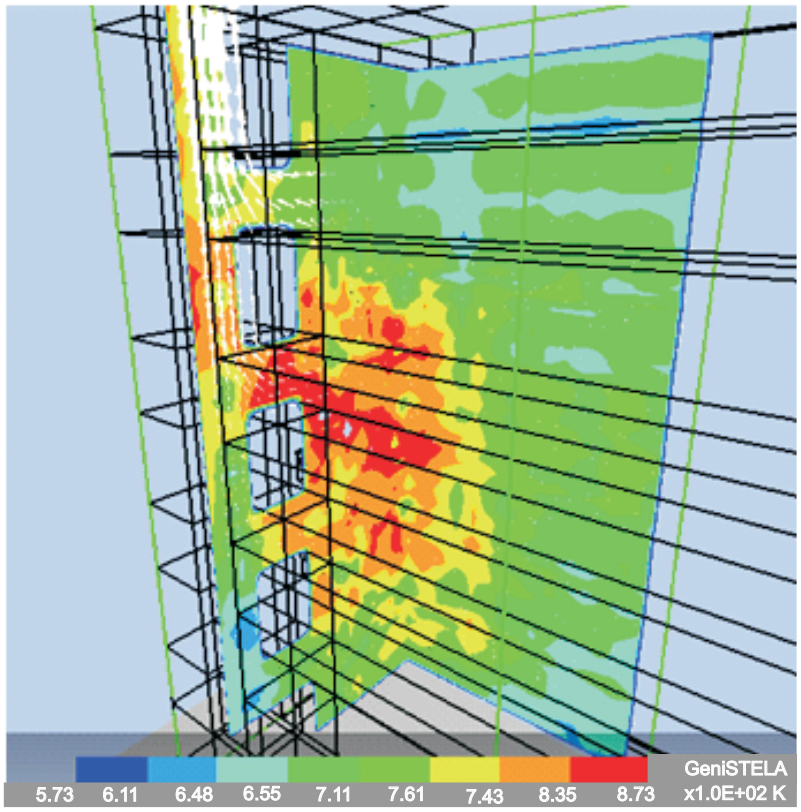

Figure 4.24: Predicted "virtual" steel temperature field at 1 hour

The performance of the *GeniSTELA* model was analysed by running simultaneous computations for different member specifications, around a default of $UC254 \times 254/73$ sections, including different types of protection system (sprayed fibre, and intumescent paint, cf. (Liang *et al.*, 2007)), protection thicknesses and section factors, i.e. flange thicknesses. Transient simulations were performed, with *GeniSTELA* called on every time step.

a. Simulation results

Figure 4.25 shows the various temperature profiles, averaged across the locations of the vertical rakes, at a time of one hour. Even at this stage of the test the non-homogenous nature of the thermal fields are clearly apparent, with some locations having predicted temperatures well in excess of the nominal heating curve, and vice versa elsewhere. However, these are seen not to have too much effect on the steel temperature; the latter is still well inside the $550°C$ contour, consistent with one hour fire rating using this protection system. There are fluctuations for the prediction of steel temperature and thermocouple temperature, which is due

to the numerical error from radiation submodel in CFD calculation. This type of error could be further improved in CFD model, which is not included in the *GeniSTELA* research here.

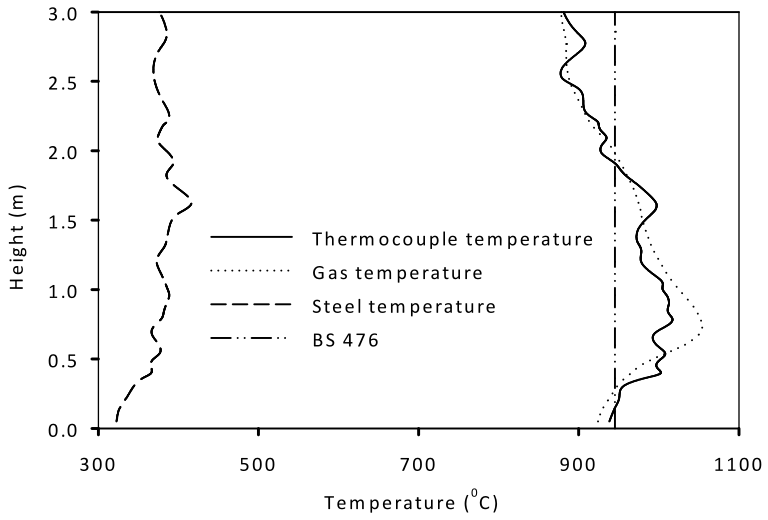

Figure 4.25: *GeniSTELA* predictions of furnace temperature profiles, at 1 hour

b. Sensitivity study results

Some results from a sensitivity study are shown in Figures 4.26 ∼ 4.28 for the effects of changing the steel flange thickness (spanning $UC254\times254/73, 107, 167$), protection thickness ($6.0mm$, $25.0mm$, $100.0mm$) and different types of protection material. The location examined is the same as the bottom left thermocouple location as in Figure 4.20 and $100mm$ from the specimen surface. As expected, the change of section factor as well as the protection thickness has a big effect on the heating rate. For the latter case, the two materials were chosen to be thermally equivalent, i.e. they provide the same fire resistance rating, with the initial thickness of the intumescent being about 100 times smaller than for the sprayed fibre. The computed steel temperatures are consistent with this expected equivalence.

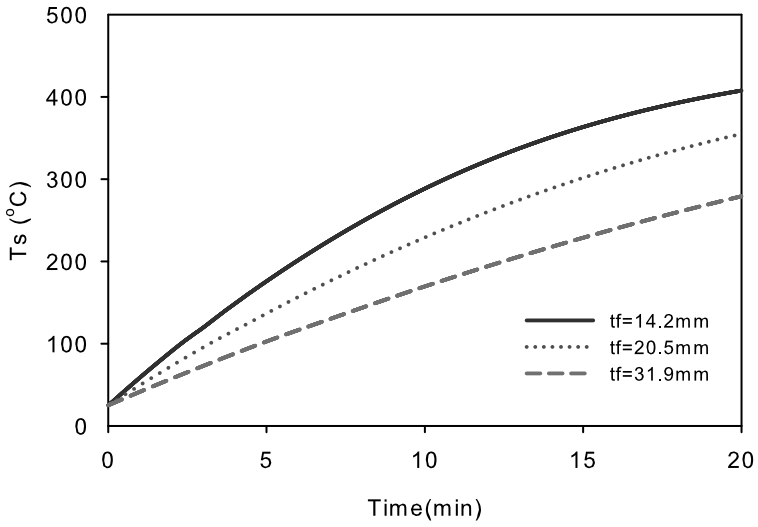

Figure 4.26: Effect of flange thickness on steel temperature

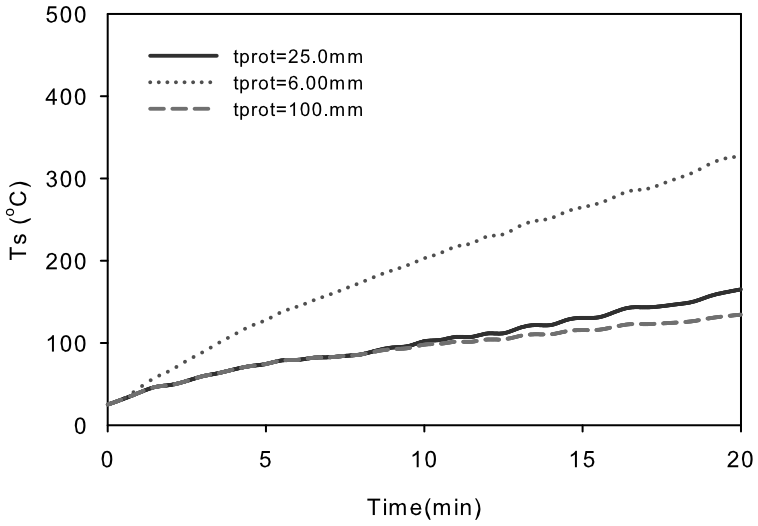

Figure 4.27: Effect of protection thickness on steel temperature

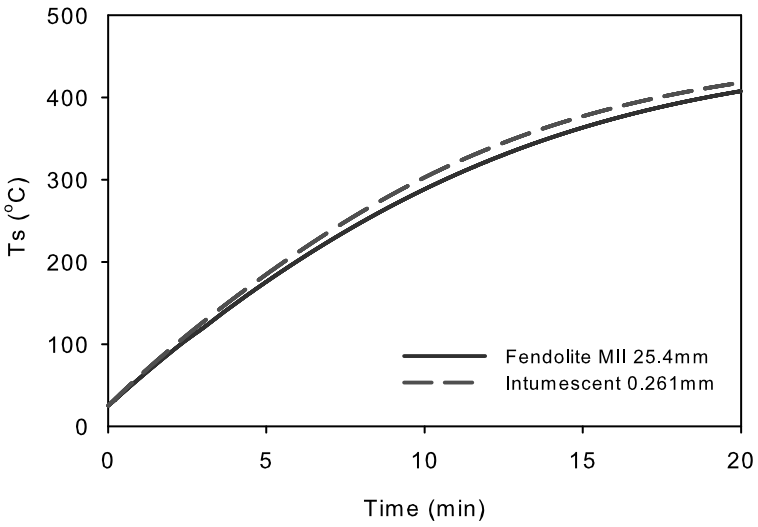

Figure 4.28: Effect of protection materials on steel temperature

4.4.2.2 BRE large compartment

The thermal response of the protected steel indicative, $UC254 \times 254/73$, in the BRE large compartment test (Welch *et al.*, 2007), is examined. The performance of the model was assessed by performing sensitivity studies, looking at the effects of a range of numerical and physical parameters. Comparisons were also made with the results from the EC3 protected member equation (BSI, 2005a; Harmarthy, 1981).

Figure 4.29 provides an illustrative comparison between the experiment and the modelling, for fire test 8.

(a) Post-flashover fire stage in BRE large compartment test 8

(b) Predicted temperature field in BRE large compartment test 8

Figure 4.29: Illustrative comparison between the experiment and modelling

a. Simulation results

Gas and steel temperatures were computed using *SOFIE* and the coupled *GeniSTELA* code. Figures 4.30 and 4.31 demonstrate that *GeniSTELA* could provide temperature field calculation results.

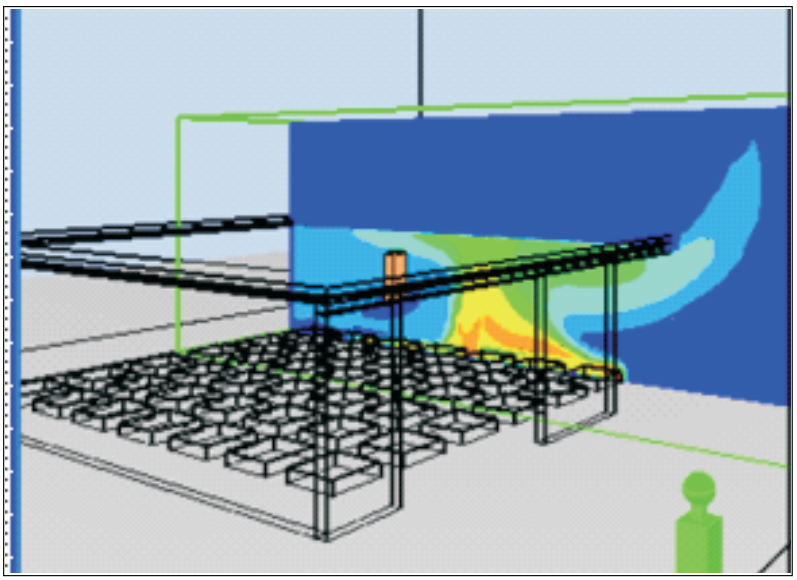

Figure 4.30: *GeniSTELA* gas temperature field graphic results

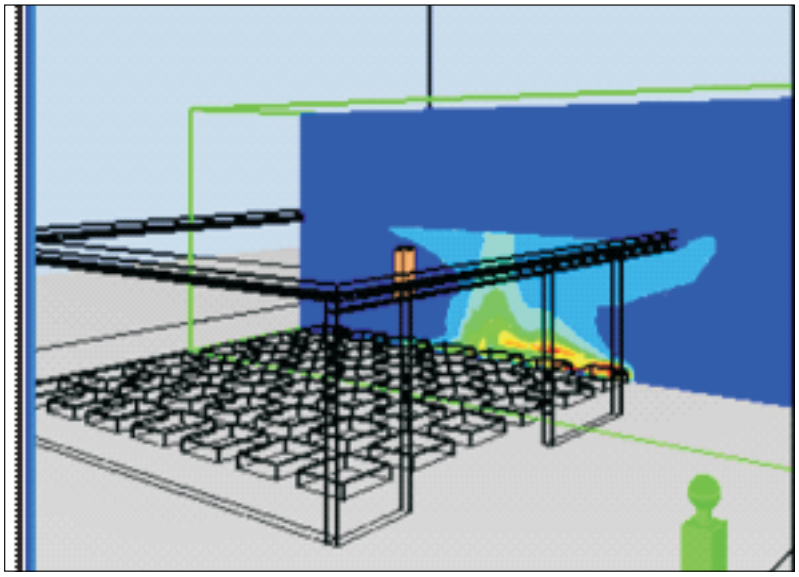

Figure 4.31: *GeniSTELA* "virtual" steel temperature field graphic results

In qualitative terms the results showed the expected differences in steel and gas temperature fields, with relatively higher steel temperatures within the depth of the compartment compared to the openings. This is consistent with the fact that the thermal exposures are more severe deeper into the fire (Welch *et al.*, 2007) and the model predictions from *GeniSTELA* are heavily influenced by the radiative terms, $\dot{q}_r''$, derived directly from the CFD calculation.

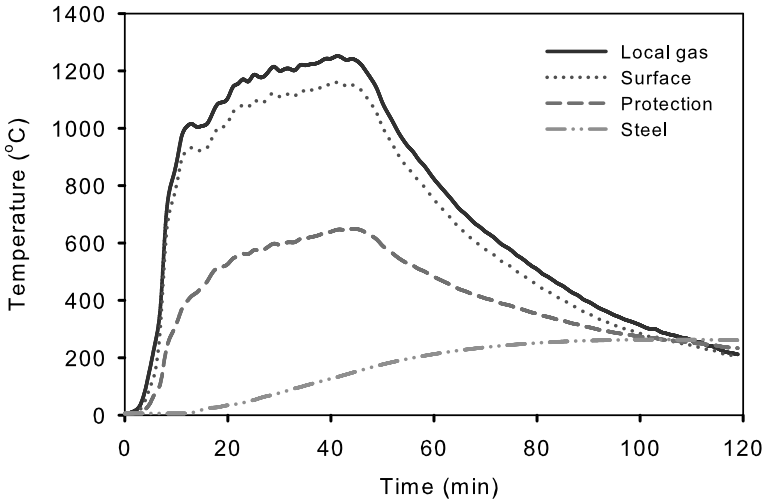

Figure 4.32: Temperatures at protected indicative, test 8

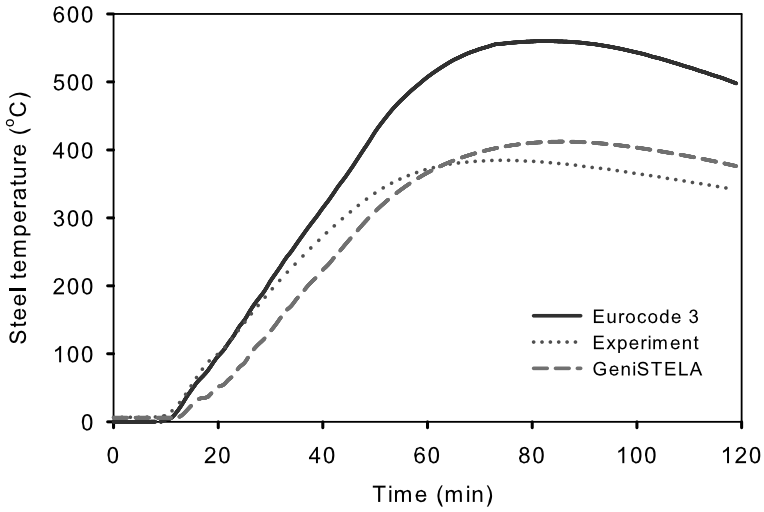

Figure 4.33: Comparison of steel temperatures

Figure 4.32 shows the temperature predictions for the protected indicative within the compartment, at thermocouple tree 7 location, as indicated in Figure 5.3 of Allan's thesis (Jowsey, 2006). The results are obtained through the spreadsheet implemented *GeniSTELA* methodology. There is a large temperature gradient across the protection. Figure 4.33 shows a comparison of the predictions of steel temperature with the test together with EC3 prediction. The figure indicates that EC3 methodology predicts well in the first $30min$, however, big discrepancy is found comparing with the experimental result. On the contrary, *GeniSTELA* predicts about 15% better than EC3 methodology, especially after the first $30min$. The effect of protection materials on the steel temperature increment is clearly shown in the first $60min$, with slower increasing. The difference between experiment and *GeniSTELA* predictions also might be attributed to uncertain input parameters which are not directly available from experiment. Overall, the EC3 prediction exceeds the measured temperature reflecting some conservatism in this semi-empirical method, while the prediction from *GeniSTELA* indicates a sufficient match with the test, provided that the CFD prediction results are reasonable.

b. Sensitivity study results

Similarly, sensitivity study for this test is also carried out. Examples of the results are shown in Figures 4.34 and 4.35, which demonstrates the effects of changing the steel flange thickness (spanning $UC254 \times 254/73, 107, 167$) and the protection

thickness (12.5 to 50mm). The results for changing the protection thermal conductivity mirror the latter, and show the expected strong influence of protection properties.

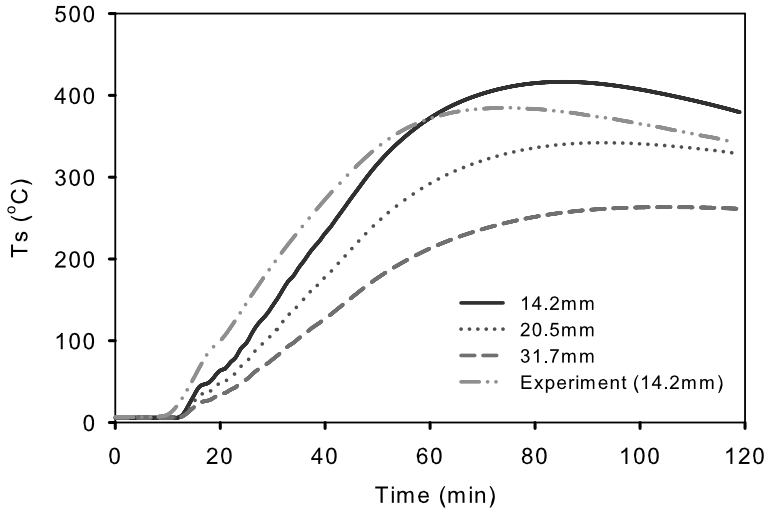

Figure 4.34: Effect of flange thickness on steel temperature

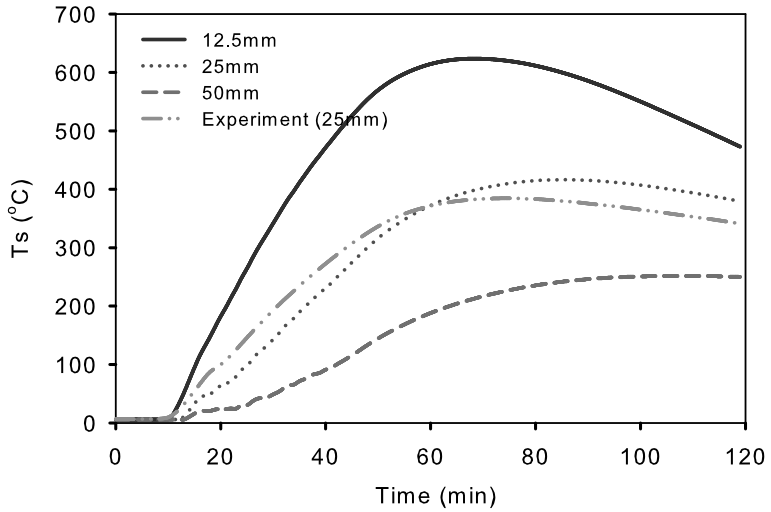

Figure 4.35: Effect of protection thickness on steel temperature

4.4.3 Remarks

The verification and validation study of *GeniSTELA* has highlighted a number of issues. The first case study, the fire resistance furnace, is illuminating since it reveals the degree of thermal exposure variation existing within the furnace even well into the test. Of course, furnace test components as a whole, e.g. beams, columns or assemblies, and it may therefore be problematic to make comparisons between the detailed local predictions of steel thermal response available from *GeniSTELA* and the global performance of components. This is a similar problem to comparing the results of CFD and zone models, and the resolution may be to take averages or characteristic values, e.g. from locations where the predicted thermal exposures most closely match the average of the standard temperature-time curves, where appropriate. Sensitivity studies reveal the expected dependencies on member specification, and the ability of the model to reproduce the thermal equivalency between different protection systems which provide the same nominal fire ratings has been shown.

For the more general case of the post-flashover fires in a large compartment fire test, reasonable matches were obtained against measured thermal response in a protected steel indicative. Here there are significant uncertainties associated with the temperature-dependent thermal properties of the protection material, and in practice even its application thickness is rather variable. The sensitivity of the results to a number of these uncertainties has been investigated on member specification, thus providing a close experimental match.

In addition, since it is almost impossible to obtain solid-phase field responses from a single experiment with no structural element inside, validation of *GeniSTELA* model with more fire scenarios is required.

Chapter 5

Application and Exploitation

5.1 Introduction

So far, this thesis has described the development, verification and validation of *GeniSTELA* as a generalised tool which could provide sufficiently accurate results, with the advantage of providing field calculation results for steel temperatures. However, whether it is applicable to practical use still relies on many factors, such as the computational cost, the ease of use, etc. One of the most important factors is the computational requirement. This has been studied for *GeniSTELA* and further improved by appropriate means. Moreover, within the afforded CPU time requirement, *GeniSTELA* is optimized with simultaneous calculations for different structural parameters and variants, significantly increasing its generality. This chapter states the investigation results for the practical use of *GeniSTELA* in regards with the CPU time and the further optimization of the methodology by simultaneous calculations. The application to the 'hypothetical benchmark scenario' has also been described, demonstrating the simultaneous thermal response calculations of different structural parameters and variants as well as the practical use of *GeniSTELA* in terms of structural fire design. The potential use in structural fire safety engineering field, in the context of models of structural response, has also been assessed and explored, illuminating further application of *GeniSTELA*.

5.2 Computational Requirements Study

In order to examine the practical use of the methodology, the overall computational requirements have been assessed in terms of the CPU time usage. Also, the potential for reducing the frequency of the calls to the *GeniSTELA* steel temperature solver has been explored by changing this from the default of every time step. The change in *GeniSTELA* call frequency is realized by introducing a time step factor variable (*tfactor*) in the model in order to increase the intervals between calls.

The study has been carried out based on the localised fire scenario, specified in the last chapter. The results show that *GeniSTELA* uses around 1% of the CPU time for the flow solver, including radiation, when called at the default interval of every time step. Simulations were then undertaken with a *tfactor* value of 10, 100 separately for the localised fire scenario, with a constant fire size, having realistic steel temperature increases in 10 minutes. Figure 5.1 shows the results for the respective steel temperature predictions, confirming that even when called once every 100 main solver time steps, i.e. with just six calls of the *GeniSTELA* solver altogether, there is a very small effect on the final steel temperature result, especially at later times. Figure 5.2 shows the evolution of the percentage temperature differences, when *GeniSTELA* is called at every 10 time steps of the main fluid flow solver or called at every 100 time steps. It is obvious that the discrepancy is only important in the early stage, with the maximum difference being only of order 10%, mostly within 3%. When the intermediate call frequency, i.e. *tfactor*= 10, is used, an even closer result could be obtained compared with the default calling frequency,with a maximum discrepancy of only 1.6%, as also seen in Figure 5.2.

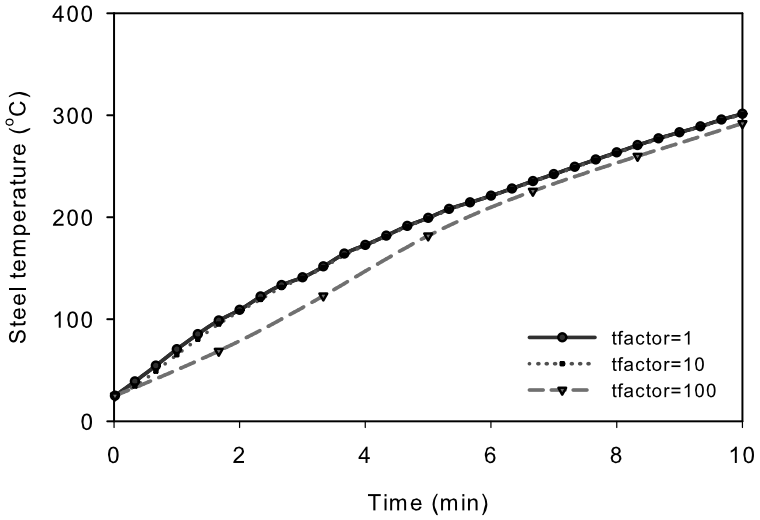

Figure 5.1: Predicted steel temperatures with *tfactor*=1, 10 and 100

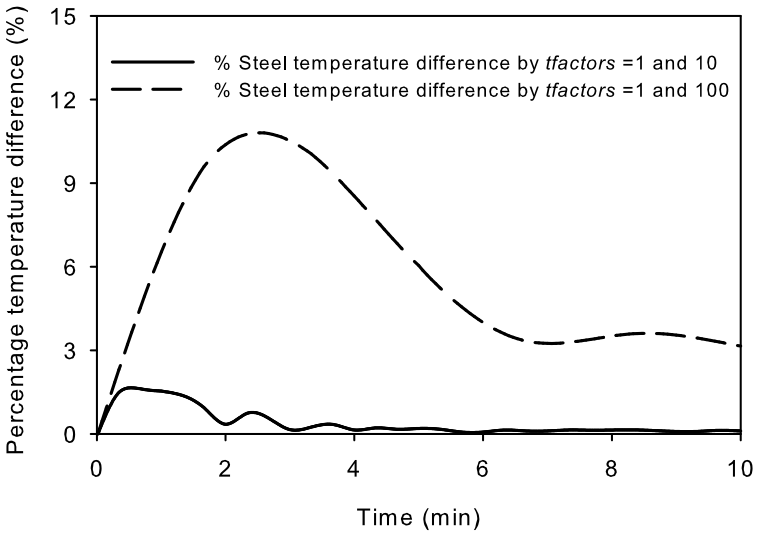

Figure 5.2: Differences in steel temperature against time using various *tfactors*

The above findings are of course only of relevance for this particular steady fire, and for more general cases, where the heat release rate may be changing rapidly, higher frequencies may be required. In practice, the frequency of the *GeniSTELA* call could be adjusted by automatic selection linked to heating rates, in order to

achieve the best efficiency. Nevertheless, this initial study suggests that a full set of parametric calculations (10 $\sim$ 100 cases) could be afforded without any significant compromise of accuracy, before the *GeniSTELA* analysis becomes the dominant part of the computation.

5.3 Simultaneous Computation

Since *GeniSTELA* is confirmed to be able to afford 10 $\sim$ 100 cases by simultaneous calculations in term of the computational requirement. An optimization scheme is made to increase the generality and efficiency of *GeniSTELA* for thermal analysis of a range of interesting cases, varying from input parameters to specifications. A library of input parameters and possible variants to the specifications are collected into a data file 'SensVari.txt', which is called each time when *GeniSTELA* is called within the fluid flow calculation. A set of thermal analysis results is therefore provided simultaneously.

An example is demonstrated below, which is based on the standard fire resistance furnace test, but using different protection material property parameters. Some of the input parameters of interest for the two simulation tests are listed in Table 5.1 below. They are input into the data file 'Sensvari.txt' within once simulation.

Table 5.1: Two different sets of parameters used within once simulation

Material types	Expansion ratio $[-]$	Protection thickness $[mm]$	Density $[kg/m^3]$	Thermal conductivity $[W/m/K]$	Specific heat $[J/kg/K]$
Sprayed fibre	1	8.0	680	0.19	970
Intumescent	50	0.268	1427	0.13	1500

As a demonstration, Figure 5.3 shows the prediction results for both cases in the early stage, at 5 minutes. According to the way how the parameters are input, the results in the figure are obtained within one simulation; hence they show clearly the simultaneous calculation of *GeniSTELA*.

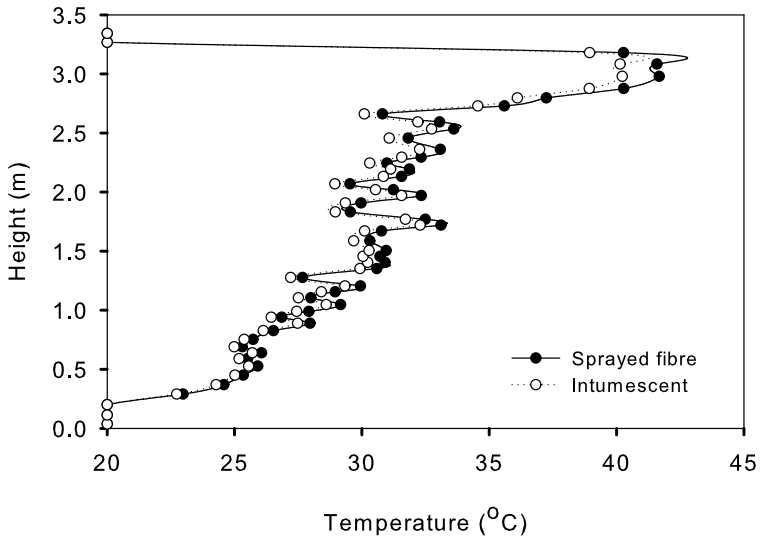

Figure 5.3: Steel temperature prediction for structural members with different protection materials at 5 minutes

For better investigation, the two predicted steel fields at 30 minutes fire rating, with vertical profile at the thermocouple locations as in the furnace test, are presented in Figure 5.4. Similarly to the above, they were obtained simultaneously for both sprayed fibre protection and intumescent protection. The aforementioned table shows their initial thermal properties adopted in the simulation. Though they are completely different in nature, they are specifically chosen for thermal equivalence with consideration of section factor Hp/A value. The two curves for $8mm$ sprayed fibre protection and $0.268mm$ intumescent protection in Figure 5.4, indicate that for either type of protection, at 30 minutes fire rating, the steel temperature failed. This is consistent with the way the material is chosen. Within this study, one hour fire rating material thermal properties have also been investigated. The steel temperature prediction against height for sprayed fibre protected structure at 1 hour fire rating, which equals to $25.4mm$ protection thickness, has also been shown in Figure 5.4. The result looks rather reasonable. In addition, comparing the overall CPU time spent on the two simultaneous cases with the one case simulation, the simultaneous calculations only result in additionally 1% CPU, which is definitely affordable and in great efficiency. In general, the study results could firstly verify the thermal protection submodel within *GeniSTELA*, and secondly justify the simultaneous computation scheme used in *GeniSTELA*.

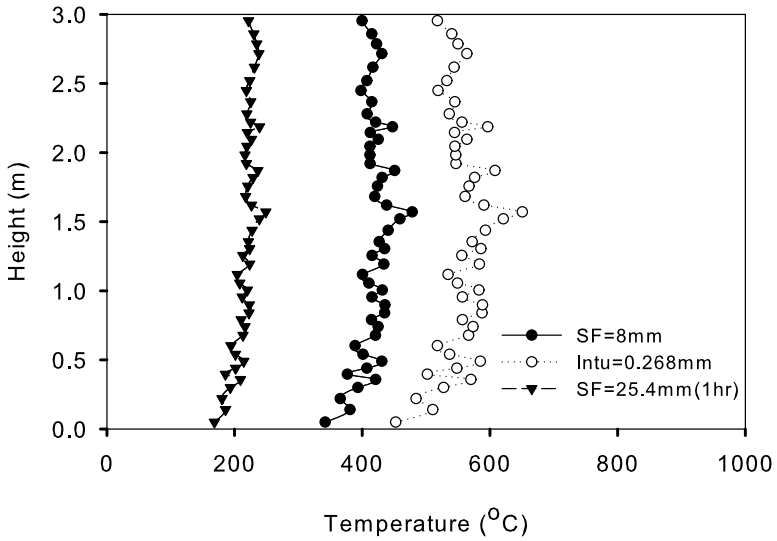

Figure 5.4: Steel temperature prediction for structural members with different protection materials at 30 minutes and 1hour for sprayed fibre protection

5.4 Brief Summary

Encouraging results concerning the computational requirements have been demonstrated which suggest that simultaneous computation of larger parametric sets, encompassing $10 \sim 100$ cases, may well be feasible. Possibilities for further efficiencies in *GeniSTELA* operation have been identified, in particular, a reduction of the call frequency, which could in principle be automated. When it is possible to assume a quasi-steady fire, much greater efficiencies can be achieved, since the *GeniSTELA* analysis can be completely decoupled from the CFD simulation, called only as a post-processing operation. Based on those findings, a simultaneous computation scheme is adopted within *GeniSTELA* for calculation many cases of interest, with varying input parameters. This scheme has been justified with test case study and modified so as to optimize *GeniSTELA*.

5.5 Application to Benchmark Scenario

5.5.1 Background

Besides the two full-scale cases application of *GeniSTELA* in last chapter for validation, the model has been applied to a 'Hypothetical benchmark scenario' as used in the *RFCS FIRESTRUC* project (Welch *et al.*, 2008). The 'Hypothetical benchmark scenario' has been studied by different partners in the *FIRESTRUC* project using different modelling methodologies. It has also been examined with *GeniSTELA*. Along with the simultaneous parametric study, the simulation results demonstrate the simultaneous computation capability of *GeniSTELA*. The detailed method-to-method comparison results demonstrate the practical use of *GeniSTELA* in terms of the prediction sensitivities and the associated computational costs, hence the possible use in the field of the structural fire design.

5.5.2 Hypothetical benchmark scenario description

The benchmark scenario involves a series of steel tubes and I-profile columns and beams inside a compartment $30m$ by $20m$ in floor area and $10m$ high, as illustrated in 5.5. A t-square fast growing pool fire with a $5.0m \times 5.0m$ fuel bed area of heptane C_7H_{17}, reaching $30MW$ in $800s$ and remains steady state afterwards, was specified such that a hot smoke layer was generated under the entire ceiling, and a layer of clear air was maintained above the floor. This allowed the performance of the different methodologies to be examined and compared in respect to beams immersed in a hot ceiling layer and columns partly engulfed in the hot layer, but heated additionally lower down by radiation from both the fire and the smoke layer. An additional feature of the fire scenarios was the adiabatic compartment boundaries, so that radiation reflected from these surfaces was also a mechanism for heat transfer.(Kumar *et al.*, 2006)

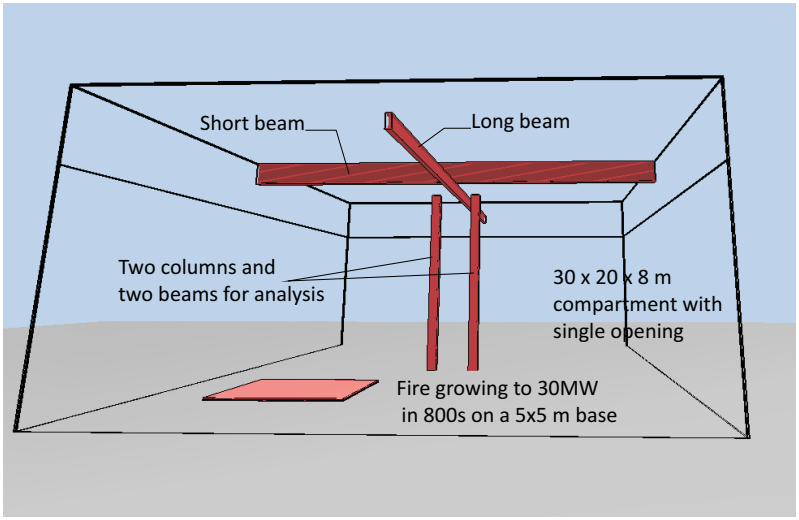

Figure 5.5: Geometry for the benchmark case

Originally, in the benchmark case reported in the *RFCS* report (Welch *et al.*, 2008), the thermal response calculations were performed for two types of column and beam elements. One is hollow, rectangular steel sections, representing the structural element with no shadow effect, and the other is steel I profile sections including a shadow effect. Details of the different sections studied were as follows:

- A long beam with $30m$ length, and with either a hollow tube with dimensions $500mm$ height $\times$ $200mm$ width $\times$ $1mm$ thickness or a IPE 500 profile steel element.
- A short beam with $20m$ length and with either a hollow tube with dimensions $1000mm \times 400mm$ and $\times 1mm$ thickness or a HL 1000 B profile steel element.
- Two columns with $8.5m$ length, with either hollow tubes with dimensions $400mm$ depth $\times$ $400mm$ width $\times 1mm$ thickness or HD 400 $\times$ 314 profile elements.

The detailed cross section dimensions are shown in Figures 5.6 $\sim$ 5.8 below:

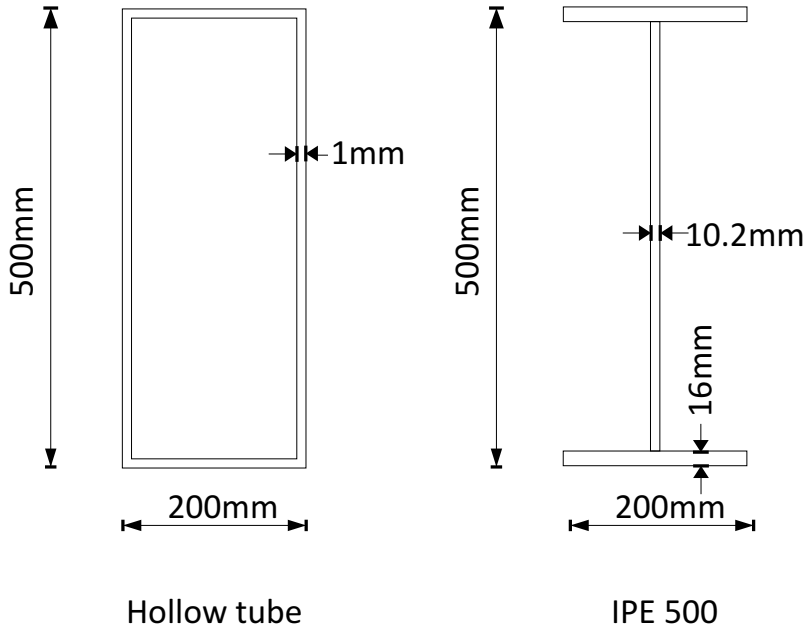

Figure 5.6: Long beam cross section

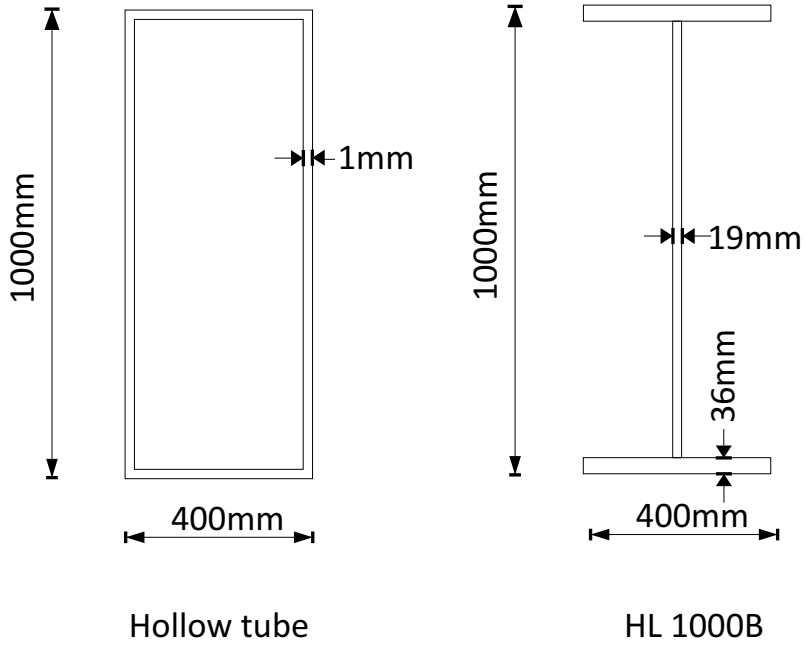

Figure 5.7: Short beam cross section

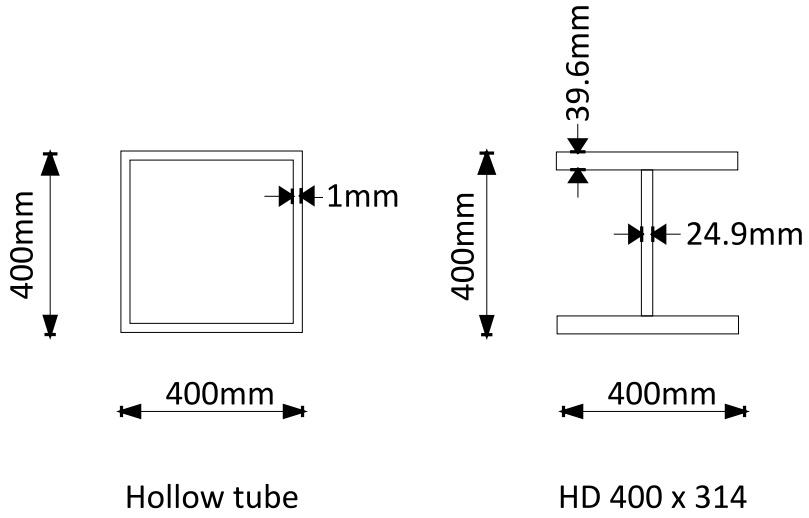

Figure 5.8: Column cross section

There was no contact between the columns and beams, so heat could not pass from one element to another. An important feature of the hollow steel sections was that no heat transfer (convection or radiation) was included inside the hollow element, i.e. the inner steel surfaces were adiabatic.

Two fire positions were considered as follows:

- Position A: Fire further away from the columns.
- Position B: Fire closer to the columns and just under the long beam.

The geometry and the positions of the elements are summarized in Figure 5.9. Overall, four scenarios were formed based on the two fire locations and two types of elements either hollow sections or I profiles.

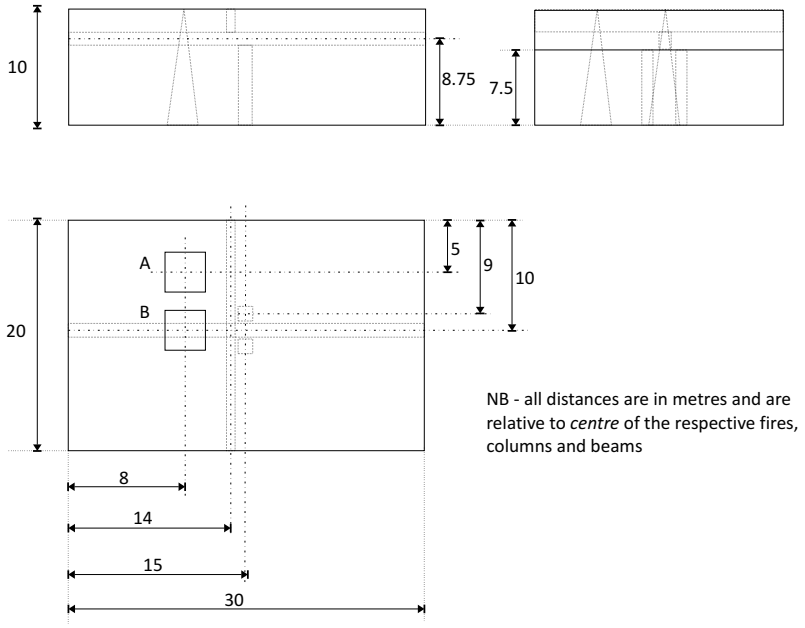

Figure 5.9: Location of fire, columns and beams for the benchmark case

However, since *GeniSTELA* is a novel simulation methodology with independent calculation for the gas phase and the solid phase, in practice no elements need to be included in the CFD calculation. Thus, the four scenarios reduce to two, with the only difference being the fire locations.

In this work, as a demonstration of *GeniSTELA* for practical use, the methodology was applied in the above specified benchmark case with fire at location A representing the non-symmetrical fire position and also applied in 71 other parametric study cases which were carried out simultaneously. As demonstrated in Table 5.2 below, the default case used the IPE B 500 section long beam protected by Fendolite MII with 1 hour fire rating thickness. Eurocode properties were assumed for the steel and the surface emissivity was set as 0.8. Among the parametric study cases, 11 cases based on the default case but with varying sections in terms of weight and type were used; four cases dealt with different fire rating thickness of Fendolite MII protection. A range of commonly used protection materials covering sprayed fibre protection, board protection and intumescent were also simulated. Sensitivity studies were carried out of moisture effect, protection material properties including thermal conductivity, thermal conductivity linear rate of change with temperature, specific heat, density and emissivity. Another three cases with very thin protection and one without protection were carried out,

providing a limit for the extreme condition and allowing the comparison with the 'hypothetical benchmark test' results obtained from other models. Those key specifications of the element, material properties and certain uncertainties for all the cases were input into the 'SensVari.txt' file, as in **Appendix D**.

Table 5.2: Case specifications and parameters

Variations		Case specifications and parameters
Steel sections	Weight	IPE B 500 (Default, long beam) IPE A 500 IPE O 500
	Weight	B UB 533X210X82 B UB 533X210X92 B UB 533X210X101 B UB 533X210X109 B UB 533X210X122
	Type	IPE B 600 HE 1000 B HL 1000 (Short beam) C HD 400X314 (Column)
Protection	Sprayed fibre protection	Fendolite MII (45min,60min,120min,180min, 240min) Cafco Balze-shield II (30min, 60min, 90min, 120min) Monokote MK5 (30min, 60min, 120min)
	Board protection	Vicuclad (30min, 60min, 120min, 240min) Monolux (60min) Plasterboard (30min, 60min)
	Intumescent	Steelguard FM 585 (30min, 60min, 90min, 120min)
	Thickness	(0, 2.54x10E-3, 2.54x10E-4, 2.54x10E-5)
Material properties	Moisture content Thermal conductivity	(0, 0.01, 0.02, 0.04, 0.08, 0.16) (0.04, 0.08, 0.16, 0.32, 0.65)
	Specific heat	(485, 970, 1940)
	Density	(340, 680, 1360)
	Emissivity	Member (0.1, 0.3, 0.5, 0.7, 0.8, 0.9, 0.95, 1.0) Fire (0.7, 0.8, 0.9, 1.0) Remote Cell (0.1, 0.8, 1.0)

The fire was to be modelled as with an effective heat of combustion of 45×10^6 J/kg, and a soot mass fraction of 0.088. The heat release rate grew to $30MW$ as shown in Figure 5.10.

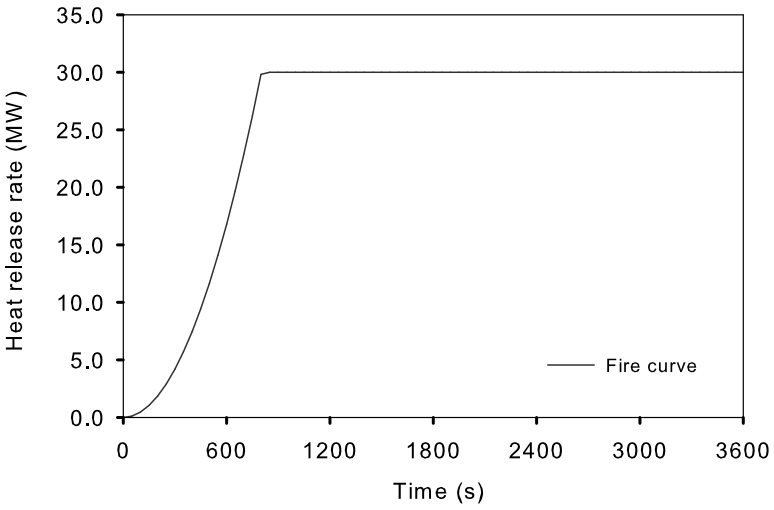

Figure 5.10: Heat release rate of benchmark fire

Various locations in beams and columns were studied to inspect the field steel temperature. Those locations are as specified in Figures 5.11 ∼ 5.13.

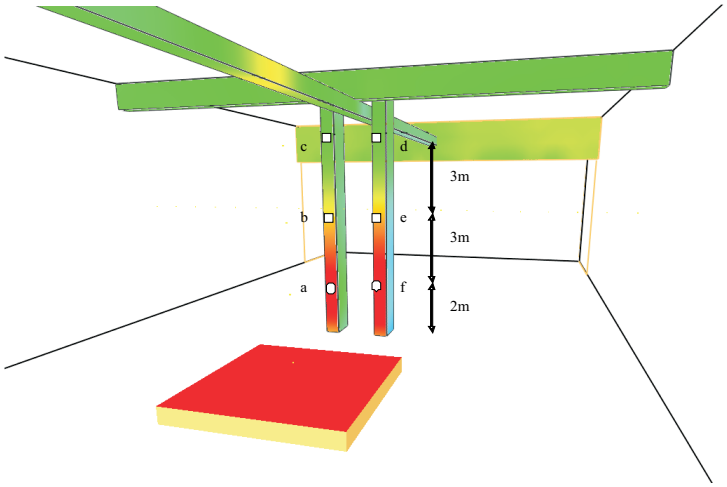

Figure 5.11: Benchmark reporting locations on columns

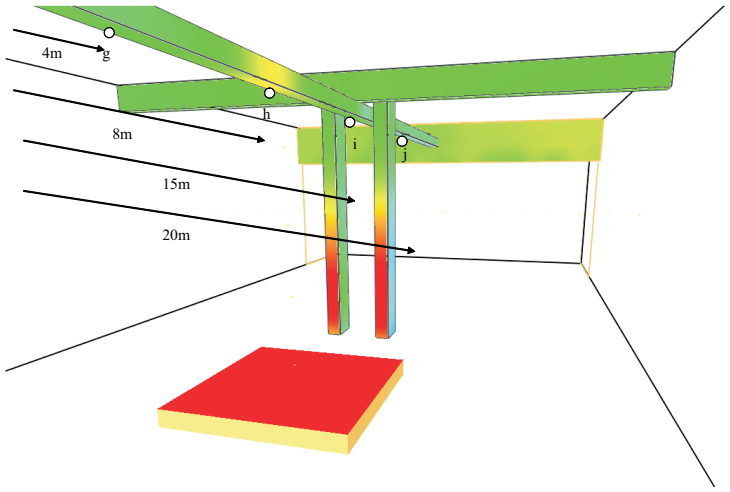

Figure 5.12: Benchmark reporting locations on long beams

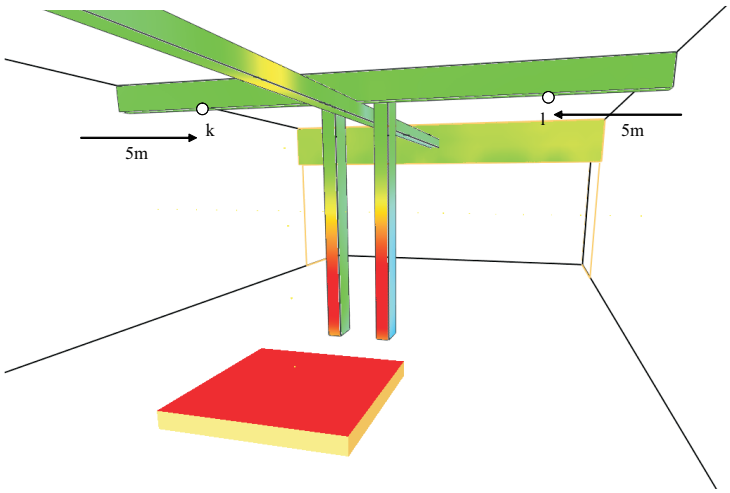

Figure 5.13: Benchmark reporting locations on short beams

5.5.3 Simulation of test cases

The computational domain was extended by $5m$ at the opening to allow for free in- and out- flow. A Cartesian rectangular CFD mesh of $64 \times 39 \times 27 = 67,392$ cells was used, with minimum cell size $0.25m$ and maximum $0.625m$ in the x axis, minimum of $0.2m$ and maximum of $0.667m$ in the y axis, and in the z axis, the minimum cell size is $0.1m$, maximum is $0.5m$. The mesh is shown in Figure 5.14

below:

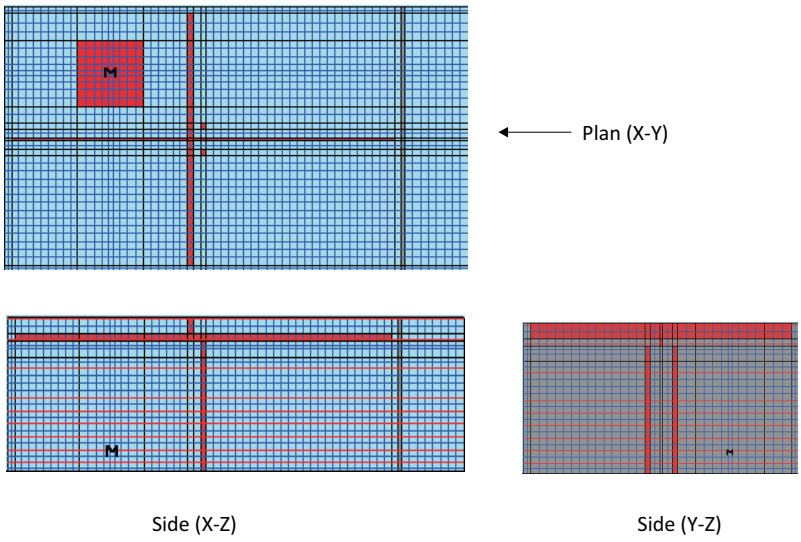

Figure 5.14: CFD mesh used in the simulation

The default 'standard $k-\varepsilon$ model' was used to model the turbulence while 'Eddy break up model' was used for the combustion. Radiation was modelled with the 'Discrete Transfer Model' using 2×4 rays. A time step of 1s was used in the CFD simulation until the end time of $3600s$. 300 iterations were used on the 1st time step, and a minimum of 10 iterations and maximum of 100 iterations thereafter. The structural elements have been modelled with *GeniSTELA*, which could allow the thermal simulation to be carried out with much larger time steps by varying the values in the 'Factors.txt' input file. In this simulation, a factor of 1 is used, indicating *GeniSTELA* steel temperature calculation was carried out at every CFD time step. The simulations were performed on a standard Windows XP computer, with a $2.99GHz$ Pentium processor, $2.0GB$ of RAM.

5.5.4 Results

Within the *FIRESTRUC* project, simulations were carried out by two-way coupling using the CFD program *VESTA* and solid-phase (FE) model *DIANA* and by one-way coupling with *FDS* (CFD) & *ANSYS* (solid), *JASMINE* (CFD) & *STELA* (solid), *JASMINE* (CFD) & *SAFIR* (solid), *SOFIE* (CFD) & *SAFIR* (solid) and *VESTA* (CFD) & *SAFIR* (solid). A series of results has been obtained

in this project, assisting comparison study of *GeniSTELA*, which have also been applied into the benchmark scenario. The CFD calculations were performed with *SOFIE* code which *GeniSTELA* is implemented into, while *GeniSTELA* was adopted for solid phase thermal analysis. The results from *GeniSTELA* were obtained through a simulation with good convergence using a 0.1% mass error criterion for each time step. Through out the one hour simulation, the velocity residuals were typically of the order of $10E-2$ to $10E-1$ per cent at the end of each time step with a value about 0.08% for the final time step.

Figure 5.15 shows the calculated development of gas temperature inside the compartment for fire at location A. From the figures, by around $840s$, gas temperatures inside the compartment have reached steady state, i.e., the further heating of the steel structure does not significantly influence the gas temperature, which is consistent with the input heat release rate. Gas temperature comparisons at different locations between *GeniSTELA* and *JASMINE-STELA* have been carried out. An example is shown in Figure 5.16, where a reasonable match is obtained through different methodologies.

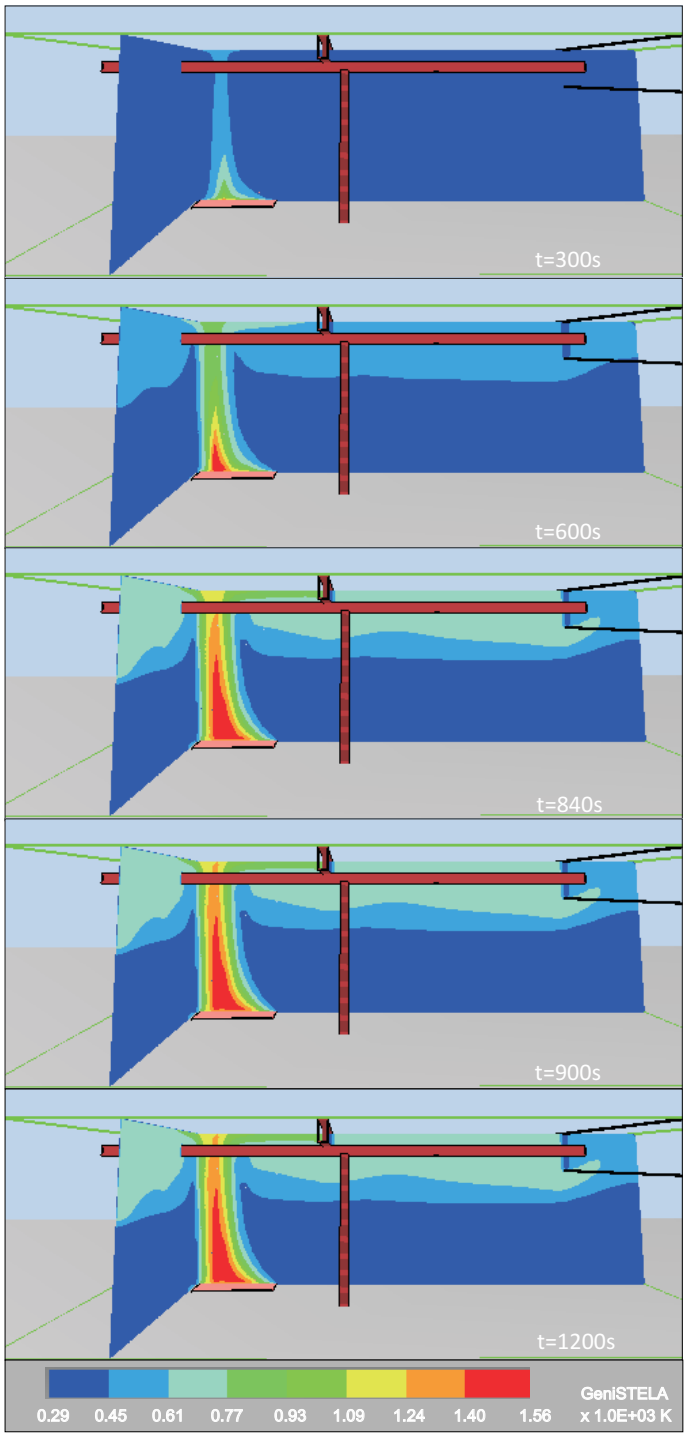

Figure 5.15: Gas temperature evolution contours for benchmark with fire at location A

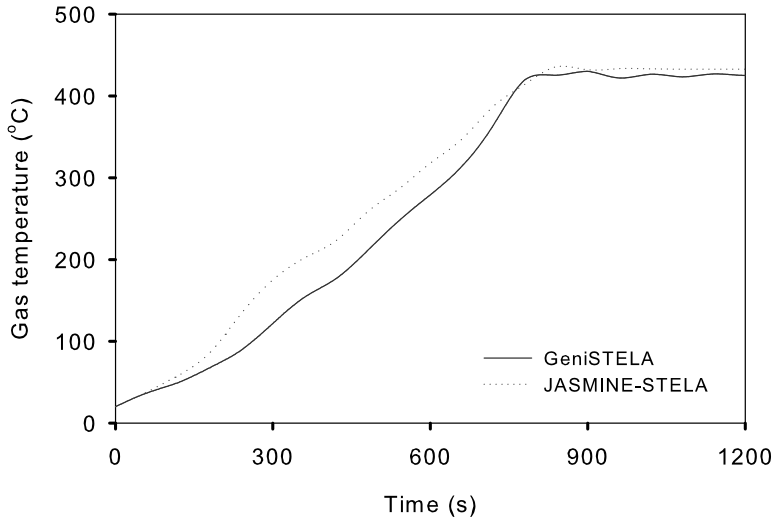

Figure 5.16: Gas temperature comparison between *GeniSTELA* and *JASMINE-STELA* at location g

A list of steel temperatures for all parametric cases has been obtained within this simulation, as demonstrated below. This demonstrates well the useful capability of *GeniSTELA* in performing simultaneous multiple case calculations, since unlike traditional methodologies which could obtain only one case simulation results in one run, *GeniSTELA*, with the assistance of input data file 'SensVari.txt' to specify varying cases, obtained the simulation results for all cases in one run.

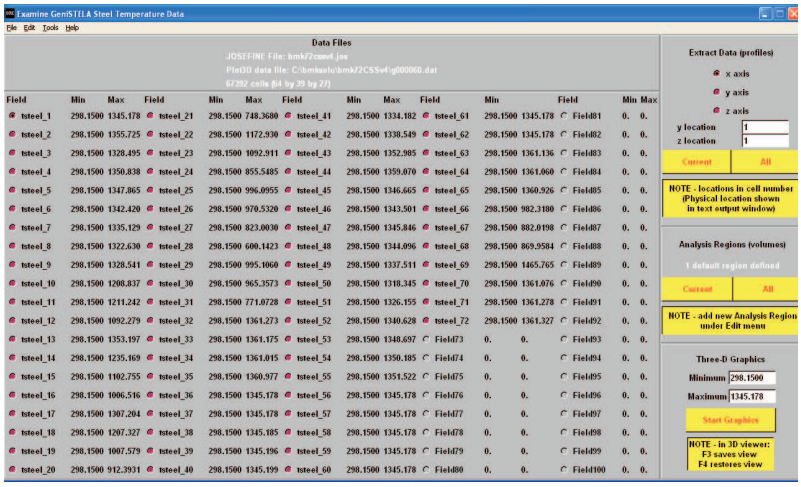

Figure 5.17: Demonstration of simultaneous calculation results

The simulation provides steel temperature field results for all parametrical study cases. As for general engineering analysis, computer graphical output is a useful tool. Figure 5.18 illustrates such a presentation of the results, which shows the *GeniSTELA* calculated steel temperatures field and vector distributions where the "virtual" two columns and beams are in close vicinity, for Fire A at 3600s of the default case. It is being viewed from the ventilation opening side. As expected, increasing temperatures were predicted at the locations close to the fire source as well as in the hot layer, due to radiation domination, revealing a possible weakness in structural member located in that position, and hence attention in design is required.

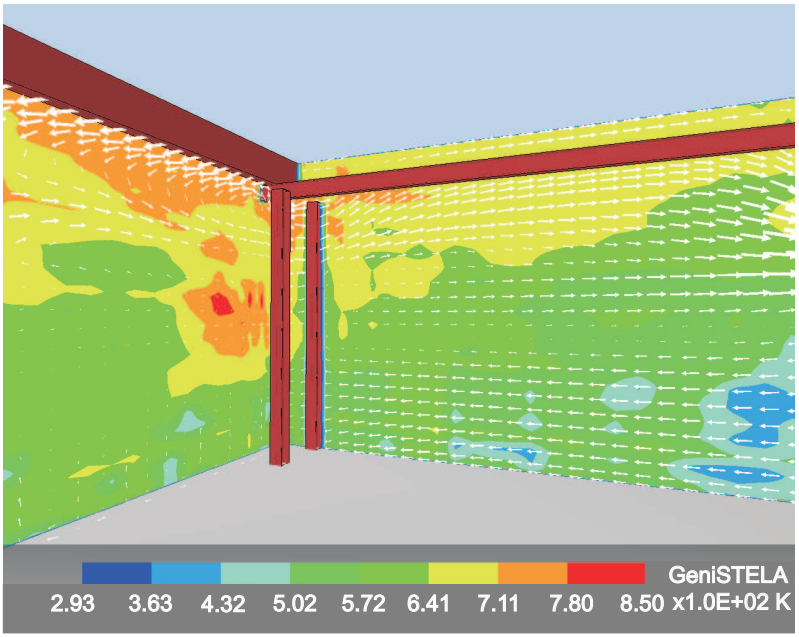

Figure 5.18: Example graphical output from *GENISTELA* at 3600s

The following results presented focus on the steel temperatures at the specified locations as mentioned in the description section. For each case among the 71 simultaneous parametric variants, only one aspect differs from the default case. This provides a good facility to inspect the key factors that might affect the results significantly, hence to improve the fire safety design in practice. The results, including those from the unprotected steel case have been compared with those obtained from other modelling methodologies specified in the *FIRESTRUC* project (Welch *et al.*, 2008), whilst model sensitivities have been examined and

demonstrated. A series of representative results are demonstrated in the following paragraphs.

5.5.4.1 Results for unprotected member case

Comparisons were made for steel temperature predictions from *GeniSTELA* and Eurocode 3 (BSI, 2005a) method. The EC3 results are obtained by implementing CFD radiative temperature output as input boundary condition, which could provide similar fire and heat flux condition, assuming the locations studied are not dominated by convection. An example of the results at location g (see Figure 5.12), representing a location in the hot layer, is shown in Figure 5.19. Similar comparison results could be obtained at other locations. Besides the above, *GeniSTELA* has also been compared with other three modelling methods reported in the *FIRESTRUC* project (*JASMINE-STELA*, *FDS-ANSYS* and *VESTA-DIANA*) (Welch *et al.*, 2008). A representative comparison result is shown in Figure 5.20 for location e.

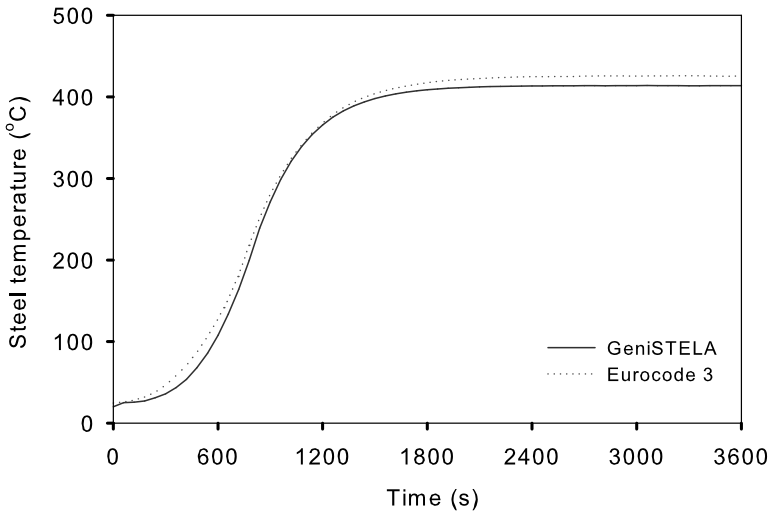

Figure 5.19: Comparison of steel temperatures for unprotected member between *GeniSTELA* and EC3 at location g

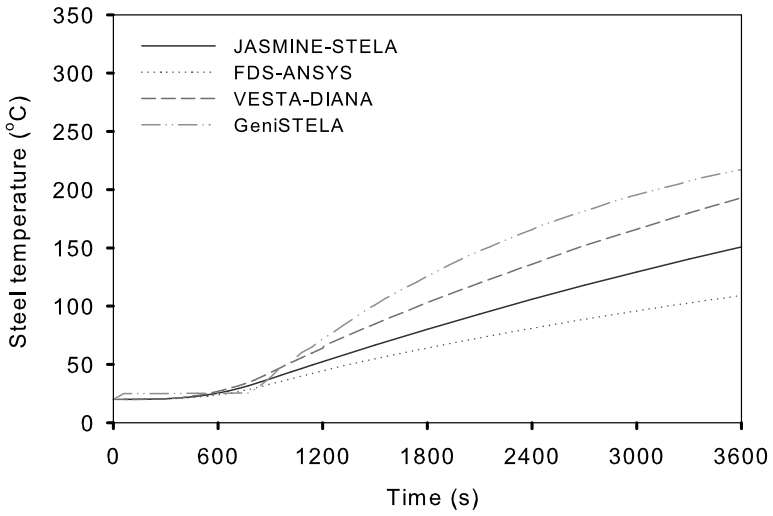

Figure 5.20: Comparison of steel temperatures for unprotected member between *GeniSTELA* and other models at location e

Good agreement has been found between the above comparisons. The comparison with EC3 method again validated the *GeniSTELA* model for unprotected steel member temperature calculations. From Figure 5.20, although the predictions from *GeniSTELA* are slightly higher than others, which might be due to the higher CFD predictions, they exhibit the same trend and the absolute difference is within an acceptable range. The maximum difference between *GeniSTELA* and *VESTA-DIANA* is 25 $°C$ at one hour, comparing 43 $°C$ between *VESTA-DIANA* and *JASMINE-STELA* and even bigger differences between others. This has provided an initial suggestion of the reliability of results from *GeniSTELA*.

A few more examples are shown below to further illustrate the application of *GeniSTELA*. Figure 5.21 shows the steel temperature predictions at three different heights along the column, where 'a' represents a location in the cold air while 'c' in the hot layer (see Figure 5.11). Figure 5.22 shows the predictions at four different locations (see Figure 5.12) along the long beam. The figures indicate that high temperatures could be obtained in the hot layer, as well as the locations close to the fire source. This is also in good agreement with the predictions from *JASMINE-STELA*, *VESTA-DIANA* and *FDS-ANSYS* as reported in the *FIRESTRUC* project (Welch *et al.*, 2008).

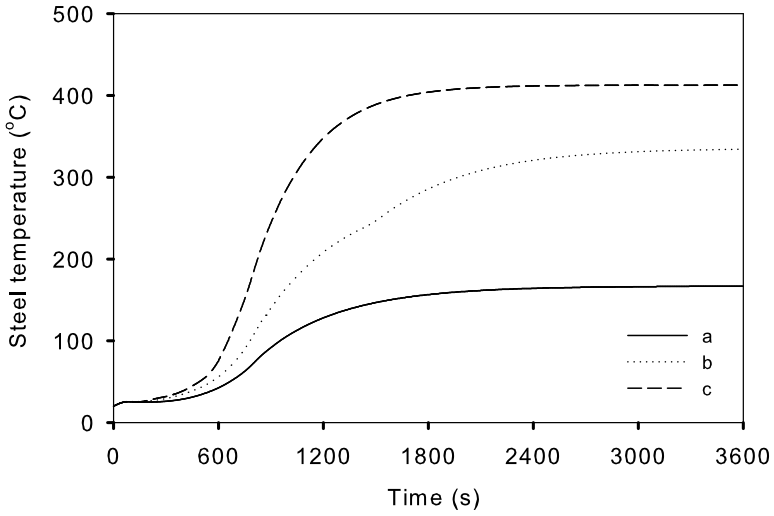

Figure 5.21: Comparison of *GeniSTELA* steel temperatures for unprotected case at different heights along the column

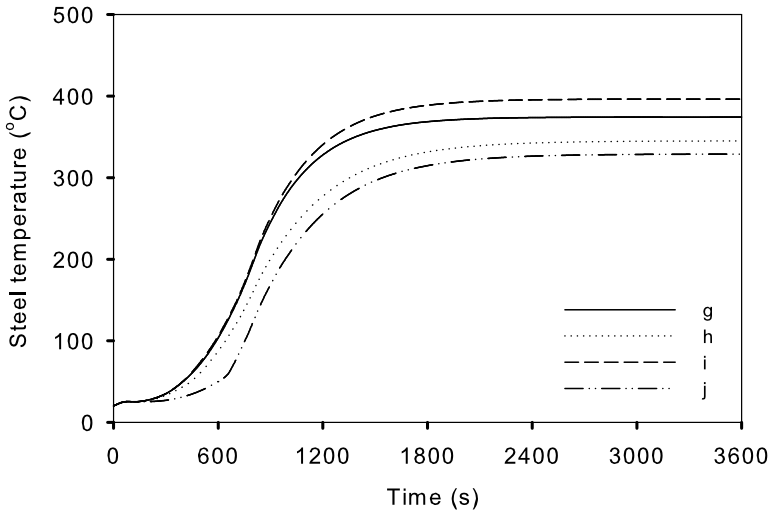

Figure 5.22: Comparison of *GeniSTELA* steel temperatures for unprotected case at different locations along the beam in hot layer

In general, the above examples of the results demonstrate that *GeniSTELA* could provide reasonable steel temperature fields for unprotected structural components. Therefore, it is possible to track the worst temperature locations for further detailed analysis, hence, facilitate the structural fire design.

5.5.4.2 Results for protected member cases

Regarding to the structural fire design, the protected cases are more of interest. A series of predicted steel temperatures at various locations for the default case have been studied, including locations a, c, g, h and j as specified previously in Figures 5.11 ~ 5.13. These cover most typical steel structure locations of interest during a fire, i.e. either structure in a cold layer or hot layer, above the fire source or away from the fire source, close to the ventilation opening or far away from the opening. Some of the results are presented in the following. Figures 5.23 and 5.24 compares the predicted steel temperatures from *GeniSTELA* with other modelling methodologies reported in the *RFCS FIRESTRUC* project (Welch *et al.*, 2008). Since other modelling methodologies simulated unprotected elements in the benchmark scenario, strictly speaking, they are not comparable with the results obtained from *GeniSTELA*. However, they could provide a reasonable limit or guidance for the *GeniSTELA* results.

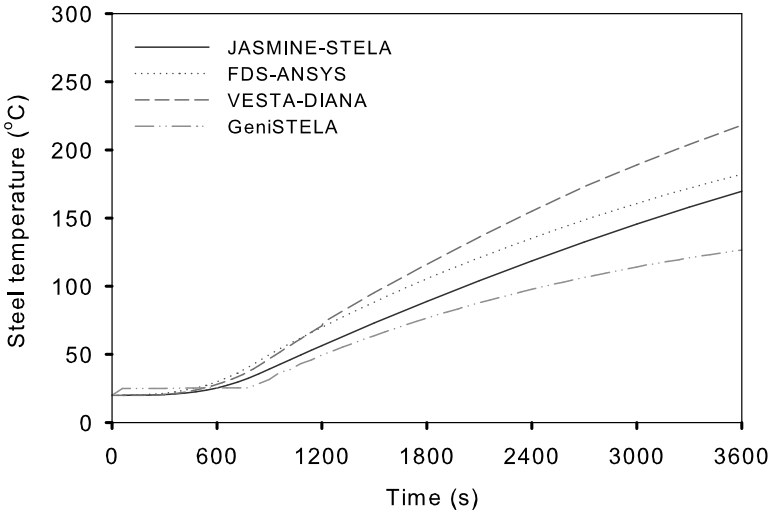

Figure 5.23: Comparison of *GeniSTELA* steel temperatures for default protected case with *FIRESTRUC* reported results for structure nearest Fire A in clear air (location a)

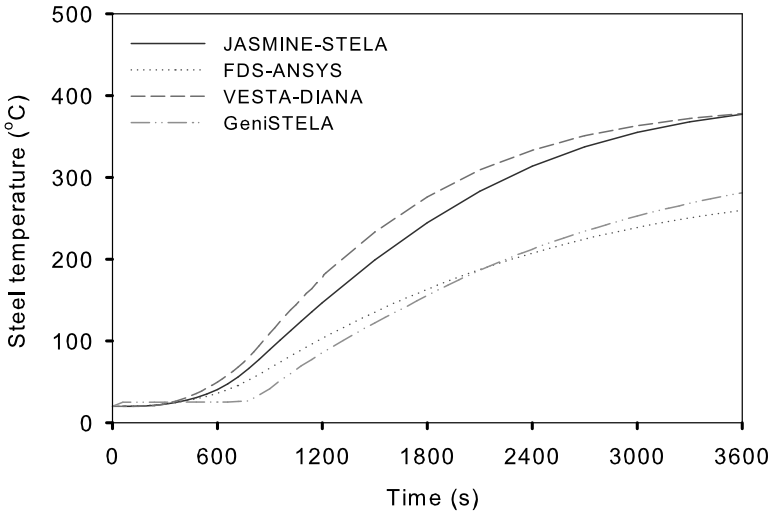

Figure 5.24: Comparison of *GeniSTELA* steel temperatures for default protected case with *FIRESTRUC* reported results for structure above Fire A in hot layer (location h)

Considering the location in the clear air layer (see Figure 5.23 for location a), it is encouraging that the results from *GeniSTELA* are in the same trend as those from other methodologies, but lower as expected due to the protection. In the hot layer, similar observations are found as seen in Figure 5.24. There is a slight discrepancy compared with *FDS-ANSYS* prediction. This might be caused by the different radiation treatment in FDS. In *JASMINE-STELA*, *VESTA-DIANA* and *GeniSTELA*, the radiation fluxes are calculated as a post-processing subroutine within the framework of the CFD and radiation models and then passed to the solid-phase model, whilst in *FDS-ANSYS*, the component radiation intensities are stored on a relatively course grid and passed to the solid-phase model in an intermediate transfer file (Kumar *et al.*, 2006). The treatment in *FDS-ANSYS* might lose some important information causing errors. This discrepancy has perhaps been amplified in this benchmark test scenario due to the adiabatic compartment surfaces. Therefore, it could be expected that the fluxes in the hot layer from FDS would be lower than those from *SOFIE*, resulting in a lower steel temperature prediction than that from *GeniSTELA*, even could be slightly lower than those with protections. The overall temperature prediction results at other locations reasonably match with other methodologies. Moreover, an expected time delay and moisture plateau have been observed in the results from *GeniSTELA*, indicating its predictive capability.

In addition, Figures 5.25 and 5.26 below have been cross plotted for a better view of the results. Figure 5.25 shows the variation in calculated steel temperature at different heights along the column while Figure 5.26 compares predicted steel temperatures at four interested locations along the long beam length. The results also suggest that higher temperatures would be expected at the locations close to the fire source in the hot layer.

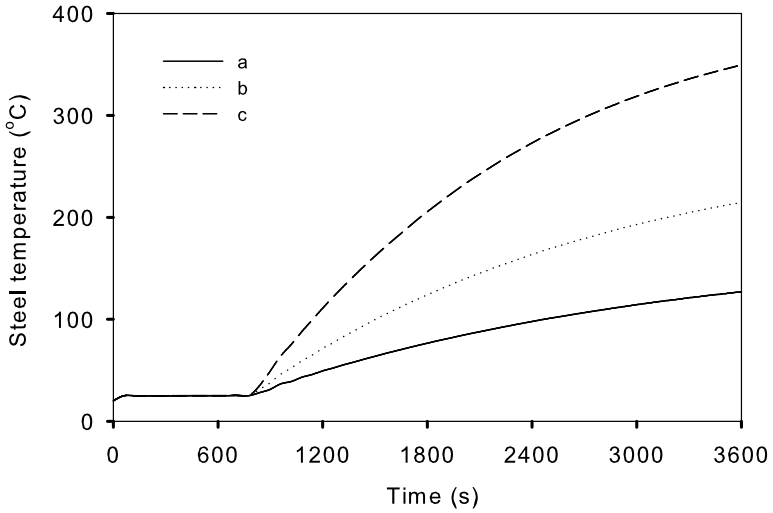

Figure 5.25: Comparison of *GeniSTELA* steel temperatures for default protected case at different heights along the column

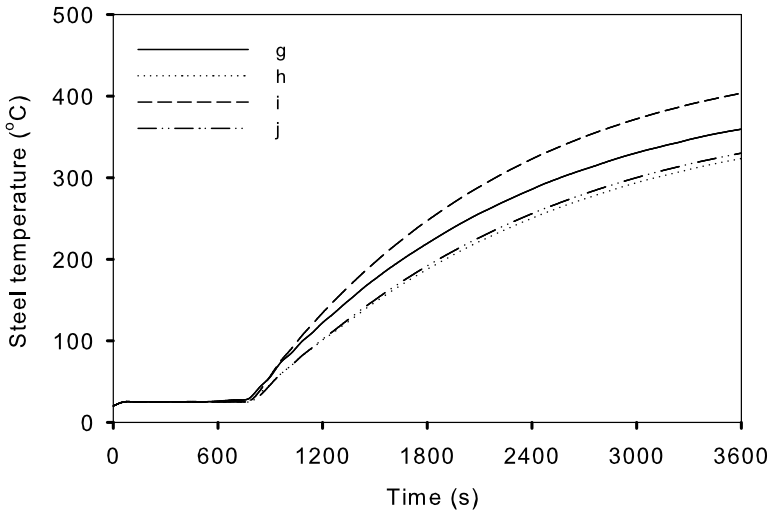

Figure 5.26: Comparison of *GeniSTELA* steel temperatures for default protected case at different locations along the beam in hot layer

5.5.4.3 Possible failure case

An additional plot is made for the cell at a location above the fire source and at the same vertical height as the lower face of long beam flange in the hot layer. High gas temperature would be predicted in the cell at this location due to high heat fluxes, and possible structure failure might occur. Figure 5.27 below shows gas temperature together with the corresponding steel temperatures for both protected and unprotected members at the same location. The gas temperature reaches 830 $°C$ while the steel temperature reaches 668 $°C$ in this specified location, i.e. exceeding the steel failure temperature. Therefore, detailed analysis is needed at this location and special care in design might be needed. This again demonstrates the utility of *GeniSTELA* and an indication of the potential practical usage in fire safety thermal design.

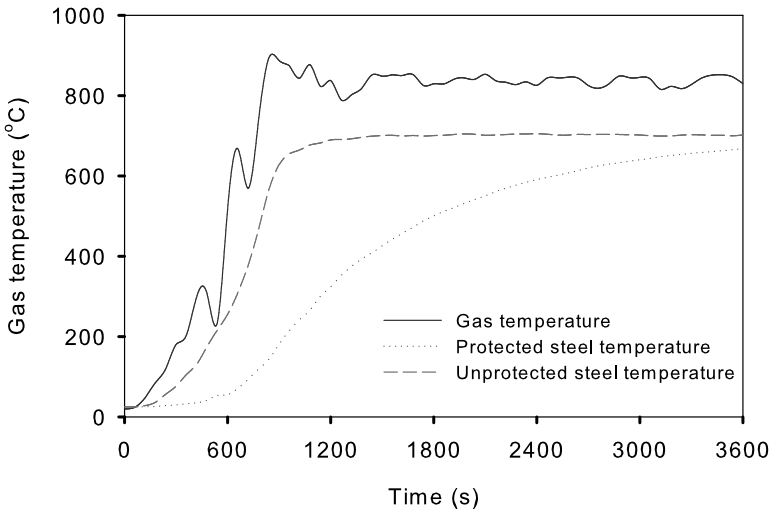

Figure 5.27: Temperature predictions at failure location

5.5.4.4 Model sensitivities

A range of calculated steel temperatures are available for parametric studies with the aid of the simultaneous calculation capabilities of *GeniSTELA*. As illustrated previously in Table 5.2, the model sensitivities to the steel section specification, protection material related issues covering protection types, fire ratings, moisture content, thermal properties such as thermal conductivity, specific heat, density, emissivity, together with fire properties have been studied. The figures below demonstrate the sensitivity variations on the basis of the default case. The results below are based on location g and similar results would be obtained from other locations such as h, i and j etc.

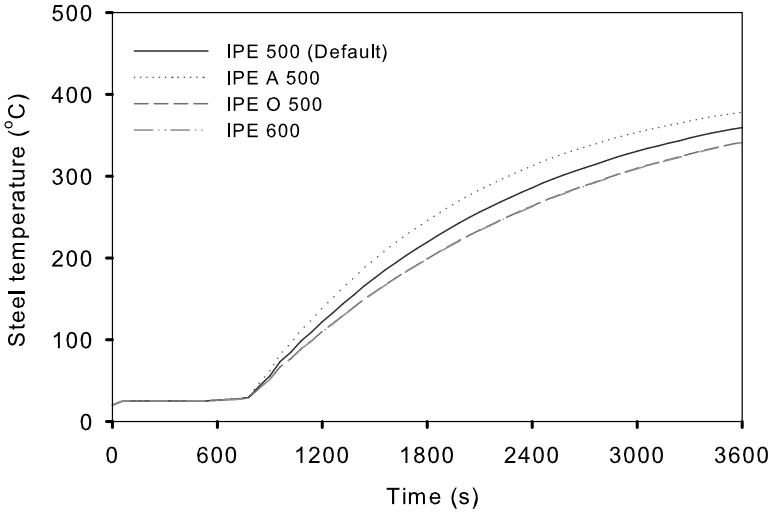

Figure 5.28: Effect of steel section types on calculated steel temperatures

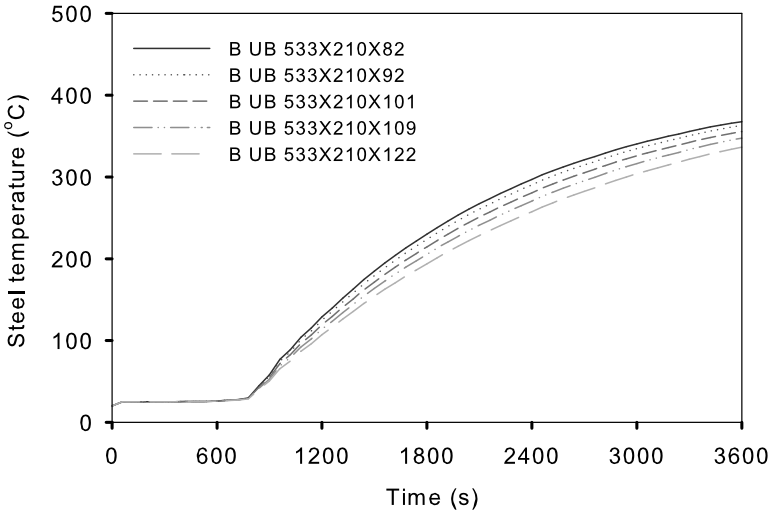

Figure 5.29: Effect of steel section weight on calculated steel temperatures

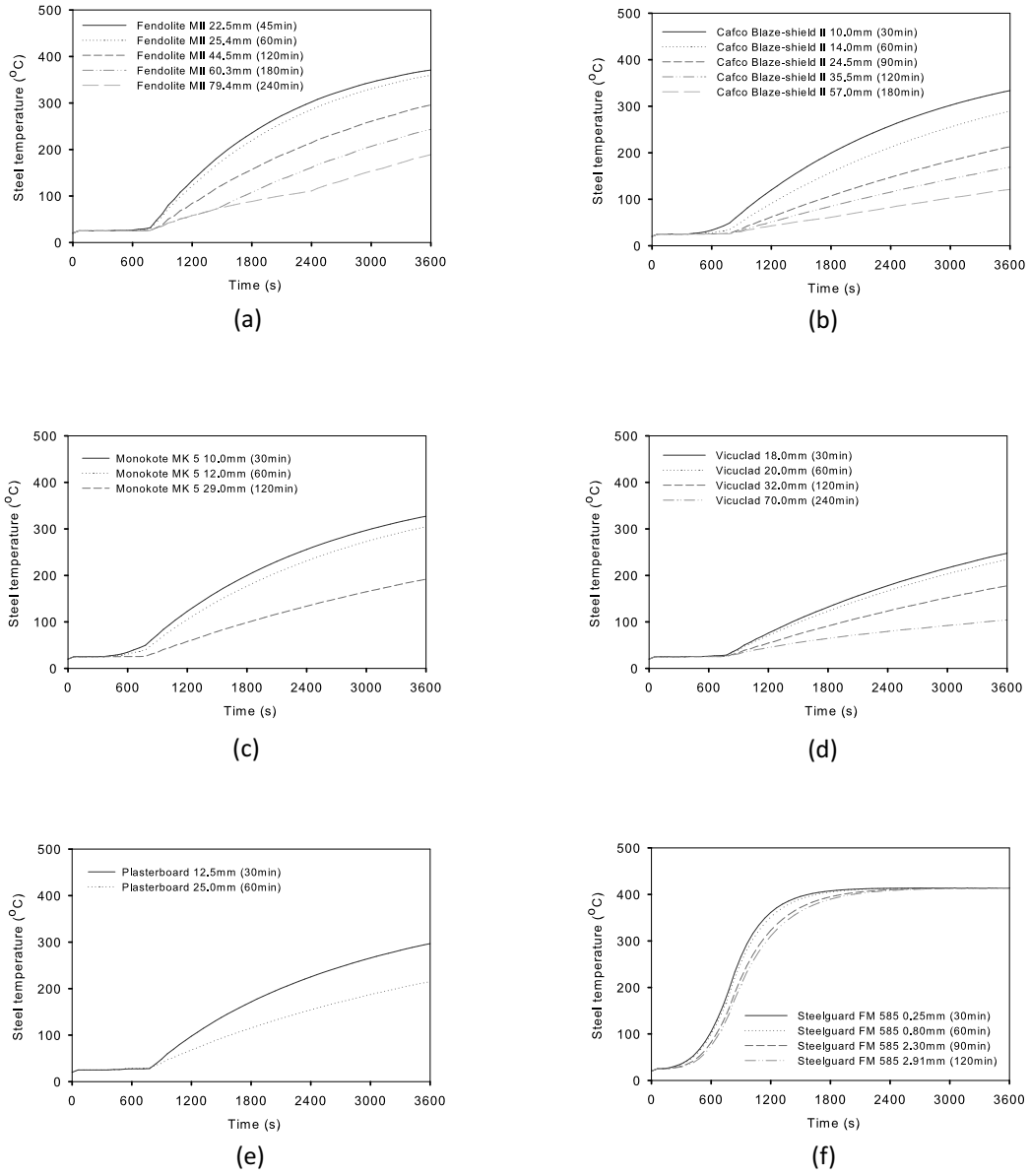

Figure 5.30: Effect of protection fire rating thickness on calculated steel temperatures

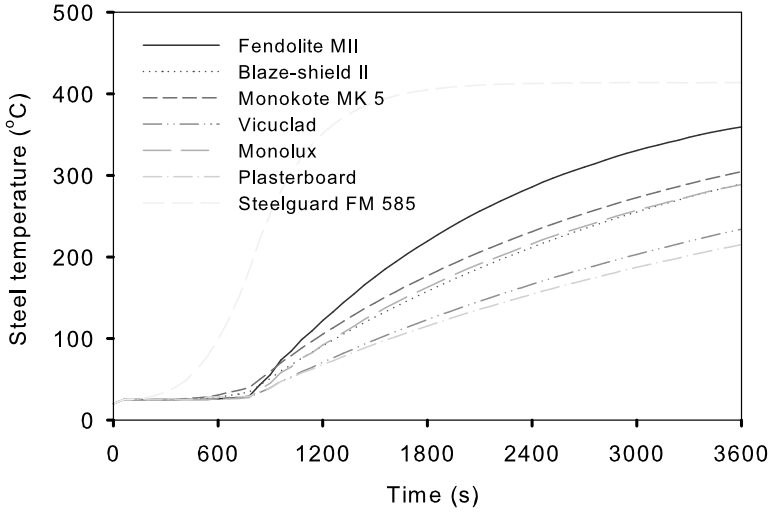

Figure 5.31: Effect of protection type on calculated steel temperatures at 1 hour fire rating thicknesses

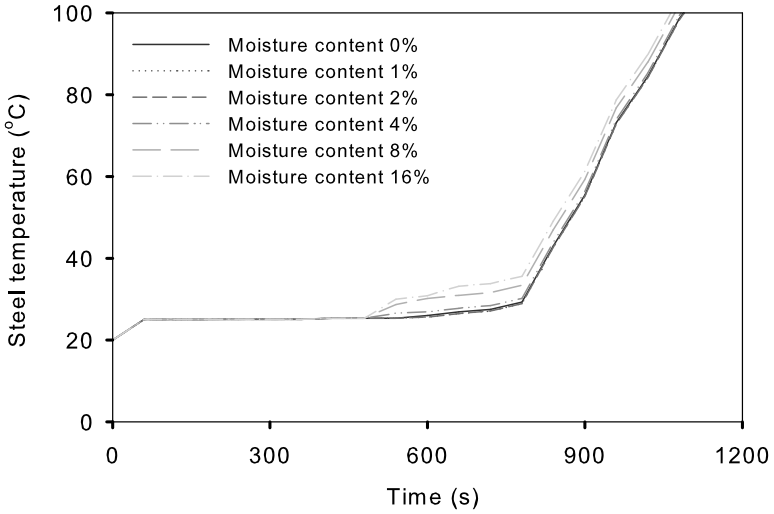

Figure 5.32: Effect of protection moisture content on calculated steel temperatures

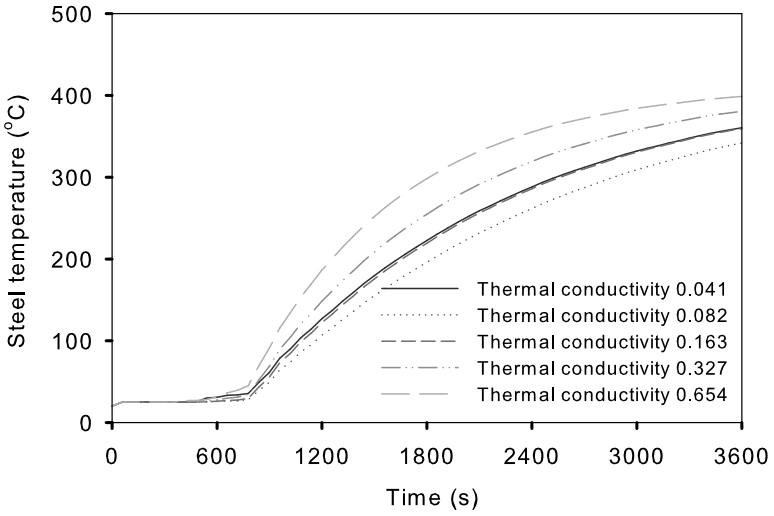

Figure 5.33: Effect of protection thermal conductivity on calculated steel temperatures

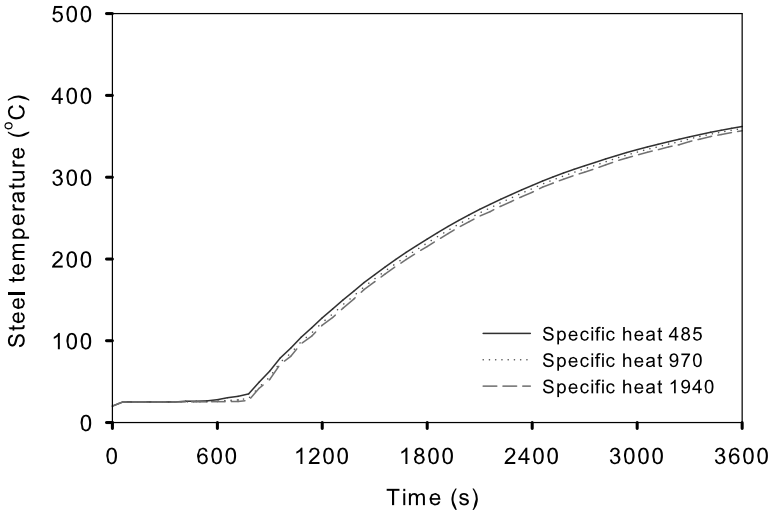

Figure 5.34: Effect of protection specific heat on calculated steel temperatures

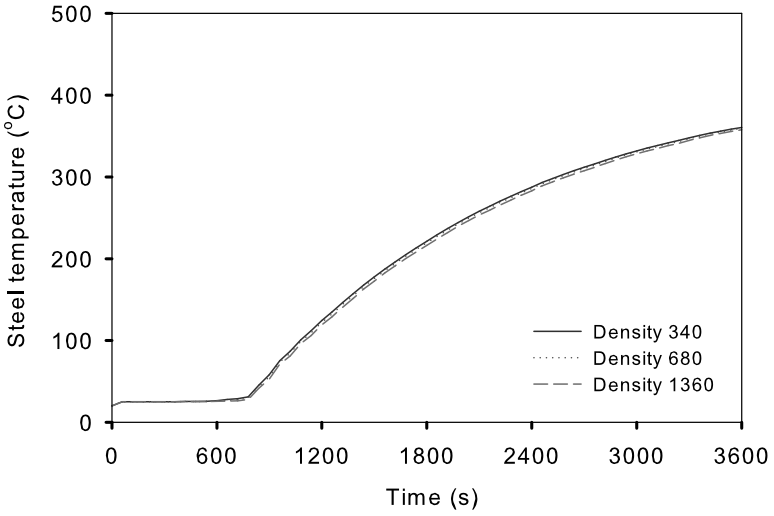

Figure 5.35: Effect of protection density on calculated steel temperatures

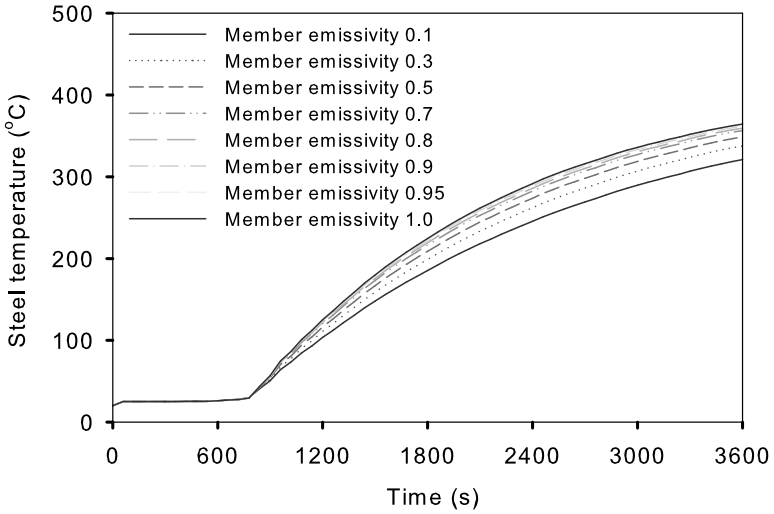

Figure 5.36: Effect of protection emissivity on calculated steel temperatures

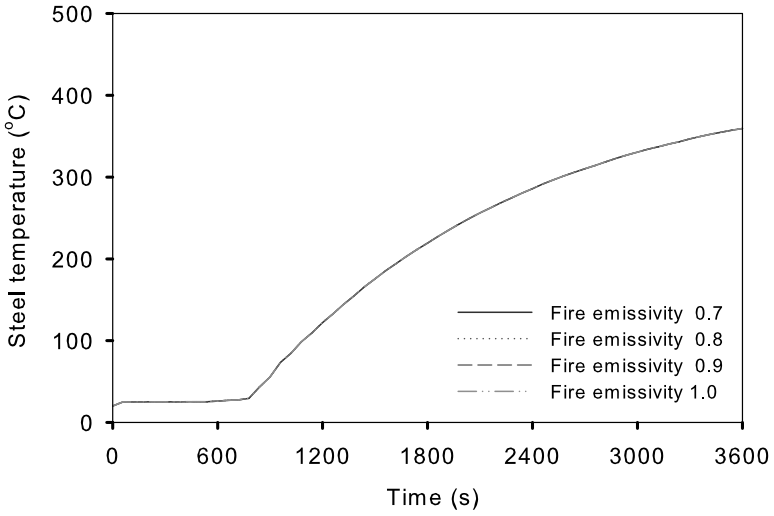

Figure 5.37: Effect of fire emissivity on calculated steel temperatures

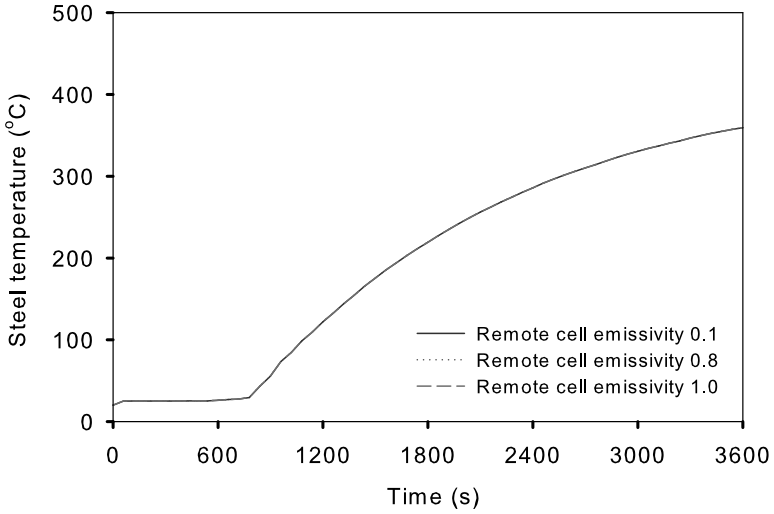

Figure 5.38: Effect of remote steel cell emissivity on calculated steel temperatures

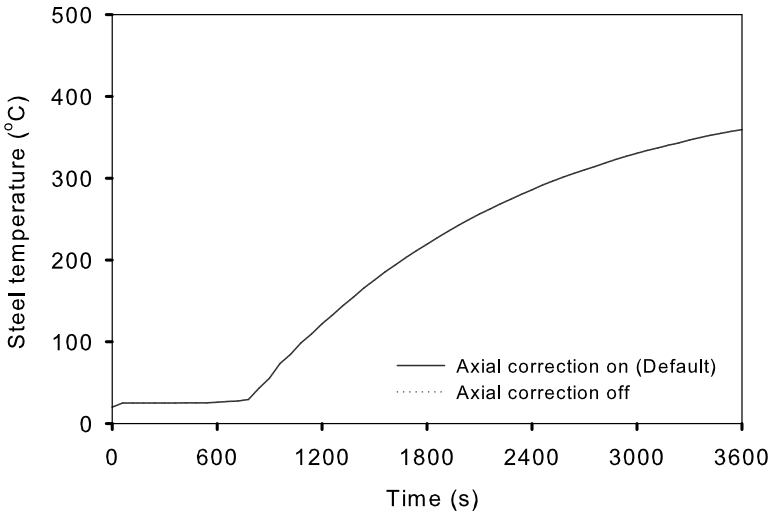

Figure 5.39: Effect of axial gradient correction on calculated steel temperatures

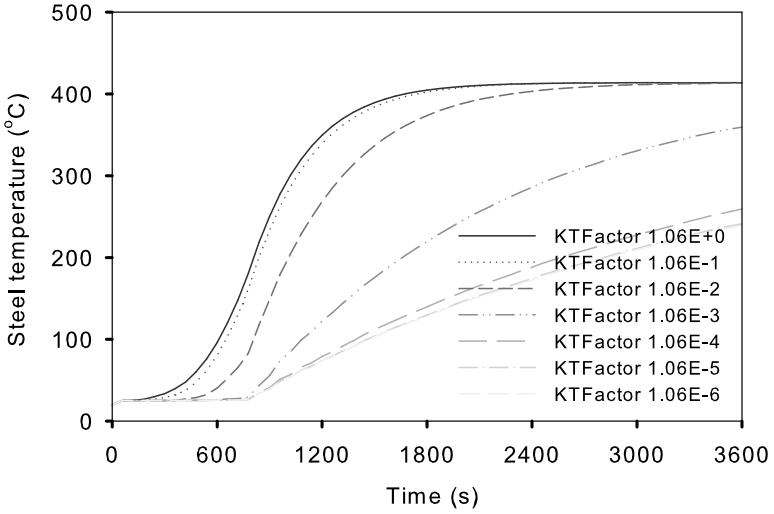

Figure 5.40: Effect of thermal conductivity linear rate of change with temperature on calculated steel temperatures

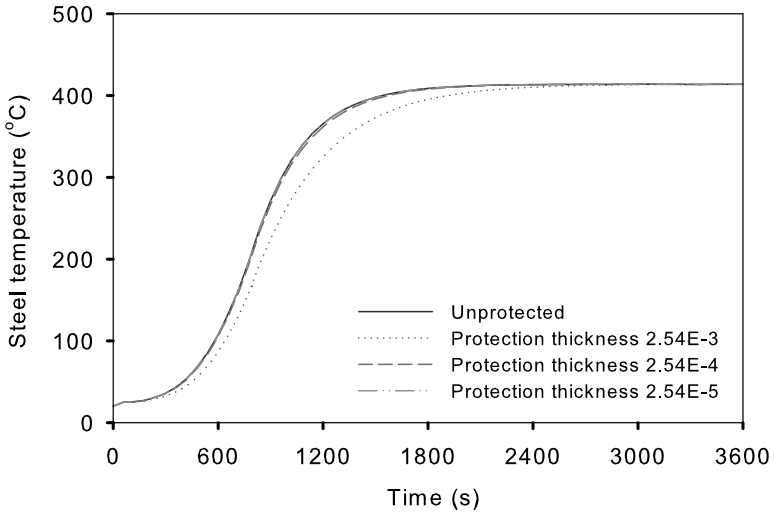

Figure 5.41: Effect of very small protection thickness and non-protection on calculated steel temperatures

From the above results, it is observed that the final steel temperature is strongly affected by the structural element geometry and the fire protection materials, as well as thermal conductivity or related affecting factors such as the KTFactor, which is the linear rate of change with temperature on conductivity. Since the thermal conductivity is strongly affecting the final steel temperature rises, they are also inspected by investigating a big range of KTFactor here. The range indicated by the above values may exceed what is physically expected, except in abnormal circumstances involving significant solid degradation, melting, etc. The moisture content could be an important factor within certain temperature range before the moisture has vanished. The emissivity effect has been studied by comparing steel temperature predictions from a range of emissivity values representing high emissivity (above 0.5) and low emissivity (below or equal to 0.5) either for the fire or for the member. It is found that the fire emissivity doesn't affect the final steel temperature prediction, but that the member surface emissivity is a key factor that may influence the temperature rise in the steel. But overall, the emissivity has a low-order effect on performance especially for the start of the heating regime when convective heat transfer is dominant, as seen in Figure 5.36 where there is a tiny difference for the first $900s$. This point is consistent with the findings by Staggs and Phylaktou (Staggs & Phylaktou, 2008). Figure 5.41 demonstrates a fairly good agreement among the steel temperature

predictions for an unprotected member and that of negligible protections.

5.5.4.5 Concluding comments

GeniSTELA has been applied to a 'hypothetical benchmark scenario', involving simultaneous calculations of 72 cases, considering different structural members and protection material parameters, etc. All the results were obtained within affordable computational requirements. The results have been compared with those from other modelling methodologies. In general, they indicate that where the structural elements do not influence the flow field and gas temperatures significantly, as in this example, acceptable calculations for the thermal response of the element can be achieved.

The results for model sensitivities to a range of parameters of interest have been found to be in good agreement with findings in literature (Wong & Ghojel, 2003). In addition, as expected, the steel temperature rise is more sensitive to the protection thickness, protection material types and thermal conductivity, hence, the correct justification of their values would be important for the accuracy of the predictions. The thicker the protection is, the slower the steel temperature rise; or with higher thermal conductivity of the protection, the energy would transfer faster in to the steel layer, thus steel temperature would rise faster. The *GeniSTELA* model capabilities, especially the protection properties submodel, have been demonstrated. Based on the results, it is useful to set certain parameters as default in modelling practice. Those parameters, such as the protection member emissivity, in a range of $0.7 \sim 1.0$; the fire emissivity as well as the remote cell emissivity for axial correction could be simply set as 1.0 by default, since their effects on the final steel temperature prediction is negligible.

The above results are based on the benchmark fire test scenario. For other fire scenarios, such as post-flashover scenario or when a lower temperature regime where convection dominates is considered, the effect of protection member emissivity on the steel temperature rise would be reduced. Or when a very long fire is considered, the steel temperature rise is much slower, the protection material thermal properties would have even stronger effects, and vice versa, for a very short fire, the effects would be reduced. Therefore, the above findings from the benchmark test scenario case study could be only a representative of the similar

fire scenario.

Overall, the results serve to illustrate the importance of using generalised methodologies in tackling fire thermal response problems, providing a possible new approach for performance-based design in particular of protected steel structures.

5.6 Exploitation

5.6.1 Introduction

The practical use of *GeniSTELA* in the aspect of thermal analysis has been previously presented. Nevertheless, the ultimate goal of the work on *GeniSTELA* is prediction and assessment of the mechanical performance of structures in fires, but so far no failure criteria beyond traditional critical temperature methods have been considered. In light of the advantages of *GeniSTELA* and literature reviews, the potential for using simplified structural analysis methods, exploiting closed-form solutions, to establish a more robust means of predicting the ultimate structural performance within this generalised framework is explored and described in this section. This involves the literature review and discussion of the state-of-the-art, together with a proposal for a simplified methodology.

5.6.2 Literature review

Structural Fire Engineering (SFE) deals, amongst other things, with specific aspects of passive fire protection in terms of analysing the thermal effects of fires on buildings and designing structural members for adequate load bearing resistance, i.e. the structural fire resistance. It covers a wide range of levels of knowledge and competence, which could be summarized into three basic aspects: fire modelling, thermal analysis and structural analysis.

GeniSTELA has been confirmed as a practical engineering tool for thermal analysis of structures in fire. For a complete structural fire engineering tool, it would be even more applicable if a reliable structural analysis methodology were to

be developed within the *GeniSTELA* framework, allowing direct use of the results in design to predict or prevent the structural failure under fire conditions. However, the theory and procedures for analysing structural behaviour under fire conditions is much more complex compared to those for structural analysis at normal temperatures. A brief literature research focused on the structural analysis methodology within the structural fire safety field has been carried out and presented here as a basis for discussion of possible further development of *GeniSTELA*.

Traditionally, most code-based design has been based on simple calculations, referencing measured fire performance in standard tests. Information on member dimensions and construction details with respect to fire resistance ratings is provided. The designers need only apply specified construction features to satisfy the code requirements. This procedure is prescriptive-based. Currently in the US, the prescriptive approach is commonly used for designing structures to resist fire (Quiel & Garlock, 2006).

More recently, performance-based procedures have been developed based on the empirical or theoretical relationships. Basically, the mechanical properties of the structural materials at elevated temperatures are incorporated into the traditional structural theory to develop a rational analysis procedure for predicting structural behaviour under fire conditions. This approach therefore provides more flexibility.

The use of advanced methods based on numerical models has become more wide spread with the progressive shift towards performance-based design. These approaches will not replace standard testing, but they can already be used in a complementary fashion, to extend the application of test data.

During this performance-based approach development stage, a variety of methods have been developed. Research such as that by Lane (Lane, 2000) and Gewain et. al (Gewain *et al.*, 2003) has emphasized the implementation of realistic fire temperature-time histories that are determined from compartment fire models. These temperature curves can then be applied to the appropriate structural sections to determine thermal and mechanical response. Usmani et. al (Usmani *et al.*, 2001) have developed analytical expressions, confirmed with the results of

computational finite-element modelling, which can be used to solve for the moment and midspan deflection in heated horizontal beams. Wang et. al (Wang *et al.*, 1995) described the use of structural subframe models to effectively capture the behaviour of a full fire-exposed building frame, with the consideration of the effects of non-uniform temperature distributions on the failure temperature and failure times of column sections with different load levels and slenderness ratios. Garlock and Quiel (Garlock & Quiel, 2006; Quiel & Garlock, 2006) have developed an even more flexible structural analysis methodology which predicts the behaviour of steel perimeter columns in a fire considering its interaction with the beam that frames into it.

In addition, recently, guidelines for the performance-based structural-fire design of steel frames have been included in the 2005 edition of AISC's Steel Construction Manual (AISC, 2005). The calculations of structural performance via "advanced" analysis methods or, where appropriate, via "simple" analysis methods have been clearly stated within these provisions. Similar to the Eurocode, the AISC manual references the changing material properties (most notably the modulus of elasticity and yield strength) of steel and concrete at elevated temperatures (AISC, 2005; Quiel & Garlock, 2006).

The AISC manual stipulates that an analysis of a structure's mechanical response must account for the deterioration of steel's strength and stiffness properties as its members' temperatures increase as well as the effects of thermal expansions and large deflection. Advanced methods must be used to capture the response of the structural frame to fire, particularly the interaction between connected structural members (AISC, 2005). Simple methods are permitted only when the assumption of uniform temperature is reasonable while support and restraint conditions remain unchanged (AISC, 2005).

5.6.3 Discussion of the state-of-the-art

According to literature research, an essentially prescriptive approach has been used by the building industry for nearly a century and is still commonly used in structural design. However, it is based on the furnace-test methodology which is principally a thermal test rather than a structural test. Besides, it considers

behaviour of an individual member without consideration of how it interacts with the surrounding structure (Quiel & Garlock, 2006).

Recently, with great willingness to adapt and implement performance-based standards among the European countries and elsewhere, the performance-based methodologies have been invoked and the development of performance-based methodologies both for thermal analysis and structural analysis has been called for. For the structural analysis methodology, it is recommended that this should be based on the performance of the structural frame as a whole, rather than the individual components. This could overcome the limitations of existing prescriptive-based methodology in terms of the interaction between different structural components.

However, complexity of solution arises with the development of performance-based methodologies. A compromise between accuracy and computational cost is also desired. Simplified performance-based approaches therefore become an important option to most practitioners.

5.6.4 Novel approach proposal

Based on the Quiel and Garlock (Garlock & Quiel, 2006; Quiel & Garlock, 2006) model concept, the structural analysis methodology within the *GeniSTELA* framework is proposed as a "simple" method by considering the protected structural component as a whole, and using a simplified structural model to represent interactions between each component, adding a spring where appropriate to represent the flexural stiffness and strength. The members are thereafter subjected to thermal expansion and thermal bowing actions due to the temperature elevation aside from dead and live loads. As illustrated in Figure 5.42, the structural component is reduced as a column and beam.

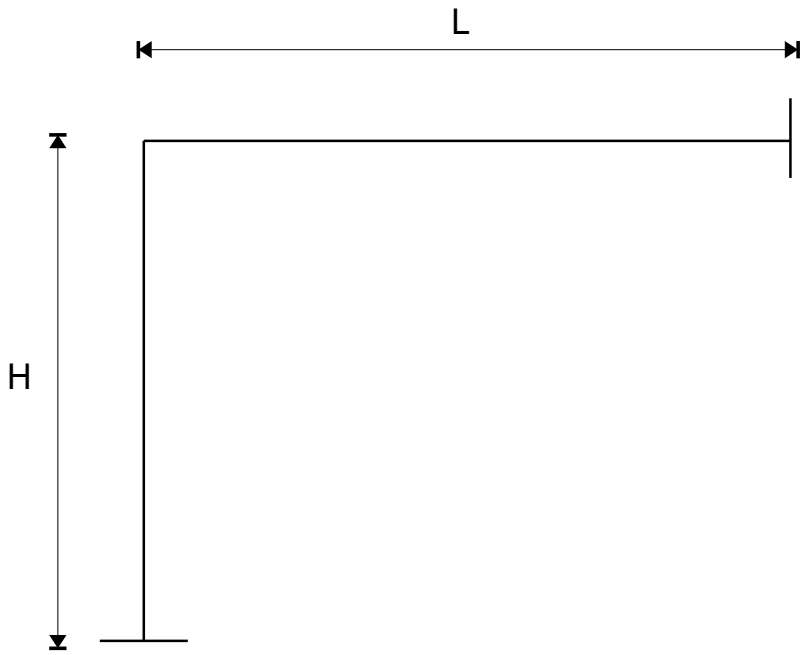

Figure 5.42: Steel flange thickness effect

Each part of the component is analysed separately, with spring of varying stiffness with time and temperature representing the interaction between each member. Figures 5.43 and 5.44 show the conceptual models for each part of the component.

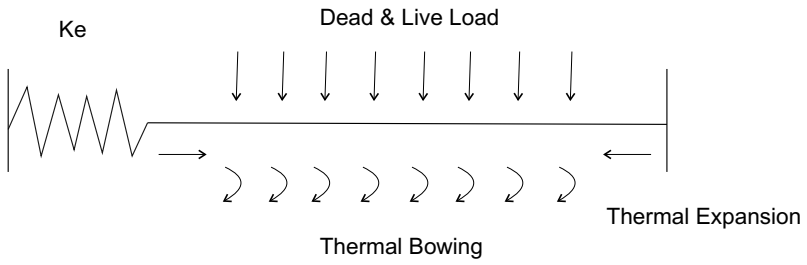

Figure 5.43: Analytical model for beam

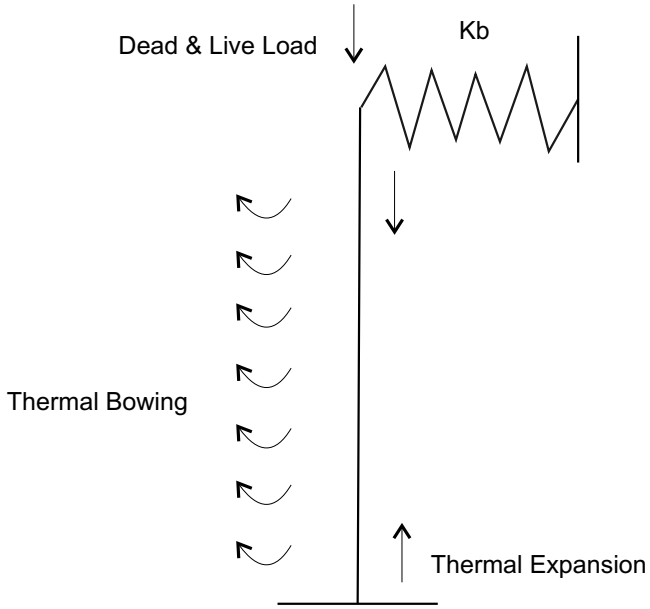

Figure 5.44: Analytical model for column

As specified in the Quiel and Garlock simplified material model (Quiel & Garlock, 2006), and based on Eurocode (BSI, 2005a), the steel strength and stiffness could be a function of temperature which is obtained through *GeniSTELA*. More precisely speaking, a field steel temperature, protection temperature and gas temperature are obtained from *GeniSTELA* and the results are further used to find out the reduction factors for temperature variation steel strength, stiffness and modulus of elasticity according to the simplified material model.

Hence, from the analytical model for beam, due to the thermal expansion, the stress-strain relationship for structural steel is obtained, with total strain as given below:

$$\varepsilon_t = \frac{\alpha \cdot \Delta T}{1 + \frac{E \cdot A}{K \cdot L}} \tag{5.1}$$

where

ε_t is the total strain including mechanical strain and thermal strain, $[-]$
α is the coefficient of linear thermal expansion, $[1/K]$
ΔT is the temperature difference is the difference between the two recorded strains, $[K]$ or $[°C]$
E is the young's modulus (modulus of elasticity), $[N/mm^2]$
A is the section area, $[m^2]$
K is the stiffness, $[N/m]$
L is the initial length before the change of temperature, $[m]$

Similarly, thermal expansion might occur when a column is considered. For this case, several hypotheses are made concerning the surroundings of the column. There is no change in column length if the compartment could be considered as part of an elevated building. In the event that the compartment is not above other levels, the column could expand freely. In any case, the equations developed previously are valid. The stiffness of the spring will just be infinite if no change in length is possible and the stiffness of the spring will minimal in the opposite case. Therefore, with the available material properties, the axial force caused by the thermal expansion could be predicted.

Another temperature change induced thermal action is thermal bowing. Current practice in fire safety engineering is to design columns assuming a uniform temperature distribution through the depth of the member. This assumption is not always verified and in some cases the thermal gradient through the depth can be important. A column on the perimeter of the building, a beam supporting a concrete slab or a column embedded in a concrete or brick wall are good examples of members developing a thermal gradient through their depth. The gradient causes the heated surface to expand more than the non heated surface and induces bending.

From above, axial load would be introduced accompanying the thermal expansion, while an additional moment would accompany the thermal bowling. If the member's expansion is retrained and at the same time is submitted to a thermal gradient, it will then undergo a moment and an axial load.

Besides the two thermal actions, other mechanical action might apply to the structural component. Ultimately, with consideration of combined mechanical and thermal actions, it should be possible to predict the structural responses in-

clude deflection, bending moment and forces within this methodology.

Appropriate assumptions are needed in this proposed novel model. For instance, the temperature envelope between the maximum and minimum temperature is narrow for the protected beam, so the lumped mass solution which assumes a uniform temperature through the section may be an accurate approximation of the section's average temperature, as stated by Quiel and Garlock (Quiel & Garlock, 2006). Therefore, within this proposed novel "simplified" structural analysis model, a uniform temperature within the member might reasonably be assumed. However, the temperature gradient effects should also be investigated. Gravity loads are not included in the novel model; it is assumed that either with or without applied gravity loads, the final structural responses, deflection, bending moment and forces, are not significantly affected.

A project developing the methodology further from that described here has been undertaken by MSc student Loïc Faure in the University of Glasgow and University of Edinburgh for further detailed development of a generalised structural analysis methodology, *GeniSTRUC*, within the *GeniSTELA* framework. The methodology is developed on the basis of detailed plastic and buckling analysis, in order to assess the structural integrity of single members taking into account a gradient along the length of the member. Springs are used to model the direct surroundings of the member. The model has been implemented in a spreadsheet and validated by comparison with FEA (Finite Element Analysis) modelling using *ABAQUS* and real events, such as the external column case study in the CTICM test (Welch *et al.*, 2008), where the thermal analysis is carried out by *GeniSTELA* while the structural mechanics analysis by the method outlined here. (Faure, 2008)

5.6.5 Conclusion

GeniSTELA efficiently provides field thermal responses for a collection of different cases, considering different structural members and protection material parameters. The potential development in terms of the structural responses has been explored. With the help of literature review, on the focus of the design methodologies, a simplified structural analysis methodology has been proposed

with the main concern being the thermal expansion and thermal bowling induced structural responses and impact on possible structural failure modes. The preliminary development of the methodology has been carried out within the *GeniSTELA* framework and applied to the CTICM test external column case. This has initially demonstrated the practical use of both *GeniSTELA* and the further development in a generalised structural analysis methodology.

Chapter 6

Conclusions

6.1 Overview

Focusing on the generalised thermal analysis methodology, various aspects have been studied. This includes the literature review of the related topics, the development of *GeniSTELA* model together with material properties submodels. The verification of *GeniSTELA* in comparison with Eurocode methodology and parametric study has been presented. Certain details of the model, such as the 3D effect correction significance, the Newton-Raphson procedure significance have been also verified with a simple universal beam case study. The model is validated with two full-scale test scenarios, the Warrington fire resistance furnace test and the BRE large compartment test. Both results demonstrate that *GeniSTELA* could provide sufficiently accurate prediction results and illustrate its generality by providing a field calculation result. The computational time requirement study indicates the practical use of the method in terms computational affordance, and the simultaneous calculation scheme improves its generality. An example regarding a hypothetical benchmark test case simulation has demonstrated the practical use of the methodology in thermal analysis of structural members in fire. The potential extension to the structural response analysis has been explored, and a proposal is suggested. A generalised structural analysis methodology is initially developed and validated with a test case study. Finally, future related research work is recommended.

6.2 General conclusions

A generalised methodology for thermal analysis of protected steel structures in fire is described. The method is based on a 1D heat transfer analysis, but appropriate corrections are developed to reconstruct a quasi-3D solution. A framework for the inclusion of treatments for intumescence effects has also been established, with provision for simple calibration in the case of each specific formulation of interest. The *GeniSTELA* implementation of the method is based on simultaneous computations spanning the range of cases of interest, providing a generalised methodology. Validation of *GeniSTELA* regarding to two full-scale cases has highlighted a number of issues to do with practical use of the code as aforementioned in the remarks of Chapter 4. The results confirm the sufficiency of the algorithms adopted and comparisons with measurements in a post-flashover compartment fire test are satisfactory. Strong dependencies on the thermal properties of the protection materials are observed in the sensitivity studies for both tests. The computational time requirement has been assessed and found to be acceptable. A demonstration example is provided based on a hypothetic benchmark test scenario, with a study of 72 parametric calculation cases, identifying the possible failure situations where attention must be paid in design practice. Computational demands are found to be acceptable, even with multiple simultaneous calculation cases. These results serve to illustrate the importance and feasibility of using generalised methodologies in tackling thermal response problems. As a complement for structural fire safety engineering design, literature on structural response analysis methodologies have been reviewed, providing an insight for developing a generalised structural analysis methodology within the *GeniSTELA* framework. A proposal is suggested and the preliminary methodology has been developed and the work is still underway. Overall study provides a possible practical new approach for performance-based design of structural members in fire.

6.3 Brief summary

The key points of the work produced could be briefly concluded and highlighted as follows:

- The results confirm the sufficiency of the algorithms adopted.
- The results also indicate some of the model sensitivities, with strong dependencies on the properties of the thermal protection materials.
- Comparisons with the measured temperatures from the full-scale fire tests show a sufficient agreement with the simulation results, which in consequence, imply the feasibility of *GeniSTELA* for application to thermal analysis of structures.
- In addition, the set of simultaneous thermal calculations executed in the model facilitates the application of *GeniSTELA* to investigate all the parameters needed.
- Parametric study is computationally tractable.

6.4 Future work

Though the methodology has been well implemented and validated, confirming *GeniSTELA* as a generalised practical tool for thermal analysis of structures in fire, there is still great potential to improve it. Further work is therefore needed to increase its generality, improve its accuracy and widen its applicability. Those future works include:

- Improve certain submodels to achieve better results, such as to generalise the protection property submodel by concerning different protection types, including profile protection and box protection.
- Consider thermal analysis of structures with a protection consisting of multi-layer materials with different properties.
- Provide a library of frequently using parametric variants for automatic selections.
- Improve the CFD gas field calculation, since for the time being, it is assumed that the structure in the compartment would not significantly affect the gas flow; however, this is true for certain cases, thus the gas field simulation results could be obtained from CFD with no structure being represented

within the compartment and input as the boundary conditions for *GeniSTELA*. For certain cases, the results would affect the surface temperature, thus leading to significant errors. A treatment for this sort of case is desired.

- Further develop of models within the *GeniSTELA* framework for calculation of structural responses.

Appendix A

Calculation of Weight Factor

By definition, the weight factor accounts for the ratio of the actual thermal energy absorption in the material to the idealised thermal energy absorption in the same material, as shown roughly in the figure below. Here the idealised thermal energy absorption refers to the idealised state that the energy penetrates through the overall thickness of the protection material.

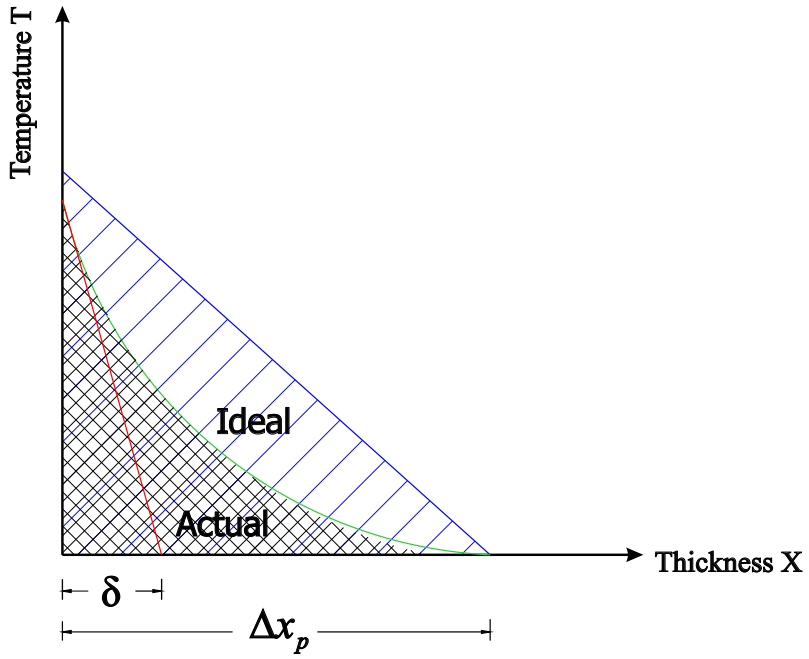

Figure A.1: Protection actual and idealised thermal energy absorption within the protection

In the above figure, the area under the green curve represents the actual thermal energy absorption while the area under the blue line represents the idealised thermal energy absorption. Due to the complexity of calculating the area under the green curve, the actual area is calculated as the area under the orange line, which is tangential to the curve. This obviously would results in another model error. However, by literature review, it is found that the influence of this error is of little significance. This has also been confirmed in the early stage of the research. Hence, the weight factor w_p is calculated as below:

$$A_{actual} = \frac{1}{2} \cdot (T - T_{initial}) \cdot \delta \tag{A.1}$$

$$A_{ideal} = \frac{1}{2} \cdot (T - T_{initial}) \cdot \Delta x_p \tag{A.2}$$

$$w = \frac{A_{actual}}{A_{ideal}} = \frac{\delta}{\Delta x_p} = \frac{2 \cdot (\frac{k_p \cdot t}{c_p \cdot \rho})^{1/2}}{\Delta x_p} \tag{A.3}$$

$$w_p = \min\{w, 1\} \tag{A.4}$$

With δ is the thermal penetration depth (Miles & Kumar, 2003),

$$\delta = 2 \cdot (\frac{k_p \cdot t}{c_p \cdot \rho})^{1/2}$$

where

A_{actual}	is the enclosed temperature area covered by actual thermal penetration depth of the protection, $[K \cdot m]$
A_{ideal}	is the enclosed temperature area covered by overall thickness of the protection, $[K \cdot m]$
$T_{initial}$	is the initial protection temperature, $[K]$
T	is the protection temperature at current time, $[K]$
δ	is the protection thermal penetration depth, $[m]$
Δx_p	is the protection overall thickness, $[m]$
k_p	is the protection thermal conductivity, $[W/(m \cdot K)]$
c_p	is the protection specific heat, $[J/(kg \cdot K)]$
ρ	is the protection density, $[kg/m^3]$
t	is either the 'true' transient time or a user prescribed 'time-to-steady-state' value, $[s]$

Appendix B

Representation of junction effect

B.1 Introduction

Four effects have been considered to generalise the quasi-3D numerical model for which the precise nature of localised heating is important. Those effects are as aforementioned: junction effect, end effect, heat sink effect and axial temperature gradient effect. Within those four effects, junction effect is considered by adding an additional correction term on the base of the uncorrected result, i.e.:

$$T_{s,junct} = T_{s,avg} + \Delta T_{s,junct} \tag{B.1}$$

where

$T_{s,avg}$	is the uncorrected steel temperature, solved from the basic 1D model governing equation, as indicated in Equation 3.1.
$T_{s,junct}$	is the steel temperature with the consideration of junction effect.
$\Delta T_{s,junct}$	is the junction effect correction term, as specified below:

$$T_{s,junct} = -\frac{\dot{q}_{rad,junct} \cdot \chi}{k_s} \tag{B.2}$$

With χ as an appropriate length scale considering the section geometry, given as:

$$\chi = \frac{4w \cdot f}{(2f \cdot d + w \cdot b)}$$

In which, f is the flange thickness; $w = t_{web}$ is the web thickness; $d = d_{web}$ is the web depth, $b = b_{flange}$ is the flange width.

And with $\dot{q}_{rad,junct}$ is the net heat flux caused by the junction effect, given by:

$$q_{r,junction} = \frac{k_s \cdot t_{web}}{d_{web} \cdot b_{flange}} \cdot (1 - \frac{h \cdot d_{web}}{k_s}) \cdot (T_s - T_a) + \frac{t_{web}}{b_{flange}} \cdot \varepsilon \cdot \sigma \cdot \left(T_a^4 - T_s^4\right)$$

In which, k_s is the thermal conductivity of section material, $[W/(m \cdot K)]$; h_c is the convection coefficient, $[W/(m^2 \cdot K)]$; T_s is steel temperature $[K]$; T_a is the ambient temperature, equals to $293.15K$; ε is the emissivity $[-]$ and σ is the Stefan-Boltzmann constant, equals to 5.67×10^{-8} $[W/(m^2 \cdot K^4)]$.

The following sections describe the derivations of χ and $\dot{q}_{rad,junct}$.

B.2 Derivation of χ

Assume χ is a length ratio which is a function of the section geometry, here defined as:

$$\chi = \frac{\xi}{X_{all}} = \frac{\xi}{(a+b)/2} \tag{B.3}$$

where ξ is the effective section geometry, reflecting the effective value in the assumption of the situation that the end flange cell transfers heat to the middle of the web directly. Therefore, the heat transfers in the flange equals to the heat in the web and also equals to the heat transfers through the effective overall section geometry, i.e.

$$2 \cdot q_f \cdot A_f = q_w \cdot A_w = q_{all} \cdot \xi \tag{B.4}$$

And:

$$A_f = f \cdot 1$$

$$A_w = w \cdot 1$$

$$q_f = k_f \cdot \frac{\Delta T_f}{\Delta x_f}$$

$$q_w = k_w \cdot \frac{\Delta T_w}{\Delta x_w}$$

$$q_{all} = k_{eff} \cdot \frac{\Delta T_{all}}{\Delta x_{all}}$$

$$k_f = k_w = k_{all} = k_{eff} = k_s$$

Therefore, Equation B.4 can be expanded as:

$$2 \cdot k_f \cdot f \cdot \frac{\Delta T_f}{\Delta x_f} = k_w \cdot w \cdot 1 \cdot \frac{\Delta T_w}{\Delta x_w} = k_{eff} \cdot \xi \cdot \frac{\Delta T_{all}}{\Delta x_{all}} \tag{B.5}$$

i.e.

$$2 \cdot k_s \cdot f \cdot \frac{\Delta T_f}{b/2} = k_s \cdot w \cdot 1 \cdot \frac{\Delta T_w}{d/2} = k_s \cdot \xi \cdot \frac{(\Delta T_f + \Delta T_w)}{(b+d)/2}$$

Two relations would be derived from above:

$$\begin{cases} \Delta T_f = \frac{w \cdot b}{2f \cdot d} \cdot \Delta T_w & (a) \\ k_s \cdot \xi \cdot \frac{(\Delta T_f + \Delta T_w)}{(b+d)/2} = k_s \cdot w \cdot 1 \cdot \frac{\Delta T_w}{d/2} & (b) \end{cases}$$

Substitute (a) into equation (b),

$$\frac{\xi}{(b+d)/2} \cdot (\frac{w \cdot b}{2f \cdot d} \cdot \Delta T_w + \Delta T_w) = w \cdot \frac{\Delta T_w}{d/2} \tag{B.6}$$

It gives:

$$\frac{\xi}{(b+d)/2} \cdot (\frac{w \cdot b}{2f \cdot d} + 1) = \frac{w}{d/2} \tag{B.7}$$

Therefore,

$$\xi = \frac{2fw \cdot (d+b)}{2f \cdot d + w \cdot b} \tag{B.8}$$

Finally, the length ratio is:

$$\chi = \frac{\xi}{(b+d)/2} = \frac{2f \cdot w \cdot (d+b)}{2f \cdot d + w \cdot b} \Big/ \frac{(b+d)}{2} = \frac{4w \cdot f}{2f \cdot d + w \cdot b} \tag{B.9}$$

Also note that the term in this derivation f is the flange thickness, $w = t_{web}$ is the web thickness, $d = d_{web}$ is the web depth and $b = b_{flange}$is the flange width.

B.3 Derivation of $\dot{q}_{rad,junct}$

$\dot{q}_{rad,junct}$ is the net heat flux causing the difference at the junction of the structural element. The derivation of its value is based on the following schematic model in Figure B.1:

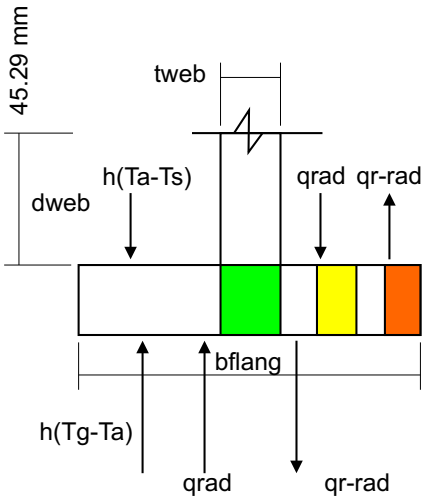

Figure B.1: Cross-section for structures with junction effect corrections

For the single 1D model cell,

$$q_{rad,face1} + q_{rad,face2} + h \cdot (T_g - T_s) + h \cdot (T_a - T_s) - 2\varepsilon \cdot \sigma \cdot T_s^4 = 0 \tag{B.10}$$

For the cell located in the junction, the heat would transfer to the web by conduction, and energy balance equation can be written as:

$$\begin{aligned} A_{flange} \cdot [q_{rad,face1} + h \cdot (T_g - T_s) - \varepsilon \cdot \sigma \cdot T_s^4] \\ +(A_{flange} - A_{web}) \cdot [q_{rad,face2} + h \cdot (T_a - T_s) - \varepsilon \cdot \sigma \cdot T_s^4] = A_{web} \cdot \frac{k_s}{d_{web}} \cdot (T_s - T_a) \end{aligned} \tag{B.11}$$

Since

$$A_{flange} = b_{flange} \cdot 1, \qquad A_{web} = t_{web} \cdot 1$$

The above equation can be expanded as:

$$\begin{aligned} & b_{flange} \cdot 1 \cdot [q_{rad,face1} + h \cdot (T_g - T_s) - \varepsilon \cdot \sigma \cdot T_s^4] \\ +(b_{flange} \cdot 1 - t_{web} \cdot 1) \cdot & [q_{rad,face2} + h \cdot (T_a - T_s) - \varepsilon \cdot \sigma \cdot T_s^4] \\ & = t_{web} \cdot 1 \cdot \frac{k_s}{d_{web}} \cdot (T_s - T_a) \end{aligned} \tag{B.12}$$

Rearrange, yields:

$$\begin{aligned} & q_{rad,face1} + q_{rad,face2} + h \cdot (T_g - T_s) + h \cdot (T_a - T_s) - 2\varepsilon \cdot \sigma \cdot T_s^4 \\ = \frac{k \cdot t_{web}}{d_{web} \cdot b_{flange}} & \cdot (T_s - T_a) + \frac{t_{web}}{b_{flange}} \cdot \left[q_{rad,face2} + h \cdot (T_a - T_s) - \varepsilon \cdot \sigma \cdot T_s^4\right] \end{aligned} \tag{B.13}$$

Compare equation Equation B.13 with B.10, the difference is the right side equation, which is also the driven force as for the junction cell temperature different from other cells. In the consequence,

$$\begin{aligned} q_{r,junction} &= \frac{k \cdot t_{web}}{d_{web} \cdot b_{flange}} \cdot (T_s - T_a) + \frac{t_{web}}{b_{flange}} \cdot [q_{rad,face2} + h \cdot (T_a - T_s) - \varepsilon \cdot \sigma \cdot T_s^4] \\ &= \frac{k \cdot t_{web}}{d_{web} \cdot b_{flange}} \cdot (T_s - T_a) + \frac{t_{web}}{b_{flange}} \cdot [\varepsilon \cdot \sigma \cdot T_a^4 + h \cdot (T_a - T_s) - \varepsilon \cdot \sigma \cdot T_s^4] \\ &= \frac{k \cdot t_{web}}{d_{web} \cdot b_{flange}} \cdot (1 - \frac{h \cdot d_{web}}{k}) \cdot (T_s - T_a) + \frac{t_{web}}{b_{flange}} \cdot \varepsilon \cdot \sigma \cdot (T_a^4 - T_s^4) \end{aligned} \tag{B.14}$$

Appendix C

Derivation of temperature dependent material properties

C.1 Specific Heat

As mentioned in the material properties section in Chapter 3, the final specific heat composes of the dry specific heat and one additional part considering the temperature dependent property and moisture effects. Literature found that the effects of moisture are normally too great to ignore, and the final effective specific heat includes the effect of moisture up to the "boiling point" (Welch, 2000). The moisture content change with temperature and time in reality is quite complex. For simplicity, the change has been considered as a linear change, shown in Figure C.1. This assumption is true for the case when the insulation has low moisture content, which is also the mostly case in practice. Thus, the case when insulation has high moisture content is not included here.

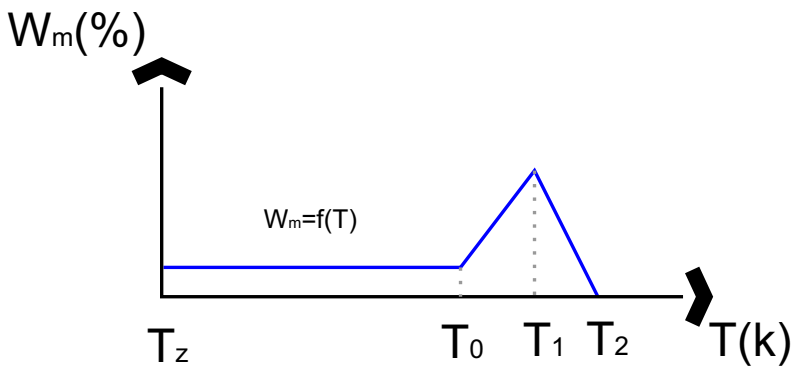

Figure C.1: Moisture content change with temperature

The figure above demonstrates the moisture content changes with the temperature as follows: ω_m is considered as a constant in the range $T_z \leq T \leq T_0$; while it increases linearly to a peak value in the range of $T_0 < T < T_1$, and reduces linearly in the range of $T_1 < T < T_2$, and finally reduced to zero; above T_2, there are no significant effects of moisture, thus can be ignored. Here, T_z is the zero Celsius degree temperature in Kelvin, $T_z = 0°C = 273.15K$. T_0, T_1, T_2 are critical temperatures regards to the boiling point of water in that material, and hence their values vary with different materials. Accordingly, c_p is divided into four regions as indicated in the green curve in Figure C.2. The additional part as a combination of the property change with temperature (pink line in Figure C.2) and moisture content change with temperature is hence denoted as $c_p^{'}$ in the figure.

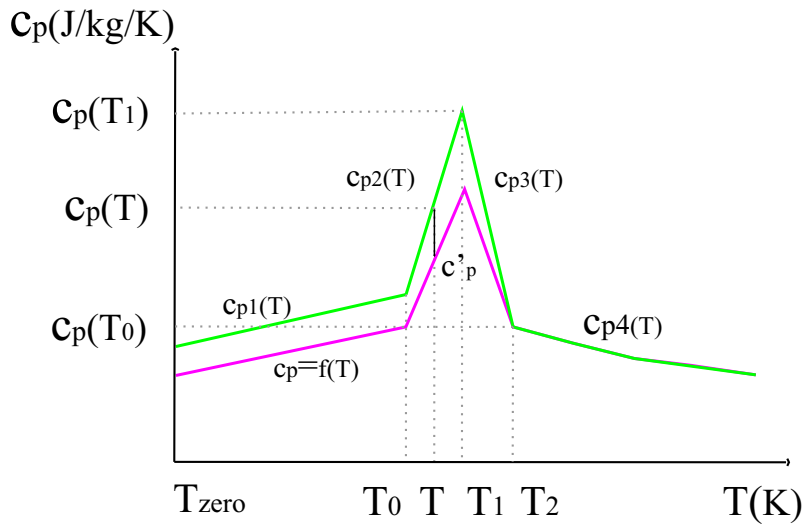

Figure C.2: Temperature dependent and moisture inclusive specific heat

To determine the additional term, correspondingly, four ranges have been divided.

In the range of $T_z \leq T \leq T_0$, $c_p^{'}$ is a constant, $c_p^{'} = c_{p,H_2O} \cdot \omega_m$;

In the range of $T_0 < T < T_1$, $c_p^{'} = c_p^{'}(T) + c_{p,moisture}^{'}$;

In the range of $T_1 < T < T_2$, $c_p^{'} = c_p^{'}(T) + c_{p,moisture}^{'}$;

In the range of $T \geq T_2$, $c_p^{'} = c_{p,H_2O} \cdot \omega_m$, and because moisture content in this temperature range is small enough to be ignored, thus, $c_p^{'} = 0$.

Detailed derivation of $c_p^{'}(T)$ is given below:

In the range of $T_0 < T < T_1$,

$$\frac{c_p^{'}(T)}{c_p(T_1) - c_p(T_0)} = \frac{T - T_0}{T_1 - T_0} \tag{C.1}$$

Then,

$$c_p^{'}(T) = a_0 + a_1 \cdot T \tag{C.2}$$

Where,

$$a_0 = \frac{c_p(T_0) - c_p(T_1)}{T_1 - T_0} \cdot T_0 \qquad and \qquad a_1 = \frac{c_p(T_1) - c_p(T_0)}{T_1 - T_0}$$

In the range of $T_1 < T < T_2$,

$$\frac{c_p'(T)}{c_p(T_1) - c_p(T_0)} = \frac{T_2 - T}{T_2 - T_1} \tag{C.3}$$

Then,

$$c_p^{'}(T) = b_0 + b_1 \cdot T \tag{C.4}$$

Where,

$$b_0 = \frac{c_p(T_1) - c_p(T_0)}{T_2 - T_1} \cdot T_2 \qquad and \qquad b_1 = \frac{c_p(T_0) - c_p(T_1)}{T_2 - T_1}$$

Since the energy stored in the system equals to the value integrated from a range of T_0 to T_2. That is to say,

$$\int_{T_0}^{T_2} c_p'(T) \cdot dT = \omega \cdot L \tag{C.5}$$

i.e.

$$\int_{T_0}^{T_1} (a_0 + a_1 \cdot T) \cdot dT + \int_{T_1}^{T_2} (b_0 + b_1 \cdot T) \cdot dT = \omega \cdot L$$

$$\Rightarrow \left[a_0 \cdot T + \frac{1}{2} a_1 \cdot T^2 \right]_{T_0}^{T_1} + \left[b_0 \cdot T + \frac{1}{2} b_1 \cdot T^2 \right]_{T_1}^{T_2} = \omega \cdot L$$

Substitute the values for a_0 and a_1, b_0 and b_1, gives Equation C.6 below:

$$\frac{c_p(T_0)-c_p(T_1)}{T_1-T_0}\cdot T_0\cdot(T_1-T_0)+\frac{1}{2}\cdot\frac{c_p(T_1)-c_p(T_0)}{T_1-T_0}\cdot(T_1+T_0)\cdot(T_1-T_0)$$
$$+\frac{c_p(T_1)-c_p(T_0)}{T_2-T_1}\cdot T_2\cdot(T_2-T_1)+\frac{1}{2}\cdot\frac{c_p(T_0)-c_p(T_1)}{T_2-T_1}\cdot(T_2+T_1)\cdot(T_2-T_1)=\omega\cdot L \tag{C.6}$$

Hence $c_p(T_1)$ is obtained as:

$$c_p(T_1)=\frac{2\omega\cdot L}{T_2-T_0}+c_p(T_0) \tag{C.7}$$

Now, substitute the calculated $c_p(T)$ value back into the function for $c_p^{'}(T)$ calculation when in the range of $T_0<T<T_1$, as specified in Equation C.2, giving:

$$c_p'(T)=\frac{c_p(T_0)-c_p(T_1)}{T_1-T_0}\cdot T_0+\frac{c_p(T_1)-c_p(T_0)}{T_1-T_0}\cdot T=\frac{T-T_0}{T_1-T_0}\cdot\frac{2\omega\cdot L}{T_2-T_0} \tag{C.8}$$

Together with the aid of the relation due to the symmetric characteristic, as also expressed as $T_0+T_2=2T_1$, the final cp'(T) is obtained:

$$c_p'(T)=\frac{T-T_0}{T_2-T_0}\cdot\frac{4\omega\cdot L}{T_2-T_0}\qquad(T_0<T<T_1) \tag{C.9}$$

Similar procedure gives the value for the range of $T_1<T<T_2$ as below: ,

$$c_p'(T)=\frac{T_2-T}{T_2-T_0}\cdot\frac{4\omega\cdot L}{T_2-T_0}\qquad(T_1<T<T_2) \tag{C.10}$$

By consideration of the moisture effect on specific heat, which decreases linearly in the range of T_0 to T_2, an additional term $c_{p,moisture}'=c_{p,H_2O}\cdot\omega\cdot\left(\frac{T_2-T}{T_2-T_0}\right)$ is added.

In summary, the final expression for $c_p^{'}$ can be obtained as:

$$c_p^{'} = \begin{cases} c_{p,H_2O} \cdot \omega_m & (T_z \leq T < T_0); \\ (\frac{T_2 - T}{T_2 - T_0}) \cdot \omega \cdot [\frac{4L \cdot (T - T_0)}{(T_2 - T_0)(T_2 - T)} + c_{p,H_2O}], & (T_0 < T < T_1); \\ (\frac{T_2 - T}{T_2 - T_0}) \cdot \omega \cdot [\frac{4L \cdot (T_2 - T)}{(T_2 - T_0)(T_2 - T)} + c_{p,H_2O}], & (T_1 < T < T_2); \\ 0, & (T \geq T_2). \end{cases} \tag{C.11}$$

Where, $c_p^{'}$ is the additional specific heat by consideration of the temperature change and moisture effect, $[J/(kg \cdot K)]$.

C.2 Thermal conductivity

Similar principle applies to the thermal conductivity derivation as to the specific heat. The final thermal conductivity composes of the initial thermal conductivity and one additional part considering the temperature dependent property and moisture effects. It can be seen in Figure C.3 below.

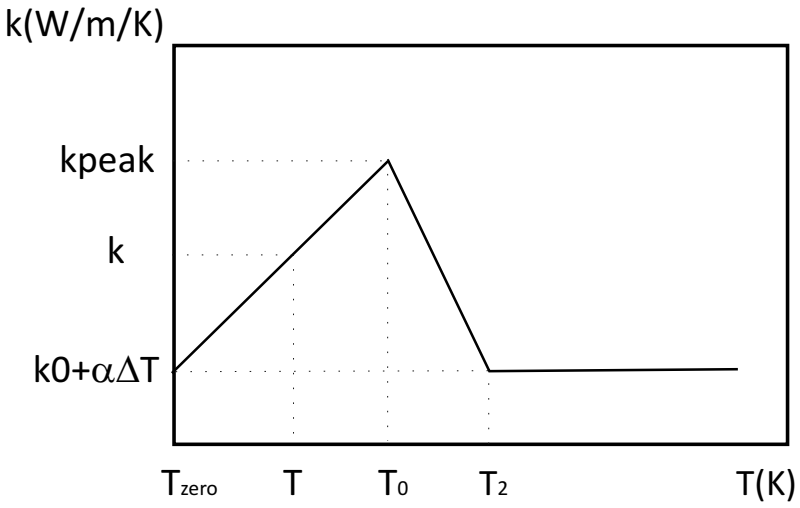

Figure C.3: Temperature dependent and moisture inclusive specific heat

As aforementioned, at temperature T_0, the thermal conductivity increases linearly to a peak value k_{peak} which equals to $(k_0 + \alpha \cdot \Delta T) \cdot (\omega_m \cdot KFactor^{KPower} + 1)^{(1/KPower)}$.

And then, it decreases linearly to the dry material thermal conductivity of a value of $(k_0 + \alpha \cdot \Delta T)$. Where ΔT is the temperature change, equals to $(T - T_z)$. According to this characteristic, three ranges are divided to obtain the final thermal conductivity.

In the range of $T_z \leq T \leq T_0$,

$$\frac{k - (k_0 + \alpha \cdot \Delta T)}{k_{peak} - (k_0 + \alpha \cdot \Delta T)} = \frac{T - T_z}{T_0 - T_z} \tag{C.12}$$

i.e.

$$k = \left(\frac{T - T_z}{T_0 - T_z}\right) \cdot [k_{peak} - (k_0 + \alpha \cdot \Delta T)] + (k_0 + \alpha \cdot \Delta T)$$

In the range of $T_0 < T < T_2$,

$$\frac{k - (k_0 + \alpha \cdot \Delta T)}{k_{peak} - (k_0 + \alpha \cdot \Delta T)} = \frac{T_2 - T}{T_2 - T_0} \tag{C.13}$$

i.e.

$$k = \left(\frac{T_2 - T}{T_2 - T_0}\right) \cdot [k_{peak} - (k_0 + \alpha \cdot \Delta T)] + (k_0 + \alpha \cdot \Delta T)$$

In the range of $T \geq T_2$,

$$k = (k_0 + \alpha \cdot \Delta T) \tag{C.14}$$

Consequently, the final thermal conductivity is summarized as below.

$$k = \begin{cases} \left(\frac{T-T_z}{T_0-T_z}\right) \cdot [k_{peak} - (k_0 + KTFactor \cdot \Delta T)] & \\ \qquad +(k_0 + KTFactor \cdot \Delta T), & (T_z \leq T \leq T_0); \\ \left(\frac{T_2-T}{T_2-T_0}\right) \cdot [k_{peak} - (k_0 + KTFactor \cdot \Delta T)] & \\ \qquad +(k_0 + KTFactor \cdot \Delta T), & (T_0 < T < T_2); \\ k = k_0 + KTFactor \cdot \Delta T, & (T \geq T_2). \end{cases} \tag{C.15}$$

Where, k is temperature dependant thermal conductivity with consideration of moisture effect, $[W/(m \cdot K)]$.

Appendix D

Parallel cases specifications

D.1 Sensvari.txt

72 simultaneous cases have been involved in the benchmark test scenario. The key input parameters for each case are listed as follows. The first line is the number of total simulation cases and from the second line onwards are the specifications or parameters for each case. Those specifications or parameters are: case number, protection 1 expansion ratio, protection 2 expansion ratio, length of steel, shape of steel (1 for I section), flange thickness, web thickness, flange breadth, web depth, protection 1 thickness, protection 2 thickness, steel thermal conductivity, KFactor, KPower, KTFactor, protection dry thermal conductivity, moisture content, water specific heat, protection dry specific heat, steel density, protection 1 density, protection 2 density, protection 1 emissivity, protection 2 emissivity, fire emissivity, remote cell emissivity for axial correction, Tmoist0, Tmoist2, Tilower, Tiupper, ipower, E, kpoly1, kpoly2, 3D correction logical flag, moisture effect on thermal conductivity logical flag.

```
72
1       1       1       30      1       0.016   0.0102  0.2     0.5     0.0254  0.025445.811
1.06E-03        0.1634229170    1000    970     8117.348        680     680     0.8     0.810.83 7 3 . 1 5
413.15  200     600     2       2.00E+06        5.97E-02        3.08E-03        1.32E-0600
2       1       1       30      1       0.0145  0.0084  0.2     0.497   0.02540.025445.811
1.06E-03        0.1634229170    1000    970     8159.323        680     680     0.8     0.810.83 7 3 . 1 5
413.15  200     600     2       2.00E+06        5.97E-02        3.08E-03        1.32E-0600
3       1       1       30      1       0.019   0.012   0.202   0.506   0.0254  0.025445.8111 . 0 6 E - 0 3
0.1634229170    1000    970     8049.955        680     680     0.8     0.8     1       0.8373.154 1 3 . 1 5
200     600     2       2.00E+06        5.97E-02        3.08E-03        1.32E-06        0       0
4       1       1       30      1       0.0132  0.0096  0.2088  0.52830.02540.025445.81
1       1.06E-03        0.1634229170    1000    970     7973.275        680     680     0.80.810.83 7 3 . 1 5
413.15  200     600     2       2.00E+06        5.97E-02        3.08E-03        1.32E-0600
5       1       1       30      1       0.0156  0.0101  0.2093  0.53310.02540.025445.81
1       1.06E-03        0.1634229170    1000    970     7940.1  680     680     0.80.810.83 7 3 . 1 5
413.15  200     600     2       2.00E+06        5.97E-02        3.08E-03        1.32E-0600
6       1       1       30      1       0.0174  0.0108  0.21    0.5367  0.02540.025445.81
1       1.06E-03        0.1634229170    1000    970     7942.793        680     680     0.80.810.83 7 3 . 1 5
413.15  200     600     2       2.00E+06        5.97E-02        3.08E-03        1.32E-0600
7       1       1       30      1       0.0188  0.0116  0.2108  0.53950.02540.025445.81
1       1.06E-03        0.1634229170    1000    970     7928.357        680     680     0.80.810.83 7 3 . 1 5
413.15  200     600     2       2.00E+06        5.97E-02        3.08E-03        1.32E-0600
8       1       1       30      1       0.0213  0.0127  0.2119  0.54450.02540.025445.81
1       1.06E-03        0.1634229170    1000    970     7921.528        680     680     0.80.810.83 7 3 . 1 5
413.15  200     600     2       2.00E+06        5.97E-02        3.08E-03        1.32E-0600
9       1       1       30      1       0.019   0.012   0.22    0.6     0.0254  0.025445.8111 . 0 6 E - 0 3
0.1634229170    1000    970     8077.331        680     680     0.8     0.8     1       0.8373.154 1 3 . 1 5
200     600     2       2.00E+06        5.97E-02        3.08E-03        1.32E-06        0       0
10      1       1       30      1       0.036   0.019   0.3     1       0.0254  0.025445.811
1.06E-03        0.1634229170    1000    970     8003.67         680     680     0.8     0.810.83 7 3 . 1 5
413.15  200     600     2       2.00E+06        5.97E-02        3.08E-03        1.32E-0600
11      1       1       20      1       0.036   0.019   0.4     1       0.0254  0.025445.811
1.06E-03        0.1634229170    1000    970     7990.179        680     680     0.8     0.810.83 7 3 . 1 5
413.15  200     600     2       2.00E+06        5.97E-02        3.08E-03        1.32E-0600
12      1       1       8.5     1       0.0396  0.0249  0.401   0.399   0.02540.025445.811
1.06E-03        0.1634229170    1000    970     7904.896        680     680     0.8     0.810.83 7 3 . 1 5
413.15  200     600     2       2.00E+06        5.97E-02        3.08E-03        1.32E-0600
13      1       1       30      1       0.016   0.0102  0.2     0.5     0.0222  0.022245.811
1.06E-03        0.1634229170    1000    970     8117.348        680     680     0.8     0.810.83 7 3 . 1 5
413.15  200     600     2       2.00E+06        5.97E-02        3.08E-03        1.32E-0600
14      1       1       30      1       0.016   0.0102  0.2     0.5     0.0445  0.044545.811
1.06E-03        0.1634229170    1000    970     8117.348        680     680     0.8     0.810.83 7 3 . 1 5
413.15  200     600     2       2.00E+06        5.97E-02        3.08E-03        1.32E-0600
15      1       1       30      1       0.016   0.0102  0.2     0.5     0.060325        0.06032545.811
1.06E-03        0.1634229170    1000    970     8117.348        680     680     0.8     0.810.83 7 3 . 1 5
413.15  200     600     2       2.00E+06        5.97E-02        3.08E-03        1.32E-0600
16      1       1       30      1       0.016   0.0102  0.2     0.5     0.079375        0.07937545.811
1.06E-03        0.1634229170    1000    970     8117.348        680     680     0.8     0.810.83 7 3 . 1 5
413.15  200     600     2       2.00E+06        5.97E-02        3.08E-03        1.32E-0600
17      1       1       30      1       0.016   0.0102  0.2     0.5     0.01    0.01    45.8113 . 0 0 E - 0 4
0.0459  0.54    1000    300     8117.348        256     256     0.8     0.8     1       0.8298.152648.15
200     600     2       2.00E+06        5.97E-02        3.08E-03        1.32E-06        0       0
18      1       1       30      1       0.016   0.0102  0.2     0.5     0.014   0.014   45.8113 . 0 0 E - 0 4
0.0459  0.54    1000    300     8117.348        256     256     0.8     0.8     1       0.8298.152648.15
200     600     2       2.00E+06        5.97E-02        3.08E-03        1.32E-06        0       0
19      1       1       30      1       0.016   0.0102  0.2     0.5     0.0245  0.024545.811
3.00E-04        0.0459  0.54    1000    300     8117.348        256     256     0.8     0.810.82 9 8 . 1 5
2648.15 200     600     2       2.00E+06        5.97E-02        3.08E-03        1.32E-0600
```

```
20 1 1 30 1 0.016 0.0102 0.2 0.5 0.0355 0.035545.8113.00E-04
0.0459 0.54 1000 300 8117.348 256 256 0.8 0.8 1 0.8298.152648.15
200 600 2 2.00E+06 5.97E-02 3.08E-03 1.32E-06 0 0
21 1 1 30 1 0.016 0.0102 0.2 0.5 0.057 0.057 45.8113.00E-04
0.0459 0.54 1000 300 8117.348 256 256 0.8 0.8 1 0.8298.152648.15
200 600 2 2.00E+06 5.97E-02 3.08E-03 1.32E-06 0 0
22 1 1 30 1 0.016 0.0102 0.2 0.5 0.01 0.01 45.8111.20E-04
0.0924 0.4 1000 550 8117.348 315 315 0.8 0.8 1 0.8298.152248.15
200 600 2 2.00E+06 5.97E-02 3.08E-03 1.32E-06 0 0
23 1 1 30 1 0.016 0.0102 0.2 0.5 0.012 0.012 45.8111.20E-04
0.0924 0.4 1000 550 8117.348 315 315 0.8 0.8 1 0.8298.152248.15
200 600 2 2.00E+06 5.97E-02 3.08E-03 1.32E-06 0 0
24 1 1 30 1 0.016 0.0102 0.2 0.5 0.029 0.029 45.8111.20E-04
0.0924 0.4 1000 550 8117.348 315 315 0.8 0.8 1 0.8298.152248.15
200 600 2 2.00E+06 5.97E-02 3.08E-03 1.32E-06 0 0
25 1 1 30 1 0.016 0.0102 0.2 0.5 0.018 0.018 45.8111.25E-04
0.0875 0 1000 880 8117.348 400 315 0.8 0.8 1 0.8373.154 13.15
200 600 2 2.00E+06 5.97E-02 3.08E-03 1.32E-06 0 0
26 1 1 30 1 0.016 0.0102 0.2 0.5 0.02 0.02 45.8111.25E-04
0.0875 0 1000 880 8117.348 400 315 0.8 0.8 1 0.8373.154 13.15
200 600 2 2.00E+06 5.97E-02 3.08E-03 1.32E-06 0 0
27 1 1 30 1 0.016 0.0102 0.2 0.5 0.032 0.032 45.8111.25E-04
0.0875 0 1000 880 8117.348 400 315 0.8 0.8 1 0.8373.154 13.15
200 600 2 2.00E+06 5.97E-02 3.08E-03 1.32E-06 0 0
28 1 1 30 1 0.016 0.0102 0.2 0.5 0.07 0.07 45.8111.25E-04
0.0875 0.01 1000 880 8117.348 400 315 0.8 0.8 1 0.8373.154 13.15
200 600 2 2.00E+06 5.97E-02 3.08E-03 1.32E-06 0 0
29 1 1 30 1 0.016 0.0102 0.2 0.5 0.019 0.019 45.8112.00E-05
0.1795 0.5 1000 550 8117.348 768 768 0.8 0.8 1 0.8298.152648.15
200 600 2 2.00E+06 5.97E-02 3.08E-03 1.32E-06 0 0
30 1 1 30 1 0.016 0.0102 0.2 0.5 0.0125 0.012545.811-
4.00E-05 0.14 0.44 1000 400 8117.348 950 950 0.8 0.8 10.8373.154 81.15
200 600 2 2.00E+06 5.97E-02 3.08E-03 1.32E-06 0 0
31 1 1 30 1 0.016 0.0102 0.2 0.5 0.025 0.025 45.811
-4.00E-05 0.14 0.44 1000 400 8117.348 950 950 0.8 0.8 10.8373.154 81.15
200 600 2 2.00E+06 5.97E-02 3.08E-03 1.32E-06 0 0
32 1 1 30 1 0.016 0.0102 0.2 0.5 0.00025 0.0002545.811
1.06E-03 0.1634229170 1000 1500 8117.348 1427 1427 0.8 0.810.83 7 3 . 1 5
413.15 200 600 2 2.00E+06 5.97E-02 3.08E-03 1.32E-0600
33 1 1 30 1 0.016 0.0102 0.2 0.5 0.0008 0.000845.811
1.06E-03 0.1634229170 1000 1500 8117.348 1427 1427 0.8 0.810.83 7 3 . 1 5
413.15 200 600 2 2.00E+06 5.97E-02 3.08E-03 1.32E-0600
34 1 1 30 1 0.016 0.0102 0.2 0.5 0.0023 0.002345.811
1.06E-03 0.1634229170 1000 1500 8117.348 1427 1427 0.8 0.810.83 7 3 . 1 5
413.15 200 600 2 2.00E+06 5.97E-02 3.08E-03 1.32E-0600
35 1 1 30 1 0.016 0.0102 0.2 0.5 0.00291 0.0029145.811
1.06E-03 0.1634229170 1000 1500 8117.348 1427 1427 0.8 0.810.83 7 3 . 1 5
413.15 200 600 2 2.00E+06 5.97E-02 3.08E-03 1.32E-0600
36 1 1 30 1 0.016 0.0102 0.2 0.5 0.0254 0.025445.811
1.06E-03 0.1634229170.01 1000 970 8117.348 680 680 0.8 0.810.83 7 3 . 1 5
413.15 200 600 2 2.00E+06 5.97E-02 3.08E-03 1.32E-0600
37 1 1 30 1 0.016 0.0102 0.2 0.5 0.0254 0.025445.811
1.06E-03 0.1634229170.02 1000 970 8117.348 680 680 0.8 0.810.83 7 3 . 1 5
413.15 200 600 2 2.00E+06 5.97E-02 3.08E-03 1.32E-0600
38 1 1 30 1 0.016 0.0102 0.2 0.5 0.0254 0.025445.811
1.06E-03 0.1634229170.04 1000 970 8117.348 680 680 0.8 0.810.83 7 3 . 1 5
413.15 200 600 2 2.00E+06 5.97E-02 3.08E-03 1.32E-0600
39 1 1 30 1 0.016 0.0102 0.2 0.5 0.0254 0.025445.811
1.06E-03 0.1634229170.08 1000 970 8117.348 680 680 0.8 0.810.83 7 3 . 1 5
413.15 200 600 2 2.00E+06 5.97E-02 3.08E-03 1.32E-0600
40 1 1 30 1 0.016 0.0102 0.2 0.5 0.0254 0.025445.811
1.06E-03 0.1634229170.16 1000 970 8117.348 680 680 0.8 0.810.83 7 3 . 1 5
413.15 200 600 2 2.00E+06 5.97E-02 3.08E-03 1.32E-0600
```

```
41    1    1    30    1    0.016 0.0102    0.2    0.5    0.0254    0.025445.811
1.06E-03    0.040855729 0    1000  970   8117.348    680   680   0.8   0.810.83 7 3 . 1 5
413.15    200   600   2    2.00E+06    5.97E-02    3.08E-03    1.32E-0600
42    1    1    30    1    0.016 0.0102    0.2    0.5    0.0254    0.025445.811
1.06E-03    0.081711459 0    1000  970   8117.348    680   680   0.8   0.810.83 7 3 . 1 5
413.15    200   600   2    2.00E+06    5.97E-02    3.08E-03    1.32E-0600
43    1    1    30    1    0.016 0.0102    0.2    0.5    0.0254    0.025445.811
1.06E-03    0.326845834 0    1000  970   8117.348    680   680   0.8   0.810.83 7 3 . 1 5
413.15    200   600   2    2.00E+06    5.97E-02    3.08E-03    1.32E-0600
44    1    1    30    1    0.016 0.0102    0.2    0.5    0.0254    0.025445.811
1.06E-03    0.653691668 0    1000  970   8117.348    680   680   0.8   0.810.83 7 3 . 1 5
413.15    200   600   2    2.00E+06    5.97E-02    3.08E-03    1.32E-0600
45    1    1    30    1    0.016 0.0102    0.2    0.5    0.0254    0.025445.811
1.06E-03    0.163422917 0    1000  485   8117.348    680   680   0.8   0.810.83 7 3 . 1 5
413.15    200   600   2    2.00E+06    5.97E-02    3.08E-03    1.32E-0600
46    1    1    30    1    0.016 0.0102    0.2    0.5    0.0254    0.025445.811
1.06E-03    0.163422917 0    1000  1940  8117.348    680   680   0.8   0.810.83 7 3 . 1 5
413.15    200   600   2    2.00E+06    5.97E-02    3.08E-03    1.32E-0600
47    1    1    30    1    0.016 0.0102    0.2    0.5    0.0254    0.025445.811
1.06E-03    0.163422917 0    1000  970   8117.348    340   680   0.8   0.810.83 7 3 . 1 5
413.15    200   600   2    2.00E+06    5.97E-02    3.08E-03    1.32E-0600
48    1    1    30    1    0.016 0.0102    0.2    0.5    0.0254    0.025445.811
1.06E-03    0.163422917 0    1000  970   8117.348    1360  680   0.8   0.810.83 7 3 . 1 5
413.15    200   600   2    2.00E+06    5.97E-02    3.08E-03    1.32E-0600
49    1    1    30    1    0.016 0.0102    0.2    0.5    0.0254    0.025445.811
1.06E-03    0.163422917 0    1000  970   8117.348    680   680   0.1   0.110.83 7 3 . 1 5
413.15    200   600   2    2.00E+06    5.97E-02    3.08E-03    1.32E-0600
50    1    1    30    1    0.016 0.0102    0.2    0.5    0.0254    0.025445.811
1.06E-03    0.163422917 0    1000  970   8117.348    680   680   0.3   0.310.83 7 3 . 1 5
413.15    200   600   2    2.00E+06    5.97E-02    3.08E-03    1.32E-0600
51    1    1    30    1    0.016 0.0102    0.2    0.5    0.0254    0.025445.811
1.06E-03    0.163422917 0    1000  970   8117.348    680   680   0.5   0.510.83 7 3 . 1 5
413.15    200   600   2    2.00E+06    5.97E-02    3.08E-03    1.32E-0600
52    1    1    30    1    0.016 0.0102    0.2    0.5    0.0254    0.025445.811
1.06E-03    0.163422917 0    1000  970   8117.348    680   680   0.7   0.710.83 7 3 . 1 5
413.15    200   600   2    2.00E+06    5.97E-02    3.08E-03    1.32E-0600
53    1    1    30    1    0.016 0.0102    0.2    0.5    0.0254    0.025445.811
1.06E-03    0.163422917 0    1000  970   8117.348    680   680   0.9   0.910.83 7 3 . 1 5
413.15    200   600   2    2.00E+06    5.97E-02    3.08E-03    1.32E-0600
54    1    1    30    1    0.016 0.0102    0.2    0.5    0.0254    0.025445.811
1.06E-03    0.163422917 0    1000  970   8117.348    680   680   0.95  0.9510.83 7 3 . 1 5
413.15    200   600   2    2.00E+06    5.97E-02    3.08E-03    1.32E-0600
55    1    1    30    1    0.016 0.0102    0.2    0.5    0.0254    0.025445.811
1.06E-03    0.163422917 0    1000  970   8117.348    680   680   1     110.8373.15413.15
200   600   2    2.00E+06    5.97E-02    3.08E-03    1.32E-06    0    0
56    1    1    30    1    0.016 0.0102    0.2    0.5    0.0254    0.025445.811
1.06E-03    0.163422917 0    1000  970   8117.348    680   680   0.8   0.80.70.83 7 3 . 1 5
413.15    200   600   2    2.00E+06    5.97E-02    3.08E-03    1.32E-0600
57    1    1    30    1    0.016 0.0102    0.2    0.5    0.0254    0.025445.811
1.06E-03    0.163422917 0    1000  970   8117.348    680   680   0.8   0.80.80.83 7 3 . 1 5
413.15    200   600   2    2.00E+06    5.97E-02    3.08E-03    1.32E-0600
58    1    1    30    1    0.016 0.0102    0.2    0.5    0.0254    0.025445.811
1.06E-03    0.163422917 0    1000  970   8117.348    680   680   0.8   0.80.90.83 7 3 . 1 5
413.15    200   600   2    2.00E+06    5.97E-02    3.08E-03    1.32E-0600
59    1    1    30    1    0.016 0.0102    0.2    0.5    0.0254    0.025445.811
1.06E-03    0.163422917 0    1000  970   8117.348    680   680   0.8   0.810.13 7 3 . 1 5
413.15    200   600   2    2.00E+06    5.97E-02    3.08E-03    1.32E-0600
60    1    1    30    1    0.016 0.0102    0.2    0.5    0.0254    0.025445.811
1.06E-03    0.163422917 0    1000  970   8117.348    680   680   0.8   0.811373.15413.15
200   600   2    2.00E+06    5.97E-02    3.08E-03    1.32E-06    0    0
61    1    1    30    1    0.016 0.0102    0.2    0.5    0.0254    0.025445.811
1.06E-03    0.163422917 0    1000  970   8117.348    680   680   0.8   0.810.83 7 3 . 1 5
413.15    200   600   2    2.00E+06    5.97E-02    3.08E-03    1.32E-0610
```

```
62    1    1    30    1    0.016 0.0102    0.2    0.5    0.0254    0.025445.811
1.06E-03    0.1634229170    1000 970    8117.348    680    680    0.8    0.810.83.15473.15
200    600    2    2.00E+06    5.97E-02    3.08E-03    1.32E-06    0    0
63    1    1    30    1    0.016 0.0102    0.2    0.5    0.0254    0.025445.811
1.06E+00    0.1634229170    1000 970    8117.348    680    680    0.8    0.811373.15413.15
200    600    2    2.00E+06    5.97E-02    3.08E-03    1.32E-06    0    0
64    1    1    30    1    0.016 0.0102    0.2    0.5    0.0254    0.025445.811
1.06E-01    0.1634229170    1000 970    8117.348    680    680    0.8    0.811373.15413.15
200    600    2    2.00E+06    5.97E-02    3.08E-03    1.32E-06    0    0
65    1    1    30    1    0.016 0.0102    0.2    0.5    0.0254    0.025445.811
1.06E-02    0.1634229170    1000 970    8117.348    680    680    0.8    0.811373.15413.15
200    600    2    2.00E+06    5.97E-02    3.08E-03    1.32E-06    0    0
66    1    1    30    1    0.016 0.0102    0.2    0.5    0.0254    0.025445.811
1.06E-04    0.1634229170    1000 970    8117.348    680    680    0.8    0.811373.15413.15
200    600    2    2.00E+06    5.97E-02    3.08E-03    1.32E-06    0    0
67    1    1    30    1    0.016 0.0102    0.2    0.5    0.0254    0.025445.811
1.06E-05    0.1634229170    1000 970    8117.348    680    680    0.8    0.811373.15413.15
200    600    2    2.00E+06    5.97E-02    3.08E-03    1.32E-06    0    0
68    1    1    30    1    0.016 0.0102    0.2    0.5    0.0254    0.025445.811
1.06E-06    0.1634229170    1000 970    8117.348    680    680    0.8    0.811373.15413.15
200    600    2    2.00E+06    5.97E-02    3.08E-03    1.32E-06    0    0
69    1    1    30    1    0.016 0.0102    0.2    0.5    0    0    45.8111 . 0 6 E - 0 3
0.1634229170    1000 970    8117.348    680    680    0.8    0.8    1    1373.15413.152 0 0
600    2    2.00E+06    5.97E-02    3.08E-03    1.32E-06    0    0
70    1    1    30    1    0.016 0.0102    0.2    0.5    0.00254    0.0025445.811
1.06E-03    0.1634229170    1000 970    8117.348    680    680    0.8    0.811373.15413.15
200    600    2    2.00E+06    5.97E-02    3.08E-03    1.32E-06    0    0
71    1    1    30    1    0.016 0.0102    0.2    0.5    0.000254    0.00025445.811
1.06E-03    0.1634229170    1000 970    8117.348    680    680    0.8    0.811373.15413.15
200    600    2    2.00E+06    5.97E-02    3.08E-03    1.32E-06    0    0
72    1    1    30    1    0.016 0.0102    0.2    0.5    0.0000254    0.000025445.811
1.06E-03    0.1634229170    1000 970    8117.348    680    680    0.8    0.811373.15413.15
200    600    2    2.00E+06    5.97E-02    3.08E-03    1.32E-06    0    0
```

Bibliography

Abbott, M.B. & Basco, D.R. (1989). *Computational fluid dynamics: an introduction for engineers*. Longman Group UK Limited, UK. 2.5.1

ABCB (2001). *Fire Engineering Guidelines*. Australian Building Codes Board, Australia. 2.4.6, 2.4.6

Abrams, M.S. (1979). Behaviour of inorganic materials in fire. *Design of Buildings for Fire Safety,* ASTM STP, **685**, 14–75. 2.4.2

AIAA (2005). Verification and validation. *URL=http://www.eng.auburn.edu/users/cjroy/Research/cfd-aiaa.html*. 4.4

AISC (2005). Specification for structural steel buildings - load and resistance factor design (LRFD)(ANSI/AISC 360-05) and commentary. *American Institute of Steel Construction (AISC), Chicago, IL*. 5.6.2

Alpert, R. (2002). Ceiling jet flows. In SFPE *handbook of fire protection engineering*, pp. 2–18 to 2–31, 1st edn. 2.2

Anderberg, Y. & Haksever, A. (1982). Comparison between measured and computed structural response of some reinforced concrete columns in fire. *Fire Safety Journal*, **4**, 293–297. 2.4.3

Anderson, D.A. (1997). *Computational Fluid Mechanics and Heat Transfer*. Taylor and Francis Inc., Philadelphia, USA, 2nd edn. 2.4.5, 3.2.2

Bailey, C.G. (2006a). Advances in fire engineering design of steel structures. *Structures and Buildings*, 21–35. 2.2, 2.4.4, 2.5, 2.5.1

Bailey, C.G. (2006b). Indicative fire tests to investigate the behaviour of cellular beams protected with intumescent coatings. *Fire Safety Journal*, **36**, 689–700. 2.4.4

Bartholmai, M. & Schartel, B. (2007). Assessing the performance of intumescent coatings using bench-scaled cone calorimeter and finite difference simulations. *Fire and Materials*, **31**, 187–205. (document), 2.4.4, 3.6.2, 3.10

Bartholmai, M., Schriever, R. & Schartel, B. (2003). Influence of external heat flux and coating thickness on the thermal properties of two different intumescent coatings using cone calorimeter and numerical analysis. *Fire and Materials*, **27**, 151–162. 2.4.4, 3.6.2, 3.6.2, 3.6.2

Baum, H.R. (2005). Simulating fire effects on complex building structures. In *Proc. 8th Int. Symp. Fire Safety Science*, 3–18, Beijing, China. 2.5.1

Bizri, H., Becker, J.M. & Bresler, B. (1974). FIRES-T3 - computer program for the fire response of structures-thermal. technical report report No. UCB FRG 74-1. Tech. rep., University of California, Berkeley. 2.4.3

BRE (2003). BRE report: JOSEFINE – a description of the fire engineering interface. Tech. rep., Building Research Establishment. 2.4.1, 2.5.1, 3.6.2.2

BSI (1993). ISO 5660-1: Fire tests on building materials and structures - part 15: Method for measuring the rate of heat release of products. Tech. rep., British Standards Institution. 3.6.2.1

BSI (1999). Fire resistance tests: general requirements. BS EN 1363-1. Tech. rep., British Standards Institution. 2.5.1

BSI (2001). Method for determination of the fire resistance of elements of construction: Part 20. BS 476-20. Tech. rep., British Standards Institution. 2.5.1

BSI (2002a). Eurocode 1: Actions on structures - part 1-2: General actions - actions on structures exposed to fire. Tech. rep., British Standards Institution. 2.2, 2.4.5, 2.4.6

BSI (2002b). Test methods for determining the contribution to the fire resistance of structural members - applied protection to steel members, DD ENV 13381-4. Tech. rep., British Standards Institution. 2.4.1

BSI (2002c). Test methods for determining the contribution to the fire resistance of structural members-part2: Vertical protective members, DD ENV 13381-2. Tech. rep., British Standards Institution. 2.4.1

BSI (2003a). Eurocode 2: Design of concrete structures - part 1-2: General rules - structural fire design. Tech. rep., British Standards Institution. 2.4.6

BSI (2003b). Eurocode 6: Design of masonry structures - part 1-2: General rules - structural fire design. Tech. rep., British Standards Institution. 2.4.6

BSI (2003c). Eurocode 9: Design for aluminium structures - part 1-2: Aluminium fire design. Tech. rep., British Standards Institution. 2.4.6

BSI (2005a). Eurocode 3: Design of steel structures - part 1-2: General rules - structure fire design. Tech. rep., British Standards Institution. (document), 1.1, 2.4.1, 2.2, 2.4.1, 2.4.2, 2.3, 2.4.2, 2.4.6, 2.4.6, 2.5.1, 2.5.1, 4.1, 4.3, 4.3.2, 4.3, 4.3.2, 4.3.2, 4.3.4, 4.4.2.2, 5.5.4.1, 5.6.4

BSI (2005b). Test methods for determining the contribution to the fire resistance of structural members - part1: Horizontal protective members, DD CEN/TS 13381-1. Tech. rep., British Standards Institution. 2.4.1

Carslaw, H.S. & Jaeger, J.C. (1959). *Conduction of Heat in Solids*. Oxford University. 2.3.1, 2.3.1, 3.2.1

Christopher, A. (1999). *Essential heat transfer*. Longman, Essex. 2.3.1, 2.3.1, 2.4.6, 2.4.7

Desanghere, S. & Joyeux, D. (2005). Development of design rules for the fire behaviour of external steel structures. Tech. Rep. 7210-PR-380. 2.4.4

Drysdale, D. (1999). *An Introduction to Fire Dynamics*. John Wiley and Sons, Inc., New York, 2nd edn. (document), 2.2, 2.1, 2.3.1, 2.3.1, 2.3.1, 2.3.1, 2.4.5, 2.4.5, 2.4.6

Edwards, D. & Menard, W. (1964). Comparison of models for correlation of total band absorption. *Applied Optics*, **3**, 621–625. 2.4.6

Edwards, D.K. & Balakrishnan, A. (1972). Thermal radiation by combustion gases. *International Journal of Heat and Mass Transfer*, **16**, 25–40. 2.4.6

Edwards, D.K. & Balakrishnan, A. (1973). Self absorption of radiation in turbulent molecular gases. *Combustion and Flame*, **20**, 401–417. 2.4.6

Edwards, D.K. & Matavosian, R. (1984). Scaling rules for total absorptivity and emissivity of gases. *Journal of Heat Transfer*, **106**, 684–689. 2.4.6, 2.5.1

Faure, L. (2008). *Generalised Method for Fire Structural Analysis*, MSc thesis, University of Edinburgh. 5.6.4

Fernandez-Pello, C. & Rein, G. (2004). Fire modelling: development and applications. In *Computational simulation models in fire engineering and research*, 1–6, University of Cantabria, Santander, Spain. 2.2

FSD (2002). Char 21 fire retardant paint on steel structures: design guide based on prENV13381-4, No. 02-024-RevB. Tech. rep. 2.4.4

Garlock, M. & Quiel, S. (2006). Combined axial load and moment capacity of fire exposed beam-columns with thermal gradients. In *Proc. of 4th Int. Workshop on Structures in fire*, Aveiro, Portugal. 5.6.2, 5.6.4

Gewain, R., Iwankiw, N. & Alfawakhiri, F. (2003). Facts for steel buildings: fire,. *American Institute of Steel Construction (AISC), Chicago, IL*. 5.6.2

GEXCON (2008). Flame ACceleration Simulator. *URL = http://www.gexcon.com/index.php?src=flacs/flacs.html.* 2.2

GHOJEL, J.I. (1998). A new approach to modelling heat transfer in compartment fires. *Fire Safety Journal*, **31**, 227–237. 2.2, 2.4.6, 2.5.1, 2.5.1

GOLDSMID, H. (1965). *The thermal properties of solids*. Routledge and Kegan Paul Ltd., London. 2.4.2

GOODE, M.G. (2004). Fire protection of structural steel in high-rise buildings, report No. GCR 04-872. Tech. rep., NIST. 2.4.4

HAMILTON, D. & MORGAN, W. (1952). *Radiant interchange configuration factors*. NACA Tech. 2.3.1

HARADA, K. & TERAI, T. (1988). Numerical simulation of fire resistance test of a concrete slab. In *Proc. 2nd Int. Symp. Fire Safety Science*, 707–717. 2.4.3

HARMARTHY, T.Z. (1965). Effect of moisture on the fire endurance of building elements. ASTM STP *385*, 74. 2.4.3

HARMARTHY, T.Z. (1981). The fire resistance test and its relation to real world fires. *Fire and Materials*, **5**, 112–122. 4.4.2.2

HARMARTHY, T.Z. (1993). *Fire safety design and concrete*. Longman Scientific and Technical, Harlow. 2.5.1

HARMARTHY, T.Z. (1995). Properties of building materials. In SFPE *Handbook of fire protection engineering*, 141–155, NFPA, Boston, 2nd edn. 2.4, 2.4.2

HE, M., KASSAB, A.J., BISHOP, P.J. & MINARDI, A. (1995). An iterative FDM/BEM method for the conjugate heat transfer problem – parallel plate channel with constant outside temperature. *Engng Anal Bound Elem*, **15**, 43–50. 2.3.3

HOLMAN, J. (1988). *Thermodynamics*. McGraw-Hill, New York, 3rd edn. 2.3.1, 2.3.1, 2.3.1

HOLMAN, J. (1997). *Heat transfer*. McGraw-Hill, New York, 8th edn. 2.4.2, 2.4.5

HOSTIKKA, S. (2003). Computation of fire emissivity for Eurocode heat transfer equations. Tech. rep., VTT Technical Research Centre of Finland. 2.4.6

HOTTEL, H. & SAROFIM, A. (1967). *Radiative Transfer*. McGraw-Hill Book Company, USA. 2.4.6

INCROPERA, F. & DEWITT, D. (1996). *Introduction to heat transfer*. John Wiley and Sons, Inc., 3rd edn. 2.3.1, 2.3.1

JEANES, D.C. (1984). Technical report 84-1. Tech. rep., Society of Fire Protection Engineers. 2.5.1

JIMENEZ, M., DUQUESNE, S. & BOURBIGOT, S. (2006). Characterisation of the performance of an intumescent fire protective coating. *Surface and Coatings Technology*, **201**, 979–987. 2.4.4

JONES, W. & WHITELAW, J. (1982). Calculation methods for reacting turbulent flow: a review. *Combustion and Flame*, **48**, 1–26. 2.4.5

JOWSEY, A. (2006). *Fire Imposed Heat Fluxes for Structural Analysis*. Ph.D. thesis, University of Edinburgh. 2.2, 2.4.6, 2.5.1, 4.4.2.2

KANURY, A. (1975). *Introduction to combustion phenomena*. Gordon and breach, London. 2.4.5

KAVIANG, M. (2002). *Principles of heat transfer*. John Wiley and Sons, Inc., New York. 2.3.2, 2.4.6, 2.4.7

KAWAGOE, K. (1958). Fire behaviour in rooms. Tech. Rep. 27, Building Research Institute. 2.2

KAYE, G.W.C. & LABY, T.H. (1986). *Table of Physical and Chemical Constants and Some Mathematical Functions*. Longman, London and New York, 15th edn. 2.4.2

KINSELLA, E.V. (2007). *Tools for thermal analysis of intumescent materials*, MEng thesis, University of Edinburgh. 3.6.2

KUMAR, S., WELCH, S., MILES, S., CAJOT, L.G., HALLER, M., OJANGUREN, M., BARCO, J., HOSTIKKA, S., MAX, U. & RÖHRLE, A. (2002). Natural fire safety concept - the development and validation of a CFD-based engineering methodology for evaluating thermal action on steel and composite structures. Tech. Rep. ISBN 92-894-9594-4, European Commission. 2.2

KUMAR, S., WELCH, S., MILES, S., CAJOT, L.G., HALLER, M., OJANGUREN, M., BARCO, J., HOSTIKKA, S., MAX, U. & RÖHRLE, A. (2005). Natural fire safety concept - the development and validation of a CFD-based engineering methodology for evaluating thermal action on steel and composite structures, report No. ISBN 92-894-9594-4. Tech. Rep. ISBN 92-894-9594-4, European Commission,. 1.1, 2.5.1, 4.4.2.1

KUMAR, S., MILES, S., WELCH, S., VASSART, O., ZHAO, B., LEMAIRE, A., NOORDIJK, L., FELLINGER, J. & FRANSSEN, J. (2006). FIRESTRUC - integrating advanced three-dimensional modelling methodologies for predicting thermo-mechanical behaviour of steel and composite structures subjected to natural fires. Tech. Rep. 7, BRE; Arcelor Profil Luxembourg S.A.; CTICM; TNO Efectis; Université de Liège. 1.1, 5.5.2, 5.5.4.2

KUMARAN, M.K. (1996). Task 3: Material properties. Tech. rep., IEA Annex 24. 2.4, 2.4.1

LANE, B. (2000). Performance-based design for fire resistance. *Journal of Modern Steel Construction, AISC*, 54–61. 5.6.2

LENNON, T. & MOORE, D. (2003). The natural fire safety concept - full-scale tests at cardington. *Fire Safety Journal*, **38**, 623–643. 1.1, 4.4, 4.4.1.2, 4.4.1.2

Lewis, M.J., Moss, J.B. & Rubini, P.A. (1997). CFD modelling of combustion and heat transfer in compartment fires. In *Proc. of 5th Int. Symp. on Fire Safety Science*, 463–474. 1.1

Liang, H. & Welch, S. (2006). A novel engineering tool for thermal analysis of structural members in natural fires. In *Proc. of 4th Int. Workshop on Structures in fire*, Aveiro, Portugal. 3.6

Liang, H., Welch, S., Stratford, T. & Kinsella, E. (2007). Development and validation of a generalised engineering methodology for thermal analysis of structural members in fire. In *Proc. of 5th Int. Seminar Fire and Explosion Hazards*, Edinburgh, UK. 4.4.2.1

Lie, T.T. (1972). *Fire and Buildings*. Applied Science, London. 2.5.1

Malhotra, H.L. (1982). *Design of Fire Resisting Structures*. Surrey University Press, Surrey. 2.5.1

Melinek, S.J. & Thomas, P. (1987). Heat flow to insulated steel. *Fire Safety Journal*, **12**, 1–8. 2.5.1

Miles, S.D. & Kumar, S. (2003). JASMINE technical summary. Tech. rep., Building Research Establishment. 2.4.1, A

Mooney, J. (1992). Surface radiant-energy balance for structural thermal analysis. *Fire Master*, **16**, 61–66. 2.4.6

Özisik, M. (1985). *Heat transfer - a basic approach*. McGraw-Hill book company. 2.3.1

Papanicolaou, E., Giebert, D., Koch, R. & Schulz, A. (2001). A conservation-based discretization approach for conjugate heat transfer calculations in hot-gas ducting turbomachinery components. *International Journal of Heat and Mass Transfer*, **44**, 3413–3429. 2.3.3

PATANKAR, S.V. (1978). *Numerical heat transfer and fluid flow: series in computational methods in mechanics and thermal sciences*. Hemisphere publishing corporation, USA. 2.3.3, 2.5.1

PITTS, D.R. & SISSOM, L.E. (1977). *Schaum's Outline Series: Theory and Problems of Heat Transfer*. McGraw-Hill, New York, USA. 2.3.1, 2.4.2

POWELL, A.C. (2004). Necessary dimensionless numbers: forced convection and natural convection equations.
URL = http://www.processassociates.com/process/dimen/dn_all.htm. 2.4.5

QUIEL, S. & GARLOCK, M. (2006). A performance-based design approach for steel perimeter columns subject to fire. In *Proc. of 4th Int. Workshop on Structures in fire*, Aveiro, Portugal. 5.6.2, 5.6.3, 5.6.4, 5.6.4, 5.6.4

ROACHE, P. (1998). *Verification and validation in computational science and engineering*. Hermosa, Albuquerque, New Mexic. 4.4

ROHSENOW, W. & CHOI, H. (1961). *Heat, mass and momentum transfer*. Prentice-Hall, London. 2.4.5

RUBINI, P.A. (1996). Numerical methods for turbulent flows. Tech. rep., Cranfield University. 2.5.1

RUBINI, P.A. (1997). SOFIE-simulation of fires in enclosures. Tech. rep., Cranfield University. 2.4.1, 2.5.1, 4.1

SBI (1976). *Fire engineering design fo steel structures*. Swedish Institute of Steel Construction. 2.4.6

SCHLEICH, J., CAJOT, L., PIERRE, M., MOORE, D., LENNON, T. & KRUPPA, J.E.A. (2003). Natural fire safety concept - full scale tests, implementation in the Eurocodes and development of an userfriendly design tool. Tech. Rep. 7210-060, Office for Official Publications of the European Communities. 1.1, 4.4, 4.4.1.2, 4.4.1.2

SFPE (2002). SFPE *Handbook of Fire Protection Engineering*. Society of Fire Protection Engineers, 3rd edn. 2.4.6, 2.4.6

Siegel, R. & Howell, J. (1980). *Thermal radiation heat transfer*. McGraw-Hill, New York, 2nd edn. 2.3.1

Siegel, R. & Howell, J. (1992). *Thermal radiation heat transfer*. Taylor and Francis, London, 3rd edn. 2.4.6

Smith, C.I. & Stirlad, C. (1983). Analytical methods and the design of steel framed buildings. In *International Seminar on Three Decades of Structural Fire Safety*, 155–200, Fire Research Station, Herts, UK. 2.4.6

Smith, T.F., Shen, Z.F. & Friedman, J.N. (1982). Evaluation of coefficients for the weighted sum of grey gases model. *Journal of Heat Transfer*, **104**, 602–608. 2.4.6

Staggs, J. & Phylaktou, H. (2008). The effects of emissivity on the performance of steel in furnace tests. *Fire Safety Journal*, **43**, 1–10. 5.5.4.4

Tan, K.H., Wang, Z.H. & Au, S.K. (2004). Heat transfer analysis for steelwork insulated by intumescent paint exposed to standard fire conditions. In *Proc. of 3rd Int. Workshop on structures in fire*, Ottawa, Canada. 3.6.2

Thomas, P. & Bullen, M. (1979). On the role of $k\rho c$ of room lining materials in the growth of room fires. *Fire and Materials*, **3**, 68–73. 2.2

Thomas, P., Heselden, A. & Law, M. (1967). Fully developed compartment fires: two kinds of behaviour. Tech. rep. 2.2

Touloukian, Y. & Dewitt, D. (1972). *Thermophysical Properties of Matter. Vol.8: Thermal radiative properties of nonmetallic solids and Vol.9:Coatings*. New York : IFI/Plenum. 2.4.6

UoE (2007). FireGrid. *URL = http://www.firegrid.org*. 1.1

USMANI, A., ROTTER, J., LAMONT, S., SANAD, A. & GILLIE, M. (2001). Fundamental principles of structural behaviour under thermal effects. *Fire Safety Journal*, **36**, 721–744. 5.6.2

WANG, Y., LENNON, T. & MOORE, D. (1995). The behaviour of steel frames subject to fires. *Journal of Constructional Steel Research*, **35**, 291–322. 5.6.2

WARNE, S.S.J. (1991). Introduction to thermal analysis. In E. Charsley & S. Warrington, eds., *Thermal analysis-techniques and applications*, Royal society of chemistry, Leeds. 2.5

WELCH, S. (2000). Developing a model for thermal performance of mansonry exposed to fire. In *Proc. 1st Int. Workshop. Structures in Fire*, Copenhagen. 2.4.3, 3.6.1, C.1

WELCH, S. (2004). Structural fire engineering design: fire and thermal response. *BRE digest 488*. 2.5.1

WELCH, S. & PTCHELINTSEV, A. (1997). Numerical prediction of heat transfer to a steel beam in a localised fire. In *Proc. 2nd Int. Sem. on Fire and Explosion Hazard of Substances and Venting of Deflagrations*, VNIIPO, Moscow. 2.5.1, 4.4.2.1

WELCH, S. & RUBINI, P. (1997). Three-dimensional simulation of a fire-resistance furnace. In *Proc. 5th Int. Symp. Fire Safety Science*, 1009–1020. (document), 2.5.1, 4.4, 4.1, 4.4.1.1, 4.4.2.1

WELCH, S., JOWSEY, A., DEENY, S., MORGAN, R. & TORERO, J. (2007). BRE large compartment fire tests - characterising post-flashover fires for model validation. *Fire Safety Journal*, **42**, 548–567. 1.1, 4.4, 4.4.1.2, 4.4.1.2, 4.4.2.2, 4.4.2.2

WELCH, S., MILES, S., KUMAR, S., LEMAIRE, T. & CHAN, A. (2008). FIRESTRUC - integrating advanced three-dimensional modelling methodologies for predicting thermo-mechanical behaviour of steel and composite structures subjected to natural fires. In *Proc. 9th International IAFSS Symposium*, Karlsruhe, Germany. 2.5.1, 5.5.1, 5.5.2, 5.5.4, 5.5.4.1, 5.5.4.1, 5.5.4.2, 5.6.4

WICKSTRÖM, U. (1979). TASEF-2 - a computer program for temperature analysis of structures exposed to fire. Tech. rep., Dept. of Structural Mechanics, Lund Institute of Technology. 2.4.3

WICKSTRÖM, U. (1985). Temperature analysis of heavily-insulated steel structures exposed to fire. *Fire Safety Journal*, **9**, 281–285. 2.5.1, 4.3

WICKSTRÖM, U. (2007). Adiabatic surface temperature for calculating heat transfer to fire exposed structures. In *Interflam 2007. (Interflam '07). International Interflam Conference, 11th Proceedings.*, vol. 2, 943–953, London, UK. 4.3

WILLIAMS, F.A. (1982). Urban and wildland fire phenomenology. *Progress in Energy and Combustion Science*, **8**, 317–354. 2.4.5

WONG, M.B. (2005). Size effect on temperatures of structural steel in fire. *Journal of Structural Engineering*, **16**, 16–20. 2.4.6

WONG, M.B. & GHOJEL, J.I. (2003). Sensitivity study of heat transfer formulations for insulated structure steel components. *Fire Safety Journal*, **38**, 187–201. 2.5.1, 3.2.2, 3.7, 4.3, 4.3.4, 4.3.4, 5.5.4.5

WONG, M.B. & GHOJEL, J.I. (2005). Heat transfer model for unprotected steel members in a standard compartment fire with participating medium. *Journal of Constructional Steel Research*, **61**, 825–833. 2.5.1

WONG, M.B., GHOJEL, J.I. & CROZIER, D.A. (1998). Temperature-time analysis for steel structures under fire conditions. *Structural Engineering and Mechanics (Struct Eng Mech)*, **6**, 275–289. 2.4.6

YAPICI, H. & BASTURK, G. (2004). CFD modelling of conjugate heat transfer and homogeneously mixing two different fluids in a stirred and heated hemispherical vessel. *Computer and Chemical Engineering*, **28**, 2233–2244. 2.3.3

Zhai, Z.Q. & Chen, Q.Y. (2004). Numerical determination and treatment of convective heat transfer coefficient in the coupled building energy and CFD simulation. *Building and Environment*, **39**, 1001–1009. 3.2.2